# ADVANCED INHERENT DAMPING MODELS AND THEIR APPLICATION IN SEISMIC LOSS OPTIMIZATION OF VISCOUS DAMPERS


## ARUN MANKAVU PUTHANPURAYIL


A thesis submitted in partial fulfilment of the requirements for the Degree of Doctor of Philosophy in Earthquake Engineering

Under the supervision of by:

**Professor Rajesh P. Dhakal (Primary Supervisor)**

**Professor Athol J. Carr**

**Associate Professor Oren Lavan (Technion-Israel Institute of Technology, Israel)**

Examined by:

**Professor (Emeritus) Andrei M. Reinhorn** (University at Buffalo-SUNY, Buffalo, New York)

**Professor Andreas J. Kappos** (City University, London)

August 2018


Department of Civil and Natural Resources Engineering, College of Engineering

UNIVERSITY OF CANTERBURY Christchurch, New Zealand.

# Abstract

The effectiveness of passive control strategies in achieving the objectives of a performance based design is well accepted in the structural engineering community. Though the damper design and installation techniques are well advanced, the science of optimal positioning of dampers incorporating direct performance indicators (the initial cost and Expected seismic loss) have not been adequately explored. The research presented in the thesis sheds new light into this less explored area and presents itself with innovative strategies for the optimal positioning of dampers keeping a strong focus on the practical feasibility of the developed framework.

This thesis tries to address the issue of a realistic optimum in terms of damper quantification and distribution. A realistic optimum may only be reached when the epistemic uncertainties inherent in the modelling of the bare frame is minimized. One of the common sources of epistemic uncertainty in the modelling of a bare frame is the inherent damping modelling. An accepted and popular method of damping modelling is to adopt a proportional viscous damping called Rayleigh damping. Issues associated with this damping model have been identified in literature and it is an agreed fact that a complete holistic change in the damping modelling is imperative. In this direction, the first part of the thesis develops a whole new paradigm of damping modelling in which the damping matrix is developed at the element level and assembled to system level in a similar manner to mass or stiffness matrices. Element level formulation of damping incurs no additional computational penalty and reflects the contribution of the elements in a more realistic manner. Six new damping models with increasing rigor are introduced into the nonlinear seismic dynamic analysis scenario. Also, a possible most pragmatic approach to damping modelling is identified which is devoid of the un-realistic issues associated with the extension of the classical Rayleigh damping into nonlinear seismic dynamic analysis.

Adopting the most realistic in-structure damping model recommendation from the first part of the thesis, the second part of the thesis addresses the issue of developing a generic framework which can simultaneously optimize the initial cost of the dampers as well as the seismic loss likely to be incurred in frame buildings with optimally distributed dampers in an earthquake. To this end, an aggregate gradient based multi-objective strategy adopted from the literature is applied to optimally quantify and distribute dampers in frame buildings. The expected loss is computed as per classical Pacific Earthquake Engineering Research (PEER) seismic risk assessment framework. A polynomial based interpolation is used to compute the expected loss conditioned on engineering demand parameters (EDPs). Gradients for the optimization framework is computed analytically using the highly efficient Adjoint Variable Method for linear frames and with finite difference schemes for nonlinear case. Efficiency of the framework is demonstrated using a four-storey linear and nonlinear 2D frame and an eight-storey linear 3D asymmetric system. The results are presented in the form of Pareto front which is plotted between the initial cost and the expected seismic loss. Pareto front presents a set of feasible solutions and presents the owner and other stakeholders with a powerful decision-making tool, as it clearly shows the implication of the decisions made.

So, in nutshell, this thesis presents itself with an advanced first order gradient based multi-objective framework for viscous damper quantification and distribution, incorporating realistic advanced inherent damping models which enables the practitioners/ stakeholders to make more informed decisions.

# ACKNOWLEDGEMENTS

This thesis would not have been possible, without the inspiration and support of my supervisors Professor Rajesh P. Dhakal, Professor Athol J. Carr and Associate Professor Oren Lavan (Technion-Israel institute of technology). I am deeply indebted to Prof. Dhakal for initiating and shaping this project, for standing by my side in all difficult times, believing in me and for motivating me to go ahead with my area of interest, for constantly observing my progress and making very constructive comments which helped me a lot in completing this thesis. Throughout the period of my project, both Prof. Carr and Dr. Lavan have constantly motivated me and sometimes even mesmerised me with their deep insights in nonlinear structural dynamics and nonlinear optimization. Thank you very much; without all the three of you, I would never have reached this point where I am now.

I would also like to express my deepest gratitude to my examiners, Prof. Andrei M. Reinhorn of SUNY, Buffalo, US and Prof. Andreas J. Kappos of City University, London, UK for critically reviewing my thesis and making very constructive comments which improved my thesis to a very high standard. I am also deeply indebted to Prof. Harm Askes of University of Sheffield for generating in me a deep interest in computational dynamics which led me to pursue this research.

I would also like to acknowledge the significant financial support provided by Earthquake Commission (NZ) and the University of Canterbury. Thanks also goes to my colleagues in Beca Ltd. (NZ): Dr. Richard Sharpe, Rob Jury, David Wood and Murray Chalmers for very informative discussions on the socio-economic impact of the Christchurch and Kaikoura earthquakes. My deepest gratitude goes to my wife Sona, who endured and loved me through all the ups and downs during the whole period of my PhD., and who persistently instilled in me the confidence that I can do this. A deep thanks goes to my mom, dad and brother for morally supporting me in all my endeavours in life. Last but not at all least and the most important, I would like to express my gratitude to the Almighty for the invisible blessings and inspiration which helped me overcome the difficult moments of this thesis and accomplishing its completion.

**ABSTRACT**

**ACKNOWLEDGEMENTS**

# 1. Introduction

## 1.1 Motivation

Conventional capacity design strategy relies on the "evasion" of seismic forces by enduring large inelastic deformations in the structure. This results in heavy economic losses. Past earthquakes have exemplified this aspect. The $M_w = 7.8$, 14th November 2016 Kaikoura earthquake in New Zealand is a very recent example of the economic losses mainly incurred due to the adoption of this philosophy. Although this earthquake resulted in only two deaths, the earthquake-related damages to buildings and infrastructure were roughly estimated as $\approx NZ\ \$15$ billion. Similarly, the damage and business disruption in the 2010 and 2011 Canterbury earthquakes amounted to be around $\geq NZ\ \$40$ billion which corresponds to approximately 20% GDP (Pampanin 2015); it must be noted that this figure -does not represent the socio-fabric disruption which would result in extensive migration of people and economic activities. Similar observations could be made from past events in other parts of the world; for example, the 1989 M6.9 Loma Prieta earthquake caused more than *US* $8 billion in direct damage (several buildings and bridges suffered total and partial collapse) although no major loss of life occurred (Wada et al., 2004). Similar observations were made for 1995 Kobe earthquake (*US* $102.5 billion in damage, 2.5% of Japan's GDP at the time) and 1999 Chi-Chi earthquake which caused about *US* $10 billion worth of damage (Wada et al., 2004).

So, reviewing these observed facts, a pressing question arises, "is the present philosophy of capacity design adequately catering to the present needs of the modern society in highly seismic

countries like New Zealand?". In a nutshell, considering the facts cited above, the answer would be negative. The primary focus of the present design philosophy is life safety and there is no absolute necessity for an engineer to consider the economic loss as part of his/her design.

The author's personal communications with experienced engineers practicing in Wellington who were involved in building assessments/retrofits after the 2010-11 Canterbury and the 2016 Kaikoura earthquakes expressed the view that, there is a general feeling among the public that the level of seismic damage incurred in these earthquakes is not acceptable and should be minimized. This expectation from the society necessitates a complete paradigm shift from the "dissipation by degradation" philosophy of the present seismic design approach to "dissipation without degradation" to achieve both "economic resilience" and "life safety". This shift of focus in the seismic design philosophy demanded by the public community may only be brought to fruition by adopting low damage technologies like base isolation, viscous dampers etc. Since the incorporation of low damage technologies increases the initial investment in the construction of the structure, there arises a need for developing a robust and generic optimal design framework for minimizing the initial cost along with simultaneously ensuring optimal returns by minimizing the seismic loss. Conceptually, this generic optimization framework may be developed by amalgamating a seismic loss framework into an optimization scheme.

In this thesis, the Pacific Earthquake Engineering Research (PEER) framework for loss estimation is adopted. The PEER framework relies on seismic hazard and response simulation (performance assessment) to estimate damage and monetary losses during a seismic event.

In mathematical form, the PEER framework is given as (Aslani and Miranda, 2005)

$$\lambda(DV) = \int\int\int G(DV \mid DM)\,dG(DM \mid EDP)\,\underline{dG(EDP \mid IM)}\,d\lambda(IM) \qquad (1.1)$$

Where $G(X|Y)$ denotes the complementary cumulative distribution of X conditioned on Y; *DV* denotes the decision variable (in the present study it is the seismic loss), *DM* denotes the damage measure; *EDP* denotes the engineering demand parameter; *IM* denotes the intensity measure.

The underlined term in eq. (1.1) is the performance assessment process. The uncertainty in the performance assessment is quantified through Incremental Dynamic Analysis (IDA). IDA is the procedure in which the analytical model of a structure is subjected to increasing intensities of earthquakes and quantifying the performances in terms of mean or median responses along with dispersions. In the PEER loss estimation framework described in eq. (1.1), this response is extrapolated to seismic loss which gives the decision maker a more tangible parameter of societal significance.

Though the procedure of IDA is simple, it presents itself with a considerable amount of uncertainties which can be classified as epistemic and aleatoric in nature. Aleatoric uncertainties deal with the inherent uncertainties in the source, selection of ground motion etc. where the analyst has no direct control. One way to reduce this uncertainty is to increase the number of ground motions selected at an intensity so that there is less dispersion in the suite of ground motions. The epistemic uncertainty or the modeling uncertainty is related to the inherent uncertainties in the mathematical model mainly attributed to the selection of the model, the parameters involved etc. One prime source of uncertainty in this category is the selection of the inherent damping model for representing the in-structure damping phenomenon exhibited by a structure during its dynamic response.

This thesis primarily addresses the issue of developing a generic framework for optimally designing viscous dampers in such a way that it minimizes both the "initial cost" and "seismic loss". So, to arrive at a realistic optimum, the epistemic uncertainty (due to the inherent

damping models) associated with IDA should first be alleviated. For this aspect, the thesis proposes new novel damping models which do not have untoward effects in the IDA study. Using these models, a generic multi-objective framework for designing viscous dampers by simultaneously minimizing “initial cost” and “seismic loss” is presented.

## 1.2 Objectives

The main aim of this thesis is to develop optimal quantification and positioning strategies for passive dampers and to redefine the concept of optimum in the light of loss assessment philosophy. Specific objectives concerning the proposed research are as follows:

1. To develop new elemental level damping models for more realistic dynamic analysis (i.e. IDA).

2. To identify a preferred damping model for IDA-based seismic performance evaluation studies

3. To develop efficient multi-objective optimization framework for optimally sizing and distributing viscous dampers along the height of linear frames.

4. To develop multi-objective optimization framework for optimally sizing and distributing viscous dampers along the height of the nonlinear frames

## 1.3 Organisation of the thesis

This dissertation presents significant advances in two areas of research: **a.** Modelling of inherent damping in nonlinear time history analysis **b.** Seismic loss based optimization for design of viscous dampers.

**Chapter 2** summarizes the present state of the art in inherent damping modelling and optimal distribution methodologies for added dampers.

**Chapter 3** develops a novel modeling approach to damping by developing discrete elemental damping models.

**Chapter 4** develops a new methodology based on Classical Newmark time integration method for solving convolution damping models.

**Chapter 5** further develops the elemental damping formulation developed in chapter 3 by adapting local continuum based damping models into nonlinear dynamic analysis.

**Chapter 6** further develops the elemental damping formulation proposed in chapter 3 by adapting non-local elasticity based damping models.

**Chapter 7** consolidates the performance of the proposed inherent damping models for nonlinear time history analysis and attempts to outline a recommended model.

**Chapter 8** illustrates the interpolation based loss estimation methodology. The method of computation of loss is a modified version of the method proposed by Ramirez and Miranda (2009).

**Chapter 9** develops a multi-objective optimization problem which is solved using a first-order aggregate gradient-based method developed by Izui et al (2014). The parent frame is assumed to remain linear. The optimization framework is described in detail and the implementation steps are outlined. The polynomial based loss computation methodology described in chapter 8 is used for the computation of the loss objective. The efficiency of the proposed framework is illustrated by a numerical study on a 4-storey planar linear frame and a 3D 8 storey RC asymmetric frame structure. It is shown that the proposed methodology is very efficient.

**Chapter 10** investigates the multi- objective optimization problem when the parent frame becomes nonlinear. A generic framework of the optimization is presented in chapter 9.0 is extended to the nonlinear scenario. Efficiency of the proposed framework is illustrated by numerical study on a 4 storey.

**Chapter 11,** presents the conclusion and recommendations for future research.

# 2. Literature Review

**Book Chapter**

Puthanpurayil, A., Dhakal, R.P. and Carr, A.J. (2013) Optimal passive damper positioning techniques: State-of-the-art. In N.D. Lagaros, V. Plevris and C.C. Mitropoulou (Ed.), *Design Optimization of Active and Passive Structural Control Systems*: 85-111. Athens: IGI-Global. http://dx.doi.org/10.4018/978-1-4666-2029-2.ch004.

**International Conference**

Puthanpurayil, A., Dhakal, R.P. and Carr, A.J. (2011) *Modelling of In-Structure Damping: A Review of the State-Of-The-Art*. Auckland, New Zealand: 9th Pacific Conference on Earthquake Engineering, 14-16 Apr 2011. In PCEE 2011: Building an Earthquake-Resilient Society: Paper 91 (Conference published)

**Abstract** This chapter presents a consolidated review of the state of the art in both in inherent damping modelling and optimal positioning of viscous dampers.

## 2.1 Introduction

The primary focus of this thesis is to develop an optimization framework for viscous damper design which simultaneously optimizes the loss incurred due to earthquakes and initial cost. It is the belief of the author that a realistic optimum in viscous damper quantification and distribution may only be reached when the uncertainties associated with the modelling of the parent structure is considered. One of the prime most uncertainty associated with modelling of the parent structure is in representing the phenomenon of inherent damping in the dynamic analysis. So, in the first sub-section of this chapter, all the inherent damping models used in both linear and nonlinear dynamic analysis as applied to seismic engineering are reviewed in detail and existing shortcomings are identified. In the second part of this chapter a full detail account of the existing methodologies of optimal damper positioning is presented and limitations are identified.

## 2.2 Part 1: A review of the state of the art in inherent damping modeling

In structural dynamics, the observed decay in the free-vibration of a structure is referred to as *damping.* This damping phenomenon is believed to come from energy dissipation in the structural and non-structural members caused by small scale hysteresis, friction and possible visco-elastic effects. Lord Rayleigh (1877) modelled the decay mechanism as viscous damping for purely mathematical convenience though he stated that he had no physical justification for doing so. Validating this above statement, the contextual description on the dissipative forces proportional to velocity presented in the book (Lord Rayleigh 1877) comes with an assumption statement which reads as follows, "*with a degree of approximation sufficient for acoustics purposes"* (refer pg. 37 of Lord Rayleigh (1877)). It is interesting to note here that Lord Rayleigh himself in his book recognizes that the main cause of dissipation is friction and arrives at the concept of viscous force only as a convenient alternative mathematical representation mimicking the effects of friction. The assumption of viscosity as formulated by Rayleigh automatically implied that the relevant state variables controlling the damping phenomenon are only the instantaneous velocities. Recorded observations of Lord Kelvin based on a series of experiments on torsional oscillation of wires reported by A.E.H Love in his book on "A treatise on the mathematical theory of elasticity" published in 1906 (Love 1906) reports that damping could be hysteretic in nature as it depends on the previous state of the body. More recently, observations like Lord Kelvin were made by other researchers as well; refer Adhikari (2000). These earlier and recent observations are in contradiction to the simple viscous model assumed by Lord Rayleigh. But nevertheless, Rayleigh damping remains a popular choice of dynamic analysts for modelling in-structure damping phenomenon.

At the present time, there are no generally accepted physical models for the damping phenomenon and the viscous model proposed by Lord Rayleigh is largely used by engineers

as the inclusion of some means of expressing the required damping. For the past sixty years or so engineers have accepted the viscous damping approximation to the damping phenomenon in the belief that as the damping forces are small then any inaccuracy in the modeling will not have a great effect on the structural response (Wilson and Clough 1962). In an elastic analysis with 5% viscous damping model the damping forces are only of the order of 10% of the other forces observed in the structure (Carr 2007). In a linear elastic model of the structure, the damping is usually simplified to the level of prescribing the modal damping, as the use of the free-vibration modes is the most efficient way of carrying out the analysis (Chopra 2012).

In nonlinear dynamic analyses the application of modal damping is not so easily implementable, and a damping matrix of some form is required for the time-history analyses. The predominant energy dissipation in the inelastic dynamic analysis is accounted for by the member hysteresis models, but the analysis still needs to cover the effective energy dissipation associated with the parts of the inelastic members which remain elastic, the members which are assumed to be linear elastic and the *un-modelled* members or sections of the structure (Carr 1997; Scanlan 1970).

One way to form the damping matrix is by using the Rayleigh damping concept. Based on Rayleigh formulation, the damping coefficient matrix $\mathbf{C}$ can be assumed as (Chopra 2012),

$$\mathbf{C} = \alpha\mathbf{M} + \beta\mathbf{K} \tag{2.1}$$

where $\alpha$ and $\beta$ are damping proportionality constants evaluated as a function of the system frequencies using a preconceived damping ratio. **M** and **K** are the mass and stiffness matrices. As the damping is computed at system level in a standard dynamic analysis scenario, from here on in this thesis this model will be called as global Rayleigh damping model; but it must be noted that Rayleigh formulation in itself has no such limitation. Originally this formulation was proposed for linear dynamic analysis (Wilson and Clough 1962).

In the case of nonlinear structural dynamics there are different phenomenological approaches adopted for the adaptation of global Rayleigh damping into the inelastic analysis scenario. From an implementation point of view, most commercial software seems to incorporate global Rayleigh damping predominantly in two forms: one is by using the initial stiffness based matrix and the other one is by using the tangent stiffness based matrix.

If the initial stiffness matrix is used then eq. (2.1) becomes,

$$\mathbf{C} = \alpha\mathbf{M} + \beta\mathbf{K}_{initial} \tag{2.2}$$

where $\mathbf{K}_{initial}$ is the stiffness matrix computed at the beginning of the analysis. Note that $\alpha$ and $\beta$ are also computed at the beginning of the analysis and remains constant throughout the analysis. If tangent stiffness matrix is used then eq. (2.1) becomes (Sharpe 1974),

$$\mathbf{C} = \alpha\mathbf{M} + \beta\mathbf{K}_{T} \tag{2.3}$$

where $\mathbf{K}_T$ is the current tangent stiffness matrix and is constantly updated as the analysis proceeds, unlike $\alpha$ and $\beta$ which are computed at the beginning of the analysis and remain constant throughout the analysis.

### 2.2.1 Is Rayleigh damping valid for nonlinear structural dynamics?

Rayleigh dissipation function was originally formulated for capturing the decay phenomenon in the field of acoustics which is predominantly linear in nature (Rayleigh 1877; Adhikari 2000). So critically reviewing the fact that the dissipation function was originally formulated for the field of acoustics, a very pressing question arises, "*how can the adaptation of this function to the realm of linear/nonlinear structural dynamics to represent the decay phenomenon be justified?"* To the best knowledge of the author there exists a clear lack of clarity on the justification of this adaptation to the field of structural dynamics. Wilson and

Clough (1962) reported that the form of the damping matrix as given in eq. (2.1) was a simplification adopted in a report by Berg under the pretext that the effect of damping on the response of a structure is small. In the case of linear dynamics this can be justified, and the decaying phenomenon exhibited in nature is mimicked closely with no unwanted effects; but in the case of nonlinear dynamics, the scenario is totally different as will be discussed below.

Other than the popularity and familiarity of the use of global Rayleigh model in the elastic dynamic analysis, its adaptation to nonlinearity as outlined above does not relate to any physical reason. Also, the mathematical convenience the global Rayleigh damping possesses in linear modal analysis arguably no longer exists in the case of nonlinear analysis (PEER 2010). However, to date, global Rayleigh damping is the most popular choice for modelling damping in nonlinear analysis mainly due to its familiarity, computational efficiency (it uses the already computed **M** and **K** matrices) and its easiness of implementation in a commercial software platform.

Past studies have shown that the most important shortcoming in the use of global Rayleigh damping in inelastic dynamic analysis is the appearance of un-realistic damping forces/moments on the onset of yielding (Carr 2007). One of the earliest studies to point out this issue when using global Rayleigh damping in inelastic analysis was by Crisp (1980). Crisp had observed damping moments of the order of values close to the yielding moments of the girders spanning into the joint in a six-story frame when initial stiffness based global Rayleigh damping was used.

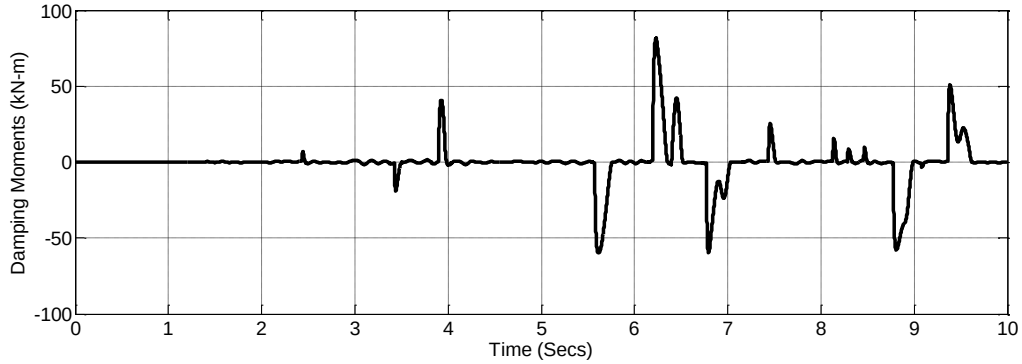


Fig.2.1 Damping moment plot for the four-storey frame for the first storey middle node

Fig. 2.1 represents the appearance of such un-realistic damping actions in the nonlinear time-history analysis of a four-storey frame the details of which are given in Appendix 3. The plot in Fig. 2.1 is of the middle beam-column junction in the first storey. The yielding moment of the girder meeting the joint was computed as 100 kNm. It can be clearly seen from Fig. 2.1 that damping moments are like instantaneous, velocity-based, force impulses which are almost like adding instantaneous viscous dampers at the onset of nonlinearity. Previous and recent studies highlight the fact that the presence of such damping moments affects the member moments and, as a result, the structural displacement response.

Shing and Mahin (1987) studied the use of viscous and numerical damping to eliminate the effects of spurious higher frequency dependent effects in pseudo dynamic testing. Their findings gave an indication that viscous damping properties can be substantially changed by nonlinear deformations. They also recommended that numerical damping is better than viscous damping for mitigating higher frequency effects in pseudo dynamic testing. Other relevant earlier studies which highlighted the effects of incorrectly modelling the inherent damping was by Tsopelas et.al. (1997) and Whittaker et al. (1998). In Whittaker et al. (1998) the significance of damping is highlighted especially in the light of estimating the responses for the performance

based seismic design procedures. Sarlis and Constantinou (2010) again re-emphasized the significance of the issues associated with modelling inherent damping in SAP 2000 software when used for modelling triple pendulum friction isolator.

### 2.2.2 Previous studies on improvisation of Rayleigh damping in nonlinear dynamic analysis

Several studies had been conducted to mitigate the issues associated with the use of global Rayleigh damping in inelastic analysis. A very brief overview of the research effort to date will be presented here to give a snapshot of the current state of the art in inherent damping modelling.

One of the earlier studies in this direction was by Leger and Dussault (1992) where global Rayleigh damping model with updated coefficients was proposed to eliminate the spurious damping forces. Their model can be expressed as;

$$\mathbf{C} = \alpha_{tan\,gent}\mathbf{M} + \beta_{tan\,gent}\mathbf{K}_{tan\,gent} \qquad (2.4)$$

where $\alpha_{tan\,gent}$ and $\beta_{tan\,gent}$ are updated variable coefficients reflecting the current changes in the system frequencies due to changes in the global stiffness. Though more generic in concept, this is rarely used in practice due to the requirement of computation of the system eigenvalues in every time step which puts a heavy penalty on the computational side if done for a large system. In addition, Zareian and Medina (2010) observed that the performance of this approach may be questionable in the case of a highly nonlinear structure.

To eliminate the un-realistic forces, Bernal (1994) suggested an alternative methodology by assembling damping matrix using stiffness matrix condensed to the size of degrees of freedom of mass and expanding to full coordinates by populating the columns and rows with zeros. This is mainly done to eliminate the spurious damping forces associated with the massless degrees

of freedom. The method proposed requires the damping matrix to be assembled restricting the Caughey series (explained later in this section) to zero or negative.

Hall (2006) investigated in detail the issues associated with global Rayleigh damping model and suggested a capped viscous damping model comprising only of the stiffness component of global Rayleigh model with certain bounds imposed in accordance with the actual physical mechanism. Charney (2008) gave a detailed set of recommendations to eliminate the issues associated with global Rayleigh damping. On the outset, the best strategy as described by Charney (2008) was the overall elimination of the use of global Rayleigh damping in inelastic dynamic analysis and suggested the use of nonlinear frictional or hysteretic damping with smooth hysteretic rules like Bouc hysteresis (1967). Charney (2008) also observed that if global Rayleigh damping is used the best option might be to use the Leger and Dussault model (1992). If this is not possible, then Charney suggested the use of tangent stiffness based global Rayleigh damping. Charney (2008) also gave a warning that, if initial stiffness based global Rayleigh model is used, where stiffness is based on the elastic stiffness of the structure, extreme caution need to be exercised. Charney (2008) also presented an excellent review of the damping procedures used by some of the current commercial software. Recommendations were also given for modifications of the damping models in existing software and for new software.

Recently Zareian and Medina (2010) proposed an approach by reformulating the damping matrix with a Rayleigh type matrix with a time invariant stiffness matrix assembled by assigning zero stiffness proportional damping to the degrees of freedom that have the potential to experience inelastic deformation. An equivalent 8 degree of freedom element was proposed with a combination of an elastic beam element in the middle and two - rotational springs at the ends. In the computation of the damping matrix, only the stiffness proportional components of the elastic beam element stiffness were accounted and no damping is assigned to the semi-rigid springs. This provides a means of reducing the spurious damping forces and maintaining

numerical stability in the inelastic dynamic analysis. The responses were compared to tangent stiffness proportional global Rayleigh damping with constant coefficients with reasonable agreement.

Jehel et al. (2014) investigated in detail the stiffness proportional part of the global Rayleigh damping and developed tools for controlling the modal damping ratio throughout the time history analysis. Analytical formulas were developed for both initial stiffness based global Rayleigh damping and tangent stiffness based global Rayleigh damping for controlling the modal damping ratio. Though there exists a simple formula for controlling the modal damping when tangent stiffness based global Rayleigh damping is used, no such direct formula exists when initial stiffness is used.

Till now only global Rayleigh damping model and its associated issues along with suggested modifications for improvisations have been discussed; though the modifications helped in improving the mathematical model primarily by reducing the unrealistic forces, still the basic model used is the global Rayleigh formulation and it is worthwhile to emphasize Charney's (2008) observation of totally avoiding global Rayleigh model altogether. To the knowledge of the author, todate no such effort exists in the literature. In quest of this, the rest of the section very briefly reviews the suitability of other damping models described in the literature for the nonlinear seismic analysis.

### 2.2.3 Other damping models

In the realm of dynamic analysis, global Rayleigh model is not the only damping model. More generic models are available in literature. Caughey (1960) derived a general form of the viscous damping matrix with orthogonal properties. Global Rayleigh damping could be looked upon as a special case of Caughey damping with only first two terms in the series. Though generic in its mathematical format, Caughey model has serious practical limitations especially with

deriving the terms in the series (Charney 2008). Also from a commercial software implementation perspective, mathematical rigor demanded by Caughey damping presents serious limitations. Wilson and Penzien (1972) presented a more direct and efficient procedure for direct evaluation of the Caughey type damping matrix as compared to the original Caughey's formulation. Here on in this thesis, this model will be referred to as global Wilson-Penzien model. Theoretical details of the model are presented in Wilson and Penzien (1972) and for implementation refer to Crisp (1980). This model has the benefit of independently assigning damping ratios to all modes giving better control of the damping ratio and hence negligible unrealistic damping forces throughout the inelastic analysis. But the main limitations of this model were that, it produced a fully populated damping matrix which violated the efficient skyline storage format used in commercial packages and also required the computation of all system eigenvectors and eigenvalues which altogether diminished its popularity in the commercial implementation scenario (Charney 2008). Due to these reasons as far as the author is aware very few software packages implement this model; *Ruaumoko* and *Perform3D* are the two commercial software in the authors' knowledge which implement the global Wilson-Penzien model (Carr 2007; PERFORM 3D 2006). It must be noted that *Perform3D* applies this method for a maximum of 50 modes whereas *Ruaumoko* applies the method for all modes (Carr 2007; PERFORM 3D 2006). In Chopra and McKenna (2016), an improvisation of global Wilson-Penzien damping is suggested by incorporating lesser number of modes compared to the complete number required by the classical global Wilson-Penzien format. Though the idea of using global Wilson-Penzien as the recommended model is not new (Crisp 1980, Carr 2007), the suggestion to use a reduced number of modes in the damping matrix computation is an improvisation; but, unfortunately, how many modes should be used in a relatively unsymmetrical complex structure to represent the *un-modelled* dissipation in a reasonable manner is still a question which needs further research.

In literature, there are other models also like non-viscous damping models which, according to Woodhouse (1998), could be considered as the most generic damping model within the domain of linear analysis. To the knowledge of the author, these models have not been extended into the nonlinear realm of dynamic analysis mainly because their application to analysis of large scale structures could be very cumbersome (Charney 2008). In chapter 4, an efficient numerical technique called AAR method is developed to solve this type of convolution damping model which can be efficiently applied in both linear and nonlinear time domain analysis as demonstrated in chapters 5 & 6.The other category of models comprises of the frequency independent models which includes the Coulomb model, hysteretic model and modified hysteretic model (Muravski 2004). Fig. 2.2 summarizes a broad overview of the existing popular discrete damping models used presently in practice.

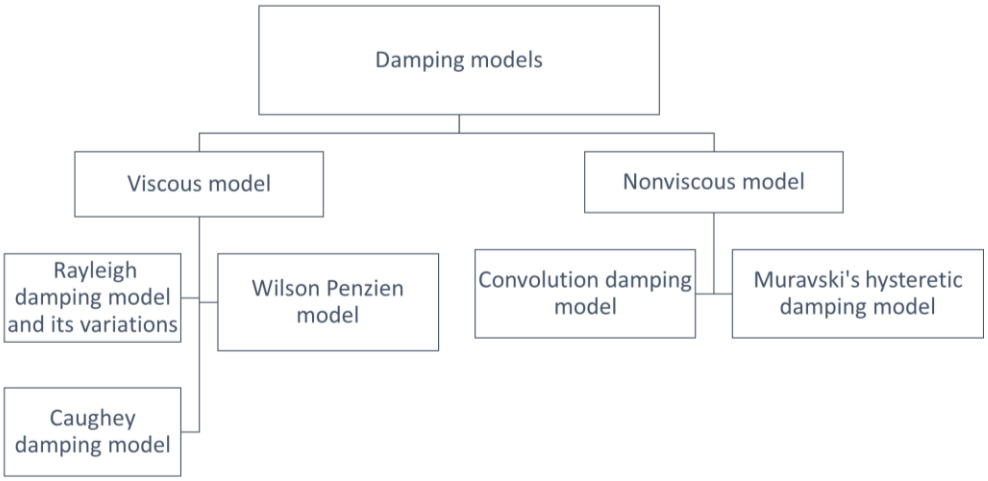


Fig.2.2 Broad classification summary of existing discrete damping models

In addition to these discrete global models, there are continuum models which incorporate the damping effect at a continuum level; refer to (Adhikari 2000; Banks and Inman 1991) for more detailed review of these types of models. Again, to the knowledge of the author, no effort has been made to extend these models into the domain of nonlinear dynamic analysis mainly due to the complication involved in implementing in an existing commercial software platform

along with the computational and parameterization demands posed by these models. Chapters 5 and 6 develop numerical implementation schemes for adapting the continuum damping models into the nonlinear dynamic analysis domain.

Reviewing all the shortcomings described above, required attributes for an ideal empirical mathematical model representing damping might be listed as follows: (a) elimination of unrealistic forces/moments associated with the damping phenomenon as the analysis progresses (b) ease of implementation in an existing commercial software framework (c) no explicit increase in the computational time due to the choice of the damping model. The first attribute, the presence of the unrealistic damping forces, may result in considerable inaccuracies in displacements and internal forces whereas the other two attributes are more related to the practical utility of the model from a commercial implementation point of view. Addressing these attributes, a new paradigm shift in inherent damping modelling for nonlinear dynamics is presented in chapter 3 which is further extended in chapters 5 and 6.

## 2.3 Part 2: Review of the optimal quantification and positioning of viscous dampers

This section attempts to give a brief overview of the present state of the art for optimal quantification and positioning of viscous dampers.

The effectiveness of control strategies in achieving the objectives of performance-based design is well accepted in structural engineering community. The theory of structural control as a field was mainly enriched by mechanical and aerospace engineering and its adoption in structural engineering is rather more recent. The introduction of control techniques in structural engineering was mainly necessitated due to the growing demand for minimizing damage during a seismic event.

The adoption of control strategies to structures presented the structural engineering community with new challenges due to the inherent uncertainties associated with the system as well as with the excitation sources. The uncertainties associated with the excitation sources result in the inherent record to record randomness at a location. As no two earthquake-induced ground motions are similar, it is uncertain whether a system proven to work for a structure in one ground motion will work equally efficiently in another ground motion. The inherent system uncertainties differ with respect to the type of control strategy adopted. Before delving into the details, we briefly describe the classification and types of structural control used in practice. Structural control is mainly divided into four types (Wada et al. 2004):

- Seismic Isolation
    - The art of insertion of mechanical devices between the sub-structure and super-structure which decouples the system from the damaging components of the earthquake ground motion.
- Passive control
    - Mechanical devices distributed through the structure to provide "added damping" to the system to reduce the response to controllable limits.

- Active control
    - Includes computer controlled actuators which provide seismic resistance by imposing forces on the structure to counter-balance the ground motion induced forces.

- Semi-active control/ Hybrid control
    - Semi-active/Hybrid control is a combination of active and passive control which includes a combination of dampers and isolators.

The focus of this section is on the passive viscous control techniques. In line with this focus, the issues discussed herein would be limited to those associated with passive viscous control. In deciding a passive control strategy, say for a building, two questions need to be answered; (i) what type of device is the most efficient? and (ii) how should they be positioned in different floors and distributed across the height of the building? In the process, two system issues associated with passive control must be dealt with (Takewaki 2009):

- local amplification of responses in the elements where a control device is attached; and
- optimal quantification and the interaction between the structure and dampers distributed throughout the structure.

The first issue/uncertainty needs to be addressed mainly in the structural design process and is directly linked to the modelling uncertainties; in the previous section the uncertainty associated with the parent structure modelling are discussed in detail. Chapters 3,5 & 6 discusses more advanced modelling techniques that will aid in reducing this first uncertainty. The second needs to be addressed in the optimal quantification and positioning strategies (Takewaki 2009). Focusing on the second system uncertainty, the main purpose of this section is to present a consolidated review of the existing state-of-the-art on optimal positioning of dampers. Some inherent assumptions made in deciding the optimal positioning techniques in previous studies are critically scrutinized.

### 2.3.1 Previous Studies

This section presents a consolidated review on the state-of-the-art for optimal passive damper design. Wherever possible and relevant, comprehensive outlines of the contents of respective works are presented. At the end of this section, some limitations inherent in the current optimal damper placement methods are pointed.

An optimal viscous damper design may involve simultaneous optimization of stiffness and damping. This will depend on whether the structure is being newlybuilt or whether the structure is being retrofitted. Even in the case of retrofitting additional stiffness may be added. Simultaneous optimization of stiffness and damping is possible, and some of the literature presented in this section do present efficient techniques to do this; but this thesis is limited to optimization of damping my means of addition of viscous dampers only.

Fig. 2.3 presents the broad classification of optimal damper design methodologies.

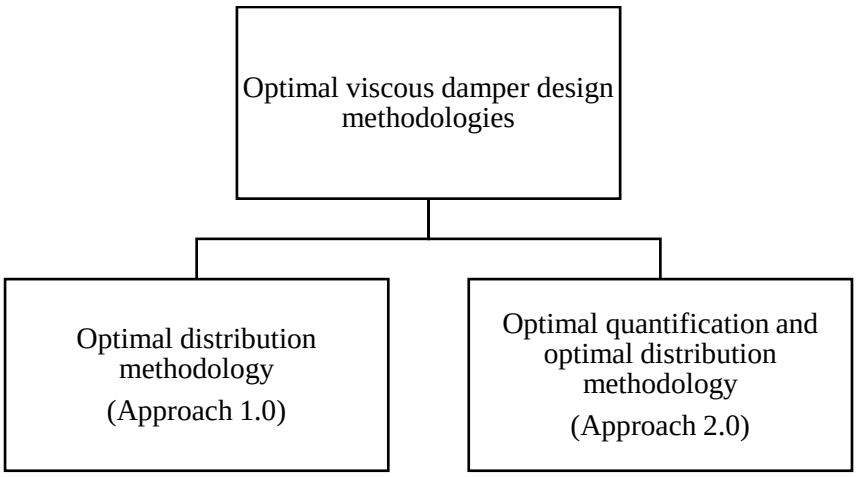


Fig. 2.3 Classification of optimal damper design methodologies

Broadly, optimal damper design techniques maybe classified into two categories: first category primarily address the problem of identifying the optimal distribution for a given total added damping to achieve the best performance (minimize damage measures); second category of methods simultaneously determined the "optimal quantity" and "optimal distribution" to achieve a prescribed performance. In section 2.3.1.1. the first category of methods is reviewed whereas section 2.3.1.2 presents a detailed review of the second category of optimization techniques where "quantification" and "allocation" of viscous dampers is done simultaneously.

### *2.3.1.1 Optimal positioning strategies for a given quantity of damping*

One of the early major works in this direction was the study carried out by Desilva (1981) in which he derived a gradient algorithm for controlling the vibration of a flexible system by optimally inserting control devices. His work included a complete mathematical formulation for slender beams in vibration due to flexure. Thereafter, Constantinou and Tadjabakhsh (1983) obtained an optimum damping coefficient for a damper located in the first story of a shear building subjected to stationary white noise ground accelerations. In this work, analytical expressions were formulated for calculating the maximum displacements of each floor. Parametric studies were conducted to determine the effect of structural damping and the inherent structural flexibility on the control parameters.

Cheng and Pantelides (1988) pioneered an approach in which the locations of active controllers were optimized in terms of a controllability index. This controllability index as defined by them is a measure associated with the structure's response to a specific earthquake. The basic idea underlying the controllability index method is that a controller is optimally placed when it is located at a position where the displacement or relative displacement response of the uncontrolled system is the maximum. Though it was done in the context of active control, the philosophy was very much applicable for addressing the positioning issues in passive control.

Zhang and Soong (1992) pioneered an extension to the above described controllability index method to address the issue of locating passive dampers. They developed a sequential procedure for the optimal placement of the damper devices. This procedure is called the Sequential Search Algorithm (SSA), and it determines the optimal location index by evaluating the random seismic response of a structure using the transfer matrix method. The mean square values of the inter-story drifts are used as optimal location indices. The procedure starts with determining the best location for the first damper. It was shown that the best position for the first damper is the location where the inter-story drift of the uncontrolled frame is the maximum (Cheng and Pantelides 1988). After determining this location, the damper is added, and the

procedure is repeated incorporating the added stiffness and damping and the optimal location for the second damper is determined. This procedure is repeated till all dampers are placed. In this method, the earthquake excitation is modeled as a stationary stochastic process.

Hahn and Sathiavageeswaran (1992) proved through a series of sensitivity analyses that to get an optimum response for a shear building with uniform stiffness during an earthquake, the dampers should be placed in the lower half of the building. This study mainly focused on assessing the effect of distribution of visco-elastic dampers. They also proved that tall buildings are more sensitive to changes in the distribution of dampers as compared to low-rise buildings. Gurgoze and Muller (1992) came up with a numerical method for optimally placing the dampers and to determine their capacities based on an energy criterion. One common observation that could be made in these works is that all of them considered shear buildings with either uniform story stiffness or with specified story stiffness. In other words, in the optimality problem considered, stiffness of the parent frame was never considered as a design variable. So predominantly these methods were applicable for retrofitting schemes or newly built structures where stiffness optimization is not considered feasible.

Tsuji and Nakamura (1996) made a significant advancement by pioneering an algorithm to derive an optimum set of stiffness of a shear building frame along with the optimum set of viscous damping devices, imposing necessary behavioral constraints. The constraints imposed were on maximum inter-story drifts due to a set of spectrum compatible ground motions, on upper bounds of the damping coefficient of each damper and on the sum of the damping coefficients of all dampers. Optimum problem addressed in this study was to find a minimum cost design. The method proposed by Tsuji and Nakamura was more efficient in the sense that it produces an ordered set of optimum design of shear buildings with viscous dampers by minimizing the sum of the story stiffness subjected to the current constraints, and each design in the ordered set could be a ‘candidate design’ corresponding to various upper bound levels

of damper damping coefficients. On the other hand, the method developed by Zhang and Soong (1992) was more intuitive as their ultimate solution only approximately optimizes the objective function. Connor and Klink (1996) and Connor *et al.* (1997) introduced the concept of a quasi-optimal distribution in which the damper devices are proportional to the stiffness distribution.

Takewaki (1997a, 1997b, 1998) introduced a new approach of smart passive damper placement techniques with a series of algorithms based on the concepts of inverse problem and optimal criteria based design approaches. The problem pioneered by Takewaki was to find the optimal damper placement to minimize the sum of the amplitudes of the transfer functions evaluated at the undamped fundamental natural frequency of the structural system. A constraint was imposed on the sum of the damping coefficients of the added dampers. This was a single criterion approach because only the damping coefficients of the added dampers were considered as a design variable, whereas the story stiffness was pre-specified.

Subsequently, Takewaki (1999) came up with an approach of stiffness-damping simultaneous optimization for displacement-acceleration simultaneous control. The structural system considered was a shear building model and both stiffness and damping coefficients of the added dampers were considered as design variables. This is a two-step design method. In the first step, a design is obtained by satisfying the optimality conditions for a specified set of total story stiffness capacity and total damper capacity. In the second step, a series of optimal designs is obtained sequentially for various stiffness and damping capacity levels. Deformation is reduced in both steps while acceleration is reduced only in the second step. This is a very significant work as it considers acceleration also as a quantity that needs to be controlled. To the knowledge of the author, most of the earlier works were mainly concentrated on drift reduction as the primary objective, whereas this was the first work which explicitly aimed to minimize both displacement and acceleration responses through minimization of the weighted

sum of mean-square inter-story drifts and a mean square top floor absolute acceleration. Takewaki also showed that increases in total stiffness capacity and total damper capacity are effective in reducing the inter-story drift, but increase of only the total damper capacity reduces the floor acceleration.

Takewaki and Yoshitomi (1998), Takewaki and Uetani (1999) and Takewaki (2000) described a systematic procedure for determining the optimal positioning of dampers in planar moment resisting frames by minimizing the dynamic compliance subjected to a constraint on the sum of the damping coefficients of the dampers. Dynamic compliance is defined as the sum of the transfer function amplitudes of inter-story drifts evaluated at the undamped fundamental natural frequency. The systematic procedure developed is called the steepest direction search algorithm. This again is a significant advancement because most of the earlier researchers were only considering shear building models. Takewaki consolidated all his work on optimal damper positioning in the form of a textbook (Takewaki 2009). In addition to the works mentioned above, the book illustrates the procedures by which the steepest direction search algorithm could be extended to three dimensional systems. This book also describes the procedures by which the effect of soil-structure interaction could be incorporated in optimal positioning of dampers and gives an overview of the design of shear buildings with uncertainties using the principle of critical excitation. Some additional useful references on this are Takewaki and Nakamura (1995, 1997), and Takewaki (2000a, 2000b).

Gluck et al (1996) pioneered and adapted the optimal control theory using a quadratic regulator to design and place control devices based on their deformations and velocities. They considered linear passive viscous and visco-elastic devices, represented them by fully effective Kelvin model using a full state static feedback. This work holds a significant place in the literature, as it adapted the well-established active control theories for passive devices. Wu et al. (1997) applied the sequential search algorithm (SSA) developed by Zhang and Soong (1992)

to 3-D torsional coupled structures and carried out an investigation into the effect of ground motion characteristics on optimal distribution.

Shukla and Datta (1999) reconfirmed the efficiency of the SSA method through a parametric study using visco-elastic dampers. Frequency domain approach was employed for determining the responses to both broad and narrow band ground motions. The study shows that the optimal placement of dampers is sensitive to the nature of excitation force. This is an important observation because it implies that what is optimal for one specific ground motion need not be optimal in a different ground motion. This raises serious concern on the use of the term 'optimality' because of the high inherent uncertainty in the ground motions. One approach to address this uncertainty is to use the principle of critical excitation (Takewaki 2007). As it falls beyond the scope of the present chapter no further discussion on this aspect is presented; interested readers should refer to other relevant works such as Takewaki (2000a-d, 2001a-g, 2004a-b, 2005, 2007), Ahamadi (1979), Drenick (1970, 1973, 1977a-b), Drenick and Park (1975), Iyengar (1970, 1972, 1989), Iyengar and Manohar (1985, 1987); to name a few.

Moreschi (2000) and Singh and Moreschi (2001, 2002) introduced a gradient based approach and employed genetic algorithm approaches as an alternative to address the problem of optimal placement of dampers. The performance index to be minimized was defined as a function of the system response obtained by considering a stochastic description of the input motion defined by Kanai-Tajimi spectral density function. The application of genetic algorithm is especially suitable where the performance index is not a continuous function of the design variables. The basic assumption in the study was that the parent frame remains linear. State space approach was used for the analysis. Numerical results were reported for both shear building model and torsional building model.

Garcia (2001), and Garcia and Soong (2002) developed the simplified sequential search algorithm method (SSSA) which is basically a simplified form of the SSA method originally developed by Soong. To show the efficiency of the proposed method a comparison of the proposed SSSA with other methods was presented. The other methods used for comparison were the optimal design using optimal control theory (Gluck et al 1996) and the optimal design using the minimum transfer functions (Takewaki 1997). It was shown that the optimal distribution of dampers obtained is sensitive to ground accelerations. In this study too, the parent frame was assumed to remain linear. Palazzo et al (2004) presented a new approach to optimally locate dampers by assessing the power balance of structures subjected to seismic actions described by a response spectrum. Modal state space approach was used for response evaluation and optimization.

Trombetti and Silvestri (2004, 2006, 2007) developed an efficient mass proportional damping (MPD) system and showed its utility. In this scheme, the dampers are placed in such a way that they are connected to a fixed point and are sized to be proportional to each storey mass. The scheme is based on the mass proportional damping component of the Rayleigh viscous damping matrices. Shear building model was used for the study, and it is assumed that the first mode of vibration controls the dynamic response. In an earlier work (Trombetti et al. 2003), they had proved that within the class of Rayleigh damping, the first modal damping ratio of the mass proportional damping system is always higher than the first modal damping ratio of stiffness proportional damping system and other Rayleigh damping systems. They compared their scheme with the algorithm proposed by Takewaki (1997) to show its efficiency. Later, Takewaki (2009) agreed that the MPD scheme is efficient, but expressed his concern regarding its practical application. From an implementation perspective, author also wish to emphasize here that the MPD scheme would be impracticable unless there is a fixed point associated with every degree of freedom to which the dampers could be attached.

Martinez-Rodrigo and Romero (2003) described a simple numerical methodology that leads to an optimum retrofitting option with nonlinear fluid viscous dampers. In the last decade, there have been several studies on optimal damper positioning. Ayidin et al (2007) presented an alternative to Takewaki's method by considering the transfer function amplitude of base shear evaluated at the fundamental frequency as the objective function. Planar building frames with a soft storey were investigated in this study. The efficiency of the proposed method was illustrated by a comparison with Takewaki's method. Ajeet and Shirkhande (2007) showed that the efficiency of optimally placed dampers is maximum in symmetric buildings and its efficiency reduces as plan irregularity increases. Cimellaro (2007) addressed the issue of simultaneous optimal distribution of stiffness and damping for retrofitting structures by optimizing a generalized objective function that combines absolute acceleration, displacement and base shear transfer function. This method basically modified the method proposed by Takewaki (1997). In order to highlight the efficiency of the proposed method a comparison with the methods of Takewaki (1997) and Aiydin et al (2007) was carried out. Di Paola and Navarra (2009) discussed the stochastic responses of MDOF structures with nonlinear viscous dampers to a seismic excitation. Similar studies were also conducted by Fujita et al. (2014).

#### *2.3.1.2 Optimal quantification and optimal positioning techniques*

Lavan and Levy (2005) presented a methodology for the optimal design of supplemental viscous dampers for regular and irregular building models by minimizing the added damping subjected to a constraint on energy based global damage index for an ensemble of realistic ground motions. A gradient based optimization scheme was used in this study, which tried to address the effect of strength irregularity caused by different story stiffness. This work was an improvement as compared to most of the studies documented earlier because it considered nonlinearity in the parent frame and the quantity of dampers was not determined *a priori.* Lavan and Levy (2004, 2006a) also presented a methodology for the optimal design of

supplemental viscous dampers in which the parent frame remains elastic. The problem of minimizing the added damping was achieved by solving an equivalent optimization problem subjected to a constraint on the maximum inter-story drift for a frame excited by an ensemble of ground motion records. The other significant contribution of these two works is that they achieved the optimum design for an ensemble of realistic ground motions rather than for a stationary or non-stationary stochastic excitation as used in majority of the other methods recorded in this section. Again, Lavan and Levy (2006b) extended this methodology into the optimal design of viscous dampers for 3D irregular framed structures. In this study too, an ensemble of realistic ground motions was used, and the parent frame is assumed to be linear. The added damping was minimized and subjected to a constraint on inter-story drifts on floor edges. A gradient based optimization algorithm was used and a variational approach was adopted for the derivation of the gradient of the constraint.

Lavan et al (2008) developed a non-iterative optimization procedure for seismic weakening and damping of inelastic structures. The procedure determines the optimal location and amount of weakened structural components and added damping devices in inelastic structures. The methodology proposed assumes proportional changes in strength and stiffness which is a limitation. Cimellaro et al. (2009) extended the above proposed methodology into a more generic design strategy in which uncoupled changes of strength and stiffness are allowed for the control of buildings experiencing inelastic deformations during seismic response.

More recently, Lavan and Dargush (2009) examined a multi-objective seismic design optimization in which the maximum interstory drift and maximum acceleration were considered as the primary control parameters. The multi-objective problem was formulated in Pareto optimal sense (Pareto 1927) and a genetic algorithm based approach was adopted to identify the Pareto front. The result of this multi-objective optimization is a family of Pareto front solutions providing the decision makers with an opportunity to understand the tradeoff

between the drift and acceleration. Both linear and nonlinear parent structural frames were considered in the study. The nonlinear parent frame was idealized as a yielding shear frame which also considers the new retrofitting techniques based on weakening and damping described in Lavan et al (2008). The other most important contribution of this work was the consideration of 'cost of the damper' as an external constraint. Although not described here in detail, some other related studies include: Pollini et al. (2015), Lavan (2015), Lavan & Amir (2014), Taflanidis (2014), Takewaki et al (2010), Lavan and Levy (2010), Viola and Guidi (2009), Cimellaro and Retamales (2007), Levy and Lavan (2006), Wongprasert and Symans (2004), Xu et al (2003, 2004), Tan et al (2005) and Xi Lin (1999) and interested readers should refer to these.

A very brief consolidated summary of the methods (both approaches 1.0 and 2.0) are given in fig. 2.4. Since there are large number of methods that falls into the category of approach 1, the figure only consolidates some very popular methods to give a broad overview of the existing methodologies. For more details on the methodologies reader should refer to the relevant sections above.

All the above-mentioned studies investigated different optimal positioning techniques; but some of the assumptions and approaches adopted remain common to all. Reviewing these assumptions and approaches, we identify the following limitations:

- *Inherent assumption of linear elastic behavior of the parent frame*

  Except for Lavan and Levy (2005), Lavan et al (2008), Cimellaro et al (2008), Lavan and Dargush (2009), and Lavan (2015), majority of all other studies discussed above assumed the parent frame to remain elastic during a seismic action. Inherent assumption of linearity assumes that there need to be an initial sufficient quantity of damper in the parent structure so as not to incur parent frame inelasticity. So, this might

simply mean that the whole of optimization would be a small perturbation on this initial quantity. Chapter 10 presents a generic optimization framework in which optimal quantity and distribution of the viscous dampers is achieved by considering parent frame inelasticity.

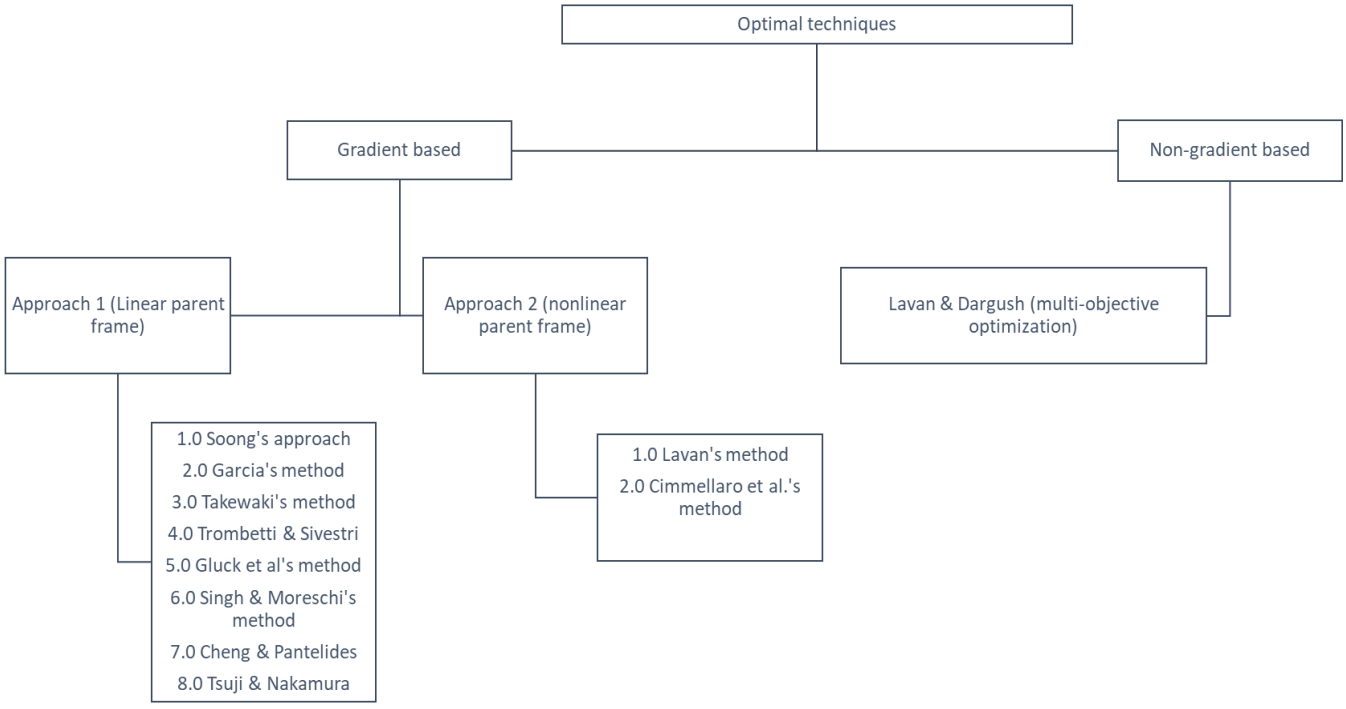


Fig. 2.4 a brief overview of the different optimization techniques

- *No explicit consideration of the seismic loss*

  Except for Taflanidis (2014), majority of the optimization formulation described above considers allowable inter-storey drifts or allowable accelerations as their performance measures; though these performance measures lend themselves to the performance-based design framework, none of the measures explicitly considered the economic impacts and the measures were mainly derived from code requirements. So, from an engineering perspective, as the underlying economic impact was not directly reflected, the obtained response reduction due to a specific distribution of dampers translated to

a much less tangible criterion in decision making. In this thesis, Chapters 9-10 presents generic optimization formulations which consider the underlying seismic loss and initial cost as explicit criteria.

- *Lack of multi-objective optimization framework*

  Except for Lavan and Dargush (2009), majority of the optimization uses single objective optimization framework. Even in Lavan and Dargush (2009), the zero-order optimization methodology of Genetic Algorithm is used. The initial cost and the seismic loss are competing parameters. So, a single optimization is not very helpful to the decision maker. Chapters 9 and 10 present a first order multi-objective optimization framework in which both the initial cost and the seismic loss is treated as competing objectives. The whole Pareto front is generated for an easier decision making.

## 2.4 Conclusion

A state of the art review on inherent damping modelling and optimal quantification and positioning of viscous dampers is presented. The issues associated with the use of classical Rayleigh model of damping are highlighted in full detail. A critical review of the optimal quantification and positioning of dampers is also presented with possible highlights on the short comings of the existing methods and a brief outline of how this thesis addresses those issues.

# 3. Discrete Elemental damping formulation

**Journal (Published)**

Puthanpurayil, A., Lavan, O., Carr, A. and Dhakal, R.P. (2016) Elemental Damping Formulation: An Alternative Modelling of Inherent Damping in Nonlinear Seismic Dynamic Analysis. *Bulletin of Earthquake Engineering* (Early access online): 1-30.http://dx.doi.org/10.1007/s10518-016-9904-9.

**Abstract:** To date, nonlinear dynamic analysis for seismic engineering predominantly employs the classical Rayleigh damping model and its variations. Though earlier studies have identified issues with the use of this model in nonlinear seismic analysis, it remains the popular choice for engineers as well as for software providers. In this chapter a new approach to modelling damping is initiated by formulating the damping matrix at an elemental level. To this regard, two new elemental level discrete damping models adapted from their global counterparts are proposed for application in nonlinear dynamic analysis. Implementation schemes for these newly proposed models using Newmark incremental method and revised Newmark total equilibrium method is outlined. The performance of these proposed models, compared to existing models, is illustrated by conducting nonlinear dynamic analyses on a four-story RC frame designed to Eurocodes. The incremental dynamic analysis study presented in the chapter illustrates the fact that both proposed models seem to produce more reliable results from an engineering perspective in comparison to the global models.

## 3.1 Introduction

From reviewing all the damping models presently existing in literature in chapter 2, it could be clearly seen that none of the models used in practice currentlysatisfies all the necessary attributes to be classed as an ideal mathematical model representing the *un-modelled* dissipation phenomenon. Again, as already stated in the previous section, avoiding global Rayleigh model altogether and replacing it by a different mathematical formulation would be the best approach to model inherent damping. But to date, to the understanding of the author, no progress has been made in that direction and most of the expended research effort on modelling damping for conventional structures (RC or steel) in the nonlinear domain has been to empirically correct the Rayleigh formulation and adapt it to the nonlinear scenario. Though models other than global Rayleigh exist, their application is very limited due to the reasons already discussed. So, a totally new approach to modelling inherent damping in conventional structures is required. The author believes that all criteria mentioned above could be achieved by considering the damping effects at the element level. At this level, moment /forces due to damping could be avoided or considerably reduced, the computational effort is very small due to working with small matrices, and the changes to existing computational frameworks are relatively minor.

The main objective of this chapter is to initiate an effort to adopt a new approach of modelling inherent damping at the element level. The scope of the present study covers the mathematical adaptation, implementation and assessment of the newly developed models. Two elemental damping models are developed. Furthermore, their implementation schemes with minor modifications in the already existing classical nonlinear framework are developed. The performance of the proposed models in the nonlinear range is assessed in comparison with the

global Rayleigh damping and global Wilson-Penzien damping models. Out of the two models developed, one model is derived from the global Rayleigh model referred hereafter as the *elemental Rayleigh damping* and the second one is derived from global Wilson Penzien model referred hereafter as *elemental Wilson Penzien model*. The scope of this study does not include the quantification of computational benefits associated with the elemental models, although it is believed to be more efficient compared to the already existing models described in section 2.2. of chapter 2, mainly due to the reduced eigen parameter computation as will be illustrated in later sections. It is also illustrated that the reformulation of the global Wilson-Penzien model at elemental level, which results in the elemental Wilson-Penzien damping matrix, eliminates both impediments described in section 2.2.3 of chapter 2 regarding the global Wilson-Penzien model (fully populated damping matrix and requirement of complete eigen parameter estimation). The matrix obtained in elemental Wilson-Penzien formulation follows a skyline pattern identical to that of the stiffness matrix. Also from a performance assessment perspective, incremental dynamic analysis (IDA) is conducted for a four-story RC frame which qualitatively highlights the fact that elemental damping models may give more reliable results mainly due to the presence of reduced un-realistic damping forces. So due to all these aspects, the author believes that the elemental damping formulation offers a more reliable modelling approach for the damping phenomenon in conventional structural systems. Although not documented elsewhere, personal communications with Prof. Reinhorn indicated that in one of the earlier versions of IDARC 2D an attempt to incorporate a similar version of elemental damping was initiated. Author unfortunately could not retrieve any published document to map the level of development that had taken place in this direction.

## 3.2 Overview of the proposed elemental models

Fig.3.1 represents the most generic classifications possible for the proposed elemental damping models with their respective sub-classifications. In this study, the author investigates the performance of all models except the updated elemental Wilson Penzien model illustrated with boxes with dashed lines. The updated elemental Wilson Penzien model is investigated in Chapter 7.0.

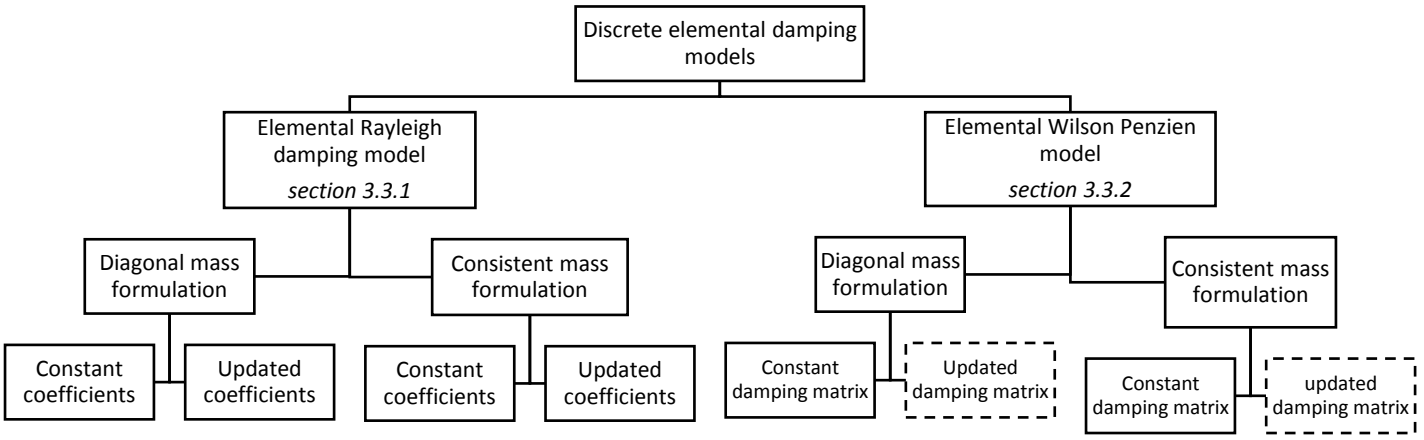


Fig.3.1 Schematic generic classification of the proposed elemental damping models

## 3.3 Proposed elemental damping models for discrete systems

The focus of this chapter is the formulation, implementation and assessment of elemental discrete damping models. As is well understood, normally the global damping models are applied at a system level, i.e. the global models are mathematically introduced into the assembled space discretized equation just before the time integration. In contrast to this, the element damping matrix is derived by the introduction of the damping matrix into the space discretized equation at element level before assemblage into a system matrix. So due to this approach, the element damping matrix

can be defined in a similar manner to element mass and element stiffness matrix and then the system damping matrix is obtained by assembling the element damping matrix similar to mass and stiffness matrix using the matrix assembling procedure used in finite elements. For the derivation of all the elemental models in this section, a semi-discretized version of Euler-Bernoulli beam enhanced with the damping force is used. It should also be noted that, though the derivations of these models are based on beam elements, their extension to higher order finite elements can be done with no extra effort.

Mathematically, a damping enhanced spatially discretized Euler-Bernoulli beam is governed by the equation as,

$$\mathbf{M}_e\ddot{\mathbf{d}}_e(t)+\mathbf{C}_e\dot{\mathbf{d}}_e(t)+\mathbf{K}_e\mathbf{d}_e(t)=\mathbf{f}_e(t) \tag{3.1}$$

where $\mathbf{M}_e, \mathbf{C}_e$ and $\mathbf{K}_e$ are the elemental mass, elemental damping and elemental stiffness matrices of size $N_e \times N_e$. Bold capital letters denote the matrices and bold small letters denote the vectors throughout this chapter. Here, $N_e$ refers to the number of degrees of freedom of the element. $\ddot{\mathbf{d}}_e(t), \dot{\mathbf{d}}_e(t)$ and $\mathbf{d}_e(t)$ are the elemental acceleration, velocity and displacement vectors and $\mathbf{f}_e(t)$ is the elemental force vector. $\mathbf{M}_e$ and $\mathbf{K}_e$ are derived using the standard classical Hermitian cubic polynomials. Based on the way $\mathbf{C}_e$ is derived, two types of damping matrix formulations are proposed in this section. They are described in the following sections.

### 3.3.1 Elemental Rayleigh damping

The main motivation behind the proposed formulation of elemental Rayleigh damping is to reduce the spurious damping forces exhibited by the global Rayleigh damping when the system becomes inelastic without compromising the conceptual simplicity of global Rayleigh damping. The

mathematical formulation exactly follows the phenomenological approach adopted by the global Rayleigh damping, but computed at elemental level.

Mathematically the elemental Rayleigh damping coefficient matrix can be represented as,

$$\mathbf{C}_e = \alpha_{eRD}\mathbf{M}_e + \beta_{eRD}\mathbf{K}_e \tag{3.2}$$

where, $\alpha_{eRD}$ and $\beta_{eRD}$ are elemental damping proportionality parameters given by

$$\left.\begin{aligned} \alpha_{eRD} &= 2\xi_{eR1}\frac{\omega_e^i\omega_e^j}{\omega_e^i+\omega_e^j} \\ \beta_{eRD} &= 2\xi_{eR2}\frac{1}{\omega_e^i+\omega_e^j} \end{aligned}\right\} \tag{3.3}$$

In the above equations, $\omega_e^i$ and $\omega_e^j$ are the $i^{th}$ and $j^{th}$ elemental undamped frequencies computed using the elemental mass matrix $\mathbf{M}_e$ and elemental stiffness matrix $\mathbf{K}_e$.

One important aspect to be noted is that, over here elemental frequencies are used for the computation of the damping proportional parameters. One of the justifications for this could be reached from the fact that the overall system damping is a net effect of summation of the damping in all elements. This implies that the damping matrix should be derived from the elemental deformations in a similar manner to the elemental mass or stiffness matrices before the system matrices are assembled. So, due to this reason, to reflect the effect of the elemental deformations, the proportionality parameters for elemental Rayleigh damping are computed using the elemental frequencies. The other main reason to use the elemental frequencies is due to the fact that it would aid in properly capturing the local nonlinearity in the damping matrix more appropriately as compared to the use of global frequencies by allowing flexibility in computing a variable damping

proportional parameter, i.e. variable $\alpha_{eRD}$ and $\beta_{eRD}$ since the eigen computation demand at elemental level is negligible compared to the system level. $\xi_{eR1}$ and $\xi_{eR2}$ in eq. (3.3) are proportionality parameters relating the elemental frequencies with the elemental damping proportional parameters. In the present study, it is proposed to be called *elemental Rayleigh damping ratios* which need to be parametrized as outlined in section 3.7. For the ease of parametrization, $\xi_{eR1}$ is assumed to be equal to $\xi_{eR2}$ and assumed to be constant for all elements in section 3.7. But there is no such stringent requirement for them to be constant; in fact, $\xi_{eR1}$ and $\xi_{eR2}$ can be parametrized for each element and can vary from element to element exhibiting high level of flexibility in modelling inherent damping altogether. This may be very important when different materials comprise the model, e.g. in soil-structure interaction problems. The use of the term '*elemental'* in the name *'elemental damping ratio'* should be understood in the context that it mainly relates the elemental frequencies to the elemental damping proportional parameters unlike the global Rayleigh damping ratio which relates the global system frequencies.

As illustrated in Fig. 3.1, based on how elemental mass matrix $\mathbf{M}_e$ is formulated, two possible modelling options are available: diagonal mass formulation and consistent mass formulation. More details on the element mass formulation is given in section 3.4. In each of these mass formulation classifications, depending on the way the damping proportional parameters are computed it is possible to divide the model further into two sub-classes (as explained below).

a. *Elemental damping proportional parameters $\alpha_{eRD}$ and $\beta_{eRD}$ remaining constant*

In this case, $\alpha_{eRD}$ *and* $\beta_{eRD}$ are computed from elemental frequencies based on the initial stiffness properties of the corresponding element at the beginning of the analysis and remain constant

throughout the analysis. By adopting this approach, the instantaneous nonlinearity of the structure won't be reflected in the damping proportional parameters. Nevertheless, this does not mean that the damping matrix $\mathbf{C}_e$ needs to be constant as the nonlinearity can be reflected in the element stiffness matrix. With this approach, the element damping matrix in eq. (3.2) becomes,

$$\mathbf{C}_e = \alpha_{eRD(constant)}\mathbf{M}_e + \beta_{eRD(constant)}\mathbf{K}_{e(tangent)} \tag{3.4}$$

where $\alpha_{eRD(constant)}$ and $\beta_{eRD(constant)}$ are the constant damping proportional parameters for the element. Conceptually this is very similar in manner to the tangent stiffness based global Rayleigh damping. But in section 3.8, it would be shown that this elemental model performs better than the global model in terms of reducing the un-realistic damping forces. One of the other major advantages of this approach from a computational point of view is that the eigenvalue computations need only be done once and only at the element level which requires far less computational effort compared to the eigenvalue computation at a system level.

b. *Elemental damping proportional parameters $\alpha_{eRD}$ and $\beta_{eRD}$ varying with elemental stiffness*

In this case, $\alpha_{eRD}$ and $\beta_{eRD}$ vary as the analysis progresses reflecting the elemental nonlinearity. So, in each time step elemental undamped frequencies are calculated using the current elemental stiffness and elemental mass and the proportionality parameters are computed. It does involve an eigenvalue computation at every time step, but the computational effort involved is much smaller as it is done at elemental level. So, with this approach eq. (3.2) would become,

$$\mathbf{C}_e = \alpha_{eRD(tangent)}\mathbf{M}_e + \beta_{eRD(tangent)}\mathbf{K}_{e(tangent)} \tag{3.5}$$

where $\alpha_{eRD(tangent)}$ and $\beta_{eRD(\tan gent)}$ are the tangent damping proportional parameters. Conceptually, this is very similar to the Leger and Dussault (1992) model described in section 2.2.2 in chapter 2. However, in contrast to the Leger and Dussault model where the eigenvalue computations are done at the system level, here they are done at the element level. Thus, the proposed approach is considerably more computationally efficient. Additionally, section 3.8 illustrates the fact that this elemental model performs better than the global model in reducing the unrealistic damping forces and gives more conservative responses from an engineering perspective.

### 3.3.2 Elemental Wilson-Penzien damping

The main benefit of global Wilson Penzien damping over global Rayleigh damping as already stated is that, the spurious damping forces exhibited by global Rayleigh model in inelastic dynamic analysis is not present when in-structure damping is represented by global Wilson Penzien model (Carr 2007; Crisp 1980). As stated earlier, mainly two impediments have been preventing the wide spread use of the global Wilson Penzien model in practice; One is the requirement of the computation of all eigen parameters of the whole system for the formation of the damping matrix and the other is the fact that the damping coefficient matrix obtained is fully populated and violates the typical skyline pattern followed in commercial codes (Charney 2008). So, in this chapter, an innovative adaptation of the global Wilson Penzien formulation at the elemental level is presented. Damping matrix is formulated at the element level using elemental mode shapes and elemental frequencies. The use of elemental frequencies and elemental mode shapes can be justified from the fact that damping matrix is derived at the element level from elemental deformations and before the system matrix is assembled the damping of an element depends only on the elemental

frequencies and mode shapes. One of the main advantages of this formulation is that the eigen parameter computation needs to be performed only at the elemental level and hence the computational effort is reduced enormously when compared to that of the global Wilson Penzien model. The other advantage is that as the damping coefficient matrix is formulated at the elemental level, the skyline pattern of the stiffness matrix is preserved thereby giving a computationally efficient sparse matrix in comparison to the fully populated matrix given by the global Wilson Penzien model.

The derivation of the elemental form of the global Wilson Penzien damping follows the same procedure outlined in (Wilson and Penzien 1972), except the fact that all computations are done at element level. Let $\Phi_e$ represent the full $N_e \times N_e$ elemental modal matrix and $\omega_e^2$ represent the $N_e \times N_e$ diagonal frequency matrix. By classical modal analysis, $\mathbf{d}_e(t)$ in eq. (3.1) can be expressed as,

$$\mathbf{d}_e(t) = \Phi_e \mathbf{q}_e(t) \tag{3.6}$$

Here $\mathbf{q}_e(t)$ is the generalized coordinate. In the derivation of global Wilson Penzien model, the damping matrix is assumed to possess the same orthogonality property as the mass and stiffness matrices (Wilson and Penzien 1972). Same assumption is adopted here for the elemental damping matrix. Hence, by pre-multiplying eq. (3.1) by $\Phi_e^T$ and using eq. (3.6) we get,

$$\mathbf{M}_{di}\ddot{\mathbf{q}}_e(t) + \mathbf{C}_{di}\dot{\mathbf{q}}_e(t) + \mathbf{K}_{di}\mathbf{q}_e(t) = \mathbf{F}_e(t) \tag{3.7}$$

where, $\mathbf{M}_{di}, \mathbf{C}_{di}$ and $\mathbf{K}_{di}$ represent the diagonalized mass, damping and stiffness matrices. The individual terms in these matrices are given as follows,

$$\left.\begin{aligned} M_{di}^{i} &= \left(\phi_e^i\right)^T \mathbf{M}_e \left(\phi_e^i\right) \\ C_{di}^{i} &= \left(\phi_e^i\right)^T \mathbf{C}_e \left(\phi_e^i\right) \\ K_{di}^{i} &= \left(\phi_e^i\right)^T \mathbf{K}_e \left(\phi_e^i\right) \end{aligned}\right\rangle i = 1,2.....N_e \tag{3.8}$$

Assuming $\xi_{eWP}^{i}$ as the elemental Wilson-Penzien damping ratio corresponding to the $i^{th}$ elemental mode, elemental modal damping coefficient $C_{di}^{i}$ can be written as,

$$C_{di}^{i} = 2M_{di}^{i}\xi_{eWP}^{i}\omega_e^i \tag{3.9}$$

Now from eq. (3.8) we get,

$$\mathbf{C}_e = \left(\Phi_e^{-1}\right)^T \mathbf{C}_{di} \left(\Phi_e^{-1}\right) \tag{3.10}$$

Now again from eq. (3.8),

$$\left(\Phi_e^{-1}\right)^T = \mathbf{M}_e \Phi_e \mathbf{M}_{di}^{-1} \tag{3.11}$$

$$\left(\Phi_e^{-1}\right) = \mathbf{M}_{di}^{-1} \Phi_e^T \mathbf{M}_e \tag{3.12}$$

Now substituting eq. (3.9), eq. (3.11) and eq. (3.12) in eq. (3.10), we get,

$$\mathbf{C}_e = \Theta_e \Psi_e \Theta_e^T \tag{3.13}$$

where $\Theta_e$ is the mass normalized elemental mode shape matrix, $\Psi_e$ is a diagonal matrix with diagonal elements given by,

$$\psi_e^i = \frac{2\xi_{eWP}^{i}\omega_e^i}{M_{di}^{i}} \tag{3.14}$$

In the present study, for application convenience, $\xi_{eWP}$ is assumed to be equal for all elements. But it should be noted here that there is no restriction for $\xi_{eWP}$ to be a constant; if better parametrization methodologies are available then $\xi_{eWP}$ can be treated as a variable for each mode of each of the elements comprising the whole system. This shows the generality of the elemental Wilson Penzien formulation.

## 3.4 Notes on computation of elemental frequencies and elemental mass formulation

It is to be noted that for the implementation of the above proposed models one of the key requirements is the computation of the elemental frequencies. Computation of the elemental frequencies can be done in different ways based on the boundary conditions adopted for the element. One of the simplest way to do is to assume that before the matrix assembly the element has a free-free boundary condition. While using free-free boundary condition, on eigen computation there will be rigid body modes. These rigid body modes can be intuitively assumed to be undamped as there are no deformations associated with those modes. This methodology is assumed for the computation of elemental frequencies and mode shapes for both proposed models. Appendix 1 presents more details regarding one of the ways in which the elemental frequencies can be computed. If only beam elements (2D or 3D) are used in the study, then it is even possible to compute the elemental frequencies by using closed form solutions with appropriate boundary conditions and the damping matrix developed requires no eigen computation.

In majority of seismic analyses, normally a lumped mass system is used to represent the mass in the system; but to compute the elemental frequencies this might not be a viable option. In the present study two different mass definitions are used for defining mass; one is the lumped mass

which is used by the main program for all nonlinear computations and the other is the diagonal or consistent mass only used by the elemental damping matrix subroutine for computing the elemental frequencies needed for generating the elemental damping matrix. In a normal nonlinear analysis, generally the story level mass (floor slabs, finishes etc.) is applied to the model as nodal masses. These nodal masses can be incorporated into the elemental frequency computation for damping matrix by distributing the mass as an additional area for the element under consideration. So, this simply means, we increase the area of the element to reflect the additional mass and the mass matrix of the element used for computing the elemental frequencies and elemental damping matrix uses this altered area. It should be noted that when the mass matrix is computed using this methodology the mass is attributed to all the degrees of freedom if consistent mass/diagonal mass matrix formulation is adopted. This can be justified because in actual reality the mass is always distributed, and lumping is only a modelling convenience. In the IDA study presented in section 3.8, the effect of both consistent mass and diagonal mass formulations are investigated in the computation of damping matrix.

In the present commercial software framework, the two-part definition of mass may be considered as a small impediment in the implementation of the proposed models; but considering the computational benefits and the more reliable performance shown by these models as illustrated in section 3.8, this should not be considered as a major limitation in the adoption of these models. As a proof of this, in *Ruauomoko*, (Carr 2007) , this two-part definition of the mass matrix has already been successfully implemented.

## 3.5 Implementation of elemental damping models in Newmark incremental equilibrium framework

As most of the commercial software incorporates Newmark incremental method for solving equations of motion, in this section, steps involved in the implementation of the damping models in the Newmark incremental equilibrium framework is outlined. From the implementation point of view described in the following subsections, it could be clearly seen that there are only minor modifications needed in the existing framework for the incorporation of these proposed models. In the case of elemental Rayleigh, the modification in the existing nonlinear framework is mainly the addition of a sub-step to compute the damping matrix (step 6.2 which is described in section 3.5.1). Also for the incorporation of these models an elemental eigen computation subroutine needs to be added if higher order finite elements are used; in the case of 2D or 3D beams closed form analytical expression could be used for eigen computation. In the case of elemental Wilson Penzien with constant coefficients, the modification required is only in the eigen computation subroutine. However, the nonlinear framework remains unchanged and the same as the classical current framework since the damping matrix is computed outside the nonlinear framework and remains constant throughout the analysis. In this section, the algorithm is outlined for Newmark constant average acceleration method with $\gamma = \frac{1}{2}$ and $\beta = \frac{1}{4}$. The algorithm outlined below is equally applicable to the linear acceleration method as well with no change in the steps described. The generic equation of motion of the system is given as,

$$\mathbf{M}\ddot{\mathbf{d}}(t) + \mathbf{C}\dot{\mathbf{d}}(t) + \mathbf{K}\mathbf{d}(t) = \mathbf{f}(t) \tag{3.15}$$

where **M** is the assembled mass matrix, **C** is the assembled damping matrix, **K** is the assembled stiffness matrix and **f** (*t*) is the applied load vector. Steps involved in the algorithm are described in two separate subsections (Chopra 2012; Filippou *et al.* 1992). Fig.3.2 represents the flow chart for the implementation steps involved for elemental Rayleigh damping. In the case of elemental Wilson Penzien, the main difference is in the fact that the damping matrix remains constant and is computed at the same time as the mass matrix; so, this is not explicitly outlined as a flow chart.

### 3.5.1 Elemental Rayleigh damping

It should be noted that only the implementation of the model with tangent proportionality constants are illustrated in this section as it is deemed to be the most generic version.

- ***Initial Calculations***

1.0 Initialize the displacement vector $\mathbf{d}_{old} = \mathbf{d}(0)$ and velocity vector $\mathbf{v}_{old} = \dot{\mathbf{d}}(0)$.

2.0 Parameterize the elemental damping ratio $\xi_{eR}$ as per section 3.7

3.0 Compute the elemental frequencies using the initial elemental stiffness matrix and evaluate the initial damping proportional parameters for each element for both the models.

4.0 Assemble the system mass matrix **M**, initial system damping matrix **C** and the initial system stiffness matrix **K**

5.0 Evaluate the initial acceleration as follows,

$$\mathbf{a}_{old} = \ddot{\mathbf{d}}(0) = \mathbf{M}^{-1}\{\mathbf{f}(0) - \mathbf{C}\mathbf{v}_{old} - \mathbf{K}\mathbf{d}_{old}\} \tag{3.16}$$

- ***Calculations for each time step***

6.0 Choose a sufficiently small-time step based on the highest modal period of interest. For a typical time step,

6.1 Compute the current system tangent stiffness matrix

6.2 Compute the current system damping matrix

For a single element,

6.2.1 Compute the elemental frequencies as described in section 3.4 using the present element stiffness computed in 6.1.

6.2.2 Compute the current damping proportional constants using eq. (3.3) for elemental Rayleigh damping.

6.2.3 Compute the elemental damping matrix using eq. (3.5) for elemental Rayleigh.

Repeat the same for all elements and assemble the matrices to obtain the system damping matrix.

6.3 Compute the dynamic stiffness matrix $\overline{\mathbf{K}}$ as follows

$$\overline{\mathbf{K}} = \frac{4}{\Delta T^2}\mathbf{M} + \frac{2}{\Delta T}\mathbf{C}_T + \mathbf{K}_T \tag{3.17}$$

where $\mathbf{M}$ is the system mass, $\mathbf{C}_T$ is the tangent damping matrix and $\mathbf{K}_T$ is the tangent stiffness matrix.

6.4 Evaluate the effective dynamic load vector as follows,

$$\left\{\Delta\hat{\mathbf{f}}\right\} = \left\{\Delta\mathbf{f}\right\} + \mathbf{M}\left\{2\mathbf{a}_{old} + \frac{4}{\Delta T}\mathbf{v}_{old}\right\} + 2\mathbf{C}_T\mathbf{v}_{old} \tag{3.18}$$

6.5 Solve for displacement increment

$$\overline{\mathbf{K}}\Delta\mathbf{d} = \left\{\Delta\hat{\mathbf{f}}\right\} \tag{3.19}$$

6.6 Perform *state determination* to check whether there is a change in stiffness within the time step*;* for details refer (Chopra 1995; Filippou *et al.* 1992). If a change of

stiffness occurs during the time step, repeat steps 6.1 to 6.6. If there is no change in stiffness (*in a state of convergence*),

6.6.1 Compute the incremental acceleration and incremental velocity as follows,

$$\Delta\ddot{\mathbf{d}} = \left[\frac{4}{\Delta T^2}\Delta\mathbf{d} - \frac{4}{\Delta T}\mathbf{v}_{old} - 2\mathbf{a}_{old}\right] \tag{3.20}$$

$$\Delta\dot{\mathbf{d}} = \left[\frac{2}{\Delta T}\Delta\mathbf{d} - 2\mathbf{v}_{old}\right] \tag{3.21}$$

6.6.2 Compute the new acceleration and new velocity

$$\mathbf{v}_{new} = \mathbf{v}_{old} + \Delta\dot{\mathbf{d}} \tag{3.22}$$

$$\mathbf{a}_{new} = \mathbf{a}_{old} + \Delta\ddot{\mathbf{d}} \tag{3.23}$$

6.6.3 Update the $\mathbf{a}_{old}$ and $\mathbf{v}_{old}$

7.0 For all time steps repeat steps 6.1 to 6.6 in step 6.0

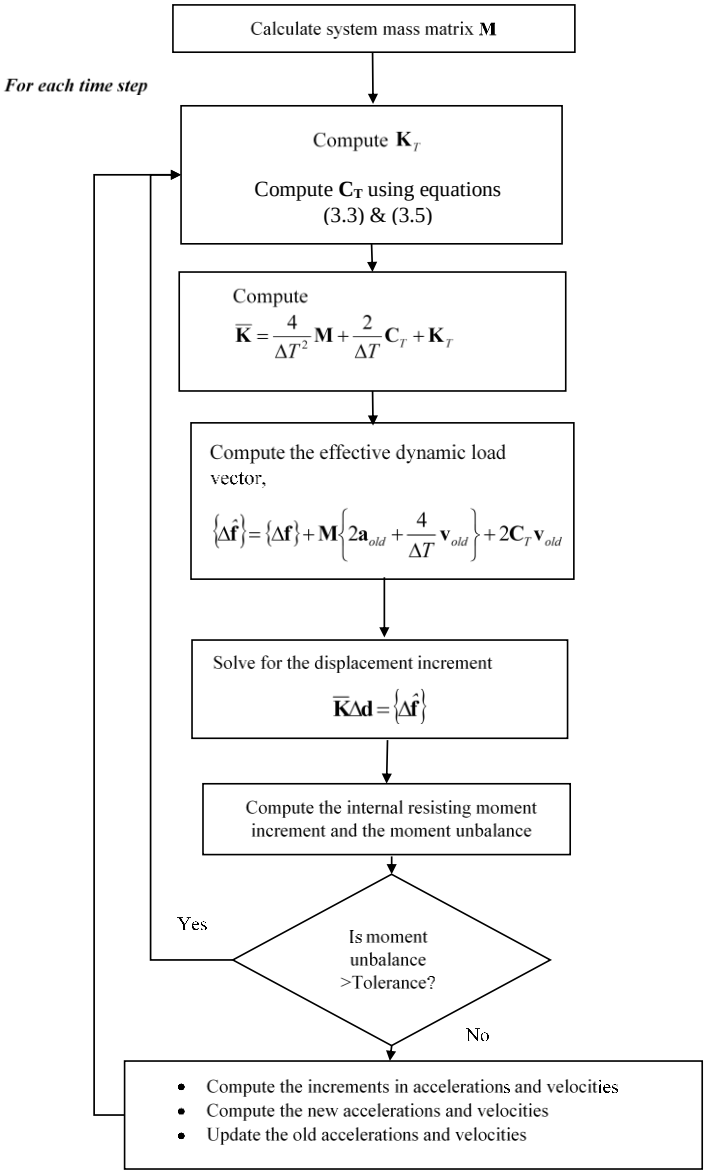


Fig. 3.2 Flow chart for the implementation of elemental Rayleigh damping

### 3.5.2 Elemental Wilson Penzien damping

Elemental Wilson Penzien damping follows the same procedure of implementation as that of elemental Rayleigh damping described in section 3.5.1, except that the damping matrix is only computed once and remains constant throughout the nonlinear analysis. So, its implementation is described here with reference to the steps outlined in section 3.5.1.

a. Perform steps 1.0 to 5.0 with $\xi_{eWP}$ assumed to be same as the global damping ratio and the elemental damping matrix computed using eq. (3.13).

b. Store the computed damping matrix for further use as it remains constant throughout the analysis.

c. Perform step 6.0, but skip step 6.2 and in step 6.3 instead of the tangent damping matrix $\mathbf{C}_T$, use the damping matrix assembled in step 4.0.

d. Repeat step 6.0 for all time steps.

## 3.6 Review of the Implementation options for the *elemental models* using revised Newmark total equilibrium method

To the knowledge of the author, most of the available commercial software packages implement the incremental version of Newmark's method described in section 3.5 for solving equations of motion in real time. One of the main issues with this formulation is that, only incremental equilibrium is checked in every time step and no check is done on the overall equilibrium of the system (Carr 2007). Due to this, normally while using the incremental Newmark version, the effects of the damping forces on the system equilibrium remain obscured. As the present focus of the numerical simulations presented in section 3.8 of this study is to investigate the performance of the proposed damping models, an alternative method called revised Newmark total equilibrium approach is adopted. A detailed account of the revised Newmark method is given in Appendix 2 (Carr 2007; Chopra 2012; Puthanpurayil *et al.* 2014). As far as the author is aware one of the commercial software which implements this method is *Ruauomoko* (Carr 2007).

The main difference between the classical incremental Newmark and the revised Newmark total equilibrium approach is that, in the classical version, the method starts with the differences in the

responses between two successive steps $\Delta T$ apart whereas in the revised Newmark total equilibrium approach, the method starts with equation of equilibrium at $t + \Delta T$. So, in the revised approach, the forces at the end of the time step are obtained by summing up the forces at the beginning of the time step with the incremental inertia, incremental damping and incremental stiffness forces (Carr 2007). This results in the computation of the inertia forces, damping forces and stiffness forces at every time step and ensures that the dynamic equilibrium is enforced (Carr 2007). This section reviews the implementation options for the elemental models developed in section 3.3 using the revised Newmark total equilibrium approach.

### 3.6.1 Elemental Rayleigh damping

The implementation scheme for the revised Newmark total equilibrium method follows the same procedure as outlined in section 3.5.1 with some modifications. The implementation steps are as follows:

a. Perform steps 1.0 to 5.0

b. Following modifications are introduced in step 6.0.

**b.1** Eq. (3.18) is modified as follows,

$$\hat{\mathbf{f}}\left(t+\Delta T\right)=\mathbf{f}\left(t+\Delta T\right)+\mathbf{M}\left\{\mathbf{a}_{old}+\frac{4}{\Delta T}\mathbf{v}_{old}\right\}+2\mathbf{C}_{T}\mathbf{v}_{old}-\mathbf{F}_{damping}\left(t\right)-\mathbf{K}_{s}\mathbf{d}_{old} \tag{3.24}$$

where $\mathbf{K}_s$ is the secant stiffness, and $\mathbf{F}_{damping}(t)$ is given by assuming secant formulation as (Carr 1997; Carr 2007),

$$\mathbf{F}_{damping}\left(t+\Delta T\right)=\mathbf{C}_{\text{sec}ant}\dot{\mathbf{d}}\left(t+\Delta T\right) \tag{3.25}$$

An alternative way to compute $\mathbf{F}_{damping}(t)$ is by using the tangent formulation (Carr 1997; Carr 2007) which is given as,

$$\mathbf{F}_{damping}(t+\Delta T)=\mathbf{C}_{secant}\dot{\mathbf{d}}(t+\Delta T)=\mathbf{C}_{secant}(t)\dot{\mathbf{d}}(t)+\mathbf{C}_{tangent}\Delta\dot{\mathbf{d}} \tag{3.26}$$

The main issue with this formulation is that the damping exhibits hysteresis and ends up with non-zero damping forces at the end of the analysis when the velocities go to zero (Carr 2007). Other than the mathematical justification inherent in the revised Newmark total equilibrium approach, no physical justification exists for such a formulation. In the present study, Secant formulation given in eq. (3.25) is adopted for all analytical studies presented in this chapter.

**b.2** In step 6.6.2, in section 3.5.1, an additional equation is incorporated as follows,

$$\mathbf{d}_{new}=\mathbf{d}_{old}+\Delta\mathbf{d} \tag{3.27}$$

**b.3** Update the $\mathbf{a}_{old}$, $\mathbf{v}_{old}$ and $\mathbf{d}_{old}$

c. With the modifications incorporated, repeat sub-steps 6.1 to 6.6 in step 6.0 in section 3.5.1 for all time steps.

### 3.6.2 Elemental Wilson Penzien damping

In the case of implementation of elemental Wilson Penzien, the procedure outlined in section 3.5.2 is followed by incorporating the respective modifications described in section 3.6.1.

## 3.7 Parameterizing the elemental damping ratio for elemental Rayleigh damping model

In elemental Rayleigh damping as described in section 3.3.1, the elemental damping ratios $(\xi_{eR1},\xi_{eR2})$ are unknowns and need to be parameterized. One way to do this is through experimental

identification procedures. But from a practical seismic analysis point of view this is not a viable option. In this section, a very simple free vibration matching procedure is outlined for the identification of the elemental damping ratio for elemental Rayleigh damping proposed in this chapter. The procedure outlined in this section directly relates the global damping ratio to elemental damping ratio. The main advantage of this approach is that the user needs to supply only the global damping ratio for two specific global system modes and the closed-form solution derived in this section will work out the elemental damping ratio. The basic assumption adopted in the development of this procedure is that all existing damping models used so far in practice, including the global Rayleigh damping model, were tuned based on snap back tests and the logarithmic decrement method. As these models are in the linear range, the responses computed using the proposed models are expected to have the same behavior when the structure remains elastic. The difference between the damping models comes into play only when the structure becomes inelastic.

### 3.7.1 Derivation of closed form parametrization of elemental damping ratio for elemental Rayleigh damping

First assuming damping matrix **C** in eq. (3.15) to be represented by global Rayleigh damping (Rayleigh damping matrix computed using global system frequency) and substituting $\mathbf{d}(t)=\Phi\mathbf{q}(t)$ in the eq. (3.15), and pre-multiplying the eq. (3.15) by $\Phi^T$ (modal matrix); for the $i^{th}$ mode we get,

$$m_i\ddot{q}_i(t)+\alpha m_i\dot{q}_i(t)+\beta k_i\dot{q}_i(t)+k_iq_i(t)=f_i(t) \tag{3.28}$$

where the terms are the $i^{th}$ modal mass, modal stiffness and the modal force vector. Now assuming a free vibration scenario, the modal force vector is assumed to be zero. So, eq. (3.28) can be re-written as,

$$m_i\ddot{q}_i(t)+\alpha m_i\dot{q}_i(t)+\beta k_i\dot{q}_i(t)+k_iq_i(t)=0 \tag{3.29}$$

Again, with elemental Rayleigh damping representing the damping matrix **C** in eq. (3.15) as,

$$\mathbf{C}=\sum_{iel=1}^{N}\mathbf{C}_{iel}=\sum_{iel=1}^{N}\left(\alpha_{iel}\mathbf{M}_{iel}+\beta_{iel}\mathbf{K}_{iel}\right)=\sum_{iel=1}^{N}\left(2\xi_{eR1}\frac{\omega_{iel}^{i}\omega_{iel}^{j}}{\omega_{iel}^{i}+\omega_{iel}^{j}}\mathbf{M}_{iel}+2\xi_{eR2}\frac{1}{\omega_{iel}^{i}+\omega_{iel}^{j}}\mathbf{K}_{iel}\right) \tag{3.30}$$

where $N$ represents the total number of elements and the $\sum$ represents the matrix assembly with proper book-keeping of the degrees of freedom. Now assuming $\xi_{eR1}=\xi_{eR2}=\xi_{eR}$ in eq. (3.30) and assuming it as constant for all elements, eq. (3.30) can be rewritten as,

$$\mathbf{C}=2\xi_{eR}\sum_{iel=1}^{N}\left(\frac{\omega_{iel}^{i}\omega_{iel}^{j}}{\omega_{iel}^{i}+\omega_{iel}^{j}}\mathbf{M}_{iel}+\frac{1}{\omega_{iel}^{i}+\omega_{iel}^{j}}\mathbf{K}_{iel}\right) \tag{3.31}$$

Now pre-multiplying eq. (3.15) by $\Phi^T$, substituting $\mathbf{d}(t)=\Phi\mathbf{q}(t)$ and substituting eq. (3.31) in eq. (3.15), we get,

$$\Phi^T\mathbf{M}\Phi\ddot{\mathbf{q}}(t)+2\xi_{eR}\Phi^T\sum_{iel=1}^{N}\left(\frac{\omega_{iel}^{i}\omega_{iel}^{j}}{\omega_{iel}^{i}+\omega_{iel}^{j}}\mathbf{M}_{iel}+\frac{1}{\omega_{iel}^{i}+\omega_{iel}^{j}}\mathbf{K}_{iel}\right)\Phi\dot{\mathbf{q}}(t)+\Phi^T\mathbf{K}\Phi\mathbf{q}(t)=\Phi^T\mathbf{f}(t) \tag{3.32}$$

Now introducing

$$\mathbf{D}=\sum_{iel=1}^{N}\left(\frac{\omega_{iel}^{i}\omega_{iel}^{j}}{\omega_{iel}^{i}+\omega_{iel}^{j}}\mathbf{M}_{iel}+\frac{1}{\omega_{iel}^{i}+\omega_{iel}^{j}}\mathbf{K}_{iel}\right) \tag{3.33}$$

and substituting in eq. (3.32) we get,

$$\Phi^T\mathbf{M}\Phi\ddot{\mathbf{q}}(t)+2\xi_{eR}\Phi^T\mathbf{D}\Phi\dot{\mathbf{q}}(t)+\Phi^T\mathbf{K}\Phi\mathbf{q}(t)=\Phi^T\mathbf{f}(t) \tag{3.34}$$

So, for $i^{th}$ mode, and neglecting the off diagonal terms, and assuming free vibration

$$m_i\ddot{q}_i(t)+2\xi_{eR}D_i\dot{q}_i(t)+k_iq_i(t)=0 \tag{3.35}$$

Now equating terms in eq. (3.35) and eq. (3.29) we get,

$$\xi_{eR}\cong\frac{\alpha m_i+\beta k_i}{2D_i} \tag{3.36}$$

Eq. (3.36) gives a direct approximate closed form relationship between the elemental damping ratio and the global damping ratio.

## 3.8 Numerical Study

To assess the performance of the elemental models proposed in this paper, a set of numerical studies are performed on a four-story reinforced concrete frame described in Arede (1997), designed in accordance with Eurocode 8 (EC8) and Eurocode 2(EC2). The frame is designed for high seismicity assuming a PGA of 0.3g. The geometric and modelling details of the frame are given in appendix 3. As the sole intention of using this frame was to test the damping models on a realistic structure designed as per the latest standards, some modelling simplifications were made. A very simple bilinear non-degrading hysteresis with bilinear factor of 0.02 and with no strength degradation is adopted in the present study. The choice of this simple hysteresis model is deliberate as the main intention is to show the effect of the damping models in a simple nonlinear scenario with no additional hysteretic complexities added which may obscure the effects of the damping models. It is acknowledged that the simplified hysteretic properties adopted for the members may not reflect the realistic hysteretic behavior of an RC structure. So, in this light, the results presented here should be looked upon as a case of nonlinearity where considerable simplifications (with regard to stiffness and strength degradation) are made, which makes the results qualitative with

respect to the specific frame, but giving a clear insight into what might happen in the case of a full-fledged nonlinear analysis. The results presented here give an indication that, the more the structure becomes nonlinear, the effect of damping models on the responses would be more prominent. A similar observation was made by Zareian and Medina (2010). Modal damping ratios of 5% are applied to the first and second modes in the global Rayleigh damping models and a constant 5% for all modes is used for the global Wilson-Penzien model. The elemental damping ratio for elemental Wilson Penzien model also assumes a constant 10% damping ratio. For elemental Rayleigh damping, the elemental damping ratios are computed by the procedure outlined in section 3.7.1 with a global damping ratio of 5%. The typical value of 5% is adopted as per the guidance in (PEER/ATC 72-1 2010) as well as due to the popular choice prevalent in the seismic analyst's community especially while modelling concrete structures.

First, a single ground motion study results are presented where the focus is on assessing the performance of the models by comparing the values of the damping moments computed. Damping moments are un-realistic forces exhibited by the models and can be computed as the product of the current damping coefficient matrix with the current velocity vector (Crisp 1980). The single ground motion study is also used to illustrate computational benefits of elemental Wilson Penzien model over the Global Wilson Penzien in terms of its altered sparse matrix in comparison to the latter's fully populated matrix. In the second part of this section an IDA study is presented as a means for a qualitative illustration of the performance of these models in a series of nonlinear analysis with different ground motions with increasing intensities. This study mainly gives a qualitative indication towards the likely performance of these models in the case of seismic performance assessments and the possible influence the choice of damping models might have on

the analysis results. It is clearly evident from the results presented below that the choice of damping models does play a pivotal role in the performance assessment studies. The abbreviations used to identify different damping models included in the plots are given in table 3.1. In all the plots presented in this section, global models are presented with continuous lines and elemental models are presented with broken lines.

| Abbreviation | Model description |
|---|---|
| ISRD | Initial stiffness based global Rayleigh damping |
| TSRD1 | Tangent stiffness based global Rayleigh damping with constant coefficients |
| TSRD2 | Tangent stiffness based global Rayleigh damping with updated coefficients |
| ELRD1 | Elemental Rayleigh damping with constant elemental proportionality coefficients (Refer eq. (3.4)) |
| ELRD2 | Elemental Rayleigh damping with updated proportionality coefficients (Refer eq. (3.5)) |
| GWP | Global Wilson Penzien model (Wilson & Penzien 1972) |
| EWP | Elemental Wilson Penzien model (Refer eq. (3.13)) |

Table 3.1 Abbreviations used in the plot

### 3.8.1 Single ground motion study

Sakaria (1999) ground motion is used for the analysis presented in this section. This ground motion was mainly chosen because it has a broad band frequency spectrum with Fourier peaks occurring between 0.5Hz and 10Hz.

#### *3.8.1.1 Damping moments of Global models vs. Elemental models*

In this section, a single ground motion is used to compare the performance of the proposed elemental models with the global models in terms of damping moments. Fig.3.3 depicts the variation of peak damping moments per story.

It can be clearly seen that elemental models have much lesser damping moments than the global Rayleigh models indicating the superiority of the models in terms of reducing the unrealistic forces. It can also be seen that, in this present study, all the elemental models seem to have lesser moments than the Global Wilson Penzien model in lower stories; thereby reinforcing the superiority of the elemental models over the global models.

One observation to be noted here which will be further investigated in the next sub-section is that elemental Wilson Penzien model used in this study uses consistent mass matrix for damping matrix computation, whereas all other models use diagonal mass formulation. Also, another interesting observation is that, although TSRD2 is believed to perform better than TSRD1 (Charney 2008), in this present study it tends to give slightly larger moments than TSRD1.

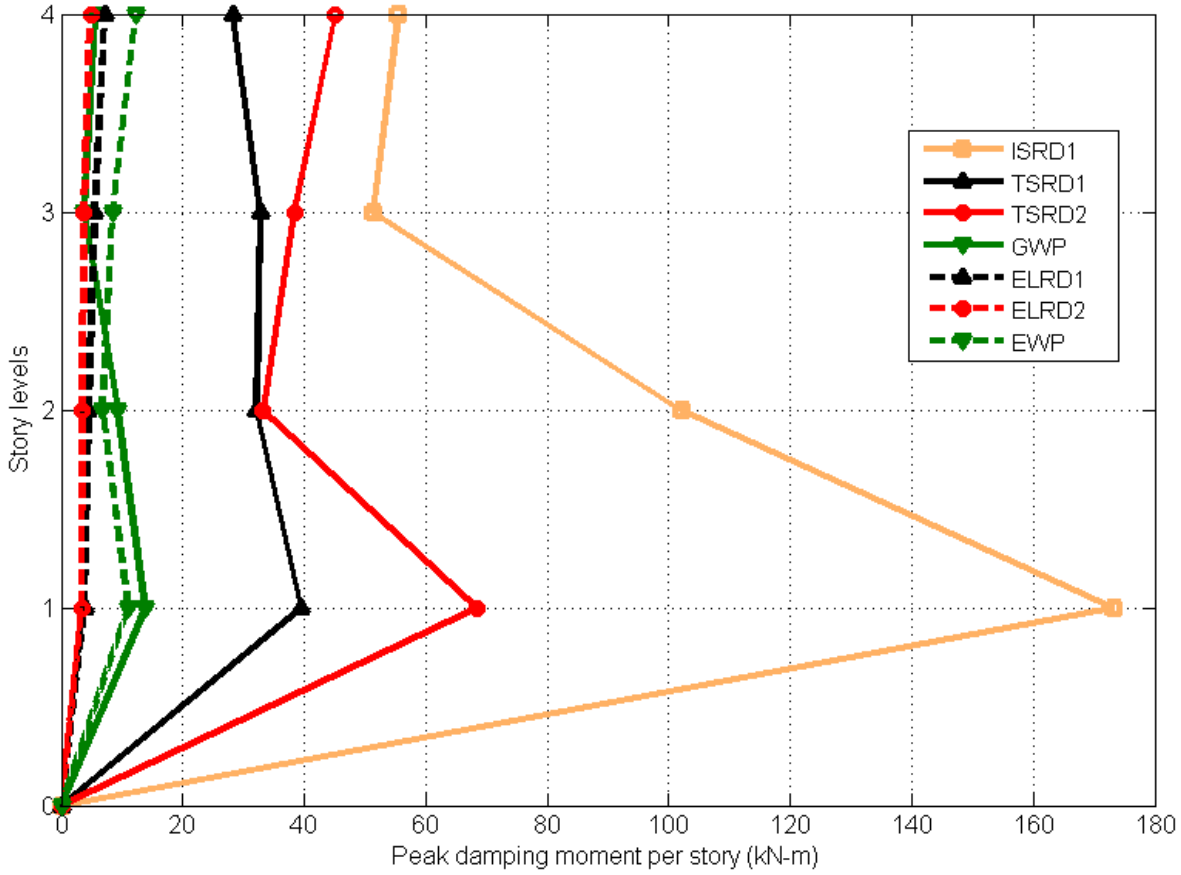


Fig. 3.3 Peak damping moments per storey for different damping models

### *3.8.1.2 Matrix pattern comparison for Global Wilson-Penzien vs. Elemental Wilson-Penzien*

One of the main reasons identified to have led to the lack of popularity of the global Wilson-Penzien model is the fully populated damping matrix obtained during its implementation. Fig. 3.4a shows this matrix for the present four-story structure. It can be clearly seen that the matrix is fully populated which is a major disadvantage as far as both the storage and the computational algorithm requirements of the present commercial software framework are concerned. Elemental Wilson Penzien on the other hand eliminates this issue as the damping matrix is defined at the elemental level and assembled to a system damping matrix. Fig. 3.4b shows the elemental Wilson Penzien

damping matrix obtained for the system. Also, the eigen computation is only done at element level. Consequently, elemental Wilson Penzien eliminates both disadvantages of global Wilson Penzien due to its elemental level formulation.

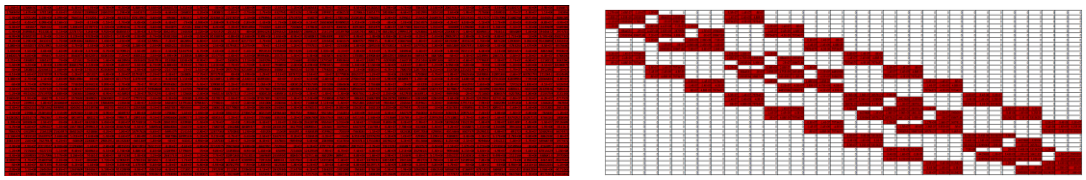

(a) (b)

Fig 3.4a damping matrix pattern of global Wilson Penzien. 3.4b. damping matrix pattern of Elemental Wilson Penzien

One important aspect about Figs. 3.4a and 3.4b that needs to be noted is that, the compared matrices in the figures do not use skyline storage or sparse algebra which is usually employed in commercial software. This is mainly done to get a full comparison on the pattern of the matrix developed.

### 3.8.2 IDA study ( Vamvatsikos and Cornell 2002; Mander et al. 2007;Bradley et al. 2009)

IDA results are presented in this section to assess the performance of the proposed models in comparison to the global models. No second order effects are considered in this study. Damping is an observed phenomenon and is highly system dependent. Hence, it is virtually impossible to state authoritatively that "*some models are better than the others".* However, it is possible to conclude with reasonable certainty that some models may perform better by giving apparently more realistic results in a conservative sense from an engineering perspective as well as from a performance assessment point of view. So, the presented IDA results should be viewed in this light

of realism. Also as the hysteretic model used is a very simple bilinear non-degrading hysteresis both in terms of stiffness as well as strength, the indications given by the curves are qualitative. In addition to assessing the performance of the elemental models, IDA study also investigates the effect of the choice of two different mass formulations described in section 3.4 for the computation of the elemental damping matrix. Hence, the study is presented in two subsections based on the way the mass used for computing the damping matrix is formulated. They are as follows:

#### *3.8.2.1 Consistent mass formulation*

In this approach, the mass matrix used for damping matrix computation adopts the classical consistent mass formulation of Euler Bernoulli beams. As the whole purpose of the IDA study is to illustrate qualitatively the effect of the choice of the damping models might have on the performance assessment studies, a set of seven artificial far-field ground motions scaled to five intensity measures (represented by the peak ground acceleration PGA) were used. To check the performance of the proposed models a parallel IDA study (not presented here) using a set of seven artificial near field ground motions scaled to same five intensity measures were also carried out. The nature of the results is found to be similar. The intensity measures to which the ground motions were scaled are 0.3g, 0.4g, 0.5g, 0.6g and 0.7g. To have similarity in comparison, the global models also adopt the consistent mass formulation for the damping matrix computation instead of the normal lumped mass formulation.

Fig.3.5a depicts the mean IDA curves for location independent peak interstory drift ratio as the engineering demand parameter (EDP). It could be clearly seen from the plots that all analyses with global damping models tend to give lower peak drifts at higher intensities as compared to the

elemental damping models. Also it can be clearly seen that as the intensities increase the difference between the global and elemental damping models become more prominent. This qualitatively suggests that from a performance assessment point of view elemental models might give a conservative estimate from an engineering perspective. This is consistent with the observation of Zareian and Medina (2010) who found a large discrepancy between the interstory drifts obtained by their model and conventional Rayleigh damping model. It is worth noting that the hysteretic model used by Zareian and Medina (2010) was more advanced and had both stiffness degradation and strength degradation incorporated.

In comparison to a standard IDA study, lesser number of ground motions is used in the present study. This is mainly justified, as the present focus is only to illustrate qualitatively the effect of the choice of different damping models on the performance assessment of structures. So considerable variation in the peak responses can be expected at higher intensities.

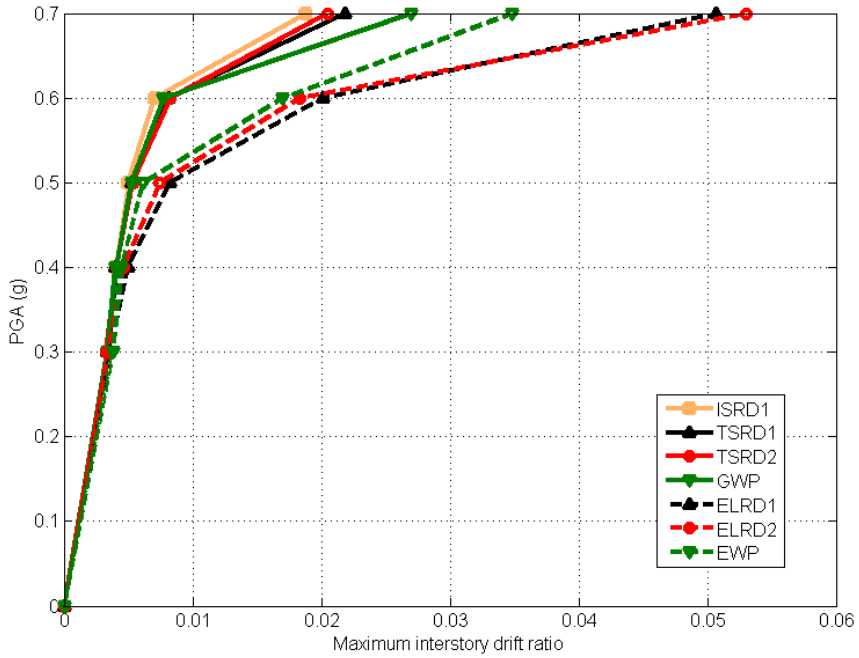


(a)

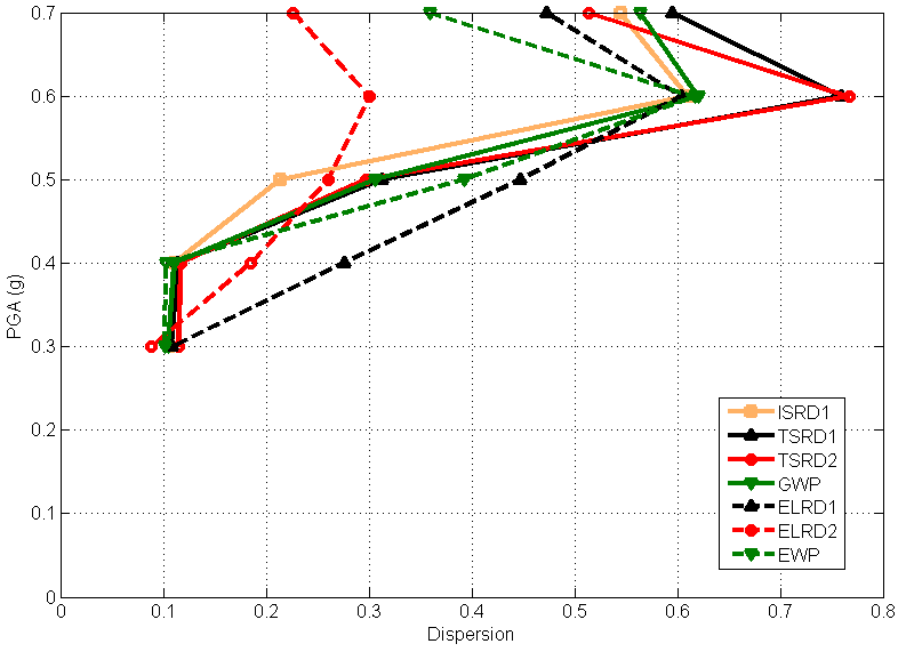


(b)

Fig. 3.5 a) IDA curves for mean interstorey drifts 3.5 b) Dispersion plots of mean interstorey drifts

This variation can be assumed to be lognormally distributed and can be quantified using dispersion $\chi$ given as (Bradley *et al*. 2009)

$$\chi = \sqrt{\ln\left(\left(\frac{\sigma_x}{\mu_x}\right)^2 + 1\right)} \tag{3.37}$$

where $\sigma_x$ and $\mu_x$ are the standard deviation and mean of the variable $x$. Fig. 3.5b depicts the dispersion of the interstory drifts for all the models. It could be seen that ELRD2 exhibits lesser dispersion in comparison to other models. If more ground motions are used the overall dispersion may be reduced. It has to be noted that the dispersion plot is only done corresponding to the five intensity measures.

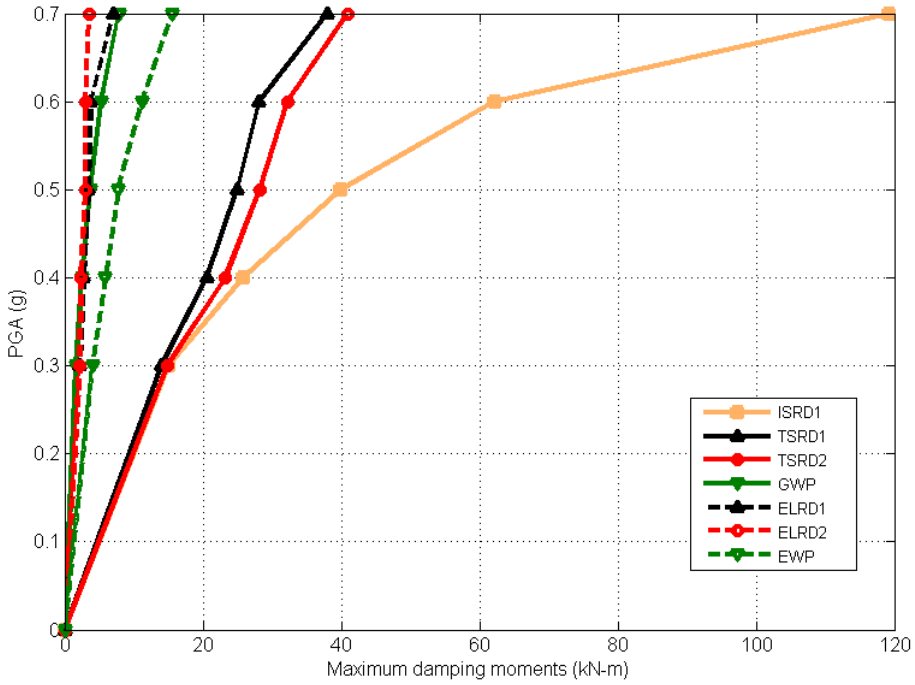


Fig. 3.6 IDA curve for peak damping moments

As already stated in the introduction, one of the key aspects of an ideal damping model is the reduction of un-realistic forces/moments due to damping. Fig. 3.6 compares the mean damping

moments predicted by the seven different damping models. High unrealistic damping forces produce inaccuracies in estimation of displacements and internal member forces (Zareian and Medina 2010). It can be clearly seen that the initial stiffness based global Rayleigh damping (ISRD) yields much higher damping moments when the intensity increases. All elemental damping models show considerably less damping moments than the global Rayleigh damping models. Except for the elemental wilson Penzien model, the other elemental models give less damping moments which are comparable to that given by the global Wilson Penzien model. Even the elemental Wilson Penzien model gives only slightly higher damping moments at higher intensities than the global Wilson Penzien model, and appears to be more promising than the global Rayleigh models in terms of damping moments and also in terms of maximum drift estimated.

#### *3.8.2.2 Diagonal mass formulation*

In this section, the mass matrix used for damping matrix computation adopts the classical diagonal mass formulation of Euler Bernoulli beams. Same set of seven artificial far field ground motions are used for this study. All the global models also adopt the diagonal mass formulation for the damping matrix computation.

Fig. 3.7a depicts the mean IDA curves for location independent maximum interstory drift ratio obtained using the different damping models. It could be clearly seen from the plots that elemental Wilson Penzien model (EWP) with diagonal mass formulation results in lower values of peak drift ratio at higher intensities as compared to the elemental Rayleigh damping models and other global models (except initial stiffness based global Rayleigh damping model). On the contrary, the elemental Rayleigh damping models give higher drifts than the global models; especially at higher intensities. This qualitatively suggests that from a performance assessment point of view elemental

Rayleigh models with diagonal mass formulation might give a conservative estimate, whereas the elemental Wilson Penzien model might give lower responses.

Fig. 3.7b depicts the dispersion plots for the inter story drifts. But here it can be seen that the dispersion of the elemental models, especially the Rayleigh based models, using diagonal mass for damping matrix computation is high. Again this can be reduced by increasing the number of ground motions used for analysis.

Fig. 3.8 shows the damping moment plots, which can be qualitatively used to explain this deviation in the behavior of elemental Wilson Penzien model. It can be seen that the damping moments of the elemental Wilson Penzien is closer to the global Rayleigh models and much higher than the other elemental models and global Wilson Penzien model.

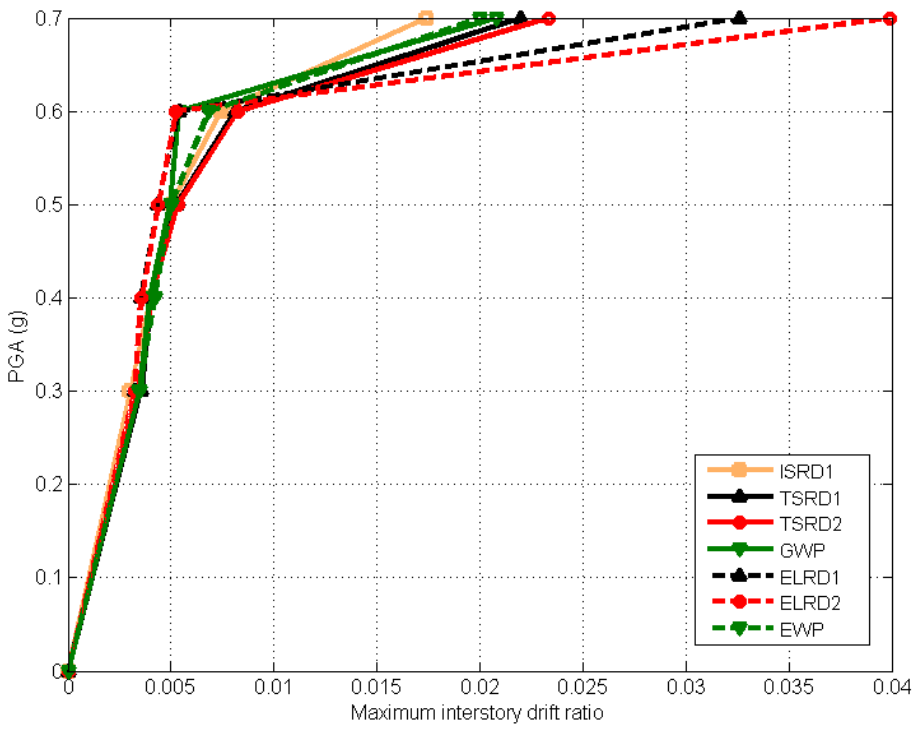


Fig. 3.7a IDA curves for mean peak interstorey drifts

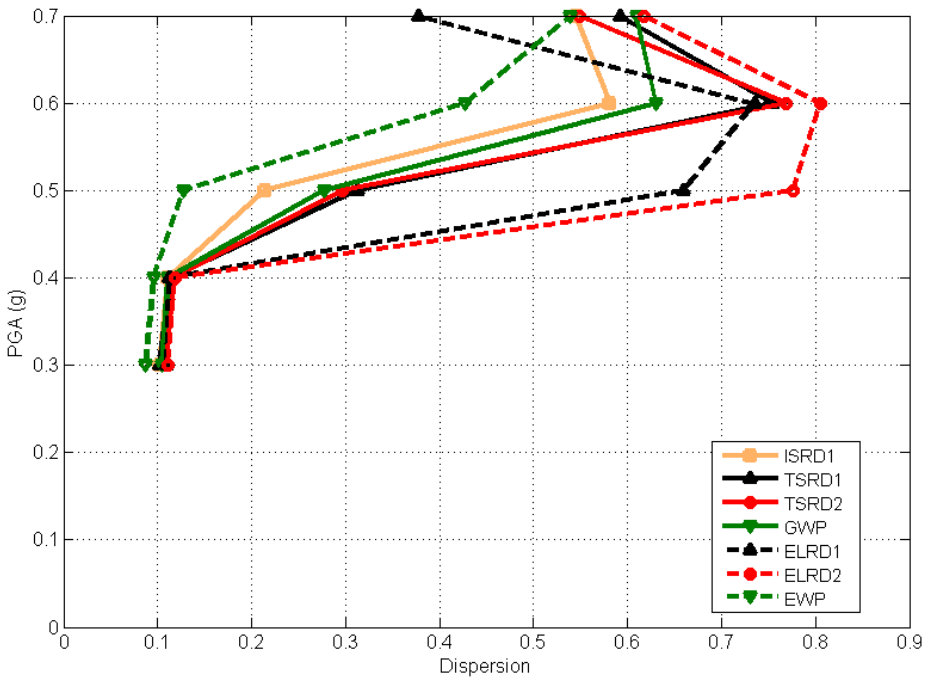


Fig 3.7b Dispersion plots for the mean interstorey drifts

So in effect elemental Wilson Penzien model with diagonal mass formulation fails to reduce the effect of the unrealistic damping forces which in a way is reflected in the drift reponse. On the other hand, it can be observed that the damping moments for elemental Rayleigh damping is very small in comparison to the global Rayleigh models and very close to the global Wilson Penzien model.

Though higher dispersion is observed as depicted in Fig. 3.7b, elemental Rayleigh model with diagonal mass formulation maybe a viable model for inelastic dynamic analysis whereas the elemental Wilson Penzien model with diagonal mass formulation may not be. It has to be noted that the dispersion plot is only done corresponding to the five intensity measures.

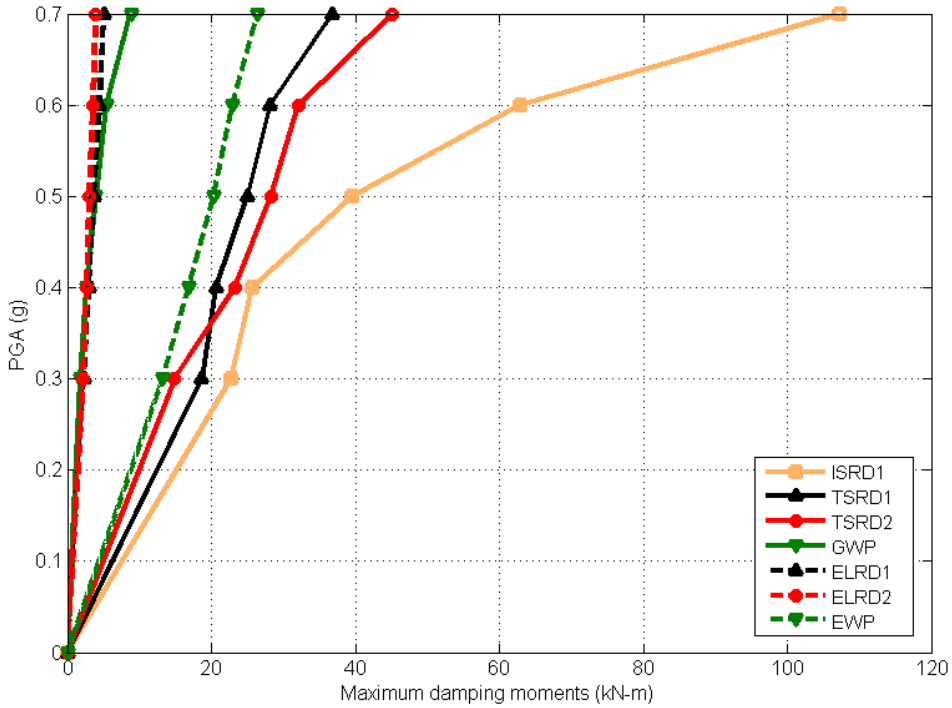


Fig. 3.8 IDA curves for peak damping moments

## 3.9 Observation on consistent mass formulation vs. diagonal mass formulation for elemental damping models

Comparing the response plots and the damping force plots presented in the previous sections 3.8.2.1 and 3.8.2.2, it can be concluded that the elemental damping models with consistent mass formulation tend to give more realistic responses from an engineering perspective; but if diagonal mass formulation need to be used, elemental Rayleigh models tend to give conservative results with reduced damping moments and higher mean interstory drifts at higher intensities, whereas elemental Wilson Penzien model with diagonal mass formulation may not be viable as it tends to exhibit higher damping moments and lower mean peak interstory drift. It should be noted that in the present study, the elemental Wilson Penzien is implemented as a constant damping matrix during the entire nonlinear dynamic analysis. So the deviation exhibited by this model could be considered as an indication for the need for the use of an updated damping matrix (element Wilson

Penzien with updated coefficients) reflecting the system nonlinearity; but this aspect is not investigated in the present chapter; but it is investigated in chapter 7.

## 3.10 Conclusions

A new approach to modelling damping in inelastic dynamic analysis is presented. The new approach relies on the elemental level derivation of the damping matrix and assembling them to obtain the global damping matrix in a way similar to mass and stiffness matrices. Two new elemental damping models are derived from the adaptation of their global counterparts. Implementation schemes for all the proposed models using both Newmark incremental approach and a revised Newmark total equilibrium approach is presented. Performance of the newly proposed models is assesed using a numerical study on a four story frame. It has been shown that all the proposed models with consistent mass formulation used for damping matrix computation seem to produce more reliable results from an engineering perspective than the global models without increasing the computational demand; thereby indicating the superiority of the proposed models. However, if diagonal mass formulation is used, then only the elemental Rayleigh damping models give conservative responses from an engineering perspective.

# 4. Development of a generic time domain implementation scheme for Non-Classical Convolution Damping Models

Puthanpurayil, A.M., Carr, A.J. and Dhakal, R.P. (2014) A generic time domain implementation scheme for non-classical convolution damping models. *Engineering Structures* 71: 88-98. http://dx.doi.org/10.1016/j.engstruct.2014.04.021. (published journal)

**Abstract:** A generic time domain integration formulation for linear systems with non-classical convolution damping models is developed in this chapter. The non-classical damping force is assumed to depend on the history of velocity through a convolution integral over a causal dissipative kernel function. The time domain implementation formulation is developed using the Newmark constant average acceleration framework. The time domain scheme developed in this chapter is referred to as AAR. To emphasize the accuracy of the proposed scheme, numerical comparisons are made for a three-degrees-of-freedom system and an axially vibrating rod problem reported in literature. The generality of the formulation is shown by simulating the response of a cantilever beam enhanced with two known standard dissipation functions: the exponential and the Gaussian model. The implementation of the proposed scheme is also presented.

## 4.1 Introduction

Structural dynamic analysis is mainly characterized by three forces: the inertia force, the damping force and the stiffness force. Out of these, the mechanics for both the inertia and the stiffness force are well understood whereas the damping force represents an observed phenomenon. Damping, in simplistic terms, could be defined as the process by which a certain portion of the energy in a vibrating system is irreversibly lost causing decay in the system response. Despite having a large amount of literature on the subject, the underlying physics is only known in a phenomenological ad-hoc manner, making damping an overall mystery in the general dynamic analysis of structures. A major reason of this could be the fact that there is no single universally accepted model for damping (Woodhouse 1998). The ambiguity involved in the modelling of damping is mainly due to the intricacies involved in understanding the *state variables* controlling the damping forces (Adhikari 2000).

In classical dynamics, for a discrete system, the damping force is predominantly represented by a viscous model, proposed by Rayleigh in 1877, through his famous dissipation function. Many studies in the past have shown that the viscous damping model suggested by Rayleigh is only a mathematical idealization and the "real damping" could be different (Woodhouse 1998; Adhikari 2000). This sort of mathematical idealization may lead to "modelling errors" in dynamic response analysis. The manifestation of these modelling errors has been obtained in various branches of engineering (Golla and Hughes 1985; Val and Segal 2005). This has paved the way for an increasing interest in other types of models which represent damping forces in a more general manner as compared to the classical viscous damping model (Adhikari and Wagner 2004).

One such model of great interest is the non-classical convolution damping model in which the damping force is represented by convolution integrals, which consider the complete history of responses other than just the instantaneous velocities as represented by viscous damping model (Adhikari 2000). The damping force $\mathbf{f}(t)$, using such a model could be expressed as,

$$\mathbf{f}(t) = \int_0^{\tau} \mathbf{C}_k g(t-\tau)\dot{u}(\tau)d\tau \tag{4.1}$$

In this equation, $g(t)$ represents the damping kernel function and $\mathbf{C}_k$ represents the damping coefficient. The kernel function $g(t)$ could represent any causal model which makes the energy dissipation functional non-negative (Adhikari 2007). Normally, $g(t)$ is taken as the normalized damping function (Cortes et al. 2009), which satisfies,

$$\int_0^{\infty} g(t)dt = 1.0 \tag{4.2}$$

In literature, this is commonly referred to as non-viscous damping model (Woodhouse 1998), because integration by parts of eq. (4.1) would result in the damping force being expressed as a function of displacement. But since damping force in its form as given in eq. (4.1) is in a convolution format depending on the history of velocities, the author prefers to address the formulation as non-classical convolution damping.

Incorporation of this model described in eq. (4.1) into the dynamic equilibrium equation would result in an integro-differential equation expressed as,

$$\mathbf{M}\ddot{\mathbf{u}}(t) + \int_0^{\tau} \mathbf{C}_k g(t-\tau)\dot{\mathbf{u}}(\tau)d\tau + \mathbf{K}\mathbf{u}(t) = \mathbf{P}(t) \tag{4.3}$$

Here, $\mathbf{M}$ and $\mathbf{K} \in R^{NxN}$ are the mass and stiffness matrices and $\mathbf{P}(t) \in R^N$ is the force vector and the convolution damping term has the same descriptions as defined above in eq. (4.1) with $\mathbf{C}_k$ representing the damping coefficient matrix. Similarly, $\ddot{\mathbf{u}}(t), \dot{\mathbf{u}}(\tau)$ & $\mathbf{u}(t)$ are the acceleration, velocity and displacement vectors. The initial conditions associated with eq. (4.3) are as follows,

$$\mathbf{u}(0) = \mathbf{u}_0 \in R^N \text{; and } \dot{\mathbf{u}}(0) = \dot{\mathbf{u}}_0 \in R^N \tag{4.4}$$

As eq. (4.3) is an integro-differential equation, no classical methods like Newmark family methods can be applied directly for its solution (Cortes et al. 2009). So, in recent years, considerable amount of research efforts has been put to solve eq. (4.3) to obtain system responses. Majority of the research conducted presented solution schemes for systems in which the damping kernel function adopts an exponential model. McTavish and Hughes (1993) adopted the double exponential model proposed by Golla and Hughes (1985) for the damping kernel function and proposed a scheme which resulted in a second order equation of motion. This second order equation of motion was then solved using classical time integration techniques. This scheme is known as the GHM method. Its main drawback is the use of a large number of internal dissipation coordinates used to capture the frequency dependent viscoelastic behaviour which enlarges the matrix size. Adhikari and Wagner (2004) proposed a time domain analysis scheme for systems with exponential damping kernel function based on an extended state space representation of the equation of motion. The efficiency of the proposed numerical method for the calculation of displacements relies on the elimination of the need for explicit calculation of the velocities and usually a large number of internal variables at each time step. Cortes et al. (2009) employed Laplace transformation on the equation of motion containing exponential damping kernel function and derived an equivalent second order equation of motion which was then solved using implicit standard time integration

schemes. The main advantage of this method was that it did not employ any internal variables which normally increase the size of the problem. The main disadvantage is that the Laplace transformation results in a differential equation with time derivative orders higher than two and the authors admit the difficulty in performing the mathematical manipulation, when the damping model has more than two exponential kernel functions.

In this chapter, a generic time domain formulation for multi-degree of freedom systems represented by eq. (4.3) is presented. This is called 'generic' because in comparison to majority of the earlier works, this formulation could be used for any causal model that the damping kernel function adopts. The other main advantage is that the formulation uses the Newmark framework with some modifications and as a result could be easily incorporated into an existing commercial software package. This aspect has been demonstrated by incorporating the proposed formulation into the commercial package "*Ruaumoko"* maintained by Professor Athol Carr. Latest version of *Ruaumoko* yet to be released gives the option of incorporating convolution damping models for nonlinear dynamic analysis of structures. Though in this chapter the implementation scheme is only shown for linear dynamics, the framework can be easily extended to the nonlinear dynamics. This is demonstrated in chapters 5 & 6. The implementation logic is presented in appendix 4.0.

## 4.2 Mathematical Derivation

In this section, the time domain formulation is developed using Newmark constant average acceleration frame work. At time *t,* the dynamic equilibrium equation with linear generic damping model of the form presented in eq. (4.1) is given by eq. (4.3).

At time $t + \Delta T$ , this equation becomes,

$$\mathbf{M}\ddot{\mathbf{u}}(t+\Delta T)+\int_{0}^{t+\Delta T}\mathbf{C}_k g(t+\Delta T-\tau)\dot{\mathbf{u}}(\tau)d\tau+\mathbf{K}\mathbf{u}(t+\Delta T)=\mathbf{P}(t+\Delta T) \quad (4.5)$$

Here, a revised Newmark constant average acceleration method (rather than the classical incremental approach) is adopted to solve the equation of equilibrium at time $t+\Delta T$ (Carr 2007). It should be noted here that, with ease a similar framework could be developed for incremental Newmark methods as well. But as this thesis mainly employs the modified Newmark total equilibrium method, so, the present framework is developed based on this.

The fundamental assumption in the classical Newmark constant average acceleration method is that the acceleration is assumed to be constant during the time step with a value equal to the average of the accelerations at the beginning and end of the time step. The classical Newmark method starts with the difference in the response between two successive time steps $\Delta T$ apart and results in solving an incremental equilibrium equation. But the revised Newmark scheme starts with equation of equilibrium at time $t+\Delta T$ (refer Appendix 2 for further details).

To have a convenient formulation for the Newmark implementation, the convolution integral is split and is given as follows;

$$\mathbf{M}\ddot{\mathbf{u}}(t+\Delta T)+\int_{0}^{t}\mathbf{C}_k g(t+\Delta T-\tau)\dot{\mathbf{u}}(\tau)d\tau+\int_{t}^{t+\Delta T}\mathbf{C}_k g(t+\Delta T-\tau)\dot{\mathbf{u}}(\tau)d\tau+\mathbf{K}u(t+\Delta T)=\mathbf{P}(t+\Delta T) \quad (4.6)$$

The above equation can be rewritten in incremental terms as (refer Appendix 2),

$$\mathbf{M}\{\ddot{\mathbf{u}}(t)+\Delta\ddot{\mathbf{u}}\}+\int_{0}^{t}\mathbf{C}_k g(t+\Delta T-\tau)\dot{\mathbf{u}}(\tau)d\tau+\int_{t}^{t+\Delta T}\mathbf{C}_k g(t+\Delta T-\tau)\dot{\mathbf{u}}(\tau)d\tau+\mathbf{K}_s\mathbf{u}(t)+\mathbf{K}_T\Delta\mathbf{u}=\mathbf{P}(t+\Delta T) \quad (4.7)$$

Here, $\Delta\mathbf{u}$ refers to increment in displacement, $\Delta\ddot{\mathbf{u}}$ refers to increment in acceleration, $\mathbf{K}_T$ refers to the tangent stiffness and $\mathbf{K}_s$ refers to the secant stiffness. For linearly elastic structures, the secant and tangent stiffness matrices are identical to the initial elastic matrices. Though the present chapter addresses only the linear dynamics scenario, the above notation of secant and tangent stiffness matrix is mainly retained to keep the generality of the Newmark integration scheme; the resulting formulation is applied in chapters 5 & 6 for nonlinear dynamics.

In eq. (4.7), both the acceleration and displacement within a time step are represented in their incremental components, whereas the velocity remains as a continuous function. There are two integral terms containing velocity functions in eq. (4.7); one varies from *0* to *t* and the other from *t* to $t+\Delta T$. So, the velocity term varies both globally (i.e. *0* to *t*) and locally (i.e. *t* to $(t+\Delta T)$). Now for convenience, let's denote the convolution integral from *0* to *t* as,

$$\mathbf{F}_{damp} = \int_0^t \mathbf{C}_k g(t+\Delta T-\tau)\dot{\mathbf{u}}(\tau)d\tau \tag{4.8a}$$

So, eq. (4.7) could be rewritten as,

$$\mathbf{M}\{\ddot{\mathbf{u}}(t)+\Delta\ddot{\mathbf{u}}\}+\mathbf{F}_{damp}+\int_t^{t+\Delta T}\mathbf{C}_k g(t+\Delta T-\tau)\dot{\mathbf{u}}(\tau)d\tau+\mathbf{K}_s\mathbf{u}(t)+\mathbf{K}_T\{\Delta\mathbf{u}\}=\mathbf{P}(t+\Delta T) \tag{4.8b}$$

In order to simplify the computation process, an assumption is made on the nature of the local variation of the velocity term (i.e. $\dot{\mathbf{u}}(\tau)$ with $'\tau'$ varying from *t* to $t+\Delta T$) which makes numerical discretisation of the continuous velocity function $\dot{\mathbf{u}}(\tau)$ possible within the time step.

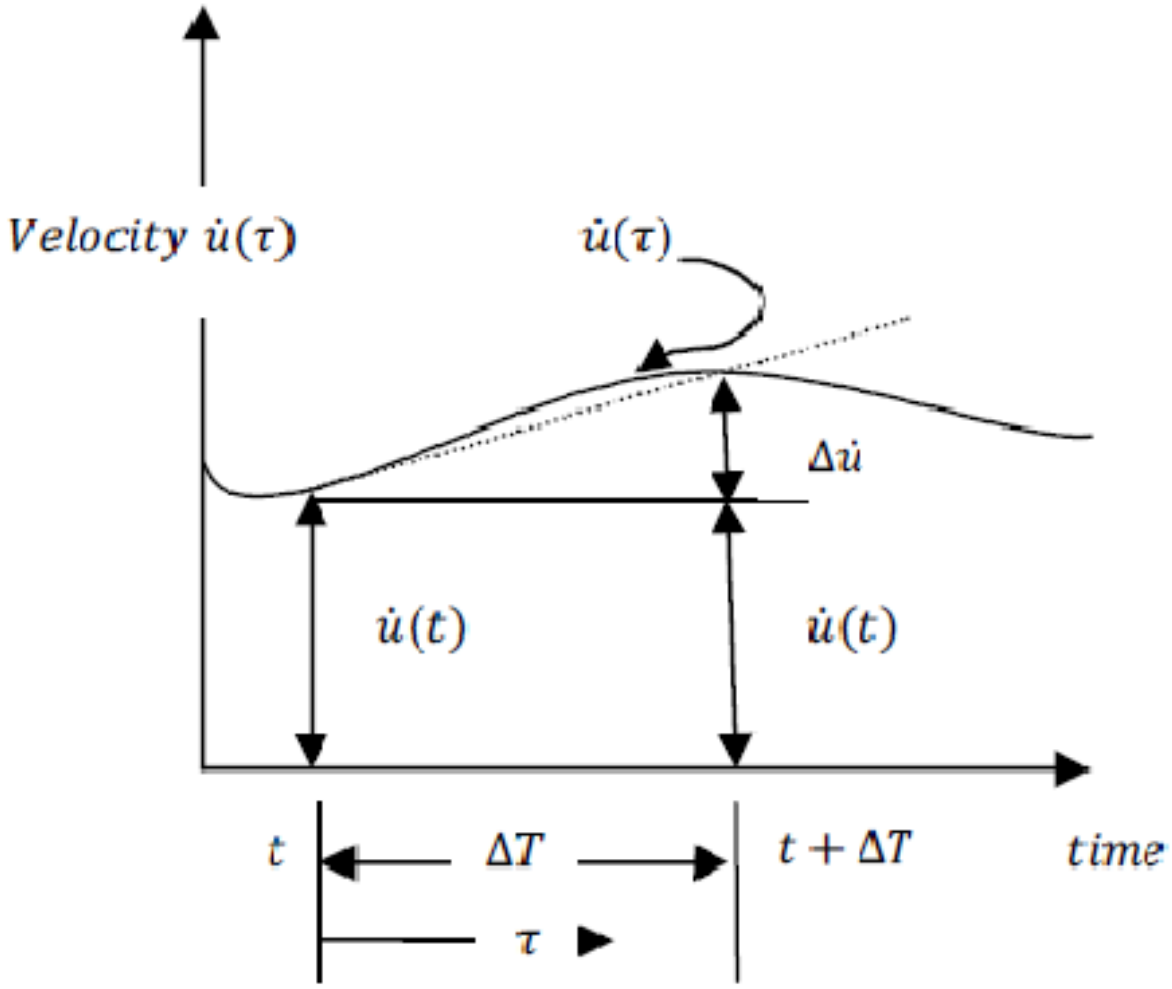


Fig. 4.1 variation of velocity within the time step

As schematically illustrated in Fig. 4.1, the velocity is assumed to have a scaled linear variation within a time step and the function $\dot{\mathbf{u}}(\tau)$ is expressed as,

$$\dot{\mathbf{u}}(\tau) = \dot{\mathbf{u}}(t) + \frac{\tau}{\Delta T}\Delta\dot{\mathbf{u}} \tag{4.9}$$

As it is within the time step, '$\tau$' varies from 0 to $\Delta T$. Note that this assumption is mainly based on the classical Newmark's constant average acceleration scheme.

Now substituting eq. (4.9) in eq. (4.8b) and rewriting it by taking the increments of acceleration, velocity and displacements on one side gives,

$$\mathbf{M}\Delta\ddot{\mathbf{u}} + \frac{1}{\Delta T}\int_{t}^{t+\Delta T}\mathbf{C}_k\, g(t+\Delta T-\tau)\tau\Delta\dot{\mathbf{u}}d\tau + \mathbf{K}_T\Delta\mathbf{u} = \mathbf{P}(t+\Delta T) - \mathbf{M}\ddot{\mathbf{u}}(t) - \mathbf{F}_{damp} - \mathbf{K}_s\mathbf{u}(t) - \int_{t}^{t+\Delta T}\mathbf{C}_k\, g(t+\Delta T-\tau)\dot{\mathbf{u}}(t)d\tau \tag{4.10}$$

From standard Newmark constant average acceleration method (refer Appendix 2), the increments of velocity and acceleration can be expressed in terms of increments of displacements as,

$$\Delta\ddot{\mathbf{u}} = \frac{4}{\Delta T^2}\Delta\mathbf{u} - \frac{4}{\Delta T}\dot{\mathbf{u}}(t) - 2\ddot{\mathbf{u}}(t) \tag{4.11}$$

$$\Delta\dot{\mathbf{u}} = \frac{2}{\Delta T}\Delta\mathbf{u} - 2\dot{\mathbf{u}}(t) \tag{4.12}$$

Now substituting equations (4.11) and (4.12) in eq. (4.10), we get;

$$\mathbf{M}\left\{\frac{4}{\Delta T^2}\Delta\mathbf{u} - \frac{4}{\Delta T}\dot{\mathbf{u}}(t) - 2\ddot{\mathbf{u}}(t)\right\} + \frac{1}{\Delta T}\int_{t}^{t+\Delta T}\mathbf{C}_k\, g(t+\Delta T-\tau)\left\{\tau\left\{\frac{2}{\Delta T}\Delta\mathbf{u} - 2\dot{\mathbf{u}}(t)\right\}\right\}d\tau + \mathbf{K}_T\Delta\mathbf{u} = \mathbf{P}(t+\Delta T) - \mathbf{M}\ddot{\mathbf{u}}(t) - \mathbf{F}_{damp} - \mathbf{K}_s\mathbf{u}(t) - \int_{t}^{t+\Delta T}\mathbf{C}_k\, g(t+\Delta T-\tau)\dot{\mathbf{u}}(t)d\tau \tag{4.13}$$

Collecting the terms containing increments of displacements on one side we get,

$$\left[\frac{4\mathbf{M}}{\Delta T^2}+\frac{2}{\Delta T^2}\int_t^{t+\Delta T}\mathbf{C}_k g(t+\Delta T-\tau)\pi d\tau+\mathbf{K}_T\right]\Delta\mathbf{u}=\mathbf{P}(t+\Delta T)+\mathbf{M}\left\{\ddot{\mathbf{u}}(t)+\frac{4}{\Delta T}\dot{\mathbf{u}}(t)\right\}-\mathbf{F}_{damp}$$
$$-\mathbf{K}_s\mathbf{u}(t)-\int_t^{t+\Delta T}\mathbf{C}_k g(t+\Delta T-\tau)\dot{\mathbf{u}}(t)d\tau+\frac{2}{\Delta T}\int_t^{t+\Delta T}\mathbf{C}_k g(t+\Delta T-\tau)\pi\dot{\mathbf{u}}(t)d\tau \tag{4.14}$$

Eq. (4.14) represents the final format of the formulation that needs to be solved iteratively. A qualitative review of eq. (4.14) would reveal the fact that the framework of Newmark is retained as such with inclusion of damping terms in integral format. This enables an easy implementation of the above formulation in existing commercial packages with minor modifications for evaluating the integrals. The assumption made in eq. (4.9) discretizes the variation of velocity function within a time step and simplifies the evaluation of the integral terms.

## 4.3 Implementation Strategy

The implementation of the above scheme (eq. 4.14) is simple and straight forward. For reducing the computational time, this equation could be used in a semi-discrete form in a numerical sense. This means that wherever velocity is not a function of the integrating parameter $(d\tau)$, a closed form solution, if it exists, could be used for evaluating the integral. In a semi-discrete format, the whole of eq. (4.14) is as shown below,

$$\left[\frac{4\mathbf{M}}{\Delta T^2}+\frac{2}{\Delta T^2}\int_t^{t+\Delta T}\mathbf{C}_k g(t+\Delta T-\tau)\pi d\tau+\mathbf{K}_T\right]\{\Delta\mathbf{u}\}=\mathbf{P}(t+\Delta T)+\mathbf{M}\left\{\ddot{\mathbf{u}}(t)+\frac{4}{\Delta T}\dot{\mathbf{u}}(t)\right\}$$
$$-\sum_{r=1}^{n+1}\mathbf{C}_k g((n+1-r)\Delta T)\dot{\mathbf{u}}\big((r-1)\Delta T\big)\Delta T-\mathbf{K}_s\{u(t)\}-\int_t^{t+\Delta T}\mathbf{C}_k g(t+\Delta T-\tau)\dot{\mathbf{u}}(t)d\tau \tag{4.15}$$
$$+\frac{2}{\Delta T}\int_t^{t+\Delta T}\mathbf{C}_k g(t+\Delta T-\tau)\dot{\mathbf{u}}(t)\pi d\tau$$

Over here the index *'n'* refers to the number of time steps such that $t = n\Delta T$ . So, in a semi-discrete form, only one numerical integration is needed to be undertaken as shown by eq. (4.15), whereas all other integrations are performed using closed form solutions. If closed form solutions are not available, then the full numerical discrete format of eq. (4.14) could be used and all the integrals could be evaluated using numerical integrations. But this might increase the computational time.

In a fully discrete format eq. (4.14) becomes,

$$\left[\frac{4\mathbf{M}}{\Delta T^2}+\underline{\frac{2}{\Delta T^2}\sum_{p=0}^{q}\mathbf{C}_k\, g(n\Delta T+\Delta T-p\Delta\tau)\big(p\Delta\tau\big)\Delta\tau+\mathbf{K}_T}\right]\Delta\mathbf{u}=\mathbf{P}(t+\Delta T)+\mathbf{M}\left\{\ddot{\mathbf{u}}(t)+\frac{4\dot{\mathbf{u}}(t)}{\Delta T}\right\}$$
$$-\underline{\sum_{r=1}^{n+1}\mathbf{C}_k\, g((n+1-r)\Delta T)\dot{\mathbf{u}}\big((r-1)\Delta T\big)\Delta T}-\mathbf{K}_s\mathbf{u}(t)-\underline{\sum_{p=0}^{q}\mathbf{C}_k\, g(n\Delta T+\Delta T-p\Delta\tau)\dot{\mathbf{u}}(n\Delta T)\Delta\tau}$$
$$+\underline{\frac{2}{\Delta T}\sum_{p=0}^{q}\mathbf{C}_k\, g(n\Delta T+\Delta T-p\Delta\tau)\big(p\Delta\tau\big)\dot{\mathbf{u}}(n\Delta T)\Delta\tau}$$

(4.16)

Over here, the local variation of the $\tau$ parameter from $t$ to $t+\Delta T$ is discretised such that $\Delta T = q\Delta\tau$ . Eq. (4.16) would require four numerical integrations per time step which would result in an increase in the computational time and the response would become more sensitive to the incremental time step. From a practical computational perspective eq. (4.16) might not be a viable scheme. But even with this disadvantage, eq. (4.16) represents the generality of the above formulation in a mathematical sense. The simulations presented in the next sections use the semi-discrete format presented in eq. (4.15). An illustration of the implementation of eq. (4.15) is presented in Appendix 4.

## 4.4 Quantitative comparison with Adhikari and Wagner scheme

In this section, to investigate the accuracy of the above derived method a comparative study is performed using the numerical results obtained by Adhikari and Wagner (2004). Two numerical examples were considered in Adhikari and Wagner (2004). The two systems studied consists of a three degree of freedom system and an axially vibrating rod. The convolution damping kernel function for both systems adopt the double exponential model. These examples were also used by Cortes et al. (2009) to show the accuracy of their method. Interestingly in that paper (Cortes et al. 2009), the plot for the second example (axially vibrating rod) disagreed with the original displacement response plotted in the work of Adhikari and Wagner (2004) by an order of $10^2$ which the author considers as a gross conversion error.

### 4.4.1 Example 1 (Three degrees of freedom system)

The three degrees of freedom system considered by Adhikari and Wagner (2004) is shown in Fig. 4.2.

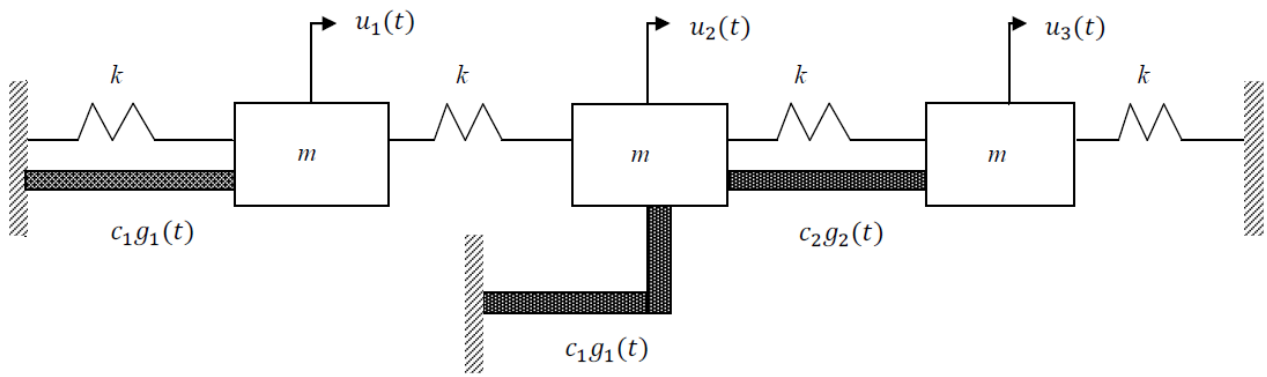


Fig. 4.2 Three degree of freedom model of Adhikari and Wagner

The equation of motion of the system with double exponential damping is given as,

$$\mathbf{M}\ddot{\mathbf{u}}(t)+\int_0^t\left[\mu_1 e^{-\mu_1(t-\tau)}\mathbf{C}_1+\mu_2 e^{-\mu_2(t-\tau)}\mathbf{C}_2\right]\dot{\mathbf{u}}(\tau)d\tau+\mathbf{K}\mathbf{u}(t)=\mathbf{f}(t) \tag{4.17}$$

Over here $\mathbf{M}$ and $\mathbf{K}$ are the mass and stiffness matrices as given below.

$$\mathbf{M}=\begin{bmatrix} m & 0 & 0 \\ 0 & m & 0 \\ 0 & 0 & m \end{bmatrix} \tag{4.18}$$

and

$$\mathbf{K}=\begin{bmatrix} 2k & -k & 0 \\ -k & 2k & -k \\ 0 & -k & 2k \end{bmatrix} \tag{4.19}$$

where $m$ =3.0 kg and $k$ =2.0 N/m.

$\mathbf{C}_1$ and $\mathbf{C}_2$ are the damping coefficient matrices and are given as below,

$$\mathbf{C}_1=\begin{bmatrix} c_1 & 0 & 0 \\ 0 & c_1 & 0 \\ 0 & 0 & 0 \end{bmatrix} \tag{4.20}$$

$$\mathbf{C}_2=\begin{bmatrix} 0 & 0 & 0 \\ 0 & c_2 & -c_2 \\ 0 & -c_2 & c_2 \end{bmatrix} \tag{4.21}$$

where $c_1$=0.6 Ns/m and $c_2$=0.2 Ns/m. Also, $\mu_1$=1.0 $s^{-1}$ and $\mu_2$=5.0 $s^{-1}$ are adopted. The external force vector $\mathbf{f}(t) = \mathbf{0}$ and the initial conditions are given as $\mathbf{u}_0 = \{1 \quad 0 \quad 0\}^T$ and $\dot{\mathbf{u}}_0 = \{0 \quad 0 \quad 0\}^T$. The system response is computed using the method described in section 4.2 and the displacement

response at the first degree of freedom $\mathbf{u}_1(t)$ is plotted in Fig. 4.3. The fundamental period of vibration of the system is 10.05 seconds.

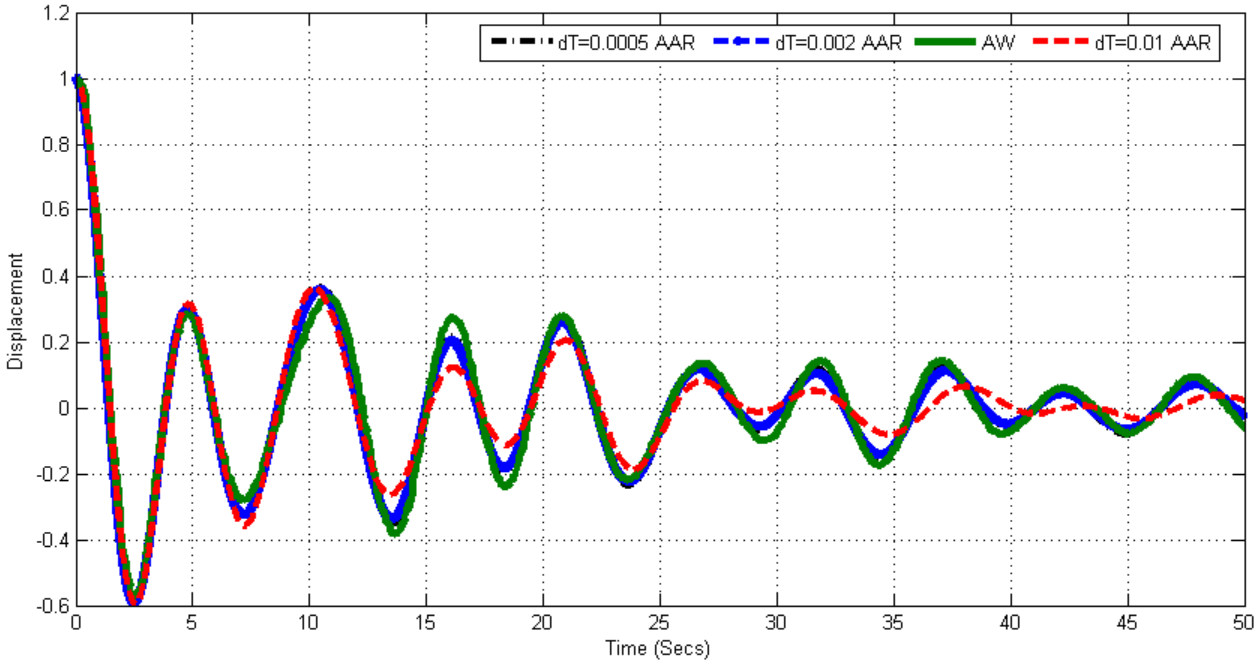


Fig. 4.3 Displacement plot for the first degree of freedom

Fig. 4.3 illustrates the fact that the proposed AAR scheme gives almost the same results as the Adhikari and Wagner method (denoted as AW) and the slight discrepancy (~ less than 1%) exhibited may be considered to be within practical limits. In the figure, 'dT' refers to time step $\Delta T$. It should be remarked that the proposed method requires smaller time steps $(\Delta T \leq 0.002s)$ as compared to the AW method $(\Delta T = 0.02s)$; hence more computational time. As the time step increases $(\Delta T = 0.01s)$, deviation from the expected response could be observed.

### 4.4.2 Example 2 (axial rod problem)

An axially vibrating rod with fixed-free boundary with double exponential damping was considered by Adhikari and Wagner (2004). The system is analysed using 80 beam elements and is shown in Fig. 4.4

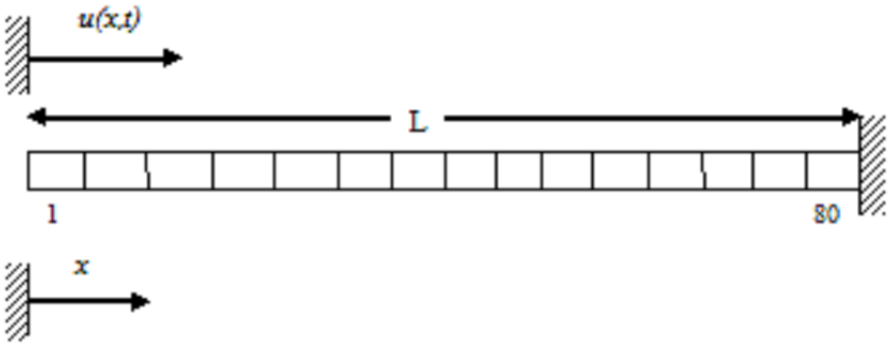


Fig. 4.4 Axially vibrating free fixed rod

The damping kernel $g(t)$ is represented by double exponential model and the equation of motion is given as,

$$\mathbf{M}\ddot{\mathbf{u}}(t)+\int_0^t\left[\mu_1 e^{-\mu_1(t-\tau)}\mathbf{C}_1+\mu_2 e^{-\mu_2(t-\tau)}\mathbf{C}_2\right]\dot{\mathbf{u}}(\tau)d\tau+\mathbf{K}\mathbf{u}(t)=\mathbf{f}(t) \tag{4.22}$$

In this equation, '$\mathbf{M}$' represents an element consistent mass matrix and is given as,

$$\mathbf{M}=\frac{\rho A\ell_e}{6}\begin{bmatrix}2 & 1\\ 1 & 2\end{bmatrix} \tag{4.23}$$

and the stiffness matrix is given as,

$$\mathbf{K}=\frac{AE}{\ell_e}\begin{bmatrix}1 & -1\\ -1 & 1\end{bmatrix} \tag{4.24}$$

$\rho$ is the mass density, $A$ is the cross section area, $E$ is the Young's modulus and $\ell_e = L/80$ is the length of an element. $L$ is the span of the beam. Numerical values adopted for these parameters are $\rho = 7.8x10^3 kg/m^3$, $E = 2x10^{11} N/m^2$, $A = 6.25x10^{-4} m^2$ and $L = 4m$.

$\mathbf{C}_1$ and $\mathbf{C}_2$ are the damping coefficient matrices and are conveniently chosen proportional to mass and stiffness (Adhikari and Wagner, 2004) and given as,

$$\mathbf{C}_1 = \alpha\mathbf{M} \text{ and } \mathbf{C}_2 = \beta\mathbf{K} \tag{4.25}$$

where,

$$\alpha = 2\xi\frac{\omega_i\omega_j}{\omega_i + \omega_j} \text{ and } \beta = 2\xi\frac{1}{\omega_i + \omega_j} \tag{4.26}$$

Here, damping ratio $\xi = 5\%$, and $\omega_i$, $\omega_j$ represents the undamped natural frequencies corresponding to the $i^{th}$ and $j^{th}$ modes. For the simulation studies, $\omega_i = \omega_1$ and $\omega_j = \omega_2$.

$\mu_1$ and $\mu_2$ are the relaxation parameters and are given as below (Adhikari and Wagner, 2004)

$$\mu_1 = \frac{1}{\gamma_1 T_{\min}} \text{ and } \mu_2 = \frac{1}{\gamma_2 T_{\min}} \tag{4.27}$$

where $\gamma_1 = 1$, $\gamma_2 = 2$ and $T_{\min}$ is the minimum period and is given by $T_{\min} = \frac{2\pi}{\omega_{\max}}$. The $\omega_{\max}$ is computed as (Adhikari and Wagner, 2004),

$$\omega_{\max} = \frac{\pi}{2L}(2N-1)\sqrt{\frac{E}{\rho}} \text{ where } N=80. \tag{4.28}$$

The problem is to find the time-domain displacement response at the free end of the rod $\mathbf{u}_1(t)$ subjected to a unit initial velocity at the same end. The forcing vector $\mathbf{f}(t) = \{0\}$ and the initial conditions applied are displacement vector, $\mathbf{u}_0 = \mathbf{0}$ and $\dot{\mathbf{u}}_0 =$ velocity vector with a unit value at the first degree of freedom and zero at all remaining degrees of freedom. The undamped fundamental period of vibration of the rod is 0.0031 seconds.

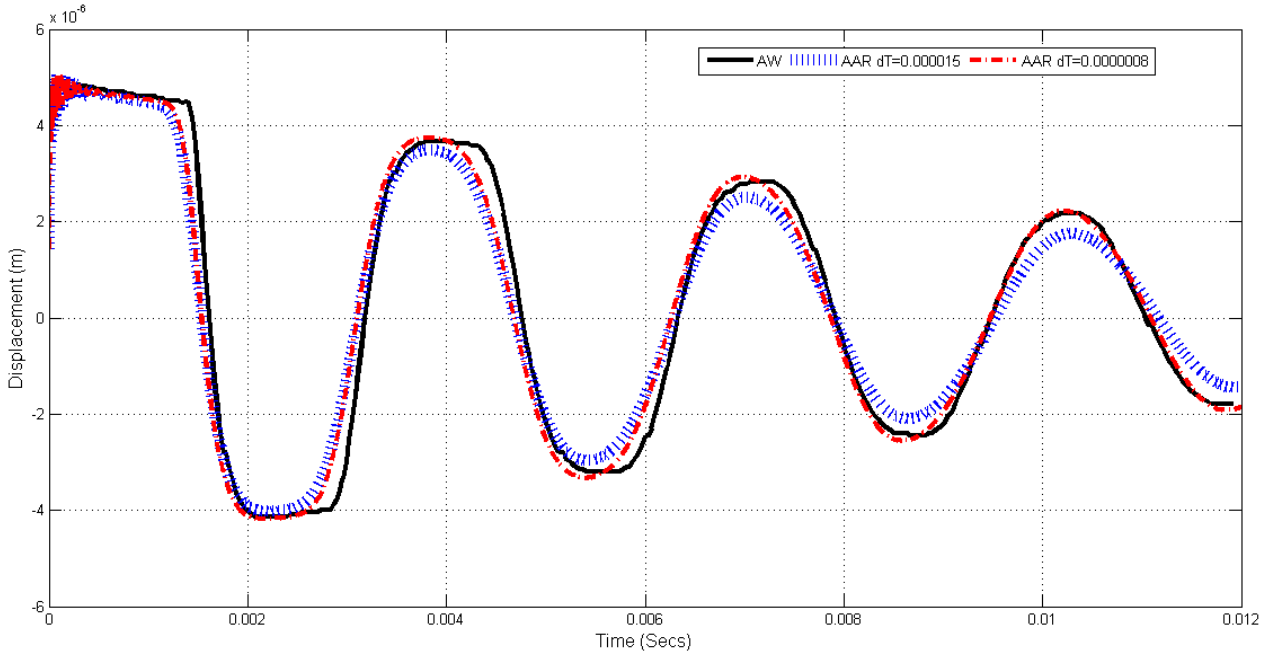


Fig. 4.5 Response of the free end of the rod for both the AW and AAR method

Fig. 4.5 represents the displacement response at the free end of the axially vibrating rod computed by the method of Adhikari and Wagner (2004) and by the method proposed in this chapter. The simulations are done for different time steps to show the sensitivity of the results. It is clear that the proposed method (AAR) gives the same response as produced by the method of Adhikari and Wagner (AW). From the plots smaller time steps $\left(\Delta T = 8x10^{-7}\, s\right)$ are needed for AAR method to arrive at a better accuracy as compared to the AW method where $\Delta T = 1.5x10^{-6}\, s$. But it could also

be seen that even a higher time step, $\Delta T = 1.5x10^{-6} s$ results in a reasonably accurate prediction which reinforces the robustness of the proposed method. The sensitivity towards the choice of time step could be attributed to the assumption of scaled linear variation of the continuous velocity function as given in eq. (4.9). This aspect is further investigated in Section 4.5.

#### *4.4.2.1 Discussion on the result for the axially vibrating rod*

The plot marked as 'AW' in Fig. 4.5 is a digitized version of the plot published in the original paper (Adhikari and Wagner, 2004). Interestingly, the original plot in Adhikari and Wagner, (2004), seems to possess an initial error. So, a further investigation is conducted in this section to review this aspect. The axially vibrating rod described in section 4.4.2 is simulated with the same initial conditions and forcing vector but with two different in-structure damping models. This is done solely to make sure that the initial error observed is a function of the choice of time step adopted in the original paper (Adhikari and Wagner, 2004) and is independent of the damping models. Classical Rayleigh damping model with $\xi = 5\%$ and the convolution double exponential damping model described in section 4.4.2 is used for the present study. For the system with classical Rayleigh model, the responses are computed using the classical Newmark's method described in Appendix 2. The system with convolution damping model is given by eq. (4.22) and is solved using the proposed AAR method given in Appendix 4.

Figs. 4.6a and 4.6b illustrate the initial error in the displacement response as a choice of the time step based on the two different in-structure damping models discussed above. Fig. 4.6a represents the displacement response of the axial vibrating rod problem using the classical Rayleigh damping.

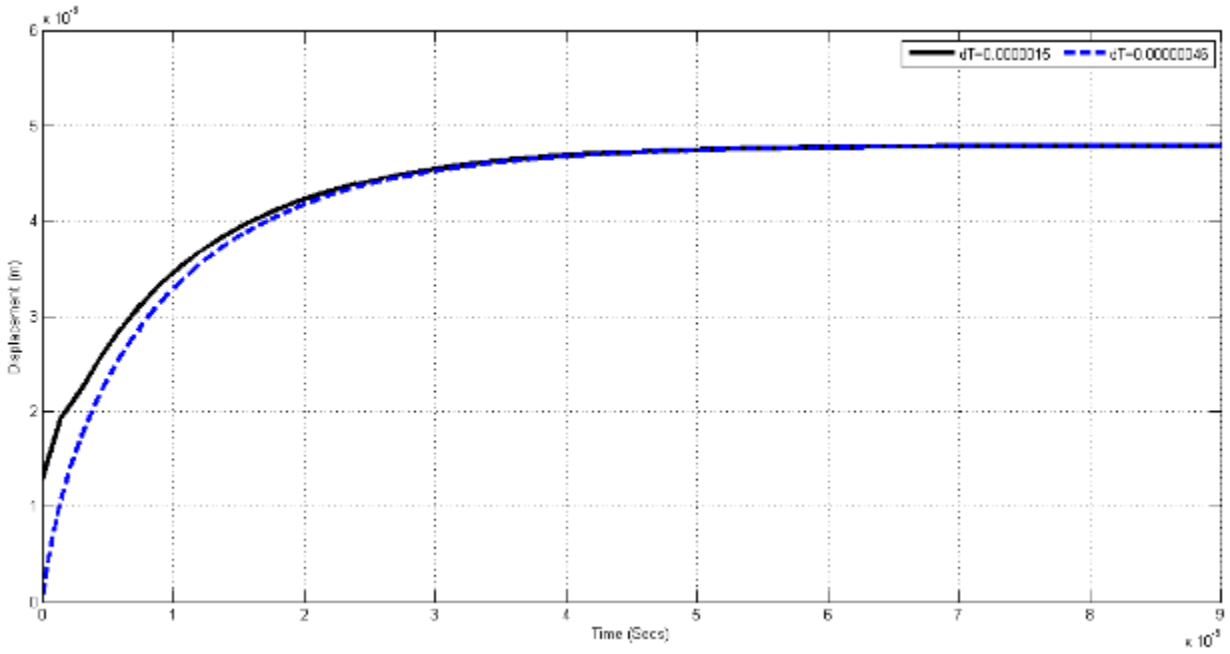


a

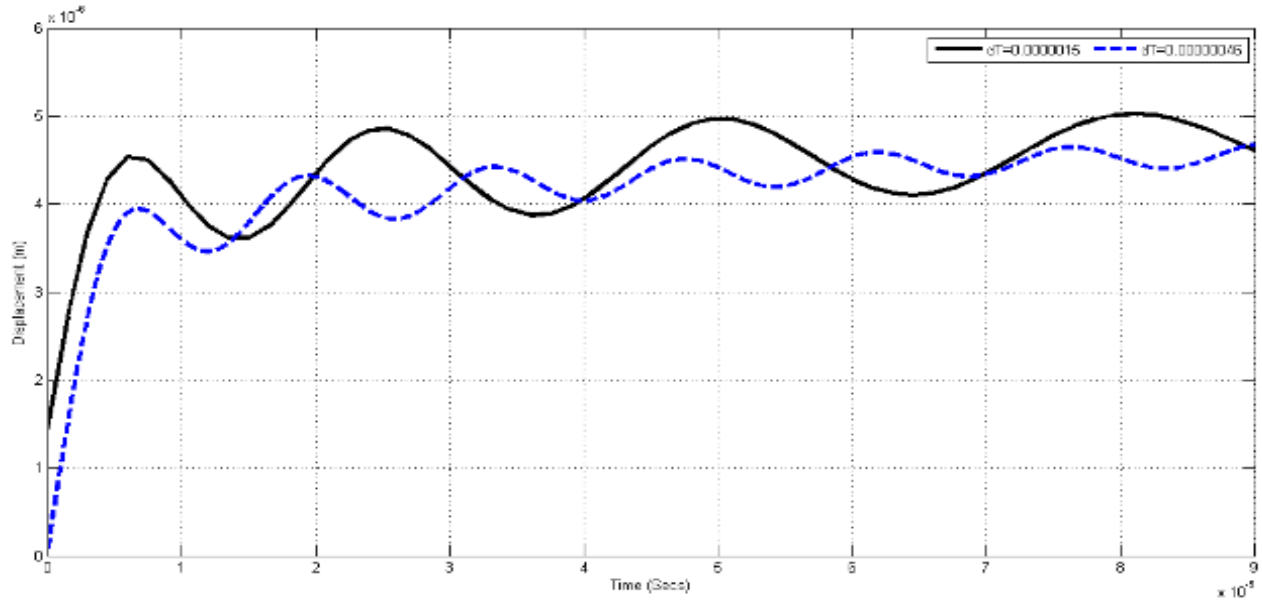


b

Fig. 4.6 a) Illustration of time step error with Rayleigh damping 4.6 b) Illustration of time step error with exponential damping

It is clearly seen that, when $'\Delta T'$ is assumed as $1.5\text{x}10^{-6}$ there is an initial error and a smaller time step show a convergence to zero initial error. Fig. 4.6b illustrates this same phenomenon being exhibited when non-classical convolution damping model based on the double exponential damping kernel is used. It could also be seen clearly that, with $\Delta T = 4.6\times10^{-7}$ the initial error is mitigated in both plots. So, this emphasises the fact that the initial error observed was an issue with the choice of the time step and is independent of the damping models. The problem being an axially vibrating rod, originally itself a much smaller time step was needed. But as the main purpose of the simulation in section 4.4.2 is to compare the accuracy of the proposed formulation with the solutions of Adhikari and Wagner (2004), the same $\Delta T$ as adopted in the original paper was used for comparison.

## 4.5 Study on the sensitivity of the choice of time step

As shown in Section 4.4, the time domain responses of the proposed AAR method are sensitive to the choice of the time step. A further investigation is presented in this section using the problem of the axial beam described in Section 4.4.2, to review the impact of the assumption made in eq. (4.9) and how well it approximates the true nature of variation of velocity within a time step. First, a large time step $'\Delta T'$ is selected and then further velocity response and damping force evaluation is carried out using time steps corresponding to $\Delta T/2, \Delta T/4, \Delta T/8$ and $\Delta T/16$.

Fig. 4.7 represents the variation of the velocity function in an analysis as a choice of time step. In these plots, the initial time step $'\Delta T'$ is assumed to be $1.5\text{x}10^{-6}$ seconds and plotted for a duration of $1.5\text{x}10^{-5}$ seconds, which is equal to $'10\Delta T'$ . From the plot, it is clear that the assumption of linear variation of velocity may not be strictly valid.

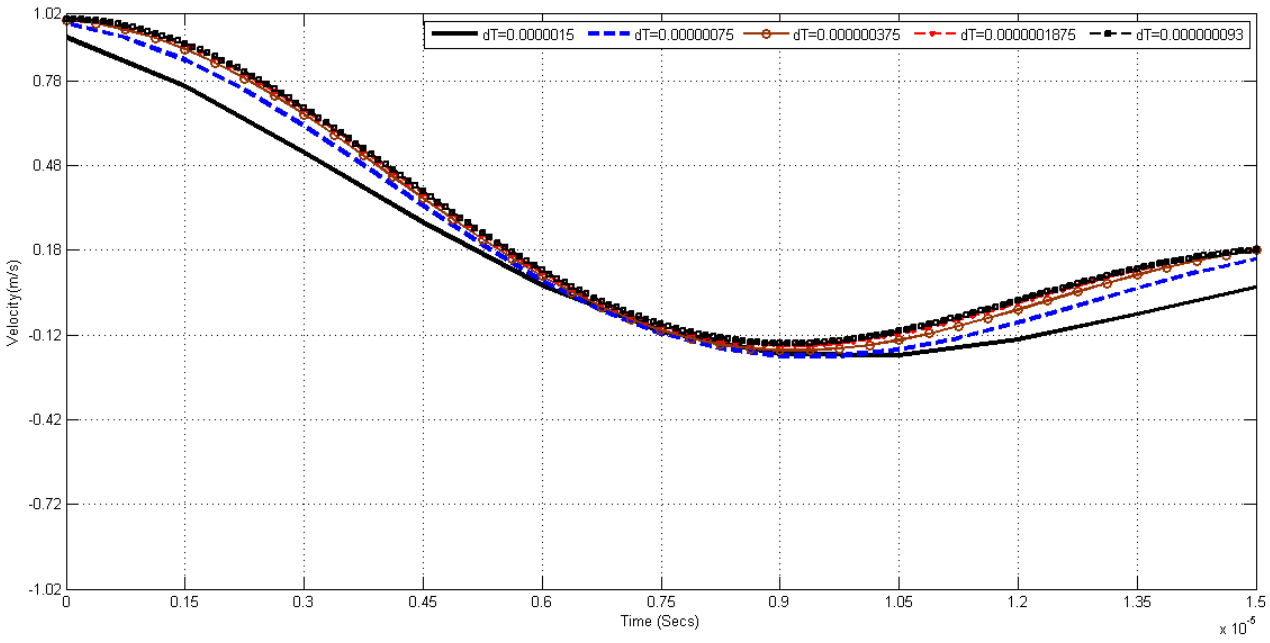


Fig. 4.7 Variation of velocity of the axially vibrating rod.

Fig. 4.8 further investigates the impact of the assumption in eq. (4.9) on the variation of the damping force in an analysis as a choice of time step. As outlined above, this figure also qualitatively reinforces the fact illustrated by Fig. 4.7, that a linear discretising assumption of velocity might not be strictly valid.

Considering the above observations, it could be argued that a better discretising assumption would be the use of a quadratic variation of velocity within the time step. But this may result in the demand for more rigorous integrations and different integration schemes, which in turn may result in making the semi-discrete format presented in eq. (4.15) invalid. This would result in a loss of both efficiency and simplicity of the proposed formulation. So, considering all the practical consequences highlighted, and as the present methodology is based on Newmark's constant average acceleration framework, the author feels that a linear discretisation of the velocity function is imperative and acceptable.

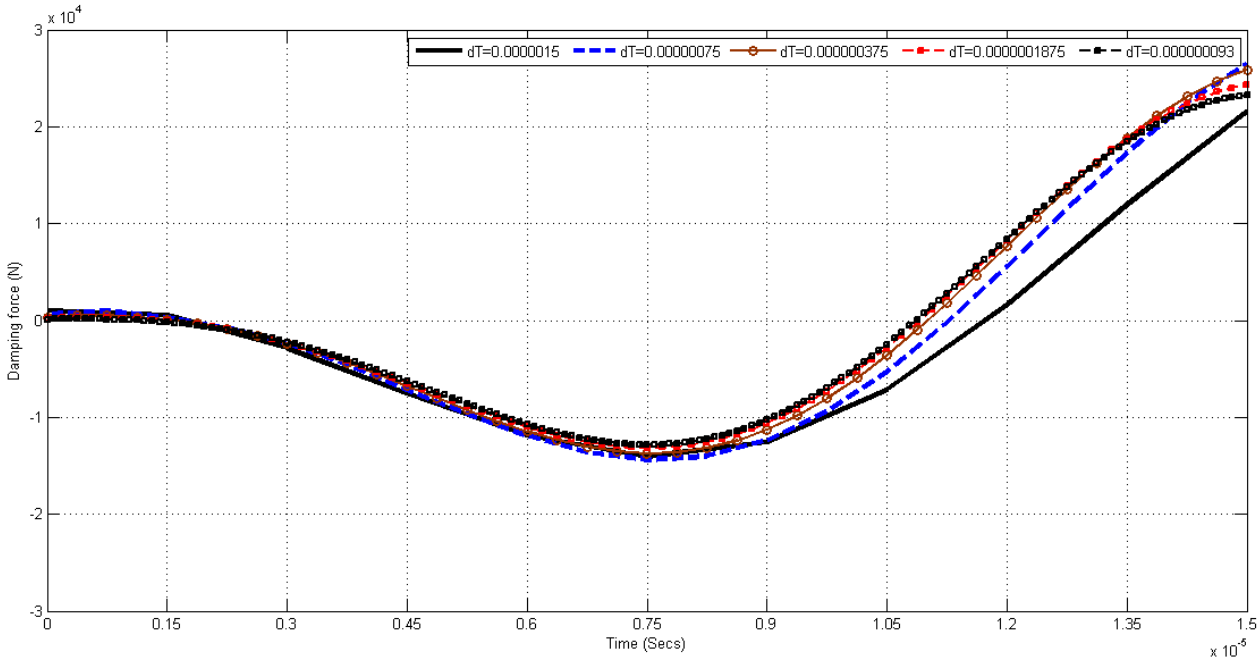


Fig. 4.8 Variation of the damping force of the axially vibrating rod

Reviewing the response calculations in the two examples discussed in Section 4.4, it could be concluded that the required smaller time steps are within practical limits and the use of a larger time step does not result in a large error. So, considering the mathematical simplicity of the AAR scheme and its ease in implementing in a commercial package, an increase in computational time due to smaller time steps should not be considered as a major impediment in accepting this as a viable scheme. Also, it could be argued that with the availability of more powerful computers, smaller time steps do not pose a major problem these days.

## 4.6 Simulation Studies using single exponential and Gaussian models

This section is devoted to demonstrating the generality of the proposed AAR scheme by emphasizing the capability to handle different causal dissipative models which the kernel function $g(t)$ adopts. To do that, numerical simulation studies are carried out on a cantilever steel beam

with kernel dissipative function of eq. (4.1) taking the form of a single exponential and a Gaussian causative model. The implementation scheme for the AAR method is given in Appendix 4. The main difference in the use of different mathematical causal models occurs in the evaluation of the closed form integrals in step 3 given in Appendix 4 (in this case the kernel function $g(t)$ adopts an exponential or Gaussian form). Timoshenko formulation illustrated in Appendix 5 is used to represent the cantilever beam. A 4m long cantilever steel beam of 100mm square cross section and subjected to a constant time independent transverse point load of 100N applied at the free end is adopted for the numerical investigation. Throughout the simulation the applied force is constant so that eventually the steady state would coincide with the static deflection. Material properties adopted are Young's modulus $E = 2x10^{11} N/m^2$ and mass density $\rho = 7.8x10^3 kg/m^3$. The system is analysed using 50 beam elements. The equation of motion for the beam with the respective damping kernel functions would be expressed as,

*Single Exponential Function*

$$\mathbf{M}\ddot{\mathbf{u}}(t) + \int_0^t \mathbf{C}_k \mu_1 e^{-\mu_1(t-\tau)} \dot{\mathbf{u}}(\tau) d\tau + \mathbf{K}\mathbf{u}(t) = \mathbf{f}(t) \tag{4.29}$$

*Gaussian Function*

$$\mathbf{M}\ddot{\mathbf{u}}(t) + \int_0^t 2\sqrt{\frac{\mu_2}{\pi}} e^{-\mu_2(t-\tau)^2} \mathbf{C}_k \dot{\mathbf{u}}(\tau) d\tau + \mathbf{K}u(t) = \mathbf{f}(t) \tag{4.30}$$

Here, $\mathbf{M}$, $\mathbf{C}_k$ and $\mathbf{K}$ represent respectively the mass, damping coefficient and stiffness matrices whereas $\mu_1$ and $\mu_2$ represent relaxation parameters for the two mathematical causal models. The response evaluations of these two systems are performed using the formulation described in

Section 4.2. For both systems, the damping coefficient matrix $\mathbf{C}_k$ has been conveniently adopted as proportional to mass and stiffness (Adhikari and Wagner, 2004) and is given as,

$$\mathbf{C}_k = \alpha\mathbf{M} + \beta\mathbf{K} \tag{4.31}$$

where,

$$\alpha = 2\xi\frac{\omega_i\omega_j}{\omega_i + \omega_j} \text{ and } \beta = 2\xi\frac{1}{\omega_i + \omega_j} \tag{4.32}$$

Here, damping ratio $\xi = 5\%$, $\omega_i$ and $\omega_j$ represent the undamped natural frequencies corresponding to the $i^{th}$ and $j^{th}$ modes, respectively. For the simulation studies, $\omega_i = \omega_1$ and $\omega_j = \omega_4$.

The author notes that the choice of $\mathbf{C}_k$ as given by eq. (4.31), although commonly used in practice (Adhikari and Wagner, 2004), has no explicit physical evidence other than the mathematical convenience it provides for the extension of a single degree of freedom model into a multi-degree of freedom model. Further research is needed to find alternate coefficient matrices so that the resulting damping models could be closer to reality. At this juncture, it must be noted that chapters 5 & 6 illustrate one alternative way of deriving this coefficient matrix which is both physically motivated and mathematically rigorous.

To provide a benchmark for a qualitative understanding of these models, a response plot of the system with classical Rayleigh viscous damping is also presented. The sole purpose of this comparison is to highlight the fact that the use of the convolution damping models along with a proper choice of the relaxation parameter can generate responses similar to the responses of the popular model used in practice; i.e. the "viscous damping model". Readers should note the fact that here viscous damping model is used as the datum for comparison just because of its popularity

in practice and not because it is the "*right damping model*". Issues associated with this model especially in nonlinear dynamics have already been discussed in chapter 2.0.

The equation of motion of such a system is,

$$\mathbf{M}\ddot{\mathbf{u}}(t) + \mathbf{C}\dot{\mathbf{u}}(t) + \mathbf{K}\mathbf{u}(t) = \mathbf{f}(t) \tag{4.33}$$

where,

$$\mathbf{C} = \alpha\mathbf{M} + \beta\mathbf{K} \tag{4.34}$$

Here $\alpha$ and $\beta$ are evaluated by eq. (4.32) using $\xi = 5\%$ and $\omega_i = \omega_1$ and $\omega_j = \omega_4$.

The undamped fundamental period of vibration of the cantilever beam is 0.196 seconds.

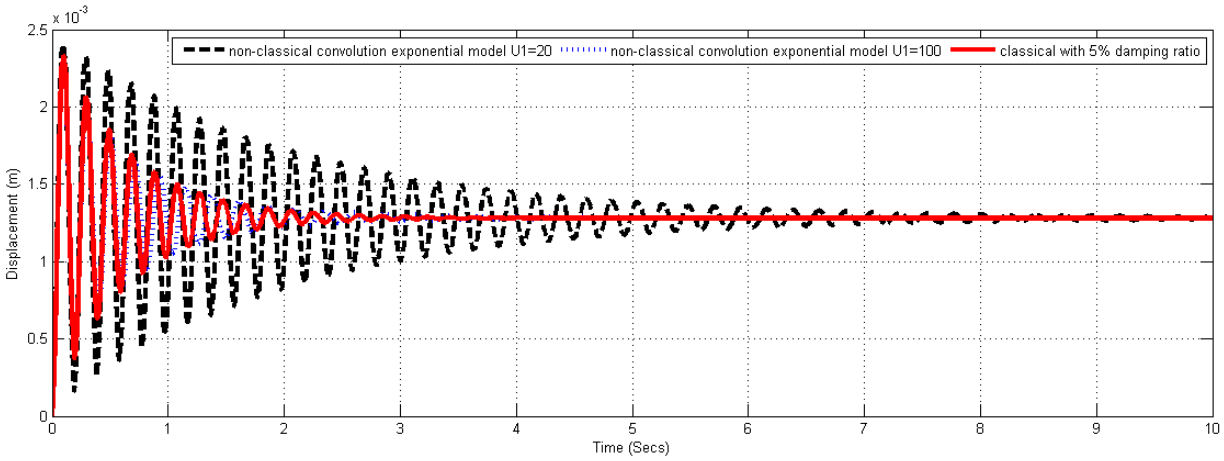


(a)

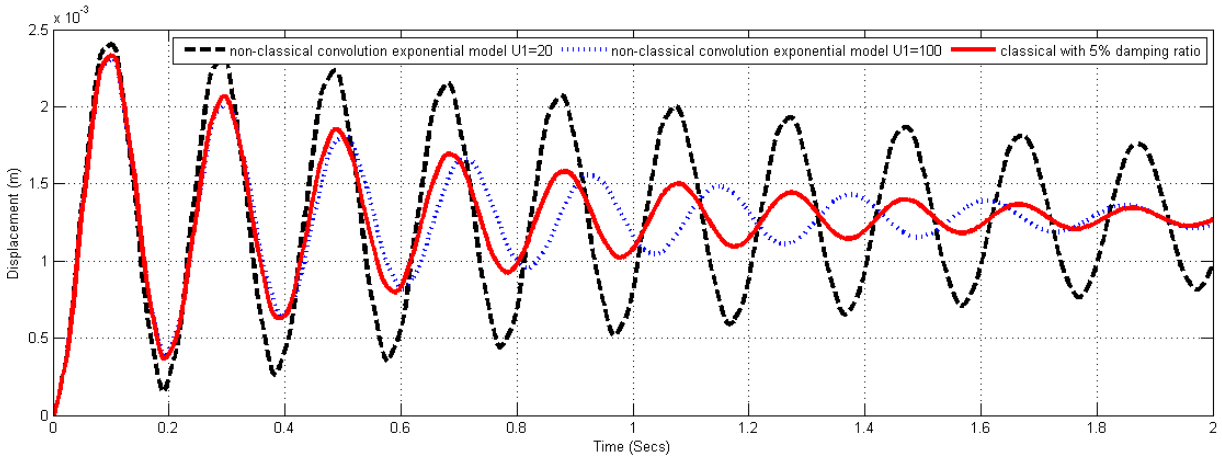


(b)

Fig. 4.9 a) Displacement response of cantilever with exponential model 4.9 b) Zoomed in plot of the displacement response of cantilever with exponential model

Figs. 4.9a, 4.9b and 4.10 depict the displacement response at the free end of the cantilever subjected to a constant transverse load with classical viscous and non-classical convolution damping models. Plots in Figs. 4.9a and 4.9b compare the response of classical viscous and exponential models while plots in Fig. 4.10 compare the classical viscous and Gaussian models.

As the responses are presented only for illustration purpose, the choice of the relaxation parameter $\mu_i (i = 1,2)$ has been arbitrary. For numerical computation, $\Delta T = 0.001\,\text{sec}$ is adopted as the time step and the simulation is performed for a total of 10 seconds (10,000-time steps). A qualitative interpretation of the zoomed-in plots clearly emphasizes the fact that higher values of $\mu_i (i = 1,2)$ give close to viscous response. As many other researchers have also made similar observations (Adhikari, 2007; Newland 1989), this reinforces the applicability and versatility of the proposed scheme.

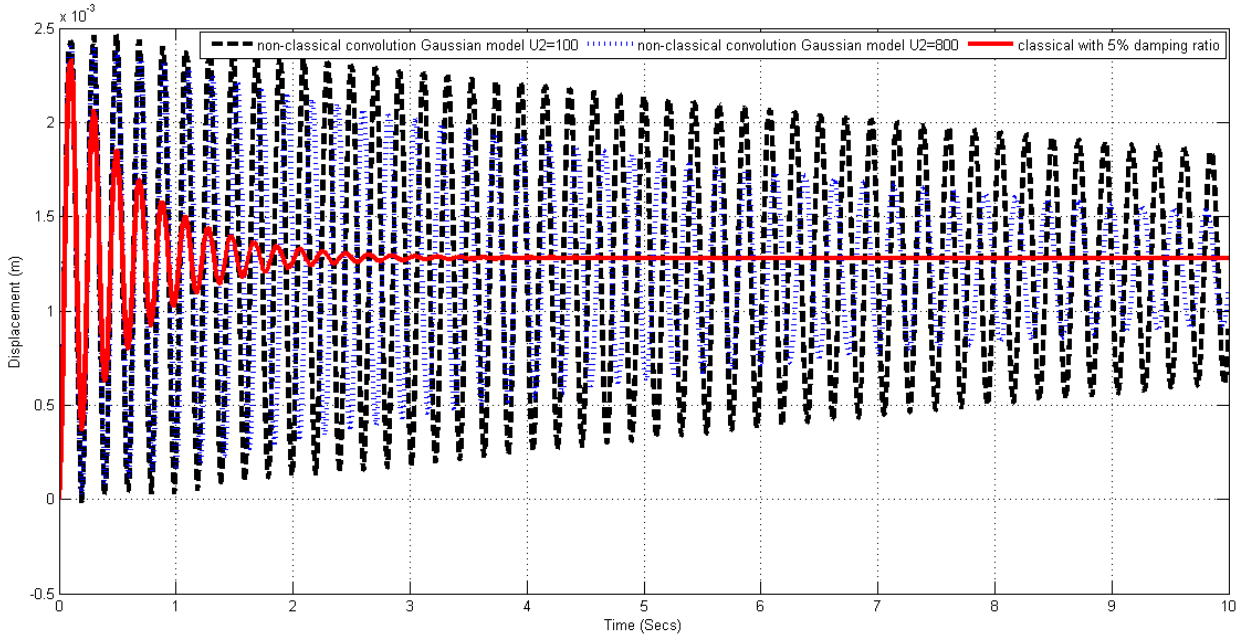


Fig. 4.10 Displacement response of cantilever with Gaussian model

## 4.7 Conclusion

A generic time domain formulation for non-classical convolution damping models is developed in this chapter. The proposed formulation called the AAR scheme is developed using the classical Newmark constant average acceleration framework. To emphasize the accuracy of the proposed scheme, numerical comparisons are presented for a three-degree-of-freedom system and an axially vibrating rod problem reported in literature. The applicability and generality of the proposed scheme is illustrated using numerical simulation of a cantilever beam with damping represented by two different causal dissipative models. Qualitative comparisons between the classical viscous and non-classical convolution damping models are also presented with no specific conclusions drawn on the suitability or applicability of these specific causal models. In contrast to other methods existing in the literature, the proposed method is generic (capable of handling any causal

dissipative models) and could be easily incorporated in an existing commercial package capable of performing dynamic analysis by Newmark integration.

# 5. Adaptation of local continuum damping models to nonlinear dynamic analysis

**Journal (Published)**

Puthanpurayil, A., Lavan., O, Carr, A. and Dhakal, R.P. (2016) Application of local elasticity continuum damping models in Nonlinear Dynamic Analysis. *Bulletin of Earthquake Engineering* https://doi.org/10.1007/s10518-018-0424-7: 27

**Abstract:** In this chapter, the new paradigm developed in chapter 3 is further applied into more mathematically rigorous local continuum damping models. These models are called local continuum models mainly since the damping stress at a point in space is a function of the strain at that point only. Semi-discretization procedures and time domain implementation schemes are outlined in detail. It has been shown that these models can be easily incorporated into the existing commercial software framework with minor modifications. The performance of these proposed models is illustrated by conducting nonlinear dynamic analysis on the same four-story RC frame used in chapter 3. The incremental dynamic analysis (IDA) study presented, outlines the fact that the proposed models perform in a more reliable manner in comparison to the classical global damping models in capturing the inherent damping phenomenon in the nonlinear scenario.

## 5.1 Introduction

Issues associated with the current state of the art in inherent damping models have been outlined in chapter 2. To alleviate the issues identified, Chapter 3 proposes a new paradigm of formulating dissipation phenomenon by defining the damping model at an element level and assembling the

elemental damping matrix in a similar manner to stiffness or mass matrix to obtain the system damping matrix. Two new models, Elemental Rayleigh and Elemental Wilson Penzien damping models, which are the elemental counterparts of the global models were proposed in chapter 3. It was shown that by adopting an elemental modelling approach the above cited issue of the appearance of un-realistic damping forces associated with the Rayleigh damping model is completely removed. Also, it was shown that the elemental models give more realistic estimate for seismic performance assessments; *but it must be remembered that still in these models, the damping force depended only on instantaneous velocities.*

Validity of the assumption of the dependence of damping forces only on instantaneous velocities was investigated by Lord Kelvin (A.E.H Love 1892). Based on a series of experiments on torsional oscillation of wires Lord Kelvin reported that the observed damping phenomenon is hysteretic in nature as the exhibited phenomenon also depended on the previous state of the body (strain history). This observation is in direct contradiction to the assumption that damping forces only depended on instantaneous velocities. Similar observations were made by Adhikari (Adhikari 2000). Though elemental viscous models proposed in chapter 3 is a real pragmatic improvement from a performance point of view and alleviated the issues highlighted in chapter 2, but still as instantaneous velocities are the only *state variables* in both models, it may be concluded that the models are not mimicking the damping phenomenon in the purest physical sense.

### 5.1.1 Motivation and scope

Observations by Lord Kelvin give a direct indication of the nature of the mathematical model needed to represent the dissipation phenomenon; the observations clearly show that the mathematical model representing the damping phenomenon should depend on the response history as well. Motivated from these facts and in quest for a more realistic representation of the damping

phenomenon in nonlinear dynamic analysis, in this chapter, the new paradigm of elemental damping modelling proposed in chapter 3, is extended to the more mathematically rigorous continuum damping models. Two advanced models already existing in literature are adapted to the nonlinear dynamic analysis domain; one is the time hysteresis model (Banks and Inman 1991) and the other is the classical Kelvin-Voigt model (Clough and Penzien 2003; Humar 2002; Banks and Inman 1991). Out of the two models, Time hysteresis model could be considered as a model in line with Lord Kelvin's observations as it depends on the strain history and exhibits hysteretic behavior. On the other hand, Kelvin-Voigt is not a hysteretic model and could be considered as a continuum version of the classical Rayleigh model. Adaptation of this model is presented in this chapter to provide a completeness to the investigation of local continuum damping models.

Scope of the present chapter mainly includes the Finite Element implementation of these models and the performance evaluation of these adapted models in nonlinear dynamic analysis based on a numerical study using a four story RC frame building designed as per Eurocodes. It should be noted that the Finite element discretization and implementation of Kelvin Voigt model is already recorded in the literature (Humar 2002; Clough and Penzien 2003) and mainly applied to elastic dynamic analysis; but as far as the author is aware none of the literature records the extension of the Kelvin Voigt model into the nonlinear scenario. Only classical Euler-Bernoulli beam enhanced with local continuum damping models are used in the present study. Simple empirical parameterization based on dimensional homogeneity presented in chapter 3 is adopted for the easy adaptation of the models to a practical inelastic analysis scenario. The incremental dynamic analysis study (IDA) presented, qualitatively highlights the fact that local continuum damping models can give more reliable results in comparison to the classical global Rayleigh damping models.

### 5.1.2 Overview of the local continuum damping models

Fig. 5.1 gives the broad generic classification of the local continuum damping models. In the present study, the implementation schemes are developed for all models and their performance is assessed using IDA study.

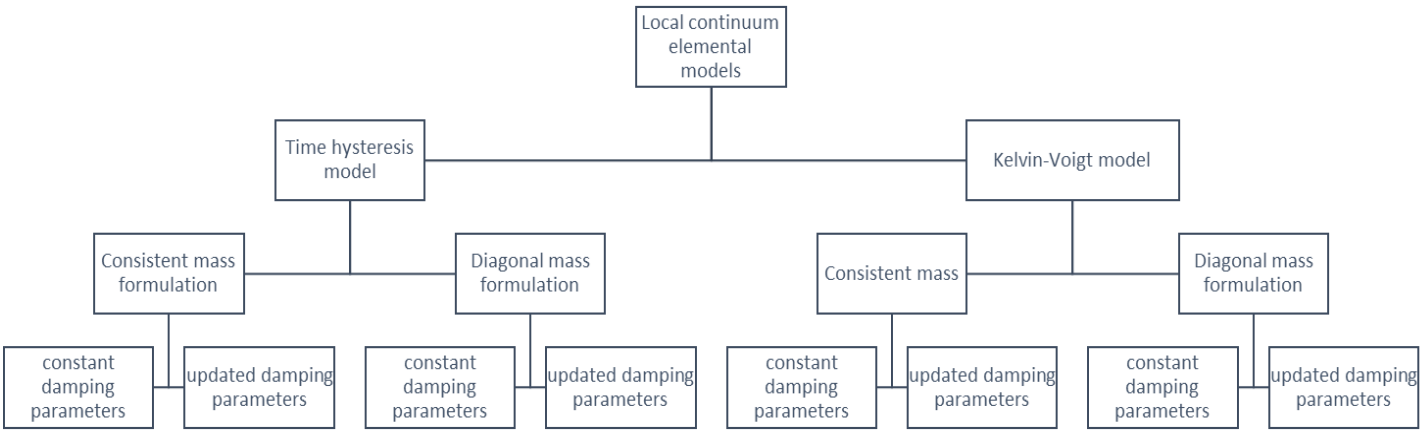


Fig. 5.1 Schematic generic classification of the local continuum damping models

## 5.2 Adaptation of local Continuum damping models into seismic analysis

This section describes in detail the Galerkin procedure used for the partial discretization of damping enhanced Euler-Bernoulli beam continuum and their parameterization adaptation based on dimensional homogeneity principles. Both time hysteresis and Kelvin-Voigt damping models are discussed. In both formulations, air damping is assumed to be represented by an external viscous damping mechanism (Humar 2002). First time hysteresis damping model is presented followed by Kelvin-Voigt damping model.

### 5.2.1 Time hysteresis model

Hysteretic nature of damping calls for a dependence of the stress on the strain history (Love A.E.H,1892). So, a quest for a better model which depends on the strain history is imperative. Golla and Hughes (Golla and Hughes, 1985) propose that one way to do this is by assuming that damping is due to material viscoelasticity in which the instantaneous stress depends not only on the instantaneous strain but also on the history of strain. Closely following their footsteps, in this section, a detailed derivation of the equation of motion for the transverse vibration of a classical Euler Bernoulli beam enhanced with time hysteresis model (Boltzmann type viscoelasticity) is presented. Galerkin partial discretization procedure is outlined for the successful finite element implementation. Main motivation is to adapt this more mathematically rigorous linear damping model into the nonlinear dynamic analysis scenario with possible minor changes in the existing computational framework adopted in a commercial software.

As per Golla and Hughes, visco-elastic stress-strain relation in continuum format is given as,

$$\sigma(x,t) = E\left( \varepsilon(x,t) + \int_0^t g(t-\tau)\frac{\partial \varepsilon(x,\tau)}{\partial \tau} d\tau \right) \tag{5.1}$$

where '*x'* denotes the spatial component and *'t'* denotes the time component; $\sigma(x,t)$ is the instantaneous stress; *E* is the modulus of elasticity; $\varepsilon(x,t)$ is the instantaneous strain and $g(t-\tau)$ is the kernel relaxation/damping function.

#### *5.2.1.1 Derivation of the time hysteresis enhanced Euler-Bernoulli beam equation*

As per classical mechanics framework, assuming a fiber model for the beam and linear strain distribution, the strain at any point 'z' on the beam from the neutral axis is given as,

$$\varepsilon(x,t) = \varepsilon_0(x,0) + \kappa(x,t)z \tag{5.2}$$

where, $\kappa(x,t)$ is the slope of the strain diagram, $\varepsilon_0$ is the initial uniform axial strain before bending.

Substituting eq. (5.2) in eq. (5.1),

$$\sigma(x,t) = E\left( \varepsilon_0(x,0) + \kappa(x,t)z + \int_0^t g(t-\tau)\frac{\partial(\varepsilon_0 + \kappa(x,\tau)z)}{\partial\tau}d\tau \right) \tag{5.3}$$

As per classical mechanics, moment *M* is given as,

$$M = \int_A \sigma(x,t)z dA \tag{5.4}$$

where *dA* refers to the differential area.

Now substituting eq. (5.3) in eq. (5.4), and assuming initial strain $\varepsilon_0 = 0$, we get,

$$M = EI(x,t)\kappa(x,t) + \int_0^t EI(x,t)g(t-\tau)\frac{\partial\kappa(x,\tau)}{\partial\tau}d\tau \tag{5.5}$$

where $I = \int_A z^2 dA$ is the second moment of area. As per classical Bernoulli hypothesis, the slope of the strain is also the curvature and eq. (5.5) can be rewritten as,

$$M = -\left( EI(x,t)\frac{\partial^2 w(x,t)}{\partial x^2} + \int_0^t EI(x,t)g(t-\tau)\frac{\partial}{\partial\tau}\left(\frac{\partial^2 w(x,\tau)}{\partial x^2}\right)d\tau \right) \tag{5.6}$$

where curvature $\kappa(x,t) = -\dfrac{\partial^2 w(x,t)}{\partial x^2}$

Now by D'Alemberts principle,

$$\rho A(x)\frac{\partial^2 w(x,t)}{\partial t^2} = -\frac{\partial^2}{\partial x^2}\left( EI(x,t)\frac{\partial^2 w(x,t)}{\partial x^2} + \int_0^t EI(x,t)g(t-\tau)\frac{\partial}{\partial \tau}\left( \frac{\partial^2 w(x,\tau)}{\partial x^2} \right) d\tau \right) \tag{5.7}$$

Now collecting all the terms on one side and equating with the applied loading we get the time hysteresis enhanced Euler-Bernoulli beam continuum equation as follows,

$$\rho A(x)\frac{\partial^2 w(x,t)}{\partial t^2} + \int_0^t EI(x,t)g(t-\tau)\frac{\partial}{\partial \tau}\left( \frac{\partial^4 w(x,\tau)}{\partial x^4} \right) d\tau + EI(x,t)\frac{\partial^4 w(x,t)}{\partial x^4} = f(x,t) \tag{5.8}$$

*5.2.1.2 Semi-discretization (spatial) of the time hysteresis damping enhanced Euler Bernoulli beam*

Euler Bernoulli beam continuum enhanced with time hysteresis damping model along with $\gamma_{air}$ representing the viscous damping constant is given as,

$$\rho A(x,t)\frac{\partial^2 w(x,t)}{\partial t^2} + \int_0^t EI(x,t)g(t-\tau)\frac{\partial}{\partial \tau}\left( \frac{\partial^4 w(x,\tau)}{\partial x^4} \right) d\tau + \gamma_{air}\frac{\partial w(x,t)}{\partial t} + EI(x,t)\frac{\partial^4 w(x,t)}{\partial x^4} = f(x,t) \tag{5.9}$$

To simplify the presentation, initial conditions are assumed to be zero and the boundary conditions are not explicitly listed as the semi-discretization is applicable to a variety of boundary conditions. Applying Galerkin procedure,

$$\int_0^{L_e} \delta^T(x)\left( \rho A(x)\frac{\partial^2 w(x,t)}{\partial t^2} + \int_0^t EI(x,t)g(t-\tau)\frac{\partial}{\partial \tau}\left( \frac{\partial^4 w(x,\tau)}{\partial x^4} \right) d\tau + \gamma_{air}\frac{\partial w(x,t)}{\partial t} + EI(x,t)\frac{\partial^4 w(x,t)}{\partial x^4} - f(x,t) \right) dx = 0 \tag{5.10}$$

Except for the time hysteresis term, rest of the terms follows standard Finite Element procedures. So, proceeding further with this term only by interchanging the order of integration and integrating by parts only the space term,

$$\int_0^t g(t-\tau)\int_0^{L_e}\delta^T(x)EI(x,t)\frac{\partial}{\partial\tau}\left(\frac{\partial^4 w(x,\tau)}{\partial x^4}\right)dxd\tau = \int_0^t g(t-\tau)\frac{\partial}{\partial\tau}\left(\begin{array}{l}\delta^T(x)EI(x,t)\dfrac{\partial^3 w(x,\tau)}{\partial x^3}\Big]_0^{L_e} \\ -\dfrac{\partial\delta^T(x)}{\partial x}EI(x,t)\dfrac{\partial^2 w(x,\tau)}{\partial x^2}\Big]_0^{L_e} \\ +\displaystyle\int_0^{L_e}\frac{\partial^2\delta^T(x)}{\partial x^2}EI(x,t)\frac{\partial^2 w(x,\tau)}{\partial x^2}dx\end{array}\right)d\tau \tag{5.11}$$

Assuming the boundary terms in eq. (5.11) to be satisfied and expressing the transverse displacements as,

$$w(x,\tau) = \mathbf{N}(x)\mathbf{d}_e(\tau) \tag{5.12}$$

and substituting these terms into eq. (5.11) the semi-discretized damping term can be given as follows,

$$\int_0^t g(t-\tau)\int_0^{L_e}\delta^T(x)EI(x,t)\frac{\partial}{\partial\tau}\left(\frac{\partial^4 w(x,\tau)}{\partial x^4}\right)dxd\tau = \int_0^t\left(\int_0^{L_e}\frac{\partial^2\mathbf{N}^T(x)}{\partial x^2}g(t-\tau)EI(x,t)\frac{\partial^2\mathbf{N}(x)}{\partial x^2}dx\right)\mathbf{d}_e(\tau)d\tau \tag{5.13}$$

Over here $\mathbf{N}(x)$ is the standard Hermitian cubic shape function and $\mathbf{d}_e(\tau)$ is the generalized coordinates. So, from an implementation point of view, the damping force vector can be given as,

$$F_{damping} = \int_0^t \mathbf{K}_e g(t-\tau)\dot{\mathbf{d}}_e(\tau)d\tau \tag{5.14}$$

Over here, $\mathbf{K}_e$ is the elemental stiffness. Now the generic semi-discretized equation of motion for the beam element is given as,

$$\mathbf{M}_e\ddot{\mathbf{d}}_e(t)+\mathbf{C}_{eair}\dot{\mathbf{d}}_e(t)+\int_0^t \mathbf{K}_e g(t-\tau)\dot{\mathbf{d}}_e(\tau)d\tau+\mathbf{K}_e\mathbf{d}_e(t)=\mathbf{f}_e(t) \tag{5.15}$$

where,

$$\left.\begin{aligned}\mathbf{M}_e &= \int_0^{L_e}\mathbf{N}^T(x)\rho A(x)\mathbf{N}(x)dx \\ \mathbf{K}_e &= \int_0^{L_e}\frac{\partial^2\mathbf{N}^T(x)}{\partial x^2}EI(x,t)\frac{\partial^2\mathbf{N}(x)}{\partial x^2}dx \\ \mathbf{C}_{eair} &= \int_0^{L_e}\mathbf{N}^T(x)\gamma_{air}\mathbf{N}(x)dx=\frac{\gamma_{air}}{\rho A_e}\mathbf{M}_e\end{aligned}\right\} \tag{5.16}$$

Any causal model which makes the damping functional non-negative can be considered as a suitable candidate for the kernel function. In this present study, the damping kernel function is adopted as an exponential one and is of the form as given in Chai and Kowalsky (2015),

$$g(t-\tau)=\frac{T_n}{\eta}e^{-\frac{1}{\eta}(t-\tau)}=\mu T_n e^{-\mu(t-\tau)}=\theta e^{-\frac{\theta}{T_n}(t-\tau)} \tag{5.17}$$

where $\eta$ is the relaxation time, $T_n$ is the fundamental period, $\mu = 1/\eta$ and $\theta = \mu T_n$

For a successful implementation of eq. (5.15) in a generic nonlinear dynamic analysis, two parameters $\mu$ and $\gamma_{air}$ need to be identified. A standard practice would be to identify these constant parameters by experimental measurements. But this might not be a viable option for a practical dynamic analyst undertaking a nonlinear dynamic analysis of a structure. So, in this study, the parameters are identified by a methodology which relies on satisfying the dimensional

homogeneity of the equations of motion given by eq. (5.15). Dimensional analysis of eq. (5.15) leads to,

$$\left.\begin{aligned}\mu &= \xi_{eTH_1}\left(\frac{\omega_e^i\omega_e^j}{\omega_e^i+\omega_e^j}\right)\\ \gamma_{air} &= \rho A_e \xi_{eTH_2}\left(\frac{\omega_e^i\omega_e^j}{\omega_e^i+\omega_e^j}\right)\end{aligned}\right\} \tag{5.18}$$

Eq. (5.18) represents the most generic form of computing the $\mu$ and $\gamma_{air}$. It should be noted here that there is absolutely no necessity to adopt the form of parameterization as described in eq. (5.18); Any dimensionally consistent form can be used for the parameterization of $\mu$ and $\gamma_{air}$. If better parametrizing options are available $\xi_{eTH_1}$ and $\xi_{eTH_2}$ can be parametrized explicitly; but for the present study we assume $\xi_{eTH_1} = \xi_{eTH_2} = \xi_{eTH}$. So, in effect the only parameter that needs to be quantified is $\xi_{eTH}$. To simplify the quantification especially from a modelling perspective, a free vibration response matching with the classical Rayleigh damping model is adopted as proposed in chapter 3. This simple method relies on matching the free vibration response of the system equipped with time hysteresis damping model to that of the response of the system with Rayleigh damping model. The underlying assumption in this method of parametrization is that in the elastic case both models (classical Rayleigh and Time hysteresis) should give very similar results and deviations only start to surface when the system gets nonlinear. As compared to Kelvin-Voigt described in the section 5.2.2, unfortunately no simple direct closed form expression exists; but as far as the implementation is concerned the free vibration parameter can be automated and has been already successfully implemented in the commercial software *Ruaumoko* maintained by Professor Athol Carr.

*5.2.1.3 Types of elemental time hysteresis damping based on modelling approaches adopted*

Broad classification of the time hysteresis damping model is depicted in fig. 5.1. Time hysteresis damping can be differentiated based on the way the mass formulations are used for the damping matrix computation. Detailed description ofthe mass formulations are given in section 5.4. Two further subclasses are obtained for each of the mass formulations and they are as explained below. One thing that needs to be noted is that in both these subclasses tangent stiffness is used for the computation of the coefficient matrix. It is also possible to incorporate the initial stiffness for the computation of the damping coefficient matrix; but the present study presents no further investigation in this regard as tangent stiffness represents the most generic framework.

a. *Constant elemental damping proportional parameters*

Over here both the damping proportional parameters $\mu$ and $\gamma_{air}$ are computed at the beginning of the analysis for all elements and remain constant throughout the analysis.

b. *Updated damping proportional parameters*

Over here, both the damping proportional parameters $\mu$ and $\gamma_{air}$ are updated every time step to reflect the current state of the element. It could be argued that this type of modelling represents a very generic scenario especially due to the fact that elemental properties change when they enter the nonlinear range. The change in the so called elemental properties will affect the deformations associated with the element and hence will affect the modal properties of the element. So, updating the damping constant parameters reflect these changes.

### 5.2.2 Kelvin Voigt Model

This section describes the semi-discretization procedure and the parametrization methodology proposed for the adaptation of the Kelvin Voigt damping model in nonlinear seismic dynamic analysis. It must be noted that semi-discretization procedure for Kelvin-Voigt using variational method is outlined in Clough and Penzien (Clough and Penzien 2003), though, there is no explicit reference to the damping model used in the context as Kelvin-Voigt. So, for mathematical completeness the discretization procedure is presented in section 5.2.2.1 using Galerkin method. Kelvin-Voigt damping model is also called the strain rate damping as it represents the resistance to internal strain. Ideally, Kelvin-Voigt damping model may be applied to any vibrating *elastic* system. In this chapter, an adaptation of this model into nonlinear dynamic analysis is proposed.

One of the main motivation in adapting the Kelvin-Voigt damping to the nonlinear scenario is due to the fact that after semi-discretization, the Kelvin-Voigt damping term reduces to a damping coefficient matrix proportional to elemental stiffness whereas the external damping term arrives at a coefficient matrix proportional to elemental mass; so in effect this model is very similar in format to the classical Rayleigh damping model applied at elemental level as proposed in chapter 3 and as a result is easily implementable in any commercial software platform capable of carrying out nonlinear dynamic analysis using classical Rayleigh damping.

#### *5.2.2.1 Semi-discretization of Kelvin Voigt damping enhanced Euler-Bernoulli beam*

The strong form of the Kelvin-Voigt damping enhanced Euler-Bernoulli beam along with external viscous damping model is given as below,

$$\rho A(x)\frac{\partial^2 w(x,t)}{\partial t^2} + F_{\text{int}}(x,t) + F_{ext}(x,t) + \frac{\partial^2}{\partial x^2}\left( EI(x,t)\frac{\partial^2 w(x,t)}{\partial x^2} \right) = f(x,t) \qquad (5.19)$$

where,

$F_{\text{int}}(x,t)=\frac{\partial^2}{\partial x^2}\left(c_s I(x,t)\frac{\partial^3 w(x,t)}{\partial t\partial x^2}\right)$ is the internal damping force caused by internal resistance to the straining of the material and $F_{ext}(x,t)=\gamma_{air}\frac{\partial w(x,t)}{\partial t}$ is the external damping force. *'x'* refers to the spatial ordinate and *'t'* refers to the time ordinate. To simplify the presentation, initial conditions are assumed to be zero and the boundary conditions are not explicitly listed as the semi-discretization is applicable to a variety of boundary conditions. $\rho, A(x), E$ & $I(x)$ refer to material density, geometric area, modulus of elasticity and second moment of area of the beam continuum. $f(x,t)$ is the externally applied load; $w(x,t)$ is the transverse displacement; $c_s$ refers to the damping coefficient which converts strain rate into stress and $\gamma_{air}$ is the external air damping coefficient. Assuming $\delta(x)$ as the test function, the weak form of eq. (5.19) is given as,

$$\int_0^{L_e}\delta^T(x)\left(\rho A(x)\frac{\partial^2 w(x,t)}{\partial t^2}+\frac{\partial^2}{\partial x^2}\left(c_s I(x,t)\frac{\partial^3 w(x,t)}{\partial t\partial x^2}\right)+\gamma_{air}\frac{\partial w(x,t)}{\partial t}+\frac{\partial^2}{\partial x^2}\left(EI(x,t)\frac{\partial^2 w(x,t)}{\partial x^2}\right)-f(x,t)\right)dx=0 \tag{5.20}$$

Here $L_e$ is the element length. Now doing integration by parts and collecting all the boundary terms on the right-hand side, the eq. (5.20) becomes,

$$\int_0^{L_e}\delta^T(x)\rho A(x)\frac{\partial^2 w(x,t)}{\partial t^2}dx+\int_0^{L_e}\frac{\partial}{\partial t}\left(\frac{\partial^2\delta^T(x)}{\partial x^2}c_s I(x,t)\frac{\partial^2 w(x,t)}{\partial x^2}\right)dx+\int_0^{L_e}\delta^T(x)\gamma_{air}\frac{\partial w(x,t)}{\partial t}dx$$
$$\int_0^{L_e}\frac{\partial^2\delta^T(x)}{\partial x^2}EI(x,t)\frac{\partial^2 w(x,t)}{\partial x^2}dx-\int_0^{L_e}\delta^T(x)f(x,t)dx=-c_s I(x,t)\frac{\partial}{\partial t}\left(\left(\delta^T(x)\frac{\partial^3 w(x,t)}{\partial x^3}\right)_0^{L_e}-\left(\frac{\partial\delta^T(x)}{\partial x}\frac{\partial^2 w(x,t)}{\partial x^2}\right)_0^{L_e}\right)$$
$$-EI(x,t)\left(\left(\delta^T(x)\frac{\partial^3 w(x,t)}{\partial x^3}\right)_0^{L_e}-\left(\frac{\partial\delta^T(x)}{\partial x}\frac{\partial^2 w(x,t)}{\partial x^2}\right)_0^{L_e}\right) \tag{5.21}$$

Assuming the boundary conditions to be satisfied in eq. (5.21) and decoupling the transverse displacement in space and time as,

$$w(x,t) = \mathbf{N}(x)\mathbf{d}_e(t) \tag{5.22}$$

where $\mathbf{N}(x)$ is the row vector of shape functions and $\mathbf{d}_e(t)$ is the vector of generalized coordinates. Substituting eq. (5.22) into eq. (5.21) and assuming $f(x,t) = 0$ for the sake of brevity,

$$\begin{aligned}&\int_0^{L_e} \mathbf{N}^T(x)\rho A(x)\mathbf{N}(x)dx\ddot{\mathbf{d}}_e(t) + \int_0^{L_e} \frac{\partial^2 \mathbf{N}^T(x)}{\partial x^2} c_s I(x,t) \frac{\partial^2 \mathbf{N}(x)}{\partial x^2} dx\dot{\mathbf{d}}_e(t) + \int_0^{L_e} \mathbf{N}^T(x)\gamma_{air}\mathbf{N}(x)dx\dot{\mathbf{d}}_e(t) \\ &+ \int_0^{L_e} \frac{\partial^2 \mathbf{N}^T(x)}{\partial x^2} EI(x,t) \frac{\partial^2 \mathbf{N}(x)}{\partial x^2} dx\mathbf{d}_e(t) = \mathbf{0}\end{aligned} \tag{5.23}$$

Employing standard $C^1$ Hermitian shape functions, the first and the last term culminates as standard elemental mass and elemental stiffness matrices.

The second and third terms in eq. (5.23) are the damping terms. Employing the standard $C^1$ Hermitian shape functions, the damping coefficient matrix for the intrinsic damping term $\mathbf{C}_{int}$ is given as,

$$\mathbf{C}_{int} = c_s \frac{1}{E}\mathbf{K}_e \tag{5.24}$$

Similarly, the external damping term $\mathbf{C}_{ext}$ is given as,

$$\mathbf{C}_{ext} = \frac{\gamma_{air}}{\rho A(x)}\mathbf{M}_e \tag{5.25}$$

A closer observation on the eqs. (5.24) and (5.25) would make the fact evident that this can be implemented very similar to elemental Rayleigh damping as described in chapter 3. Motivated

from this fact, two new proportionality constants can be developed for Kelvin-Voigt damping model representing intrinsic damping as,

$$\left.\begin{aligned}\beta_{KV} &= \frac{c_s}{E} \\ \alpha_{KV} &= \frac{\gamma_{air}}{\rho A(x)}\end{aligned}\right\} \tag{5.26}$$

So, the damping coefficient matrix using Kelvin-Voigt damping at element level is given as,

$$\mathbf{C}_{eKV} = \alpha_{KV}\mathbf{M}_e + \beta_{KV}\mathbf{K}_e \tag{5.27}$$

The consolidated spatially discretized Kelvin-voigt damping enhanced Euler Bernoulli beam equation can now be given as

$$\mathbf{M}_e\ddot{\mathbf{d}}_e(t) + \mathbf{C}_{eKV}\dot{\mathbf{d}}_e(t) + \mathbf{K}_e\mathbf{d}_e(t) = \mathbf{f}_e(t) \tag{5.28}$$

where all the coefficient matrices are as described in this section; $\ddot{\mathbf{d}}_e(t), \dot{\mathbf{d}}_e(t)$ and $\mathbf{d}_e(t)$ represent the elemental acceleration, velocity and displacement.

*5.2.2.2 Parameterization for Kelvin Voigt model*

For a successful implementation of this model, both damping parameter constants $c_s$ and $\gamma_{air}$ should be parameterized. One way to estimate these coefficients is through experimental modal analysis (Banks and Inman 1991). But this method might not be practical for a practicing engineer doing a general nonlinear dynamic analysis for structural systems. So, a simple alternative procedure based on dimensional homogeneity similar to described in chapter 3 is proposed in this study. Based on dimensional homogeneity the damping parameter constants can be empirically related to known material and geometric properties through two proportionality constants denoted as $\xi_{eKV_1}$ and $\xi_{eKV_2}$. Motivated from the elemental Rayleigh damping ratio concept proposed in

chapter 3, the proportionality constants are called here as the elemental Kelvin Voigt damping ratios. So, by dimensional homogeneity of eq. (5.19), $c_s$ and $\gamma_{air}$ can be expressed as,

$$\left.\begin{aligned} c_s &= \rho A_e \xi_{eKV_1}\left(\frac{\omega_e^i \omega_e^j}{\omega_e^i + \omega_e^j}\right) \\ \gamma_{air} &= \rho A_e \xi_{eKV_2}\left(\frac{\omega_e^i \omega_e^j}{\omega_e^i + \omega_e^j}\right) \end{aligned}\right\} \tag{5.29}$$

So, from eq. (5.27),

$$\left.\begin{aligned} \beta_{KV} &= \rho A_e \xi_{eKV_1}\left(\frac{\omega_e^i \omega_e^j}{\omega_e^i + \omega_e^j}\right)\left(\frac{1}{E}\right) \\ \alpha_{KV} &= \xi_{eKV_2}\left(\frac{\omega_e^i \omega_e^j}{\omega_e^i + \omega_e^j}\right) \end{aligned}\right\} \tag{5.30}$$

Eq. (5.30) clearly shows that there are some differences in the way the coefficients are computed in comparison to elemental Rayleigh damping (refer chapter 3). Over here $A_e$ represents area of the element; $\omega_e^i$ and $\omega_e^j$ are the $i^{th}$ and $j^{th}$ elemental undamped frequencies computed using the elemental mass and elemental stiffness matrices; the only constants that have to be parametrized are $\xi_{eKV_1}$ and $\xi_{eKV_2}$. The most apt way to do this is through experimental identification procedures in which case, in the most sophisticated scenario, a variable elemental damping ratio varying per element may be identified; but as already stated this might not be a viable option especially from a practical seismic analysis point of view. So, in this study, a simple procedure of matching proposed in chapter 3 in which the damped free vibration response of the system with elemental Kelvin Voigt damping to that of the system with classical Rayleigh damping is proposed. This method of parametrization equates the equation of motion of the system with the two damping models after pre and post multiplying the modal vector. In the case of global Rayleigh damping as

the model is proportional, a diagonal matrix is obtained, but in the case of Kelvin Voigt model, off diagonal terms are present in the damping matrix. Ignoring the off-diagonal terms, we get,

$$\xi_{eKV} \cong \frac{\alpha m_i + \beta k_i}{2\psi_i} \tag{5.31}$$

Here, $m_i$ is the $i^{th}$ modal mass, $k_i$ is the i$^{th}$ modal stiffness, $\alpha, \beta$ are classical Rayleigh coefficients computed using a pre-conceived damping ratio and

$$\psi_i = \phi_i^T \sum_{iel=1}^{N} \left[ \left( \frac{\omega_{iel}^i \omega_{iel}^j}{\omega_{iel}^i + \omega_{iel}^j} \right) \mathbf{M}_{iel} + \frac{\rho A(x)}{E} \left( \frac{\omega_{iel}^i \omega_{iel}^j}{\omega_{iel}^i + \omega_{iel}^j} \right) \mathbf{K}_{iel} \right] \phi_i \tag{5.32}$$

Eq. (5.31) gives a direct approximate closed form relationship between the elemental damping ratio and the global damping ratio. Global Rayleigh model was used for parametrization mainly because of its popularity and not because the author believes it is the "correct model". *It must be noted that the only unknown parameter that needs to be specified is the classical Rayleigh damping ratio for two specific modes of interest which makes this procedure of parametrization very practical from a dynamic analyst's point of view*. It should be also noted that this parametrization is based on the fact that, in the linear scenario, both damping models should give similar responses and the differences in responses should only happen when the system becomes nonlinear.

*5.2.2.3 Types of elemental Kelvin-Voigt damping based on modelling approaches adopted*

Fig. 5.1 depicts the classification of Kelvin-Voigt damping based on the ways in which the mass formulation and computation of the damping parameter coefficients are undertaken. A more detailed discussion on the elemental mass formulations will be presented in section 5.4. Based on the way the coefficients are computed the Kelvin-voigt model can be implemented in two different ways as outlined in fig. 5.1; one with constant $\alpha_{KV}$ , $\beta_{KV}$ and the other with variable $\alpha_{KV}$ , $\beta_{KV}$

.The first option uses the constant elemental frequencies and the second option requires the computation of the current elemental frequencies. The computation of current elemental frequencies requires eigenvalue computation at each time step, but is computationally efficient as it is done at the element level with small matrices being involved. In the present study, both options are investigated. In both these options tangent elemental stiffness is used. A third model also with constant stiffness with the above stated combination of coefficients could also be envisaged; but this option is not investigated in the present study.

## 5.3 Why we use elemental frequencies for the computation of the damping coefficients?

The main function of a mathematical damping model in nonlinear time-history analysis is to model the un-modelled dissipation. Un-modelled dissipation includes all those tiny mechanisms such as cracking of non-structural components, cracking of gravity supporting structures, cracking of plaster coating, etc., which are not included in the hysteretic response of the structural elements in a structure. To model these mechanisms explicitly is almost close to impossible. The model representing damping should mimic this un-modelled dissipation mechanism as closely as possible with minimum computational penalty and, preferably, with no untoward unexpected effects when the system becomes nonlinear. From a realistic physical point of view, there is no doubt that this un-modelled dissipation phenomenon emanates from the elements. This is because all the gravity and non-structural components contributing to this phenomenon are either attached directly or indirectly to the elements contributing to the hysteretic response. Damping occurs when these attached primary members deform to cause cracks and failure in the non-structural components,

along with the damping of the elastic portion of the inelastic members. So, in effect it is essential that the damping model be defined at the element level.

As damping in a real structural system is due to the damping in the individual components of the system, an ideal mathematical formulation representing the damping phenomenon should derive the system damping matrix from the elemental damping matrices. These elemental damping matrices before the system matrix assembly is in turn derived from the associated elemental deformations. As the elemental deformations are a function of the elemental frequencies and mode shapes, the elemental damping coefficients for both the models are computed using elemental frequencies.

## 5.4 Notes on computation of elemental frequencies and elemental mass formulations

A two part mass definition as proposed in chapter 3 is used for this study. This two part mass definition is successfully implemented in *Ruaumoko*.

Computation of elemental frequencies varies according tothe type of boundary conditions adopted. For a 2D or 3D line element, this could be derived in closed forms, though it can become a bit too tedious when more sophisticated boundary conditions are adopted. So, in the present study a very simple way of computing elemental frequencies by adopting a free-free boundary condition as outlined in Appendix 1 is adopted.

## 5.5 Implementation of time hysteresis model using Modified Newmark formulation (AAR method)

Several methods exist in literature for solving the integro-differential equation given in eq. (5.15). Interested readers can refer to Adhikari (2000), Adhikari and Wagner (2004), Cortes et al. (2009), Puthanpurayil et al. (2014). As the present work is mainly focused on inelastic analysis, AAR method outlined in chapter 4 (Puthanpurayil et al. 2014) is used for solving eq. (5.15).

Only the final form of the equation with exponential kernel function which needs to be implemented is given below (for details please refer to chapter 4),

$$\left[\frac{4\mathbf{M}}{\Delta T^2}+\frac{2}{\Delta T^2}\int_t^{t+\Delta T}\sum_{iel=1}^{N_s}\mathbf{K}_T^{iel}\theta_T^{iel}e^{-\frac{\theta_T^{iel}}{T_n}(t+\Delta T-\tau)}\tau d\tau+\frac{2}{\Delta T}\mathbf{C}_{airT}+\mathbf{K}_T\right]\Delta\mathbf{d}=\mathbf{f}\left(t+\Delta T\right)+\mathbf{M}\left\{\ddot{\mathbf{d}}(t)+\frac{4}{\Delta T}\dot{\mathbf{d}}(t)\right\}$$
$$-\sum_{r=1}^{n+1}\left[\sum_{iel=1}^{N_s}\mathbf{K}_T^{iel}\theta_T^{iel}e^{-\frac{\theta_T^{iel}}{T_n}((n+1-r)\Delta T)}\right]\dot{\mathbf{d}}\left((r-1)\Delta T\right)\Delta T-\mathbf{K}_s\mathbf{d}(t)-\int_t^{t+\Delta T}\sum_{iel=1}^{N_s}\mathbf{K}_T^{iel}\theta_T^{iel}e^{-\frac{\theta_T^{iel}}{T_n}(t+\Delta T-\tau)}\dot{\mathbf{d}}(t)d\tau$$
$$+\frac{2}{\Delta T}\int_t^{t+\Delta T}\sum_{iel=1}^{N_s}\mathbf{K}_T^{iel}\theta_T^{iel}e^{-\frac{\theta_T^{iel}}{T_n}(t+\Delta T-\tau)}\dot{\mathbf{d}}(t)\tau d\tau+\mathbf{C}_{eairT}\dot{\mathbf{d}}(t)$$

(5.33)

Over here $\mathbf{M}$ refers to system mass matrix; $\mathbf{K}_T$ refers to the system tangent stiffness matrix ; $\mathbf{K}_T^{iel}$ refers to element tangent stiffness; *iel* refers to the element number; $\mathbf{K}_s$ refers to the system secant stiffness matrix; $\mathbf{C}_{airT}$ refers to the external viscous damping matrix; $\ddot{\mathbf{d}}(t),\dot{\mathbf{d}}(t)$ and $\mathbf{d}(t)$ are the acceleration, velocity and displacement; $\theta_T$ refers to the current time hysteresis elemental damping coefficient computed by eq. (5.18) using the current elemental stiffness; $\Delta T$ refers to the time step increment. Eq. (5.33) represents the AAR formulation for nonlinear analysis and can be implemented in a computer for solving the integro-differential equation.

Implementable format of eq. (5.33) used in the algorithm below is given as,

$$\left[\frac{4\mathbf{M}}{\Delta T^2}+\frac{2}{\Delta T^2}\mathbf{I}_{damp2}+\frac{2}{\Delta T}\mathbf{C}_{airT}+\mathbf{K}_T\right]\Delta\mathbf{d}=\mathbf{f}\left(t+\Delta T\right)+\mathbf{M}\left\{\ddot{\mathbf{d}}(t)+\frac{4}{\Delta T}\dot{\mathbf{d}}(t)\right\}$$
$$-\mathbf{f}_{damp}-\mathbf{K}_s\mathbf{d}(t)-\mathbf{I}_{damp1}\dot{\mathbf{d}}(t)+\frac{2}{\Delta T}\mathbf{I}_{damp1}\dot{\mathbf{d}}(t)+\mathbf{C}_{airT}\dot{\mathbf{d}}(t) \tag{5.34}$$

where

$$\left.\begin{aligned}\mathbf{I}_{damp1}&=\int_t^{t+\Delta T}\sum_{iel=1}^{N_s}\mathbf{K}_T^{iel}\theta_T^{iel}e^{-\frac{\theta_T^{iel}}{T_n}(t+\Delta T-\tau)}d\tau\\ \mathbf{I}_{damp2}&=\int_t^{t+\Delta T}\sum_{iel=1}^{N_s}\mathbf{K}_T^{iel}\theta_T^{iel}e^{-\frac{\theta_T^{iel}}{T_n}(t+\Delta T-\tau)}\tau d\tau\end{aligned}\right\} \tag{5.35}$$

$$\mathbf{f}_{damp}=\sum_{r=1}^{n+1}\left[\sum_{iel=1}^{N_s}\mathbf{K}_T^{iel}\theta_T^{iel}e^{-\frac{\theta_T^{iel}}{T_n}((n+1-r)\Delta T)}\right]\dot{\mathbf{d}}\left((r-1)\Delta T\right)\Delta T \tag{5.36}$$

*5.5.1 Algorithm for implementation of nonlinear AAR*

The algorithm is only detailed for the case when the time hysteresis model parameters $\theta^{iel}$ and $\gamma_{air}$ are updated every time step and hence $\theta^{iel}=\theta_T^{iel}$ in this case.

- ***Initial Calculations***

1.0 Initialize the system displacement vector $\mathbf{d}_{old}=\mathbf{d}(0)$ and velocity vector $\mathbf{v}_{old}=\dot{\mathbf{u}}(0)$

2.0 Parametrize the elemental time hysteresis damping ratio $\xi_{eTH}$ as outlined in section 5.2.1.2.

3.0 Compute the elemental frequencies using the initial elemental stiffness matrix and evaluate the initial damping proportional parameters $\theta^{iel}$ and $\gamma_{air}$ for each element.

4.0 Assemble the system mass matrix **M**, initial system time hysteretic damping matrix $\mathbf{C}_{hyst}$, initial system air damping matrix $\mathbf{C}_{air}$ and initial stiffness matrix **K.**

Over here $\mathbf{C}_{hyst}(t) = \sum_{iel=1}^{N_s} \mathbf{K}^{iel} \theta^{iel} e^{-\frac{\theta^{iel}}{T_n}(t-\tau)}$; Over here $N_s$ is the total number of elements in the system.

5.0 Initialize system acceleration vector as,

$$\mathbf{a}_{old} = \mathbf{M}^{-1}\left\{\mathbf{f}(0) - \mathbf{C}_{hyst}(0)\mathbf{v}_{old} - \mathbf{C}_{air}\mathbf{v}_{old} - \mathbf{K}\mathbf{d}_{old}\right\} \quad (5.37)$$

6.0 Initialize $\mathbf{f}_{damp}$

- ***Calculation for each time step***

7.0 Choose a sufficiently small time step. For the first time step,

7.1 Compute the current tangent system stiffness matrix.

7.2 Compute the current tangent system damping matrices, $\mathbf{I}_{damp1}$, $\mathbf{I}_{damp2}$ and $\mathbf{C}_{airT}$

To demonstrate the computation of the above terms for the $j^{th}$ element,

7.2.1 Compute the elemental frequencies as described in section 3.0 using the present element stiffness obtained from step 7.1.

7.2.2 Compute the current tangent damping proportional parameters $\theta_e$ and $\gamma_{air}$

7.2.3 Compute the $\left.\begin{aligned}\mathbf{I}_{damp1}^{j} &= \int_{t}^{t+\Delta T} \mathbf{K}_T^j \theta_T^j e^{-\frac{\theta_T^j}{T_{n,j}}(t+\Delta T-\tau)} d\tau \\ \mathbf{I}_{damp2}^{j} &= \int_{t}^{t+\Delta T} \mathbf{K}_T^j \theta_T^j e^{-\frac{\theta_T^j}{T_{n,j}}(t+\Delta T-\tau)} \tau d\tau\end{aligned}\right\}$ such that on matrix assembly will result in $\mathbf{I}_{damp1}$ and $\mathbf{I}_{damp2}$

7.3 Compute the system dynamic stiffness matrix $\hat{\mathbf{K}}$

$$\hat{\mathbf{K}} = \frac{4\mathbf{M}}{\Delta T^2} + \frac{2}{\Delta T^2}\mathbf{I}_{damp2} + \frac{2}{\Delta T}\mathbf{C}_{airT} + \mathbf{K}_T \tag{5.38}$$

Where $\mathbf{K}_T$ is the tangent stiffness.

7.4 Evaluate the effective system load vector,

$$\mathbf{f}_{new} = \mathbf{f}(t+\Delta T) + \mathbf{M}\left\{\ddot{\mathbf{d}}(t) + \frac{4}{\Delta T}\dot{\mathbf{d}}(t)\right\} - \mathbf{f}_{damp} - \mathbf{K}_s\mathbf{d}(t) - \mathbf{I}_{damp1}\dot{\mathbf{d}}(t)d\tau + \frac{2}{\Delta T}\mathbf{I}_{damp1}\dot{\mathbf{d}}(t) + \mathbf{C}_{airT}\dot{\mathbf{d}}(t) \tag{5.39}$$

$\ddot{\mathbf{d}}(t), \dot{\mathbf{d}}(t)$ and $\mathbf{d}(t)$ are the system acceleration, system velocity and system displacement;

7.5 Solve for system displacement increment,

$$\hat{\mathbf{K}}\Delta\mathbf{d} = \mathbf{f}_{new} \tag{5.40}$$

7.6 Perform *state determination* to check whether there is a change in stiffness within the time step*;* for details refer (Fillipou et al. 1992). If a change of stiffness occurs during the time step, repeat steps 7.1 to 7.6. If there is no change in stiffness (*in a state of convergence*),

7.6.1 Compute the incremental acceleration and incremental velocity as follows,

$$\Delta\ddot{\mathbf{d}} = \left[\frac{4}{\Delta T^2}\Delta\mathbf{d} - \frac{4}{\Delta T}\mathbf{v}_{old} - 2\mathbf{a}_{old}\right] \tag{5.41}$$

$$\Delta\dot{\mathbf{d}} = \left[\frac{2}{\Delta T}\Delta\mathbf{d} - 2\mathbf{v}_{old}\right] \tag{5.42}$$

7.6.2 Compute the new acceleration and new velocity

$$\mathbf{v}_{new} = \mathbf{v}_{old} + \Delta\dot{\mathbf{d}} \tag{5.43}$$

$$\mathbf{a}_{new} = \mathbf{a}_{old} + \Delta\ddot{\mathbf{d}} \tag{5.44}$$

$$\mathbf{d}_{new} = \mathbf{d}_{old} + \Delta\mathbf{d} \tag{5.45}$$

7.6.3 Update the $\mathbf{a}_{old}$ $\mathbf{v}_{old}$ and $\mathbf{d}_{old}$

7.6.4 Updated $\mathbf{f}_{damp}$,$\mathbf{f}_{damp1}$ and $\mathbf{f}_{damp2}$

$$\left.\begin{aligned}\mathbf{f}_{damp1} &= \mathbf{I}_{damp1}\dot{\mathbf{u}}(t)d\tau \\ \mathbf{f}_{damp2} &= \frac{2}{\Delta T}\mathbf{I}_{damp1}\dot{\mathbf{u}}(t)d\tau\end{aligned}\right\}$$

8.0 Repeat the steps 7.1-7.6 in step 7.0 for other time steps.

## 5.6 Implementation of elemental Kelvin-Voigt damping in Newmark incremental equilibrium framework

In this section, steps involved in the implementation of the Kelvin Voigt damping model in the Newmark incremental equilibrium framework is outlined. This is very similar in manner to the implementation of elemental Rayleigh damping as described in chapter 3. Only Newmark constant average acceleration method with $\gamma = \frac{1}{2}$ and $\beta = \frac{1}{4}$ is described in this section. The algorithm is outlined in fig. 5.2 and is equally applicable to the linear acceleration method as well with similar ease. Only the implementation of the model with tangent proportionality constants are illustrated in this section and the procedure is the same for other models. Mass formulations used can be either diagonal or consistent.

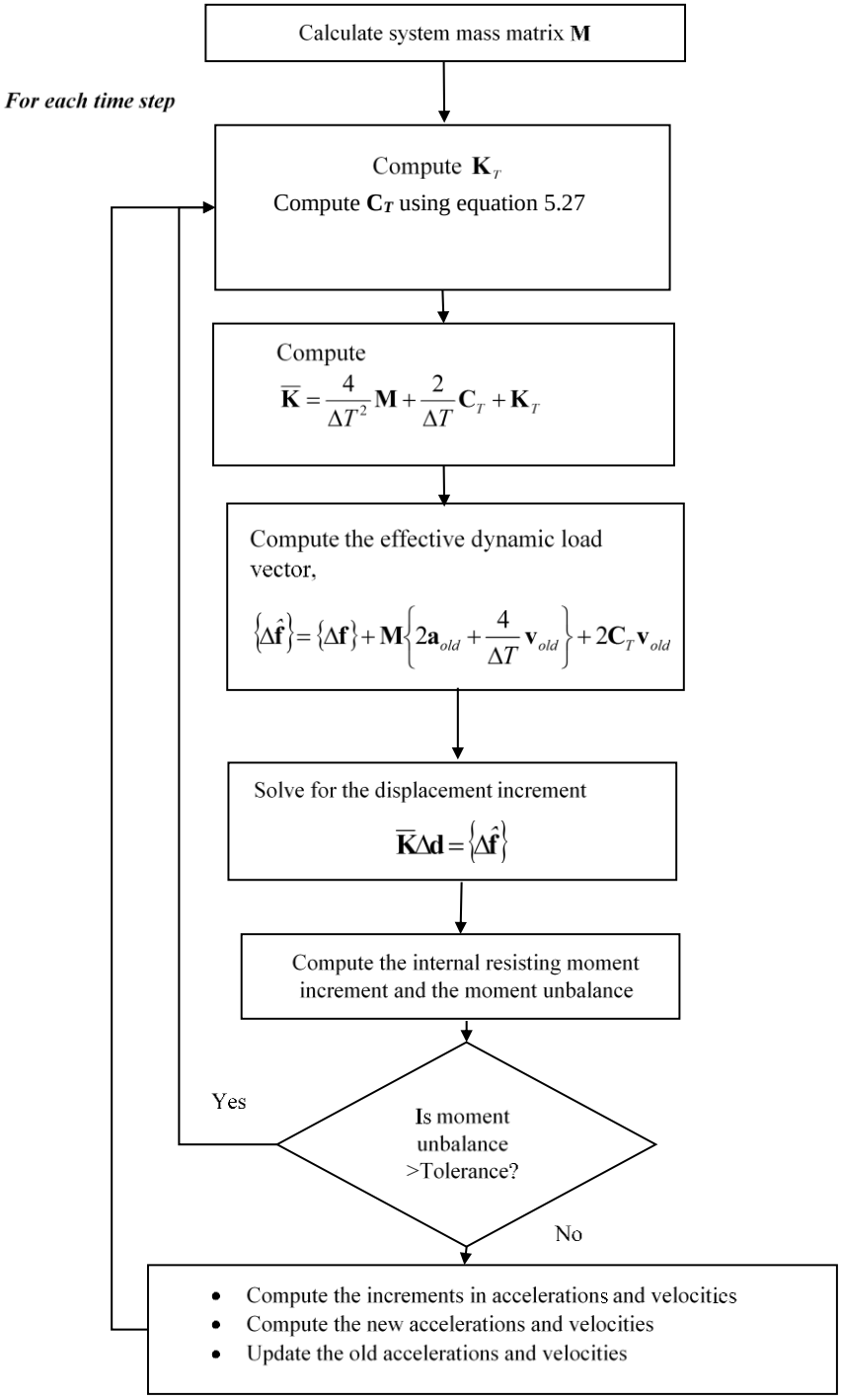


Fig. 5.2 Flow chart of incremental Newmark constant acceleration algorithm

## 5.7 Implementation of the *elemental Kelvin-Voigt model* using revised Newmark total equilibrium method

Revised Newmark algorithm is given in fig. 5.3. In comparison to fig. 5.2, the main difference exists in the computation of the effective dynamic load vector as illustrated in fig. 5.3 (Carr 2007, Puthanpurayil et al. 2014, Puthanpurayil et al. 2016).

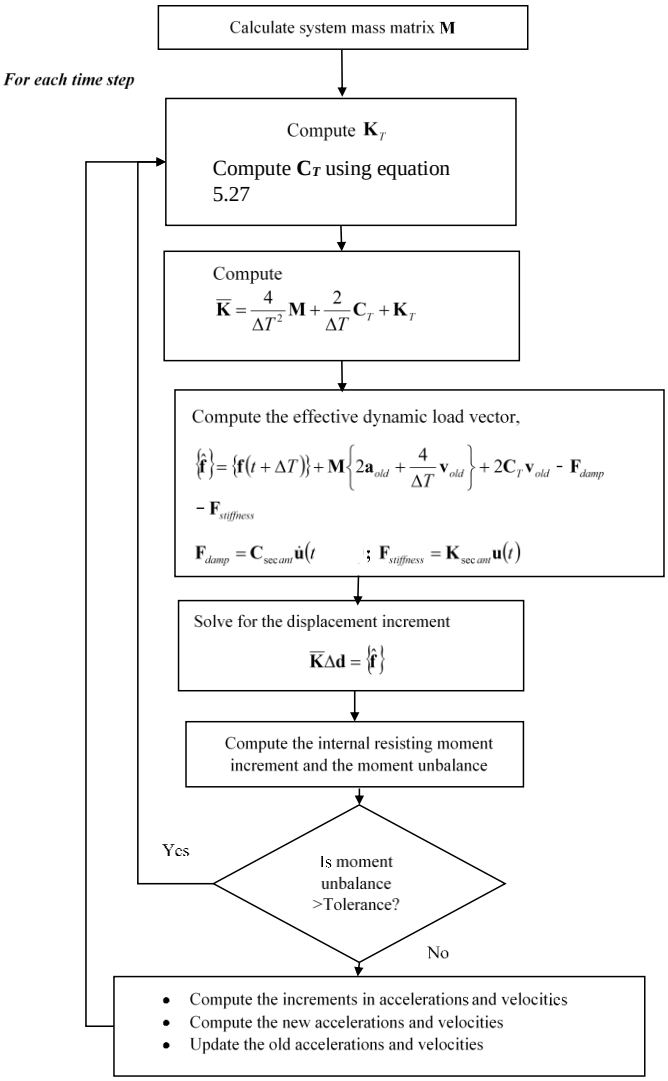


Fig. 5.3 Flow chart of revised Newmark constant acceleration algorithm

## 5.8 Numerical study- IDA study

In order to assess the performance of the proposed local continuum models an IDA study is initiated on the same four-story RC frame described in chapter 3 (Puthanpurayil et al. 2016). The geometric and material properties are given in Appendix 3.

Abbreviations used to identify different damping models included in the plots are as follows: Initial stiffness based classical Rayleigh damping (ISRD), Tangent stiffness based classical Rayleigh damping with constant coefficients (TSRD1), Elemental Kelvin-Voigt damping with constant elemental proportionality coefficients (ELKV1), Elemental Kelvin-Voigt damping with updated proportionality coefficients (ELKV2), Elemental time hysteresis model with constant damping parameters (ELTH1), Elemental time hysteresis model with updated damping parameters (ELTH2) and Wilson-Penzien/modal damping model (GWP). In all plots, global models are presented with continuous lines and elemental models are presented with broken lines. IDA study is presented in two subsections based on the way the mass used for computing the damping matrix is formulated. They are as follows:

### 5.8.1Consistent mass formulation

Euler Bernoulli consistent mass formulation is used for the damping matrix computation. A set of seven artificial far-field ground motions scaled to five intensity measures (represented by the peak ground acceleration PGA) are used for the present study. A parallel IDA study (not presented in this paper) using a set of seven artificial near field ground motions scaled to same five intensity measures were also carried out. Since similar conclusions were drawn regarding the performance

of the proposed models in the near field study, only results from far field ground motions are presented in this section. The intensity measures to which the ground motions were scaled are 0.3g, 0.4g, 0.5g, 0.6g and 0.7g.

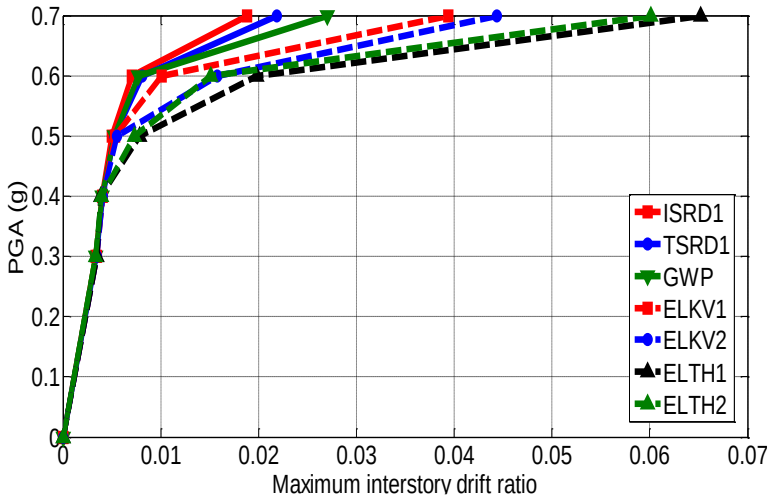


(a)

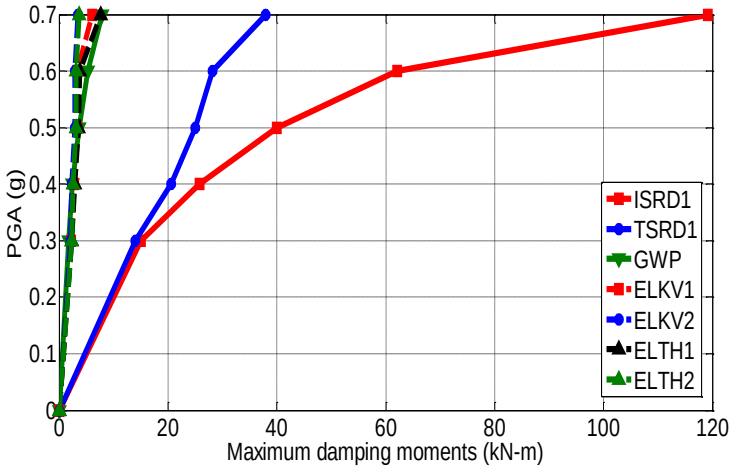


(b)

Fig. 5.4a. IDA curves for mean peak interstory drifts for consistent mass formulation. 5.4b. IDA curves for peak damping moments for consistent mass formulation.

To maintain consistency in comparison, the global models also adopt the consistent mass formulation for the damping matrix computation instead of the normal lumped mass formulation.

Fig. 5.4a illustrates the mean IDA curves for location independent peak interstory drift ratio and fig. 5.4b depicts the IDA curves for peak damping moments. Damping moments are un-realistic forces exhibited by the models. In the case of viscous damping models this can be computed as the product of the current damping coefficient matrix with the current velocity vector whereas in the case of time hysteresis model this can be computed by adding the damping forces on the right-hand side of eq. (5.33). It could be clearly seen from fig. 5.4a that as the intensity level increases the elemental damping models tend to give larger interstory drift ratios in comparison to global models and hence giving a more conservative estimate from a performance assessment point of view. Results from Zareian and Medina (2010) also emphasizes this aspect. Another important aspect that can be observed in Fig. 5.4a is that overall the elemental damping model exhibits yielding at a much earlier stage as compared to the global models and exhibits larger drifts. A very similar observation had been made by Val and Segal (2005) in which a comparison between the responses of a SDOF system with both viscous and hysteretic damping models were presented; It has been observed that structures with hysteretic damping model exhibit yielding at an earlier stage as compared to the system which uses viscous damping model. Fig. 5.4b clearly illustrates the superiority of the elemental models in comparison to the classical Rayleigh damping models in terms of the damping moments. All elemental damping models produce small un-realistic damping forces in a similar manner to global Wilson Penzien damping model (*modal damping)* epitomizing the significance of the elemental damping models in comparison to the classical Rayleigh damping models in a performance assessment scenario. Though the damping forces are small in the case of

Wilson Penzien model, the requirement of a full eigen solution and the presence of a fully populated damping matrix renders this model impracticable for practical dynamic analysis of large systems.

### 5.8.2Diagonal mass formulation

Classical diagonal mass formulation of Euler Bernoulli beams is used for generating the damping matrix. Same set of seven artificial far-field ground motions are used for this study. Over here global models also adopt the diagonal mass formulation for the damping matrix computation.

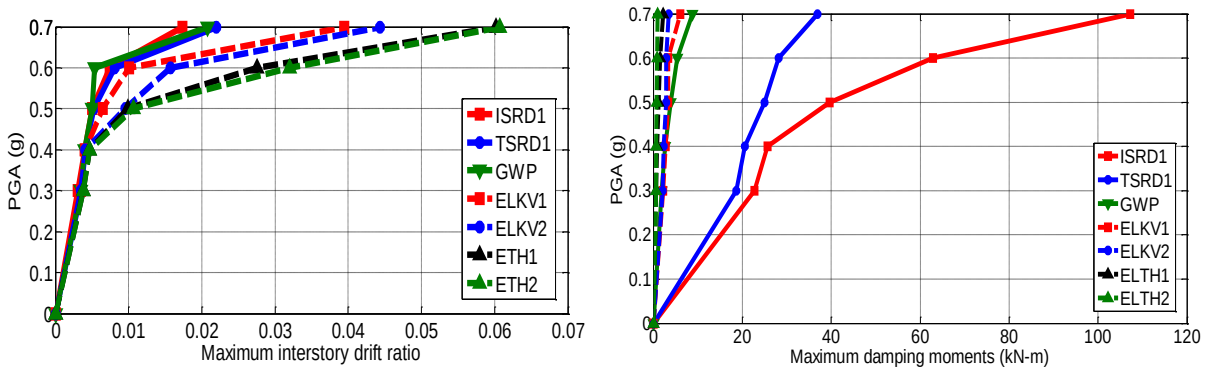


(a) (b)

Fig. 5.5a. IDA curves for mean peak interstory drifts for diagonal mass formulation. 5.5b. IDA curves for peak damping moments for diagonal mass formulation.

Fig. 5.5a depicts the mean IDA curves for location independent peak interstory drift ratio and fig. 5.5b illustrates the IDA curves for peak damping moments. In both plots similar trend as in the case of consistent mass formulation as described in section 5.8.1 is exhibited by the diagonal mass formulation. This clearly shows that if elemental damping models are used, either consistent mass or diagonal mass formulation can be used for generating the elemental mass component of the elemental damping matrix. Similar to consistent mass formulation, in the case of diagonal mass also higher peak interstory drift ratios are shown by elemental damping models when the intensity

increases. This is evidenced in fig. 5.5a. Similar trend to consistent mass formulation is exhibited for the peak damping moments as well by the diagonal mass formulation, with the elemental damping models exhibiting much lower damping moments similar to the classical modal damping model denoted as GWP. This is illustrated in fig. 5.5b.

### 5.8.3 Discussion on consistent mass vs. diagonal mass formulation

From section 5.8.1 and 5.8.2 it can be concluded that both consistent mass and diagonal mass formulations give conservative results from an engineering perspective.

## 5.9 Conclusions

A new approach to modelling damping in inelastic dynamic analysis is presented. The new approach relies on the elemental level derivation of the damping matrix and assembling them to obtain the global damping matrix in a way similar to mass and stiffness matrices. Two existing local continuum damping models existing in the linear dynamic analysis scenario are adapted and extended into the nonlinear dynamic analysis scenario. Implementation schemes for the models using the classical Newmark framework and the parametrisation methodology are presented. Performance of the extended models are assesed using a numerical study on a four story RC frame. It has been shown that all the proposed models seem to produce more reliable results than the global models without increasing the computational demand. It has also been demonstrated that for both models either consistent mass or diagonal mass can be used to generate the mass component of the damping matrix.

# 6. Application of nonlocal continuum damping models in nonlinear dynamic analysis

**Journal (Published)**

Puthanpurayil, A., Carr, A. and Dhakal, R.P. (2016) Application of nonlocal elasticity continuum damping models in Nonlinear Dynamic Analysis. *Bulletin of Earthquake Engineering* (in press).

**Abstract:** In this chapter, the new paradigm developed in chapter 3 and applied in chapter 5 is further applied to more mathematically rigorous nonlocal continuum damping models. In order to have a more generic representation of the damping phenomenon in seismic analysis, the already existing nonlocal continuum damping models have been adapted and extended to inelastic domain. Two nonlocal damping models have been studied which includeRussell's spatial hysteresis model and the extended Sorrentino model. Galerkin based Finite element schemes are developed and the numerical implementation of the models is outlined. The performances of the nonlocal models are illustrated by studying the nonlinear dynamic responses of the four-story RC frame described in chapter 3. It has been shown that in nonlinear dynamic analysis, the proposed adaptation of the nonlocal continuum damping models might be a more realistic alternative to the popular classical Rayleigh damping model.

# 6.1 Introduction

As described in chapter 2.0, other than the user familiarity and mathematical convenience there are no attributed explicit physical evidences for the adoption of Rayleigh damping model in nonlinear dynamic analysis. Chapter 3.0 introduced a new paradigm in modelling inherent damping in a nonlinear dynamic analysis which gives more realistic estimate for seismic responses in nonlinear domain; *but still the damping forces were formulated with instantaneous velocities as the only state variables.* So, in chapter 5 this new paradigm was extended to local continuum damping models. In this chapter, a step further than that described in chapter 5.0 is presented, which involves adaptation of more rigorous nonlocal continuum damping models to nonlinear dynamic analysis.

### 6.1.1 Motivation, Objective and scope

Motivated from the need for a better mathematical representation of the *un-modelled* dissipation phenomenon and the possible dependence of the damping phenomenon on the history of response and the spatial nonlocalness, in this chapter, a methodology for representing the damping phenomenon in a more generic sense for nonlinear dynamic analysis is proposed. This is achieved by adapting the already existing nonlocal (spatially and spatio-temporally) damping models to the inelastic domain. Spatially nonlocal damping models are those models in which the damping force at a point is a function of the responses at all points in the domain whereas in the spatio-temporally nonlocal damping models, the damping force at a point is a function of responses at all points in the domain along with response history. In that sense, nonlocal models are very generic in comparison to the existing classical damping models which are local in nature, both spatially and temporally. The reason for this is because till now no specific physical evidence has been provided

which shows that the damping force at a point should only be the function of the response at that point alone (Friswell *et al.* 2007). Also, one of the other main motivations for extending the nonlocal damping model can be fetched from the experimental fact that nonlocal damping models tend to represent the damping phenomenon in composite structural elements more realistically as compared to other local continuum or discrete models (Russell (1991); Banks and Inman (1991)). Most of the practical civil engineering structural elements are either macroscopically or microscopically composite in nature. So, in that sense with a proper parameterization adopted, the nonlocal damping models should represent the physical reality more closely in a simulation.

These observations cited above coupled with the fact that the *un-modelled* dissipation phenomenon is indirectly related to the member deformations, in this chapter, these models are introduced at the continuum level and once subjected to partial discretization, arrive at the element level damping matrix in a similar manner to that obtained in chapter 3.0. Also, when the damping model is introduced at the continuum level a proper representation of the member level damping in the system damping matrix is obtained with no untoward effects as exhibited by the classical Rayleigh damping model.

So, keeping the above stated motivations in focus, in this study two nonlocal damping models in ascending order of the mathematical rigor are investigated; one is Russell's model in which the damping force is nonlocal in space but depends only on the instantaneous velocity and the other is the extended Sorrentino model (Friswell et al. 2007) in which the damping force is nonlocal in space and depends on the history of velocities. Galerkin based finite element schemes are adopted for the implementation of both models. Galerkin scheme used for extended Sorrentino model is very similar in manner to that employed by Friswell *et al.* (2007) and the internal damping matrix derived is similar to the direct damping matrix derived in Friswell *et al.* (2007). Only classical

Euler beam enhanced with nonlocal damping models are used in the present study.. Numerical implementation of the proposed models using the Newmark direct integration scheme is described in detail. The performance of these models is assessed using the four-story moment resisting reinforced concrete frame described in chapter 3. Simple empirical parameterization based on dimensional homogeneity is presented for easy adaptation of the models to a practical inelastic analysis scenario. The presented single ground motion study and incremental dynamic analysis (IDA) study qualitatively highlights the fact that nonlocal damping models can give more reliable results from an engineering perspective. The objectives and scope of the present chapter are limited to the mathematical adaptation of the above mentioned nonlocal damping models into the inelastic seismic scenario.

## 6.2 Background of nonlocal damping models

This section briefly outlines chronologically the background of nonlocal damping models. Nonlocal theories have been developed through a rigorous research effort invested to accurately represent the long range intermolecular and microstructural effects which otherwise would be almost impossible to represent by using the scale-free local continuum theories. Most of these theories rely on the representation of an enrinched continuum and representing the micro-structural effects in an averaged sense (Paolo *et al.* 2013). Some of the enriched continuum theories include the integral theory (Eringen 1972,1983,1987), the gradient elasticity theory (Aifantis 1999,1984), the continnualization theories (Askes and Metrikine (2002), Metrikine and Askes (2002)) and the peridynamic theories (Silling et al. 2003, Silling, 2000). Most of these theories develop nonlocal stiffness terms (Reddy 2007, Paolo et al. 2013).

Russell (1991) pioneered the development of nonlocal damping models by the development of spatial hysteresis model. The internal damping term is described as a torque acting on a beam at a point $'x'$ due to the differential rotation of the beam at points $\xi$ "near" $x$ (Russell 1991). Banks and Inman (1991) investigated the performance of four continuum damping models which included, the viscous air damping, the kelvin-Voigt model, the time hysteresis model and Russell's spatial hysteresis model. Experimental responses of a composite cantilever beam with a tip mass was compared in this study with the analytical time histories. It has been shown that Russell's spatial hysteresis model in conjunction with the viscous air damping model gave the best quantitative agreement with the experimental results (Banks and Inman, 1991). Friswell *et al.* (2007) and Lei *et al.* (2006) proposed a non-local damping model in which the damping phenomenon is explicitly represented by internal and external damping models; internal damping is represented by the time rate of the fourth order derivative of the transverse displacement. This model was an extension of the already published Sorrentino model (2003) and henceforth from here after in this chapter it would be referred to as Extended Sorrentino model and will be denoted as ESM. The proposed nonlocal model represents the intrinsic dependence between the responses at a given point and the responses at the surrounding points of the medium (Paolo *et al.*2013, Flugge 1978). Gonzalez-Lopez and Fernandez-Saez (2012) studied the influence of parameters of the nonlocal damping models on the bending vibrations of Euler-Bernoulli beams treated with nonlocal viscoelastic damping patches. Paolo *et al.* (2013) presented the development of a nonlocal Timoshenko beam with both nonlocal damping and nonlocal stiffness components. The key assumption in the study was that the nonlocal effects were modelled as long-range volume forces and moments mutually exerted by non-adjacent beam segments. Most of these studies focused only on linear dynamics. Very recently, Sideris and Salahi (2017) introduced a gradient inelastic beam theory and a

corresponding flexibility based (FB) frame element formulation. The gradient inelastic beam theory is obtained by enriching Navier's beam theory by introducing nonlocal deformation variables to alleviate the pathogenies of Navier theory in the presence of softening section constitutive relations. The proposed FB formulation is shown to alleviate strain localization and loss of objectivity, reduce instabilities and convergence failures of the numerical solution algorithm.

Motivated by the benefits a nonlocal damping model could attribute as evidenced in these above cited studies, a methodology is proposed in this chapter to extend these models into the inelastic seismic analysis domain.

### 6.2.1 Overview of the nonlocal damping models

Fig. 6.1 gives the broad generic classification of the nonlocal continuum damping models. In the present study, the implementation schemes are developed for the models with updated damping parameters as they are the most generic and their performance is assessed using IDA. Though not presented here, the model with constant damping parameters also shows similar responses.

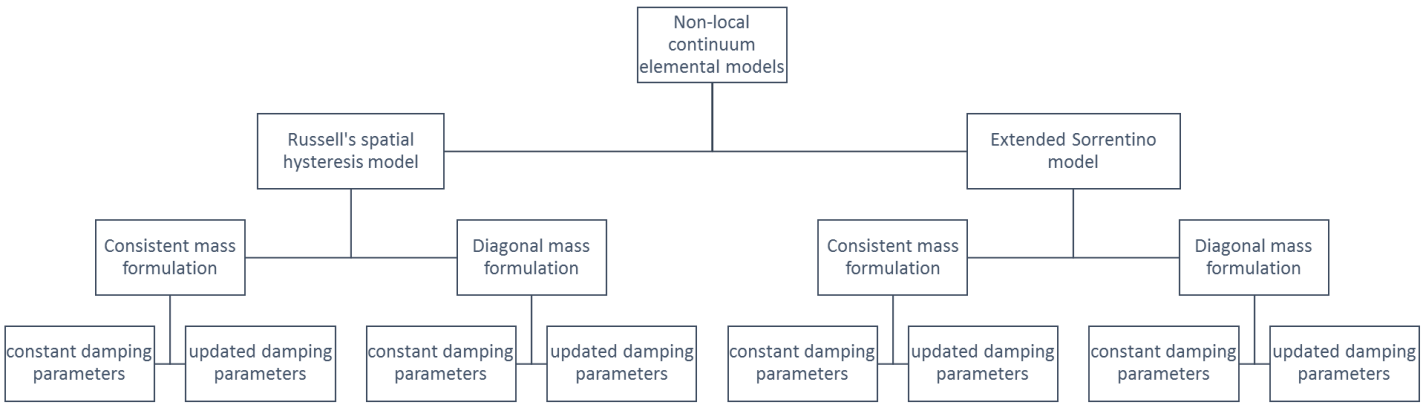

Fig 6.1 Schematic generic classification of the nonlocal continuum damping models

## 6.3 Partial discretization of nonlocal damping enhanced Euler-Bernoulli beam model

This section presents the partial discretization procedure for the classical Euler-Bernoulli beam enhanced with both the nonlocal damping models. The dimensional homogeneity based parametrization adopted for easier applicability of these models in a nonlinear dynamic analysis scenario is also described in detail. One point to be noted is that the nonlocal damping models are incorporated in the local beam theories whereas in the generic format the beam theory should also follow the nonlocal differential constitutive relationship of Eringen (Reddy 2007). Although the classical local elasticity based Euler-Bernoulli beam formulation is used, the proposed adaptation of the damping models into the nonlinear scenario illustrated is generic and can be incorporated in the nonlocal version of the Euler-Bernoulli beam theory.

### 6.3.1 Russell's spatial hysteresis model

Russell's model (Russell 1991) enhanced Euler-Bernoulli beam in differential format is given as follows:

$$\rho A(x)\frac{\partial^2 w(x,t)}{\partial t^2} + Q_i(x,\xi,t) + Q_e(x,t) + EI(x,t)\left(\frac{\partial^4 w(x,t)}{\partial x^4}\right) - f(x,t) = 0 \qquad (6.1)$$

where $w(x,t)$ represents the transverse displacement of the beam continuum, $Q_i(x,\xi,t)$ refers to internal damping forces and $Q_e(x,t)$ refers to external damping forces. $\rho, A, E$ & $I$ refer to material density, cross section area, modulus of elasticity and second moment of area of continuum. $'x'$ and $'\xi'$ refer to the spatial ordinates and $'t'$ refers to the time ordinate. $f(x,t)$ is the externally applied load on the continuum. The internal damping term is given as (Russell 1991),

$$Q_i(x,\xi,t) = -2\frac{\partial}{\partial x}\left\{\int_0^L h(x,\xi)\left[\frac{\partial^2 w(x,t)}{\partial x \partial t} - \frac{\partial^2 w(\xi,t)}{\partial x \partial t}\right] d\xi\right\} \tag{6.2}$$

Here '$L$' is the element length and the $h(x,\xi)$ is called the interaction kernel and is a function of both $'x'$ and $'\xi'$ which is a point in the neighborhood of *'x',* and in the present study Gaussian function is used as the kernel function and is given as (Banks and Inman 1991),

$$h(x,\xi) = \frac{a}{b\sqrt{2\pi}} e^{-(x-\xi)^2/2b^2} \tag{6.3}$$

where *'a'* and *'b'* are damping coefficient constants.

The external damping term can be assumed as given in (Banks and Inman 1991),

$$Q_e(x,t) = \gamma \frac{\partial w(x,t)}{\partial t} \tag{6.4}$$

To simplify the presentation, initial conditions are assumed to be zero and the boundary conditions are not explicitly stated as the semi-discretization procedure adopted here is applicable to a variety of boundary conditions. There is no absolute restriction that the damping kernel should follow a Gaussian function. In fact, the damping kernel functions can be any causal model that makes the dissipative functional non-negative (Adhikari, 2007).

The Galerkin based weak form of eq. (6.1), is given as

$$\int_0^L \delta^T \left[ \rho A(x) \frac{\partial^2 w(x,t)}{\partial t^2} + Q_i(x,\xi,t) + Q_e(x,t) + EI(x,t) \frac{\partial^4 w(x,t)}{\partial x^4} - f(x,t) \right] dx = 0 \tag{6.5}$$

Here both the mass and stiffness terms follow the standard Finite Element semi-discretization procedure. So, the rest of the presentation focuses only on the damping terms $Q_i(x,\xi,t)$ and $Q_e(x,t)$ . Substituting eq. (6.2) into eq. (6.5) and extracting the internal damping term, we get

$$\int_0^L \delta^T Q_i(x,\xi,t) dx = -2 \int_0^L \delta^T \frac{\partial}{\partial x} \left\{ \int_0^L \left( h(x,\xi) \left[ \frac{\partial^2 w(x,t)}{\partial t \partial x} - \frac{\partial^2 w(\xi,t)}{\partial t \partial x} \right] \right) \right\} d\xi dx \tag{6.6}$$

Now performing integration by parts on eq. (6.6), we get

$$= -2\delta^T \left[ \int_0^L h(x,\xi) \left\{ \frac{\partial^2 w(x,t)}{\partial t \partial x} - \frac{\partial^2 w(\xi,t)}{\partial t \partial x} \right\} d\xi \right]_0^L + 2 \int_0^L \frac{\partial \delta}{\partial x} \int_0^L h(x,\xi) \left\{ \frac{\partial^2 w(x,t)}{\partial t \partial x} - \frac{\partial^2 w(\xi,t)}{\partial t \partial x} \right\} d\xi dx \tag{6.7}$$

Similarly, the external damping term gives

$$\int_0^L \delta^T Q_e(x,t) dx = \gamma \int_0^L \delta^T \frac{\partial w(x,t)}{\partial t} dx \tag{6.8}$$

The space-time separation approach for the deflection is given as,

$$\left. \begin{aligned} w(x,t) &= \mathbf{N}(x) \mathbf{u}_e(t) \\ w(\xi,t) &= \mathbf{N}(\xi) \mathbf{u}_e(t) \end{aligned} \right\} \tag{6.9}$$

$\mathbf{N}(x)$ and $\mathbf{N}(\xi)$ are the classical cubic shape functions and $\mathbf{u}_e(t)$ is the generalized coordinate. Following classical Galerkin approach and substituting eq. (6.9) in eq. (6.7) and ignoring the boundary term, results in

$$= 2\int_0^L \left[\frac{\partial \mathbf{N}^T(x)}{\partial x}\right]\left\{\int_0^L h(x,\xi)\left[\frac{\partial \mathbf{N}(x)}{\partial x} - \frac{\partial \mathbf{N}(\xi)}{\partial x}\right]d\xi\right\}dx\dot{\mathbf{u}}_e(t) \tag{6.10}$$

So, this gives the internal spatial hysteretic damping matrix as

$$\mathbf{C}_i = 2\int_0^L \left[\frac{\partial \mathbf{N}^T(x)}{\partial x}\right]\left\{\int_0^L h(x,\xi)\left[\frac{\partial \mathbf{N}(x)}{\partial x} - \frac{\partial \mathbf{N}(\xi)}{\partial x}\right]d\xi\right\}dx \tag{6.11}$$

The spatial hysteretic damping matrix coefficients using the Gaussian kernel function given in eq. (6.3) for a beam element is given in Appendix 6. Similarly substituting eq. (6.9) in eq. (6.8), the external damping matrix is given as

$$\mathbf{C}_e = \gamma\int_0^L \mathbf{N}^T(x)\mathbf{N}(x)dx \tag{6.12}$$

Now the total damping matrix at element level can be given as,

$$\mathbf{C} = \mathbf{C}_e + \mathbf{C}_i \tag{6.13}$$

#### *6.3.1.1 Proposed dimensional homogeneity based Parametrization of Russell model*

For practical use of this model, three unknown coefficients *'a'*, *'b'* (refer Appendix 6) and $\gamma$ need to be parametrized. The most generic way of doing this is by experimental identification as illustrated in Banks and Inman (1991). From a practical structural engineering point of view, this is almost close to impossible as the structural system is not yet built. So, for the easy practical adoption of the Russell model in nonlinear seismic analysis, a simple dimensional homogenization approach as described in chapter 5 is illustrated in this section. Dimensional analysis of eq. (6.1) with kernel function adopted as the Gaussian function given in eq. (6.3) would yield the unknown damping coefficients as follows,

$$\gamma \propto \rho A(x)\left(\frac{\omega_{ei}\omega_{ej}}{\omega_{ei}+\omega_{ej}}\right) \tag{6.14}$$

$$a \propto \rho A(x)L^2\left(\frac{\omega_{ei}\omega_{ej}}{\omega_{ei}+\omega_{ej}}\right) \tag{6.15}$$

$$b \propto L \tag{6.16}$$

Here $\omega_{ei}$ and $\omega_{ej}$ are the $i^{th}$ and $j^{th}$ elemental undamped frequencies computed using the elemental mass and elemental stiffness. The form of relation presented in eqs. (6.14,6.15 & 6.16) is one of its kind; There can be various other possible options as well which may be adopted to relate the unknown damping coefficients to the elemental frequencies.

To reduce the parameterization difficulties, a single proportionality constant  is introduced using which, eqs. (6.14, 6.15 & 6.16) would take the following forms,

$$\gamma \cong \zeta_{eR}\rho A(x)\left(\frac{\omega_{ei}\omega_{ej}}{\omega_{ei}+\omega_{ej}}\right) \tag{6.17}$$

$$a \cong \zeta_{eR}\rho A(x)L^2\left(\frac{\omega_{ei}\omega_{ej}}{\omega_{ei}+\omega_{ej}}\right) \tag{6.18}$$

$$b \cong \zeta_{eR}L \tag{6.19}$$

So, from eqs. (6.17, 6.18 & 6.19), by adopting a dimensional homogeneity approach we reduce the number of unknowns from three in the original formulation to one; that is $\zeta_{eR}$ which needs to be parameterized. Motivated by classical damping ratio philosophy, $\zeta_{eR}$ is proposed to be called as the *elemental Russell damping ratio* though in the present study it will be a constant for all

elements in the system. Therefore, in the present study, in effect it is a system parameter itself like the global damping ratio but relating the elemental frequencies instead of the system frequencies. If better parameterization procedures are available, $\zeta_{eR}$ can also be varied between elements. This aspect illustrates the very generic nature of the elemental type modelling approach. The reason for adoption of elemental frequencies have been already described in chapter 5.

### 6.3.2 Extended Sorrentino model (ESM) (Friswell et al. 2007)

ESM enhanced Euler-Bernoulli classical beam equation is given as,

$$\rho A(x)\frac{\partial^2 w(x,t)}{\partial t^2} + Q_{\text{int}}(x,t) + Q_{ext}(x,t) + EI(x,t)\frac{\partial^4 w(x,t)}{\partial x^4} = f(x,t) \tag{6.20}$$

Here the spatio-temporal non-local damping model is given as (Friswell *et al.* 2007)

$$Q_{\text{int}}(x,t) = \frac{\partial^2}{\partial x^2}\left(\int_0^L \int_{-\infty}^t C_{\text{int}}(x,\xi,t-\tau)\frac{\partial^2 \dot{w}(\xi,\tau)}{\partial \xi^2} d\tau d\xi\right) = \frac{\partial^2}{\partial x^2}\left(\int_0^L \int_{-\infty}^t C_{\text{int}}(x,\xi,t-\tau)\frac{\partial^3 w(\xi,\tau)}{\partial \xi^2 \partial \tau} d\tau d\xi\right) \tag{6.21}$$

Again, the external damping can be treated as viscous damping and can be written as (Banks and Inman 1991),

$$Q_{ext}(x,t) = \gamma \frac{\partial w(x,t)}{\partial t} \tag{6.22}$$

So, with the non-local damping model incorporated, eq. (6.20) would become an integro-partial differential equation. Here $w(x,t)$ is the transverse displacement, $C_{\text{int}}(x,\xi,t-\tau)$ is the internal damping kernel functions coupled in space and time. $x$ and $\xi$ are spatial ordinates and $t$ is the time ordinate. Rest of the terms in eq. (6.20) are the standard terms used in an Euler-Bernoulli formulation with $\rho, A, E \,\&\, I$ referring to material density, cross section area, modulus of elasticity

and second moment of area of continuum. $\gamma$ is the air viscous damping coefficient and $f(x,t)$ is the externally applied load on the continuum.

#### *6.3.2.1 Significance of the damping kernel and its interpretation*

$C(x,\xi,t-\tau)$ can be conveniently assumed to be separable in space and time (Friswell *et al.* 2007). Thus, kernel can be expressed as,

$$C(x,\xi,t-\tau)=H(x)c(x-\xi)g(t-\tau) \tag{6.23}$$

In this equation, the $H(x)$ is the Heaviside step function showing the effect of the spatial term usually used when there is patch damping, $c(x-\xi)$ represents the effect of the different spatial segments (effect of adjacent elements on the element under consideration) and $g(t-\tau)$ represents the effect of the past time histories.

According to Lei et al. (2006), $C(x,\xi,t-\tau)$ emphasizes a very generic version of the damping phenomenon exhibited in structures. This is mainly because the so called classical viscous damping can be derived from this term by replacing the space term and time term by Dirac delta function as follows (Friswell *et al.* 2007),

$$C(x,\xi,t-\tau)=H(x)\delta(x-\xi)\delta(t-\tau) \tag{6.24}$$

No proportionality assumption is made in eq. (6.24) and it represents a pure viscous damping coefficient matrix. Again interestingly, a spatial hysteresis model can be derived by adopting a Dirac delta function for the time term (Friswell *et al.* 2007),

$$C(x,\xi,t-\tau)=H(x)c(x-\xi)\delta(t-\tau) \tag{6.25}$$

Similarly, a time hysteresis damping model can be obtained by adopting a Dirac delta function for the space term (Friswell *et al.* 2007),

$$C(x,\xi,t-\tau)=H(x)\delta(x-\xi)g(t-\tau) \tag{6.26}$$

### *6.3.2.2 Derivation of Galerkin implementation scheme for ESM*

The weak form of eq. (6.20) is given as,

$$\int_0^L\left(\delta^T\left(\rho A(x)\frac{\partial^2 w(x,t)}{\partial t^2}+Q_{\text{int}}(x,t)+Q_{ext}(x,t)+EI(x,t)\frac{\partial^4 w(x,t)}{\partial x^4}-f(x,t)\right)\right)dx=0 \tag{6.27}$$

The internal damping terms can be derived as,

$$\int_0^L \delta^T Q_{\text{int}}(x,t)=\int_0^L\left(\delta^T\frac{\partial^2}{\partial x^2}\left(\int_0^L\int_{-\infty}^t C(x,\xi,t-\tau)\frac{\partial^3 w(\xi,\tau)}{\partial\xi^2\partial\tau}d\tau d\xi\right)\right)dx \tag{6.28}$$

Now on integrating twice by parts, eq. (6.28) becomes,

$$\begin{aligned}&=\left[\delta^T\frac{\partial}{\partial x}\int_0^L\int_{-\infty}^t C(x,\xi,t-\tau)\frac{\partial^3 w(\xi,\tau)}{\partial\xi^2\partial\tau}d\tau d\xi\right]_0^L-\left[\frac{\partial\delta^T}{\partial x}\left[\int_0^L\int_{-\infty}^t C(x,\xi,t-\tau)\frac{\partial^3 w(\xi,\tau)}{\partial\xi^2\partial\tau}d\tau d\xi\right]\right]_0^L\\&+\int_0^L\left[\frac{\partial^2\delta^T}{\partial x^2}\left[\int_0^L\int_{-\infty}^t C(x,\xi,t-\tau)\frac{\partial^3 w(\xi,\tau)}{\partial\xi^2\partial\tau}d\tau d\xi\right]\right]dx\end{aligned} \tag{6.29}$$

Assuming the boundary terms to be satisfied, the resulting term represents the damping form which needs to be semi-discretized. Assuming a standard beam element with uncoupled axial bending interaction, the bending deformation within an element can be interpolated using the standard cubic shape functions.

$$w(\xi,\tau)=N(\xi)\mathbf{u}(\tau) \tag{6.30}$$

where $N(\xi)$ represents the spatial cubic shape functions used for standard local beam model. Here, $\mathbf{u}(\tau)$ represents the generalized nodal displacement, $x$ and $\xi$ are spatial coordinates and $\xi$ is a point in the neighborhood of $x$.

Assuming the standard Galerkin procedure for choice of the test function and substituting eq. (6.30) in eq. (6.29), we get

$$= \int_0^L \left[ \frac{\partial^2 \mathbf{N}^T(x)}{\partial x^2} \left[ \int_0^L \int_{-\infty}^t C(x,\xi,t-\tau) \frac{\partial}{\partial \tau} \left( \frac{\partial^2 \mathbf{N}(\xi)}{\partial \xi^2} u(\tau) \right) d\tau d\xi \right] \right] dx \tag{6.31}$$

Now substituting eq. (6.23) in eq. (6.31),

$$= \int_0^L \left[ \frac{\partial^2 \mathbf{N}^T(x)}{\partial x^2} \left[ \int_0^L \int_{-\infty}^t H(x) c(x-\xi) g(t-\tau) \frac{\partial^2 \mathbf{N}(\xi)}{\partial \xi^2} \dot{\mathbf{u}}(\tau) d\tau d\xi \right] \right] dx \tag{6.32}$$

Now collecting all the temporal terms together and taking it out of the main spatial integral, we get

$$= \int_0^L \left[ \frac{\partial^2 \mathbf{N}^T(x)}{\partial x^2} \left[ \int_0^L H(x) c(x-\xi) \frac{\partial^2 \mathbf{N}(\xi)}{\partial \xi^2} d\xi \right] \right] dx \int_{-\infty}^t g(t-\tau) \dot{\mathbf{u}}(\tau) d\tau \tag{6.33}$$

Now, assuming the damping patch for the entire length of the element makes the $H(x)$ a constant term, say $H_0$ (Friswell *et al.* 2007), the spatial hysteretic damping matrix is given as,

$$\mathbf{C}_{hysteretic} = H_0 \int_0^L \left[ \int_0^L \frac{\partial^2 \mathbf{N}^T(x)}{\partial x^2} c(x-\xi) \frac{\partial^2 \mathbf{N}(\xi)}{\partial \xi^2} d\xi \right] dx \tag{6.34}$$

The damping matrix obtained is given in Appendix 7.0 and is similar to direct damping matrix described in Friswell et al. (2007). In addition to the damping matrix derived in eq. (6.34), a cross

damping matrix can also be derived reflecting the effect of other elements based on the location of this element under consideration (Friswell *et al.* 2007). In the present study, only the direct damping matrix is adopted as each beam is represented by a single element and no finer spatial discretization is employed which is very typical in nonlinear seismic dynamic analyses using lumped plasticity models. If higher order finite elements like plate/shell elements are employed, cross damping matrices may be incorporated and interested readers should refer to Friswell *et al.* (2007) for more details. So, eq. (6.33) becomes,

$$= \mathbf{C}_{hysteretic} \int_{-\infty}^{t} g(t-\tau)\dot{\mathbf{u}}(\tau)d\tau \tag{6.35}$$

Rest of the other terms in eq. (6.20) follows classical discretization procedures and the total discretized equation of motion thus obtained would be as follows,

$$\mathbf{M}\ddot{\mathbf{u}} + \mathbf{C}_{hysteretic} \int_{0}^{t} g(t-\tau)\dot{\mathbf{u}}(\tau)d\tau + \mathbf{C}_{mass}\dot{\mathbf{u}}(t) + \mathbf{K}\mathbf{u}(t) = \mathbf{f}(t) \tag{6.36}$$

Here, $\mathbf{M}$ and $\mathbf{K} \in R^{NxN}$ are the element mass and element stiffness matrices given as,

$$\mathbf{M} = \int_{0}^{L} \mathbf{N}^{T}(x)\rho A(x)\mathbf{N}(x)dx \tag{6.37}$$

$$\mathbf{K} = \int_{0}^{L} \frac{\partial^2 \mathbf{N}^{T}(x)}{\partial x^2} EI(x,t) \frac{\partial^2 \mathbf{N}(x)}{\partial x^2} dx \tag{6.38}$$

and the viscous air coefficient matrix $\mathbf{C}_{mass}$ is given as,

$$\mathbf{C}_{mass} = \int_{0}^{L} \mathbf{N}^{T}(x)\gamma\mathbf{N}(x)dx \tag{6.39}$$

Eq. (6.36) is an integro-differential equation and can be solved efficiently by AAR method developed in chapter 4. The spatial and the temporal kernel function can adopt any causal dissipation function. In the present study, both spatial and temporal kernels adopt exponential functions; i.e. the following forms are adopted in the present study (Friswell *et al.* 2007),

- *Spatial kernel functions*

$$c(x-\xi)=\frac{\alpha}{2}e^{-\alpha|x-\xi|} \tag{6.40}$$

- *Time kernel functions*

$$g(t-\tau)=\frac{\mu}{2}e^{-\mu(t-\tau)} \tag{6.41}$$

Over here, $\alpha$ and $\mu$ are spatial and temporal damping constants which need to be parameterized.

#### *6.3.2.3-Dimensional homogeneity based parametrization of ESM*

Philosophically the parametrization of ESM also follows the same path as that of Russell's model. In ESM, both spatial and temporal components are present. Mainly, there are three unknown parameters which are: $\alpha$ the spatial parameter, $\mu$ the temporal parameter and $H_0$ the damping constant. Now the most sophisticated methodology would be to initiate an experimental identification procedure to parameterize these unknowns for every element comprising the system; but this is cumbersome from a practical dynamic analysis point of view and might deemed to be close to impossible in the case of a practical structural system which is yet to be constructed. A simpler and more practical methodology for parametrization is hence required. For this reason, a simple intuitive dimensional homogeneity based parametrization approach described in chapter 5 is adopted here.

By dimensional analysis, the spatial parameter $\alpha$ may be related to the elemental geometry (elemental length in this case) as follows,

$$\alpha \propto \left(\frac{1}{L}\right) \tag{6.42}$$

Introducing the concept of a proportionality constant (chapter 3.0), eq. (6.42) can be rewritten as,

$$\alpha \cong \zeta_{eSM}\left(\frac{1}{L}\right) \tag{6.43}$$

Motivated from the concept of well-known Rayleigh damping ratio, this proportionality constant is termed *extended Sorrentino elemental damping ratio*. From a dimensional homogeneity perspective, the temporal parameter $\mu$ may be related to elemental frequencies using the elemental damping ratio and may be given as,

$$\mu \cong \zeta_{eSM}\left(\frac{\omega_{ei}\omega_{ej}}{\omega_{ei}+\omega_{ej}}\right) \tag{6.44}$$

$\omega_{ei}$ , $\omega_{ej}$ are the $i^{th}$ and $j^{th}$ elemental frequencies.

Similarly, the damping constant $H_0$ may be obtained by dimensional analysis as,

$$H_0 = \zeta_{eSM}\left(\rho A(x)\right)\left(\frac{\omega_{ei}\omega_{ej}}{\omega_{ei}+\omega_{ej}}\right) \tag{6.45}$$

The biggest advantage of this modelling approach is that multiple unknowns are reduced to just parameterizing $\zeta_{eSM}$. Again, in the present study, $\zeta_{eSM}$ will be a constant for all elements in the system (Chapter 3). But if better parameterization procedures are available, the $\zeta_{eSM}$ can also be

varied between elements. Computation of elemental frequencies relies on the same justifications as outlined in chapter 5.

## 6.4 Computation of elemental frequencies and mass formulations

Detailed description of computation of elemental frequencies was presented in chapter 3.0. In the present study, a free-free boundary condition is assumed for the element before the matrix assembly and element frequencies are computed as described in Appendix 1. Rigid body modes of the element are assumed to be undamped as no deformation is associated with them.

Russell and ESM models can be implemented using either diagonal mass or consistent mass formulations. Details of implementation of the mass formulations are given in chapter 3.0. Both models are implemented in *Ruaumoko*, the 3D inelastic dynamic analysis commercial software.

## 6.5 Parameterizing elemental damping ratio

For the practical use of the above described nonlocal models in seismic analysis, the elemental damping ratio needs to be parameterized. One way of achieving this is by experimental testing and estimating the elemental damping ratio based on the recorded responses. As already mentioned in the previous chapters, one of the most generic ways of doing this might be to identify the elemental damping ratio at a component level by appropriate testing of the components which make up the

whole system. But a component level identification approach might be a very cumbersome procedure and in view of the uncertainties in the overall damping phenomenon and the uncertainties already present in nonlinear analysis, this would not be a practical option. Another approach would be to identify a system level equivalent value for the elemental damping ratio assuming it to be constant for all elements by experimental testing; but the issue with this approach is that the system which is yet to be designed needs to be existing as already built, which negates the whole purpose of a simulation. So, considering all these impediments, a very simple simulation based identification procedure similar in manner to that described in chapter 3.0 is outlined in this section for identifying elemental damping ratio. This method is adopted in the present chapter.

First, a mathematical model of the system with damping matrix represented by global Rayleigh damping model with a preconceived global damping ratio is assembled. This is then subjected to a free vibration and its responses are computed. Then the damping matrix is recomputed using the nonlocal elemental damping model with an arbitrary value for the elemental damping ratio. The elemental damping ratio is then iteratively identified to obtain a very close match to the free vibration response of the system obtained using the global Rayleigh model. The elemental damping ratio thus identified is used for all the subsequent inelastic analysis. One thing the readers must note is that Rayleigh damping was chosen as the datum damping not because it is the *"right model",* but because of its popularity and also due to the existing popular belief that Rayleigh damping reasonably mimics the damping phenomenon in linear dynamics (Wilson and Clough, 1962).

.

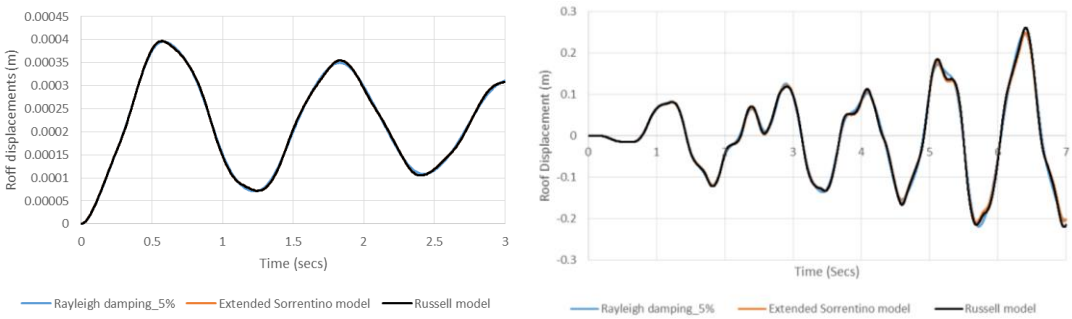


Fig 6.2a. Free vibration matching of the frame with Rayleigh damping model and the nonlocal damping models.

6.2b Elastic analysis of the four storey frame with 5% Rayleigh damping and non-local damping models

Fig 6.2a illustrates the free vibration matching for the four storey frame described in chapter 3 using the global Rayleigh damping with 5% damping ratio and with both the elemental non-local damping models. Basically, such an approach ensures that in the linear state at least, damping attributed by the non-local damping models is equivalent to that attributed by the Rayleigh damping model with 5% damping. To further verify this statement an elastic response computation from all the three models is presented using a single ground motion. Fig 6.2b illustrates the comparative response of the four-story frame subjected to an earthquake where the frame remains in its linear state. Responses from all three models are presented. It can be clearly seen that the differences in the peak responses is of the order of ~5% between Rayleigh and non-local damping models. Considering all the other uncertainties involved in time domain analysis, this slight discrepancy observed can be overlooked and this methodology of parameterization may be deemed to be acceptable. As mentioned in previous chapters, choice of Rayleigh damping as the datum is just mainly due to the popularity of the model among the analysts and not because the author believes this is the “correct model”.

Now it could be argued that this type of a parametrization calls for a free vibration analysis prior to starting the inelastic analysis which might increase the overall computational cost; but in the light of higher reliability in the responses offered by the proposed models as evidenced in the numerical study in section 6.7, this small increase in computational cost should not be considered as a major impediment in the adoption of these models as both these models exhibit higher physical and mathematical consistency as opposed to the other available damping models. Also from an implementation point of view, to minimize the user effort, this proposed free vibration matching procedure may be made into an automatic iterative process in such a way that the user need only specify the well-known global damping ratio and the automatic parametrization subroutine would compute the constant elemental damping ratio by performing free vibration matching in an iterative manner for the system.

## 6.6 Implementation of the proposed models in Newmark direct time domain integration framework

Both incremental and revised Newmark methods are discussed for elemental Russell model, but only the revised Newmark total equilibrium method is discussed for the ESM model as it uses the AAR method developed in chapter 4.

### 6.6.1 Elemental Russell model

This section presents both the incremental and total equilibrium version of Newmark direct integration scheme for elemental Russell model.

#### *6.6.1.1 Incremental Newmark framework*

In this section, the algorithm uses the Newmark constant average acceleration method with $\gamma = \frac{1}{2}$ and $\beta = \frac{1}{4}$. The algorithm outlined in fig. 6.3 is equally applicable to the linear acceleration method as well with similar ease. Only the implementation of the model with tangent proportionality constants are illustrated in this section and the procedure is the same for other models. Mass formulations used can be either diagonal or consistent.

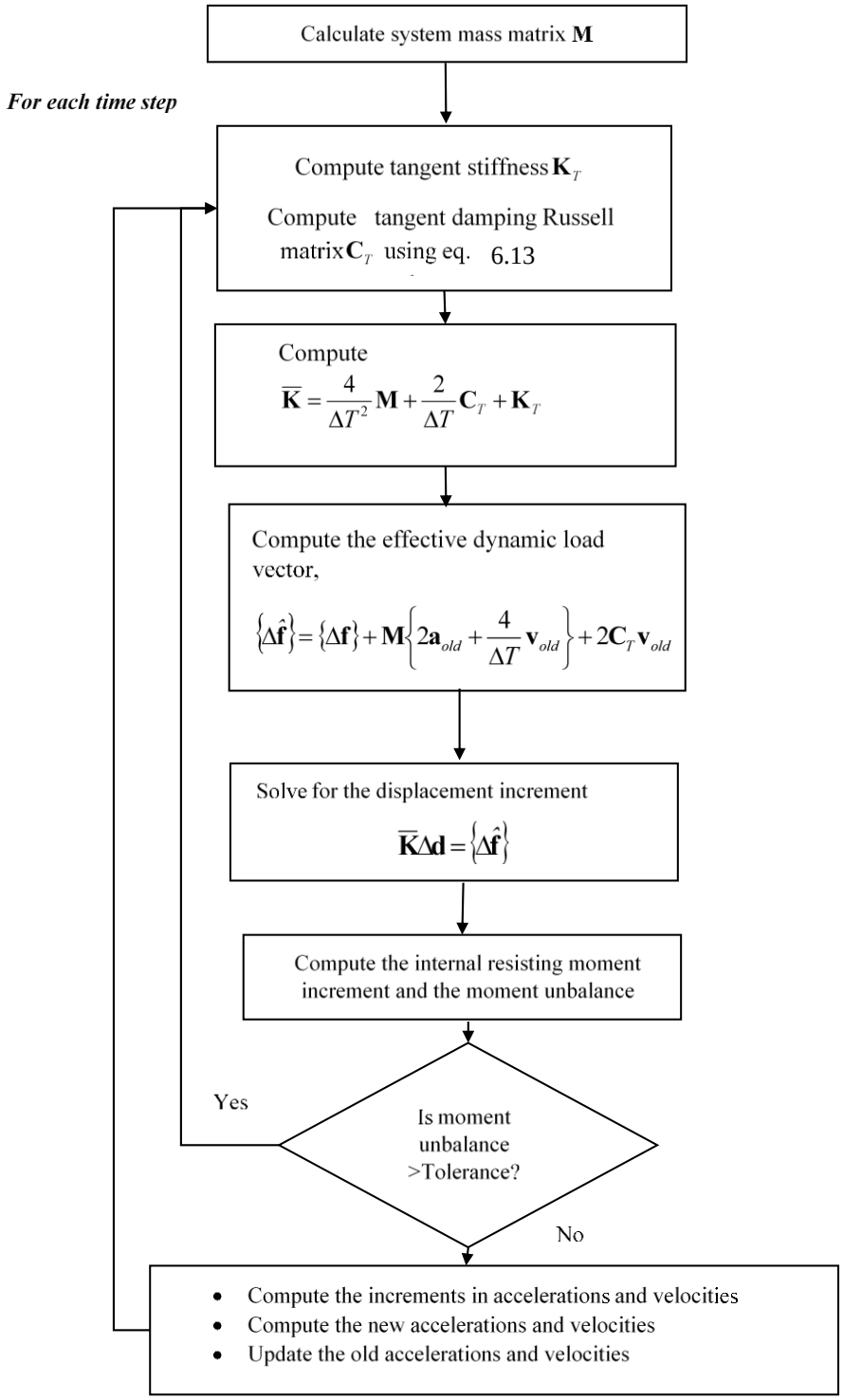


Fig. 6.3 Flow chart of incremental Newmark acceleration implementation algorithm for elemental Russell model

### *6.6.1.2 Revised Newmark total equilibrium method*

Revised Newmark total equilibrium method outlined in Appendix 2 is adapted to incorporate the Russell damping model and the algorithm is outlined in fig. 6.4.

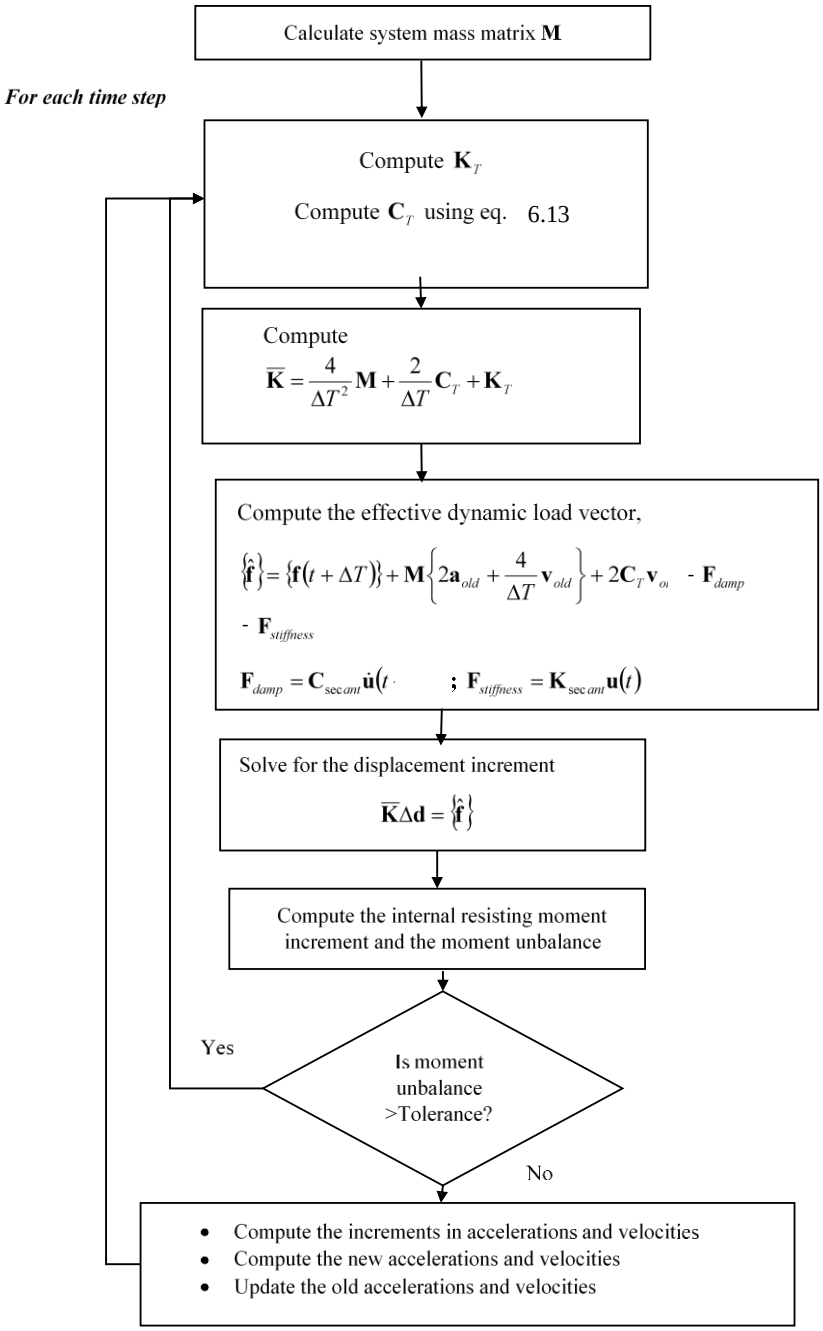


Fig 6.4 Flow chart for revised Newmark total equilibrium method for elemental Russell model.

### 6.6.2 Extended Sorrentino model

This section presents the implementation of ESM damping model using the AAR method described in chapter 4.0.

#### *6.6.2.1 Implementation of ESM using Modified Newmark formulation (AAR method)*

The final form of the equation which needs to be implemented is given below,

$$\left[\frac{4}{\Delta T^2}\mathbf{M}+\frac{2}{\Delta T^2}\int_t^{t+\Delta T}\left[\sum_{iel=1}^{N_s}\mathbf{C}_{hysteretic}^{iel}g^{iel}\left(t+\Delta T-\tau\right)\right]d\tau+\mathbf{K}_T\right]\Delta\mathbf{u}=\mathbf{P}\left(t+\Delta T\right)+\mathbf{M}\left\{\ddot{\mathbf{u}}\left(t\right)+\frac{4}{\Delta T}\dot{\mathbf{u}}\left(t\right)\right\}$$
$$-\sum_{r=1}^{n+1}\left[\sum_{iel=1}^{N_s}\mathbf{C}_{hysteretic}^{iel}g^{iel}\left(\left(n+1-r\right)\Delta T\right)\right]\dot{\mathbf{u}}\left(\left(r-1\right)\Delta T\right)\Delta T-\mathbf{K}_s\mathbf{u}\left(t\right)-\int_t^{t+\Delta T}\left[\sum_{iel=1}^{N_s}\mathbf{C}_{hysteretic}^{iel}g^{iel}\left(t+\Delta T-\tau\right)\right]\dot{\mathbf{u}}\left(t\right)d\tau$$
$$+\frac{2}{\Delta T}\int_t^{t+\Delta T}\left[\sum_{iel=1}^{N_s}\mathbf{C}_{hysteretic}^{iel}g^{iel}\left(t+\Delta T-\tau\right)\right]\dot{\mathbf{u}}\left(t\right)d\tau \tag{6.46}$$

Here, $\mathbf{M}$ refers to system mass matrix; $\mathbf{K}_T$ refers to the system tangent stiffness; $\mathbf{K}_s$ refers to the system secant stiffness matrix; $\mathbf{C}_{hysteretic}^{iel}$ refers to the elemental hysteretic damping matrix as given by eq. (6.34) of $iel^{th}$ element; $\ddot{\mathbf{u}}\left(t\right),\dot{\mathbf{u}}\left(t\right)$ and $\mathbf{u}\left(t\right)$ are the acceleration, velocity and displacement vector respectively; $g^{iel}\left(t-\tau\right)$ refers to the time hysteresis damping kernel per element; $N_s$ is the number of elements in the system and $\Delta T$ refers to the time step increment. It must be noted that the $\sum$ symbol in eq. (6.46) indicates the assembling of the elemental matrices. Implementable format of eq. (6.46) used in the algorithm below is given as,

$$\left[\frac{4\mathbf{M}}{\Delta T^2}+\frac{2}{\Delta T^2}\mathbf{I}_{damp2}+\mathbf{K}_T\right]\Delta\mathbf{u}=\mathbf{P}(t+\Delta T)+\mathbf{M}\left\{\ddot{\mathbf{u}}(t)+\frac{4}{\Delta T}\dot{\mathbf{u}}(t)\right\}-\mathbf{f}_{damp}-\mathbf{K}_s\mathbf{u}(t)-\mathbf{I}_{damp1}\dot{\mathbf{u}}(t)+\frac{2}{\Delta T}\mathbf{I}_{damp1}\dot{\mathbf{u}}(t)$$

(6.47)

where

$$\mathbf{I}_{damp1}=\int_t^{t+\Delta T}\left[\sum_{iel=1}^{N_s}\mathbf{C}_{hysteretic}^{iel}g^{iel}(t+\Delta T-\tau)\right]d\tau \tag{6.48}$$

$$\mathbf{I}_{damp2}=\int_t^{t+\Delta T}\left[\sum_{iel=1}^{N_s}\mathbf{C}_{hysteretic}^{iel}g^{iel}(t+\Delta T-\tau)\right]\tau d\tau \tag{6.49}$$

$$\mathbf{f}_{damp}=\sum_{r=1}^{n+1}\left[\sum_{iel=1}^{N_s}\mathbf{C}_{hysteretic}^{iel}g^{iel}((n+1-r)\Delta T)\right]\dot{\mathbf{u}}((r-1)\Delta T)\Delta T \tag{6.50}$$

*6.6.2.1.1 Algorithm for implementation of nonlinear AAR*

The algorithm detailed in this section adopts the time hysteresis damping kernel as per eq. (6.41). The algorithm is detailed for the case when the damping model parameters are updated every time step; i.e. $\mu_e = \mu_{eT}$ where $\mu_{eT}$ is the tangent temporal damping constant.

- ***Initial Calculations***

1.0 Initialize the system displacement vector $\mathbf{d}_{old}=\mathbf{u}(0)$ and velocity vector $\mathbf{v}_{old}=\dot{\mathbf{u}}(0)$

2.0 Parametrize the ESM damping ratio $\xi_{eSM}$ as outlined in section 6.5.

3.0 Compute the elemental frequencies using the initial elemental stiffness matrix and evaluate the initial damping proportional parameter $\mu_e$ for each element.

4.0 Assemble the system mass matrix **M**, initial system hysteretic damping matrix $\mathbf{C}_{hyst}$ and initial stiffness matrix **K.**

$$\mathbf{C}_{hyst}(t) = \sum_{iel=1}^{N_s} \mathbf{C}_{hysteretic}^{iel} \mu_e^{iel} e^{-\mu_e^{iel}(t-\tau)} \tag{6.51}$$

5.0 Initialize system acceleration vector as,

$$\mathbf{a}_{old} = \mathbf{M}^{-1}\left\{\mathbf{f}(0) - \mathbf{C}_{hyst}(0)\mathbf{v}_{old} - \mathbf{C}_{air}\mathbf{v}_{old} - \mathbf{K}\mathbf{d}_{old}\right\} \tag{6.52}$$

6.0 Initialize $\mathbf{f}_{damp}$ vector.

- ***Calculation for each time step***

7.0 Choose a sufficiently small time step. For the first time step,

7.1 Compute the current tangent system stiffness matrix.

7.2 Compute the current tangent system damping matrices $\mathbf{I}_{damp1}$ and $\mathbf{I}_{damp2}$

To demonstrate the computation of the above terms for the $j^{th}$ element,

7.2.1 Compute the elemental frequencies as described in section 6.4 using the present element stiffness obtained from step 7.1.

7.2.2 Compute the current tangent damping proportional parameter $\mu_e$ for the element

7.2.3 Compute the $\left.\begin{aligned} \mathbf{I}_{damp1}^{j} &= \int_{t}^{t+\Delta T} \mathbf{C}_{hysteretic}^{j} \mu_{e,j} e^{-\mu_j(t+\Delta T-\tau)} d\tau \\ \mathbf{I}_{damp2}^{j} &= \int_{t}^{t+\Delta T} \mathbf{C}_{hysteretic}^{j} \mu_{e,j} e^{-\mu_j(t+\Delta T-\tau)} \tau d\tau \end{aligned}\right\}$ such that on matrix assembly will result in $\mathbf{I}_{damp1}$ and $\mathbf{I}_{damp2}$

7.3 Compute the system dynamic stiffness matrix $\hat{\mathbf{K}}$

$$\hat{\mathbf{K}} = \frac{4\mathbf{M}}{\Delta T^2} + \frac{2}{\Delta T^2}\mathbf{I}_{damp2} + \mathbf{K}_T \tag{6.53}$$

where $\mathbf{K}_T$ is the tangent stiffness.

7.4 Evaluate the effective system load vector,

$$\mathbf{P}_{new} = \mathbf{P}(t+\Delta T) + \mathbf{M}\left\{\ddot{\mathbf{u}}(t) + \frac{4}{\Delta T}\dot{\mathbf{u}}(t)\right\} - \mathbf{f}_{damp} - \mathbf{K}_s\mathbf{u}(t) - \mathbf{I}_{damp1}\dot{\mathbf{u}}(t)d\tau + \frac{2}{\Delta T}\mathbf{I}_{damp1}\dot{\mathbf{u}}(t) \tag{6.54}$$

7.5 Solve for system displacement increment,

$$\hat{\mathbf{K}}\Delta\mathbf{u} = \mathbf{P}_{new} \tag{6.55}$$

7.6 Perform *state determination* to check whether there is a change in stiffness within the time step*;* for details refer (Chopra 2012; Filippou *et al.* 1992). If a change in stiffness occurs during the time step, repeat steps 7.1 to 7.6. If there is no change in stiffness (*in a state of convergence*),

7.6.1 Compute the incremental acceleration and incremental velocity as follows,

$$\Delta\ddot{\mathbf{u}} = \left[\frac{4}{\Delta T^2}\Delta\mathbf{u} - \frac{4}{\Delta T}\mathbf{v}_{old} - 2\mathbf{a}_{old}\right] \tag{6.56}$$

$$\Delta\dot{\mathbf{u}} = \left[\frac{2}{\Delta T}\Delta\mathbf{u} - 2\mathbf{v}_{old}\right] \tag{6.57}$$

7.6.2 Compute the new acceleration and new velocity

$$\mathbf{v}_{new} = \mathbf{v}_{old} + \Delta\dot{\mathbf{u}} \tag{6.58}$$

$$\mathbf{a}_{new} = \mathbf{a}_{old} + \Delta\ddot{\mathbf{u}} \tag{6.59}$$

$$\mathbf{d}_{new} = \mathbf{d}_{old} + \Delta\mathbf{u} \tag{6.60}$$

7.6.3 Update the $\mathbf{a}_{old}$ $\mathbf{v}_{old}$ and $\mathbf{d}_{old}$

7.6.4 Update $\mathbf{f}_{damp}$, $\mathbf{f}_{damp1}$ and $\mathbf{f}_{damp2}$, where,

$$\left.\begin{aligned}\mathbf{f}_{damp1} &= \mathbf{I}_{damp1}\dot{\mathbf{u}}(t)d\tau \\ \mathbf{f}_{damp2} &= \frac{2}{\Delta T}\mathbf{I}_{damp1}\dot{\mathbf{u}}(t)d\tau\end{aligned}\right\} \tag{6.61}$$

8.0 Repeat steps 7.1 to7.6 in step 7.0 for other time steps.

## 6.7 Numerical study

To assess the performance of the proposed non-local continuum models, a series of numerical studies are performed on the same four-story RC frame described in chapter 3.0 and Appendix 3. The numerical studies includes a single ground motion study and an Incremental Dynamic Analysis (IDA) study. As a bilinear hysteresis as described in chapter 3.0 for simplicity is used, the results presented in this section are more qualitative in nature.

In this study, the comparative performance of the non-local damping models is made against the most popular classical damping models used in seismic analysis which includes the initial stiffness based Rayleigh damping model, Tangent stiffness based Rayleigh damping model and the Wilson Penzien/ modal damping model. Following abbreviations are used to identify different damping models included in the plots hereafter: Initial stiffness based classical Rayleigh damping (ISRD), Tangent stiffness based classical Rayleigh damping with constant coefficients (TSRD), Elemental Russell damping with updated proportionality coefficients (ELRu), Elemental Sorrentino model with updated damping parameters (ELSM) and Wilson Penzien/modal damping model (GWP). In

all plots presented in this section, global models are presented with continuous lines and elemental models are presented with broken lines. 5% damping ratio is used by all global damping models.

### 6.7.1 Single ground motion study

An EC8 spectrum compatible artificial ground motion scaled to an intensity of 0.5g is used for this study. Only roof displacement histories are compared in this study.

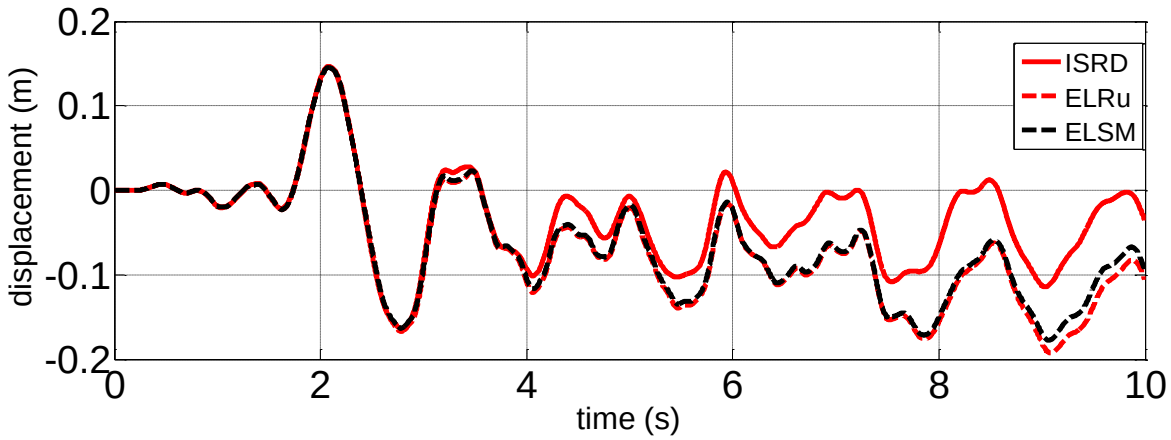


Fig 6.5 Roof displacements based on different models

Fig 6.5 illustrates the roof displacements of the four storey frame with both initial stiffness Rayleigh damping and non-local damping models. As single ground motion study was only meant to be an overview of the effects the choice of models has on the responses, only the most popular initial stiffness Rayleigh model is used in the present comparison. It can be clearly seen that different models give different responses. It is also evident that different models tend to exhibit different behavior when the system undergoes nonlinear excursions. The responses presented in fig. 6.5 are computed using consistent mass formulation. To get a better insight into the effect of the choice of damping models and different mass formulation aiding the computation of damping matrices, an IDA study is presented in the next section.

### 6.7.2 IDA study

IDA study follows the same approach as adopted in chapters 3 & 5 and investigates the effect of different mass formulations in the damping matrix computation. IDA study is presented in two subsections based on the way the mass used for computing the damping matrix is formulated. They are as follows:

#### *6.7.2.1 Consistent mass formulation*

Classical consistent mass formulation for Euler Bernoulli beam is used for the damping matrix computation. Same seven artificial far field ground motions scaled to five intensity measures (depicted in the form of peak ground acceleration PGA) as used in chapters 3 & 5 are used for the present study. Ground motions were scaled to the following intensity measures 0.3g, 0.4g, 0.5g, 0.6g and 0.7g. To maintain consistency in comparison, the global models also adopt the consistent mass formulation for the damping matrix computation instead of the normal lumped mass formulation. The responses of the global models are directly adopted from chapter 3.0.

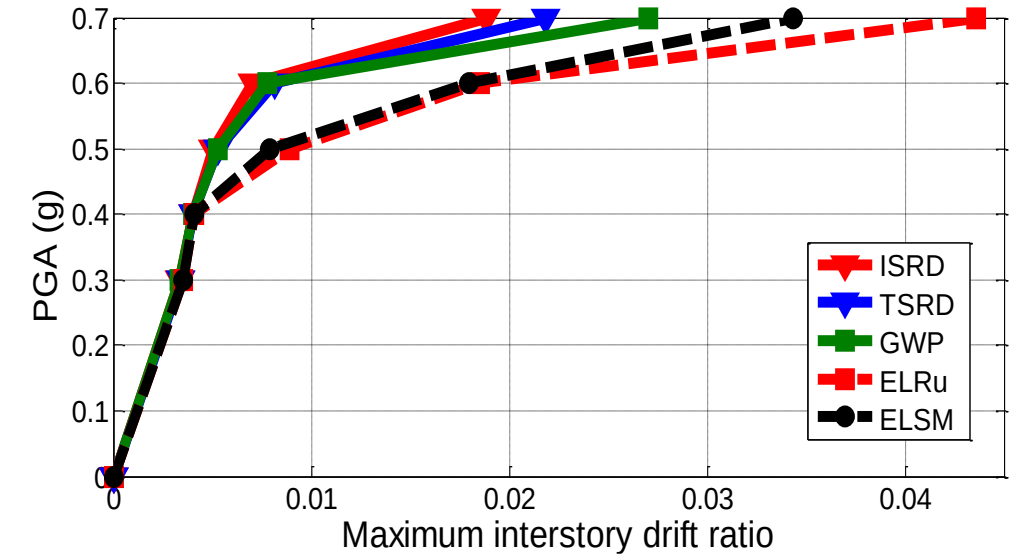


(a)

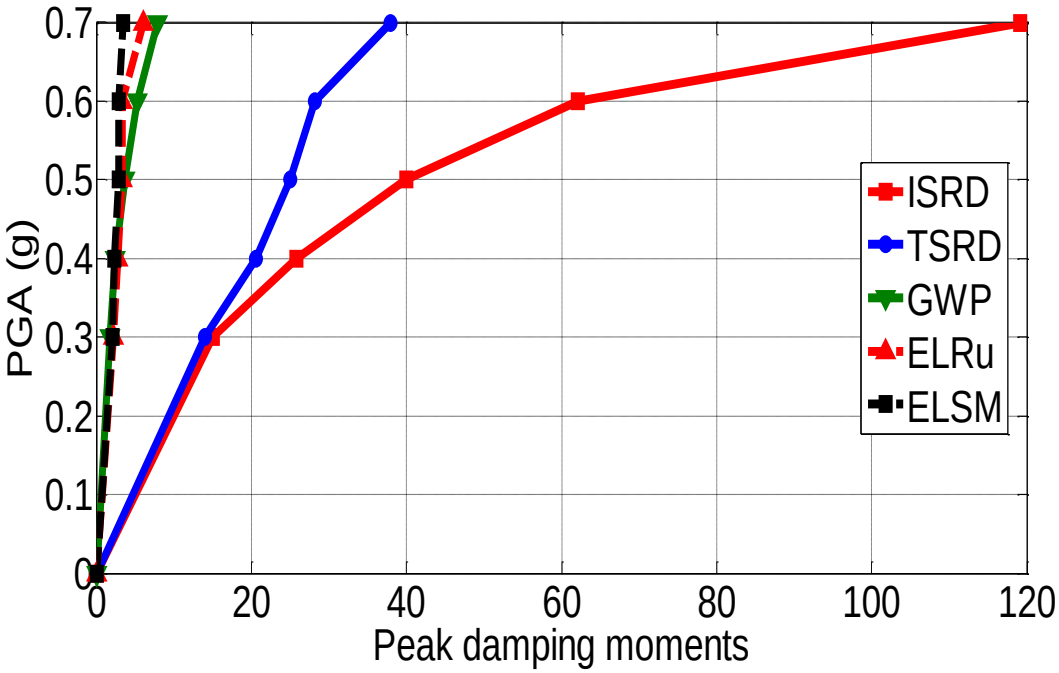


(b)

Fig. 6.6a. IDA curves for mean peak interstory drifts for consistent mass formulation. Fig.6.6b. IDA curves for peak damping moments for consistent mass formulation.

Fig.6.6a illustrates the mean IDA curves for location independent peak interstory drift ratio and fig.6.6b depicts the IDA curves for peak damping moments. In fig 6.6a, it could be seen that from 0.5g PGA onwards the responses obtained by the proposed damping models deviate from the responses of the classical damping model indicating excursion of high level nonlinearity. This is to be expected since the structure is designed for high seismicity with a design PGA of 0.3g and assumes a high ductility class with a behavior factor of 5. So, this evidences that the proposed damping models give a more conservative estimate on the onset of nonlinearity. One important point to be noted is that the pre-yield state depicted by classical damping models might not be a realistic pre-yield state as illustrated in fig 6.6a. This might result in un-conservative estimates of nonlinear responses as the analysis would still be linear when the actual system might have entered the post yield state. As mentioned in chapter 5, similar observations were presented by Val *et al.* (2005) using an elasto-slip model in which it was shown that there might be instances where the viscous damping assumption would underestimate the peak response.

Though not completely, to an extent this deviation in the behavior of the classical damping models and the proposed damping models may be explained in terms of damping moments. Damping moments are exhibited by the damping models on the initiation of nonlinearity (Carr 2007, Puthanpurayil *et al.*2016). In the case of classical viscous and spatial nonlocal viscous damping models, this can be computed as the product of the current damping coefficient matrix with the current velocity vector, whereas in the case of ESM, this can be computed by adding the damping forces on the right-hand side of eq. (6.47). Fig. 6.6b clearly illustrates the superiority of the elemental nonlocal models in comparison to the classical Rayleigh damping models in terms of the damping moments. All elemental damping models produce small un-realistic damping forces similar in manner to Wilson Penzien damping model (modal damping); epitomizing the

significance of the elemental damping models in comparison to the classical Rayleigh damping models in a performance assessment scenario. Though Wilson-Penzien model produces damping moments similar to the proposed models, it cannot be used in practice mainly attributed to the heavy computational demand imposed by the requirement of computation of all the eigen parameters of the system as described in chapter 3 (Charney 2006). Also from an engineering perspective, the proposed models predict responses in a conservative manner better than Wilson Penzien model.

#### *6.7.2.2Diagonal mass formulation*

Classical diagonal mass formulation of Euler Bernoulli beams is used for generating the damping matrix. Same set of seven artificial far field ground motions used for section 6.7.2.1 are used for this study as well. Here, global models also adopt the diagonal mass formulation for the damping matrix computation. The IDA responses for the global models depicted in fig.6.7a and 6.7b are adopted directly from chapter 3.0.

Fig.6.7a presents the mean IDA curves for location independent peak interstory drift ratio and fig.6.7b illustrates the IDA curves for peak damping moments. Both plots exhibit similar trend as in the case of consistent mass formulation as described in section 6.7.2.1. This clearly shows that if elemental damping models are used, either consistent mass or diagonal mass formulation can be used for generating the elemental frequencies. As evidenced in the plots, when the intensity increases, higher interstory drift ratios are exhibited by the elemental damping models. Fig. 6.7 b illustrates that the peak damping moments predicted using the diagonal mass formulation also show similar trend to consistent mass formulation; i.e. the elemental damping models result in much lower damping moments compared to the global Rayleigh based damping models.

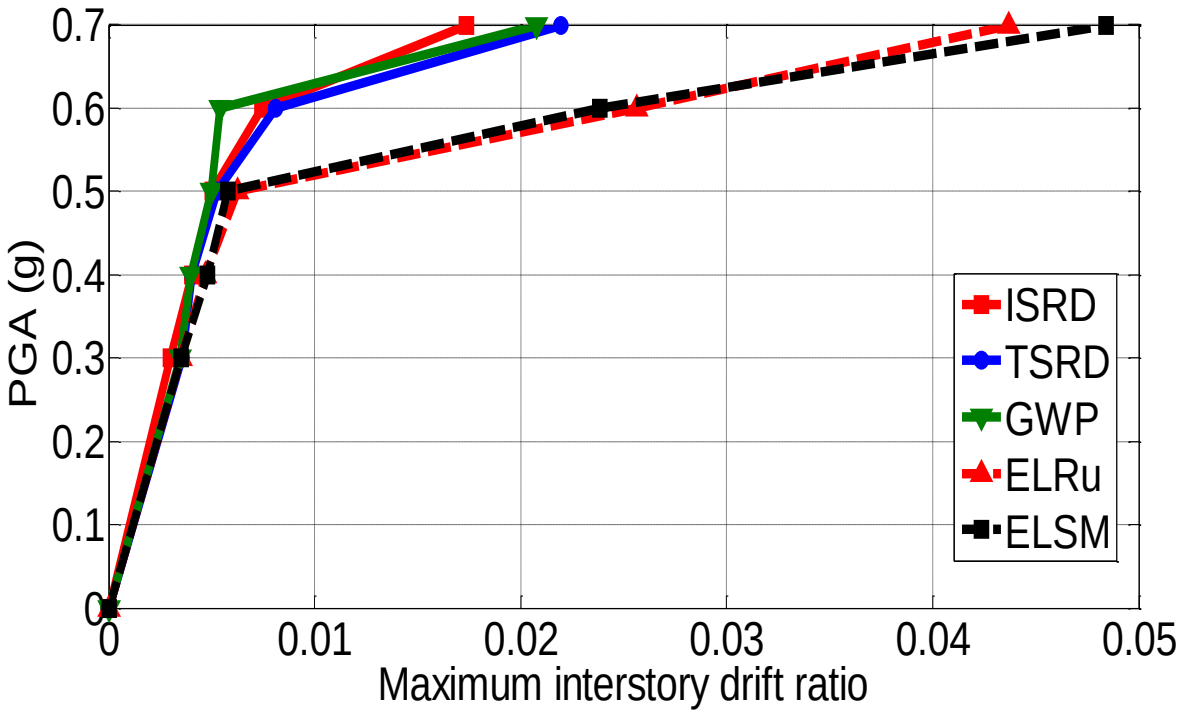


(a)

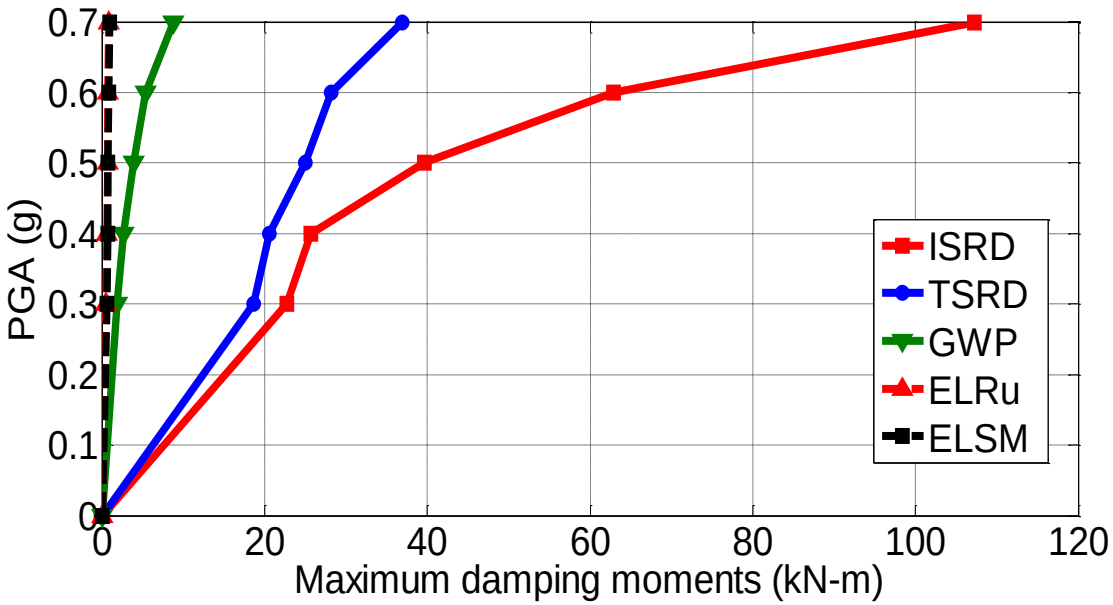


(b)

Fig. 6.7a. IDA curves for mean peak interstory drifts for diagonal mass formulation. Fig. 6.7b. IDA curves for peak damping moments for diagonal mass formulation.

#### *6.7.2.3Observation on consistent mass formulation vs. diagonal mass formulation*

Comparing the response plots and the damping moment plots presented in section 6.7.2.1 and 6.7.2.2, it could be clearly seen that both mass formulations give responses which are conservative in an engineering perspective. It has to be noted that damping is an observed phenomenon. So no authoritative conclusion can be drawn regarding the correctness of a model in representing reality except for relying on the models which give more conservative estimates of the responses of interest with little or no untoward non-physical effects. So in effect from a practical perspective, either of these mass formulations can be used in computing the elemental damping matrix for the proposed models; but considering the fact that the consistent mass formulation is more mathematically consistent, the author tends to prefer computing elemental damping matrix parameters using this formulation rather than the diagonal mass formulation. Also if consistent mass is used, as only small matrices are involved as it is computed at elemental level, there is no additional penalty in terms of computational cost.

## 6.8 Conclusions

The already existing nonlocal continuum damping models have been adapted and extended to nonlinear seismic analysis. A Galerkin based Finite element scheme is developed and the numerical implementation and parametrization of the models are outlined. Performance of these models in inelastic seismic analysis has been assessed using numerically simulated responses for a four story frame. It has been shown that nonlocal continuum damping models are better than global discrete damping models.

# 7. A comparative performance evaluation of elemental damping models

**Book Chapter**

Carr A., Puthanpurayil A.M, (2017) *Inherent damping in nonlinear time-history analyses. A recommended modelling approach.* peer reviewed book chapter (in print); this paper was also presented as a keynote by Prof. Carr in International conference on earthquake engineering and structural dynamics.

**Peer reviewed conferences**

Carr A., Puthanpurayil A.M, Lavan O, Dhakal R. (2017) *Damping Models for Inelastic Time-History Analysis.* Santiago, Chile: 16th World Conference on Earthquake Engineering (16WCEE), 9-13 Jan 2017.: 12.

Puthanpurayil A., Carr A., Lavan O. and Dhakal R. (2017) *Effect of choice of inherent damping models on reliability of Incremental Dynamic Analysis.* Wellington: ". 2017 Annual Conference of NZ Society for Earthquake Engineering (NZSEE17), 27-29 Apr 2017.: 9.

**Abstract** This chapter consolidates the responses of all damping models introduced in the previous chapters and attempts to identify a preferred model. The preferred model identified is then used for the optimization studies undertaken in the next chapters.

## 7.1 Introduction

The damping models used in - non-linear time-history analysis are trying to mimic the *unmodeled* dissipation. The overall mechanisms that contribute to this *un-modelled dissipation* are complex and need to be explicitly defined by an appropriate damping matrix. These damping matrices are created using pseudo mathematical models which tryto mimic the observed phenomenon, but have no relation with the exact physics of the process that causes

the damping phenomenon. In the other chapters of this thesis (Ch. 3.0, Ch. 5.0 & Ch. 6.0) a series of damping models with increasing rigor were proposed to reflect the damping phenomenon in inelastic dynamic analysis. The present chapter consolidates these elemental damping models proposed in other chapters and presents an investigation to identify the most appropriate damping model for nonlinear dynamic analysis. One additional contribution of this chapter is that responses computed using updated elemental Wilson Penzien model is also incorporated; in chapter 3 elemental Wilson Penzien model was implemented as a constant matrix similar to the Global Wilson Penzien model. An indication of the most suitable damping model for nonlinear dynamic analysis is also presented.

## 7.2 Overview of the elemental damping models

This section briefly consolidates the elemental damping models presented in the previous chapters. The elemental damping models are broadly classified based on the way the damping matrix is formed and is as follows:

- Discrete elemental damping models
- Continuum elemental damping models

In the discrete elemental damping models, the damping matrix is introduced at the element level after a semi-discretisation procedure is undertaken. In the continuum models the damping is introduced at the continuum level and on semi-discretisation produces the elemental damping matrix. The elemental damping matrix thus obtained is then assembled like mass and stiffness matrices. These models can be further classified based on the way the coefficients are computed and the mass formulation. In this approach, the element mass matrix may be either the element consistent mass matrix or a diagonalized version of it. The member deformation modes are

required to compute the element damping matrices (eg beams require the flexural modes and frequencies).

### 7.2.1 Discrete elemental damping models

Two elemental models described in chapter 3.0 which are the elemental counterparts of the global models fall in this category. These are the

1. Elemental Rayleigh damping (elemental adaptation of the classical Rayleigh damping)
2. Elemental Wilson-Penzien model (elemental adaptation of the classical Wilson-Penzien model).

To avoid repetition, only a very brief theoretical summary of the elemental models is given. For more details please refer to chapter 3.0.

- *Elemental Rayleigh damping model*

The form of the element damping matrix is given as,

$$\mathbf{C}_e = \alpha_{eRD}\mathbf{M}_e + \beta_{eRD}\mathbf{K}_e \tag{7.1}$$

where $\alpha_{eRD}$ and $\beta_{eRD}$ are the elemental damping coefficients. The main difference between the elemental Rayleigh damping and the classical Rayleigh damping (which is predominantly implemented at a global level) exists in the computation of these damping coefficients. In the elemental Rayleigh damping the coefficients are computed as,

$$\left.\begin{aligned} \alpha_{eRD} &= 2\xi_{eR1}\frac{\omega_e^i\omega_e^j}{\omega_e^i+\omega_e^j} \\ \beta_{eRD} &= 2\xi_{eR1}\frac{1}{\omega_e^i+\omega_e^j} \end{aligned}\right\} \tag{7.2}$$

where $\omega_e^i$ and $\omega_e^j$ are the $i^{th}$ and the $j^{th}$ elemental frequencies. $\xi_{eR1}$ and $\xi_{eR2}$ are elemental damping ratios which need to be parameterised as outlined in chapter 3.0.

- *Elemental Wilson-Penzien model*

The elemental Wilson-Penzien damping coefficients is given as,

$$\mathbf{C}_e = \Theta_e \Psi_e \Theta_e^T \tag{7.3}$$

where $\Theta_e$ is the mass normalized elemental mode shape matrix. $\Psi_e$ is a diagonal matrix with diagonal elements given by,

$$\psi_e^i = \frac{2\xi_{eWP}^i \omega_e^i}{M_{di}^i} \tag{7.4}$$

where $\xi_{eWP}$ is the elemental Wilson-Penzien damping ratio assumed to be equal for all elements and *assumed to be same as the global damping ratio (the damping ratio used for the global Wilson-Penzien model).*

In chapter 3.0 this damping matrix was only implemented as a constant matrix; but in this chapter an updated version of the matrix is also implemented and is called as the *updated elemental Wilson Penzien model*. The main difference in the implementation happens in step b in section 3.5.2.

### 7.2.2 Continuum damping models

In the continuum damping models, the damping term is introduced at the continuum level. Chapters 5.0 and 6.0 introduce the continuum damping models with increasing rigor.

Two damping forces are introduced at the continuum level to represent the internal damping action and the external damping action (mainly attributed to air resistance in a physical sense).

The external term can be very important if the structure is immersed in a fluid where there will be drag forces applied on the structure. The Euler Bernoulli beam continuum enhanced with the damping term is given as,

$$\rho A(x)\frac{\partial^2 w(x,t)}{\partial t^2} + F_{int}(x,t) + F_{ext}(x,t) + \frac{\partial^2}{\partial x^2}\left( EI(x)\frac{\partial^2 w(x,t)}{\partial x^2} \right) = f(x,t) \qquad (7.5)$$

where, $F_{\text{int}}(x,t)$ is the internal damping force caused by internal resistance and $F_{ext}(x,t)$ is the external damping force. $'x'$ refers to the spatial ordinate and $'t'$ refers to the time ordinate. To simplify the presentation, the initial conditions are assumed to be zero and the boundary conditions are not explicitly listed as the semi-discretization is applicable to a variety of boundary conditions. $\rho, A(x), E$ & $I(x)$ refer to material density, geometric area, modulus of elasticity and second moment of area of the beam continuum. $f(x,t)$ is the externally applied load; $w(x,t)$ is the transverse displacement.

The external damping force is assumed as,

$$F_{ext}(x,t) = \gamma_{air}\frac{\partial w(x,t)}{\partial t} \qquad (7.6)$$

$\gamma_{air}$ is the external air damping coefficient.

### *7.2.2.1 Spatially local continuum damping models*

Chapter 5.0 describes the spatially local continuum damping model. In this model, the damping force at a point is the function of the response at the same point.

- *Kelvin Voigt damping*

In Kelvin Voigt damping the $F_{\text{int}}(x,t)$ is given as,

$$F_{\text{int}}(x,t)=\frac{\partial^2}{\partial x^2}\left(c_s I(x,t)\frac{\partial^3 w(x,t)}{\partial t\partial x^2}\right) \tag{7.7}$$

where $c_s$ refers to the damping coefficient which converts strain rate into stress. The elemental Kelvin Voigt damping matrix is obtained by semi-discretization of equation (7.5) incorporating equations (7.6) and (7.7). As described in chapter 5.0, this model could be viewed as a continuum version of the classical global Rayleigh damping model.

- *Time hysteresis damping*

The time hysteresis damping force is given as,

$$F_{\text{int}}(x,t)=\int_0^t g(t-\tau)EI(x,t)\frac{\partial}{\partial\tau}\left(\frac{\partial^4 w(x,\tau)}{\partial x^4}\right)d\tau \tag{7.8}$$

Incorporating equations (7.6) and (7.8) in equation (7.5) and on semi-discretization, the elemental equation of motion is given as,

$$\mathbf{M}_e\ddot{\mathbf{d}}_e(t)+\mathbf{C}_{eair}\dot{\mathbf{d}}_e(t)+\mathbf{K}_e\int_0^t g(t-\tau)\dot{\mathbf{d}}_e(\tau)d\tau+\mathbf{K}_e\mathbf{d}_e(t)=\mathbf{f}_e(t) \tag{7.9}$$

where, $\mathbf{M}_e$ is the element mass matrix; $\mathbf{K}_e$ is the element stiffness matrix; $\mathbf{C}_{eair}$ is the element external damping matrix; $\ddot{\mathbf{d}}_e, \dot{\mathbf{d}}_e, \mathbf{d}_e$ are the element acceleration, velocity and displacement; $g(t-\tau)$ is the causal damping kernel function which is given as,

$$g(t)=\mu e^{-\mu t} \tag{7.10}$$

where, $\mu$ is a relaxation parameter as defined in chapter 5.

Equation (7.10) is an integro-differential equation and is solved by the AAR method developed chapter 4.0.

### *7.2.2.2 Nonlocal continuum damping models*

Chapter 6.0 describes a spatially nonlocal-temporally local model and a spatio-temporally nonlocal model. Spatially nonlocal-temporally local damping models are models in which the damping force at a point is a function of the responses at all points in the domain. In the spatio-temporally nonlocal damping models, the damping force at a point is a function of responses at all points in the spatial domain along with response history. The damping model described by Russell (1991) falls under the category of spatially nonlocal-temporally local model and the Extended Sorrentio (Friswell *et al.* (2007)) model falls under the category of spatio-temporally nonlocal model. Only very brief overview of the theory of these models is presented in this section just for completeness.

- *Russell's damping model*

In Russell model, the internal damping term is described as a torque acting on a beam at a point $'x'$ due to the differential rotation of the beam at points $\xi$ "near" $x$.

$$F_{\text{int}}(x,\xi,t) = -2\frac{\partial}{\partial x}\left\{\int_0^L h(x,\xi)\left[\frac{\partial^2 w(x,t)}{\partial x \partial t} - \frac{\partial^2 w(\xi,t)}{\partial x \partial t}\right] d\xi\right\} \tag{7.11}$$

On semi-discretization, adopting from chapter 6, the internal spatial hysteresis matrix is given as,

$$\mathbf{C}_i = 2\int_0^L \left[\frac{\partial \mathbf{N}^T(x)}{\partial x}\right]\left\{\int_0^L h(x,\xi)\left[\frac{\partial \mathbf{N}(x)}{\partial x} - \frac{\partial \mathbf{N}(\xi)}{\partial x}\right] d\xi\right\} dx \tag{7.12}$$

where, $h(x,\xi)$ is the spatial kernel function and $\mathbf{N}(x)$ is the shape function.

The Russell spatial hysteresis model incorporated elemental equation of motion can be given as,

$$\mathbf{M}_e\ddot{\mathbf{d}}_e(t)+\left[\mathbf{C}_{eair}+\mathbf{C}_i\right]\dot{\mathbf{d}}_e(t)+\mathbf{K}_e\mathbf{d}_e(t)=\mathbf{f}_e(t) \tag{7.13}$$

- *Extended Sorrentino damping model (ESM)*

ESM is a very generic model as it is a spatio-temporally nonlocal model. In the case of ESM,

$$F_{\text{int}}(x,t)=\frac{\partial^2}{\partial x^2}\left(\int_0^L\int_{-\infty}^{t}C_{\text{int}}(x,\xi,t-\tau)\frac{\partial^3 w(\xi,\tau)}{\partial\xi^2\partial\tau}d\tau d\xi\right) \tag{7.14}$$

$C_{\text{int}}$ is a spatio-temporal kernel function. Refer to chapter 6 for additional details.

For these elemental damping models, the function parameters to match the observed decay phenomenon of the structure in free-vibration must be selected by the analyst or in subsequent research. This is no different to analysts trying to match the two parameters of the Rayleigh damping to approximate the *right* amount of damping observed in the real structure. In the case of temporally nonlocal and spatio-temporally nonlocal models, the ability to choose different causal damping kernel functions has the advantage that these models would be able to model hysteretic or friction damping without introducing the difficulties with the conventional attempts to model these types of damping.

## 7.3 Incremental Dynamic Analysis Study

This section investigates the performance of the elemental damping models in comparison to the global classical damping models. This section consolidates the IDA results from Chapters 3.0, 5.0 & 6.0 along with responses of the updated elemental Wilson Penzien. Updated elemental Wilson Penzien response is incorporated into the elemental Wilson Penzien framework with appropriate modifications to the steps described in section 3.5.2. The frame description is given in chapter 3.0 & Appendix 3.0.

All existing/newly proposed elemental and existing global damping models are compared in this section. Following abbreviations are used to identify different damping models included in the plots hereafter:

- Initial stiffness based global Rayleigh damping (ISRD)
- Tangent stiffness based global Rayleigh damping with constant coefficients (TSRD),
- Global Wilson-Penzien (GWP)
- Elemental Rayleigh damping with updated proportionality coefficients (ELRD)
- Elemental Wilson-Penzien model implemented as a constant damping matrix (EWP)
- Elemental Wilson-Penzien model implemented as a tangent matrix (UEWP)
- Elemental Kelvin Voigt (ELKV)
- Elemental Time hysteresis (ELTH)
- Elemental Russell model (ELR)
- Elemental Extended Sorrentino model (EESM).

In all plots the global models are presented with continuous lines and elemental models are presented with dashed lines.

### 7.3.1 Elemental damping vs. Global damping

As stated above the elemental damping matrix computation can be done using either the consistent mass or using the diagonal mass. As similar results are obtained either in the consistent mass or diagonal mass formulation, only the consistent mass formulation results are presented in this section. No additional penalty in the form of higher computational demand occurs even if the consistent mass formulation is used as only small matrices are used for the elemental damping matrix computation. In real structures every degree of freedom is associated with mass. Hence the author believes that the consistent mass formulation is more robust in

terms of its mathematical closeness to the physical reality. More details on the effects of the mass formulations on these models are described in Chapters 3.0, 5.0 and 6.0.

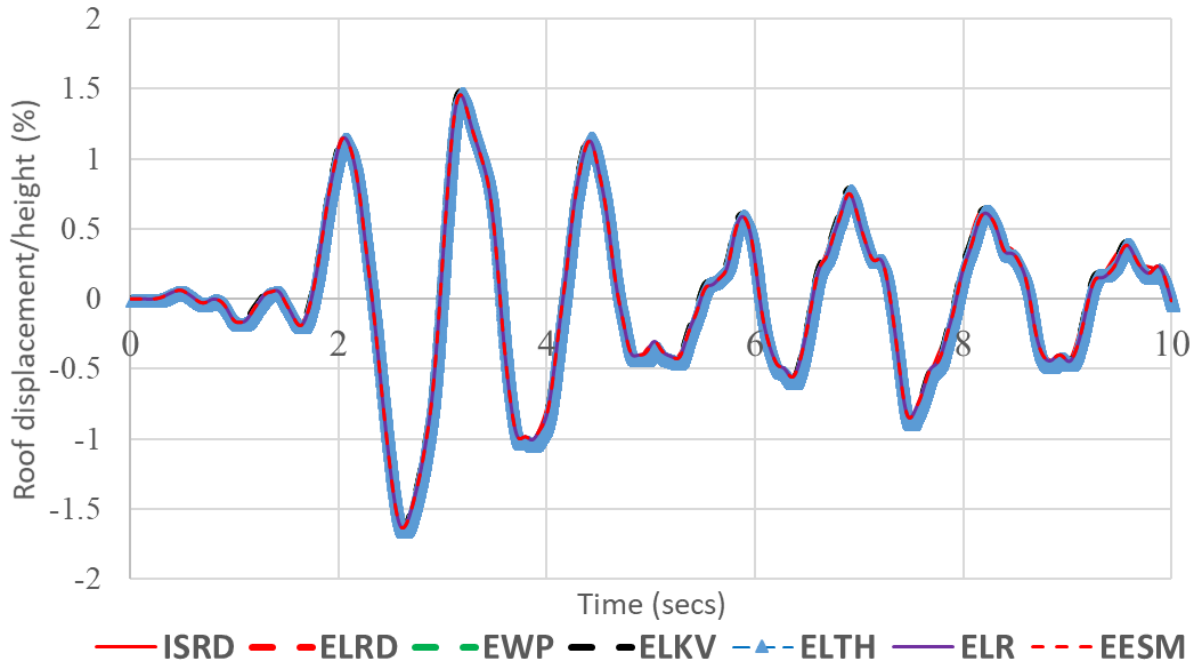


Fig. 7.1 Elastic response of the four storey frame using all the proposed elemental damping models and global Rayleigh damping model

Figure 7.1 illustrates the comparison of the elastic response of all the proposed elemental damping models to the global Rayleigh damping model. It can be clearly seen that, if no inelasticity is allowed in the analysis, all the proposed elemental damping models give very similar results to the global damping model. For lucidity, only initial stiffness Rayleigh damping is used for this comparison.

Figure 7.2 illustrates the compilation of the mean IDA curves for location-independent peak interstory drift ratio as the engineering demand parameter (EDP). Except for the curves of updated Wilson-Penzien, all other curves are adopted from chapters 3.0, 5.0 & 6.0. All the elemental damping models give higher drifts when compared to those of the global damping models. Fig. 7.3 illustrates the peak damping moments for all the models. The ISRD model

gives the highest damping moment which is higher than the yield moment of the frame. All the elemental damping models produce relatively small damping moments.

Although it is very difficult to get a direct correlation between the damping moments and its effect on the structural peak responses, it is shown that the lesser the damping moment the larger the structural response. Damping is an observed phenomenon and unless physical science comes up with an exact model for the real physics of damping all the models are mathematical approximations. From a structural perspective, a conservative approximation (from a safety point of view) would be better than an un-conservative approximation. The elemental models tend to predict more conservative responses and as a result the author believes that they produce more realistic responses with less untoward side effects.

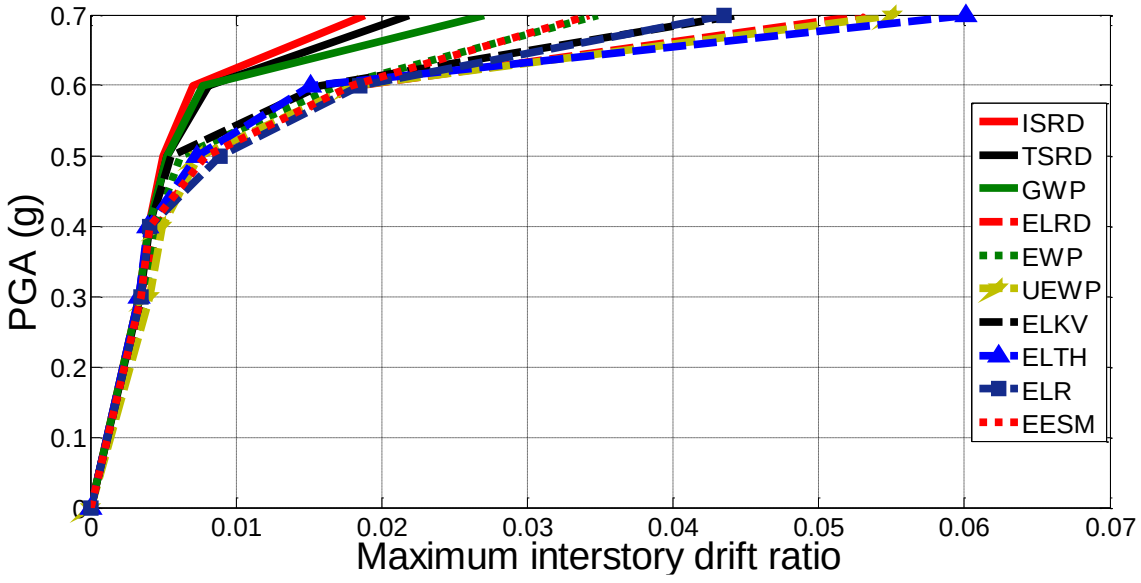


Fig. 7.2. IDA results for the interstory drift ratio

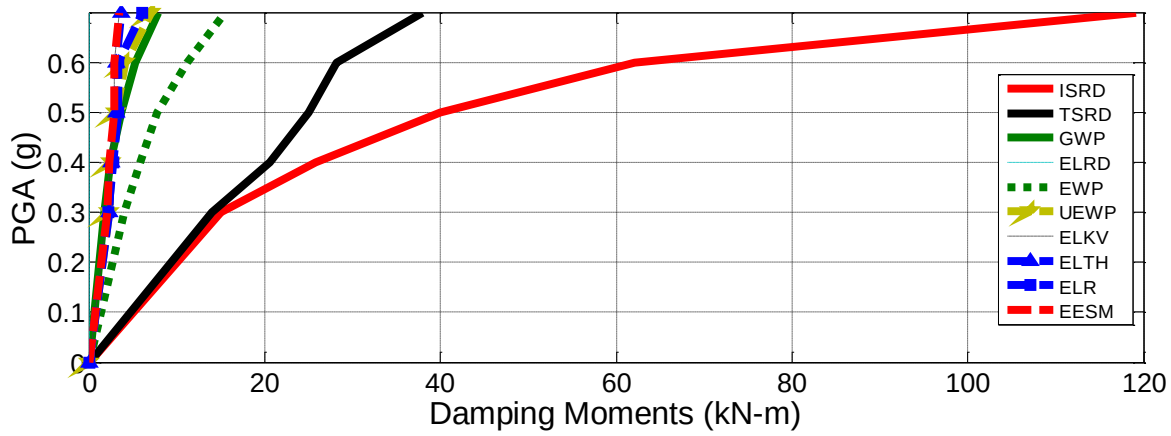


Fig. 7.3. IDA results for peak damping moment

### 7.3.2 Which might be a better model?

The author believes that updated elemental Wilson-Penzien model indicates a more realistic option than the currently commonly adopted Rayleigh models. The updated elemental Wilson-Penzien model exhibits low damping actions and show responses that are very similar to those of the more rigorous continuum damping models. Fig. 7.2 clearly illustrates that the updated Wilson-Penzien damping model results similar to the Elemental Time- Hysteresis model. The Elemental Rayleigh damping may also be a modelling option, however, explicit parametrisation is required at every element level, increasing the challenges in using it. In the case of elemental Wilson-Penzien, the same global damping ratio is applied at the element level which eases the need for explicit parametrization. Though there is a clear indication that updated elemental Wilson Penzien may be considered as a reasonable realistic damping model, the author believes that more in-depth research hasto be undertaken in this direction to confirm this.

## 7.4 Conclusions

A summary of the performance of the elemental damping models in comparison to global damping models is presented. The IDA results presented show that the elemental damping

models perform much better than the global damping models. The elemental damping models may have significant computatiuonal advantages in that the structure damping matrix itself may be dispensed with and the damping actions can be directly computed at the element level. Based on the results presented a preferred elemental damping model for the generic use in nonlinear time-history analysis is reccomended. More research needs to be done to confirm this initial insight of the preferred model.

# 8. Simplified framework for seismic loss computation

**Abstract:** In this chapter a simplified framework for seismic loss estimation to be used in the optimization scheme in the next chapter is outlined. The methodology presented in this chapter closely follows the techniques outlined in Aslani and Miranda (2005). The concepts of *lumped loss estimation approach* and *interpolation technique* to evaluate the expected loss are introduced here. As no new grounds are broken, this chapter mainly serves as a preamble to the next chapter.

## 8.1 Introduction

Present day seismic design philosophy mainly aims to ensure "life safety". As outlined in the previous chapters, this philosophy results in structures which incur heavy economic losses in moderate-severe earthquakes. So, a pressing need for a better philosophy has come to light. In the last few decades, considerable amount of research efforts has been directed towards establishing the basic framework for performance based design. Because of this, some seminal documents like Vision 2000 (SEAONC, 1995) and ASCE 41 were published. The documents outlined discrete global performance goals in an abstract manner; this was in direct contrast to documents which relied on the prescriptive life safety criterion. The abstract nature of the outlined performance goals posed difficulties in translating them to real engineering scenario. So, a need for better metrics for measuring performance was imperative. One such measure which is very close to the heart of a stakeholder or owner is the "seismic loss" (Ramirez and Miranda 2009).

Embarking on the challenge to realize the quantification of the abstract performance goals outlined in Vision 2000 document, Pacific Earthquake Engineering Research (PEER) center developed a

framework which relies on seismic hazard and response simulation to estimate damage and monetary losses during a seismic event. The framework involves a four-stage process in which the first stage is seismic hazard characterization which quantifies the frequency of exceeding a ground motion intensity measure; the second step involves estimating engineering demand parameters (EDPs) from the structural response computations; the third stage involves estimation of damage measures from fragility functions and the fourth stage involves establishing the estimated seismic loss.

In mathematical form, the PEER framework is given as (Aslani and Miranda, 2005)

$$\lambda(DV) = \int\int\int G(DV \mid DM)\,dG(DM \mid EDP)\,dG(EDP \mid IM)\,d\lambda(IM) \qquad (8.1)$$

Where $G(X \mid Y)$ denotes the complimentary cumulative distribution of X conditioned on Y; *DV* denotes the decision variable (in the present study it is the seismic loss), *DM* denotes the damage measure; *EDP* denotes the engineering demand parameter; *IM* denotes the intensity measure.

Eq. (8.1) involves three integrations of probabilistic functions and is computationally expensive. Over the years a lot of research effort has been expended for the realistic simplifications of the above rigorous format. Out of the above efforts one of the most practical approaches has been advocated by Ramirez and Miranda (2009). The proposed approach by them is referred to as the *story based loss estimation.* The main data intensive step in the PEER framework is the damage estimation (third step). Story based loss estimation relied on computing this stage beforehand and deriving the direct EDP-DV functions where EDP is the structural response parameter and DV is the decision variable (economic losses). Motivated from this, a slightly modified approach is adopted in this study. The method is very similar to the approach adopted by Ramirez and Miranda, except that instead of the loss being assessed for each storey, the loss in this case is computed for

each degree of freedom of the system. The approach proposed in this chapter is called *lumped loss estimation.* One advantage of this method is that no apriori distribution of the structural/non-structural components is needed. As the main intent of this chapter is to develop a smooth mathematical function of the loss which needs to be incorporated in the optimization framework, only a theoretical overview of the method is given here. At first, a glimpse of the rigorous method is presented; after this the simplified method is presented along with the concept of *lumped loss estimation* and *interpolation techniques* to evaluate the expected loss.

## 8.2 Overview of the rigorous theoretical format (Aslani and Miranda 2005)

This section summarizes the detailed loss assessment framework as reported in Aslani and Miranda (2005). In classical detailed loss assessment framework (PEER format), the expected annual loss or the loss expected over a period of time is computed as,

$$E[L_T] = \frac{1-e^{-\lambda t}}{\lambda} \int_0^{\infty} E[L_T \mid IM] dv(IM) \tag{8.1}$$

where,

$E[L_T]$ is the expected annual loss; $\lambda$ is the discount rate; $t$ is the period for which the rate is applied; it can be the design life of the building or remaining life of the structure; $E[L_T \mid IM]$ is the expected loss conditioned on the intensity measure *IM*; *v(IM)* is the mean annual rate of exceedance of the intensity measure

$E[L_T \mid IM]$ can be divided into two components,

$$E[L_T \mid IM] = E[L_T \mid NC, IM] P(NC \mid IM) + Total\ building\ value \times P(C \mid IM) \tag{8.2}$$

Over here,

$E[L_T \mid NC, IM]$ is the expected loss in non-collapse case; $P(NC \mid IM)$ is the probability of non-collapse for the specific ground motion intensity; $P(C \mid IM)$ is the probability of collapse for the specific ground motion intensity

The addition of viscous dampers reduces the collapse probability considerably in a major event. So, it could be argued that only non-collapse case need be considered while using viscous dampers which means no probability of collapse be computed. An alternative approach is to use a modified framework in which the whole loss is computed in such a way that there is no collapse and the effect of collapse is introduced through a Heaviside step function in such a way that when drift exceeds a certain value in any of the ground motions considered, it is deemed as a total loss. This approach is adopted in the present study. So first the loss is computed assuming no collapse and then the obtained equation is modified by introducing the Heaviside step function term. This aspect is described in more detail in section 8.3.2.

Assuming no global collapse $\left(P(NC \mid IM) = 1.0\right)$, eq. (8.2) becomes,

$$E[L_T \mid IM] = E[L_T \mid NC, IM] \tag{8.3}$$

Now

$$E\left[L_T \mid NC, IM\right] = \sum_{j=1}^{N} a_j \left(E\left[L_j \mid IM\right]\right) \tag{8.4}$$

Over here,

$a_j$ is the cost of a new $j^{th}$ component; $E\lfloor L_j \mid IM \rfloor$ is the expected loss of the $j^{th}$ component conditioned on the ground motion intensity. Note that from here on "NC" is not being explicitly stated as the computation is only done for the non-collapse case.

Now the expected loss of the $j^{th}$ component conditioned on the ground motion intensity is given as,

$$E\left[L_j \mid IM\right] = \int_0^{\infty} E\left[L_j \mid EDP_j\right] dP\left(EDP_j \geq edp \mid IM\right) \tag{8.5}$$

Over here,

$E\lfloor L_j \mid EDP_j \rfloor$ is the expected loss in the $j^{th}$ component when it is subjected to an $EDP_j$ when no collapse occurs; $P\left(EDP_j \geq edp \mid IM\right)$ is the probability of the *EDP* exceeding *edp* in the $j^{th}$ components when no collapse occurs. Again,

$$E\left[L_j \mid EDP_j\right] = \sum_{i=1}^{m} E\left[L_j \mid DS_i\right] P\left(DS = ds_i \mid EDP_j\right) \tag{8.6}$$

$E\lfloor L_j \mid DS_i \rfloor$ is the expected loss conditioned on damage state *i*. In other words, it is the loss in the $j^{th}$ component when the component is in damage state *i* and can be obtained from experimental database (Aslani and Miranda 2005). $P\left(DS = ds_i \mid EDP_j\right)$ is the probability of the $j^{th}$ component being in damage state $ds_i$ when the $EDP_j$ is experienced by the $j^{th}$ component and is given as follows (Aslani and Miranda 2005)

$$\left.\begin{aligned} P\left(DS = ds_i \mid EDP_j\right) &= P\left(DS \geq ds_i \mid EDP = edp\right) - P\left(DS \geq ds_{i+1} \mid EDP = edp\right) \\ P\left(DS \geq ds_i \mid EDP = edp\right) &= \Phi\left[\frac{Ln\left(edp\right) - Ln\left(EDP_{mean}\right)}{\sigma_{LnEDP}}\right] \end{aligned}\right\} \quad (8.7)$$

Here, $\sigma_{LnEDP}$ is the logarithmic standard deviation of EDP.

## 8.3 Simplified loss estimation adopted in this study

The above section briefly outlined the main steps involved in a detailed loss estimation framework. As the purpose of the present study is to integrate the loss estimation into a mathematically robust optimization framework some simplifications in the method is imperative.

### 8.3.1 Lumped loss estimation

Ramirez and Miranda (2009) introduced the storey based loss estimation as a more pragmatic framework for performing loss estimation. Mathematically, this concept may be looked upon as storey level lumped loss estimation, mainly because the loss is evaluated as a function of the total value of the storey.

Motivated from this, in the present study, a degree of freedom level lumping is adopted. It is a known fact that whether it is structural or non-structural components, the damage incurred is a function of the structural response corresponding to each degree of freedom. For e.g. damage to a partition wall in a bay is due to the inter-storey drift sustained between the structural nodes (beam column junction) above and below the partition wall. Similarly, in 3D asymmetric structures also this is very important as the storey exhibits different drifts in different locations. Fig. 8.1 represents a two bay two storey frame with a partition wall in the first bay in the first-floor level.

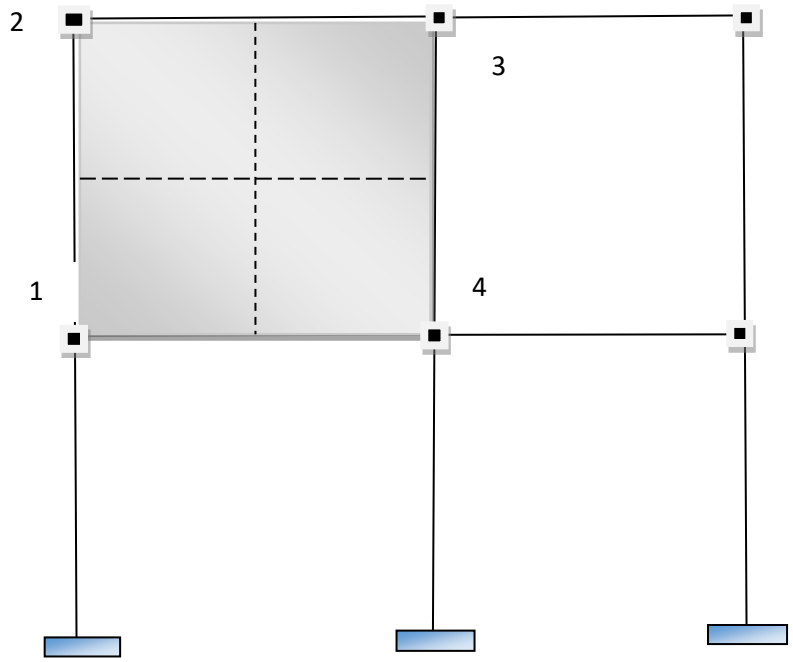


Fig. 8.1 two storey tow bay frame with partition wall

It is very clear that damage to the partition wall will be a function of the inter-storey drift of these nodes. Lumping of loss philosophy assumes that if the value of the partition wall is say $\chi$ then each node connecting it will be assigned an equal share of the value; i.e. $\chi/4$ . In other words, an influence factor is introduced which transforms the value of each component and lumps it to a specific degree of freedom. The loss incurred will then be a function of the inter-storey drift associated with that degree of freedom. This type of approach may be conveniently adopted for predominantly drift sensitive non-structural components mainly because all the drift sensitive items would be directly or indirectly connected to the parent structural members.

Damage to acceleration sensitive items would be a function of the specific floor mass acceleration alone; so, losses may be lumped to the specific floor masses and will be very similar to the Ramirez and Miranda (2009) approach. Losses may also be lumped to the acceleration felt by a specific

degree of freedom by computing/assessing the proximity of the structural node to the component under consideration.

### 8.3.2 Simplified loss framework including collapse consideration

The first simplification comes from the fact that only intensity based loss assessments are used in this study; so only EDP corresponding to a specific intensity of ground motion is adopted and the resulting loss is termed as total expected loss. Except for step 8, all the steps which are detailed below are adopted from Aslani and Miranda (2005) and Ramirez and Miranda (2009). The steps are as follows:

1. Perform linear/nonlinear time history analyses using *n* ground motions compatible with a target spectrum.
2. Compute the mean response history from the *n* response histories
3. For the $j^{th}$ component, determine the damage state using eq. (8.7)
4. Determine $E\left[L_j \mid NC, DS_i\right]$ for the $j^{th}$ component from the loss database; for the present study the loss database given in Aslani and Miranda (2005) is adopted.
5. Compute eq. (8.6) for the $j^{th}$ component
6. Repeat steps 3-5 for all components
7. Compute the total normalized expected loss conditioned on *EDP* for no collapse as follows,

$$\left.\begin{aligned} E\left[L_T \mid EDP\right] &= \sum_{j=1}^{N} \beta_j E\left[L_j \mid EDP\right] \\ \beta_j &= \mathrm{T}a_j \end{aligned}\right\} \qquad (8.8)$$

where T represents the spatial influence factor which determines the lumping.

8. Introduce the Heaviside function to reflect the collapse scenario as shown below,

$$\left.\begin{aligned}\Psi &= E\left[L_T \mid NC, EDP\right]H\left(d_{al} - X\right) + Total\ building\ value \times H\left(X - d_{al}\right)\\ \mathrm{X} &= Env\left(\max_i\left(\left\{\max_t\left(abs\left(\mathbf{H}_T\mathbf{u}_1(t)\right)\right), \max_t\left(abs\left(\mathbf{H}_T\mathbf{u}_2(t)\right)\right), .., \max_t\left(abs\left(\mathbf{H}_T\mathbf{u}_{N_{gm}}(t)\right)\right)\right\}\right)\right)\end{aligned}\right\} \quad (8.10)$$

Over here, $\Psi$ represents the expected total loss conditioned on EDP, $d_{al}$ refers to the capping drift, *H* refers to the Heaviside step function, $\mathbf{H}_T\mathbf{u}_i(t)$ refers to the drift, *Env* refers to envelope. The use of Heaviside step function reflects the fact that when the computed drift exceeds an allowable capping drift, total loss is assumed. It should be understood here that exceeding this capping drift does not mean physical collapse of the structure, but mainly relates to a situation of complete financial loss as the structure gets written off due to non-reparability or non-usability. So, the selection of capping drift is very important. Even the definition of no-reparability or non-usability is subjective and depends on lots of other associated societal aspects. This is further discussed in section 9.3.1.1.

### 8.3.3 Expected loss of a component conditioned on a specific EDP

Figs.8.2a and 8.2b represent the typical functions of expected loss conditioned on EDP; this is obtained by evaluating eq. (8.6) and is obtained from Aslani and Miranda (2005). It maybe seen that the expected loss for the partition walls is more than 1.0 as obtained in Aslani and Miranda (2005). This 20% increase in loss may be attributed to the additional associated cost for removing the debris and all.

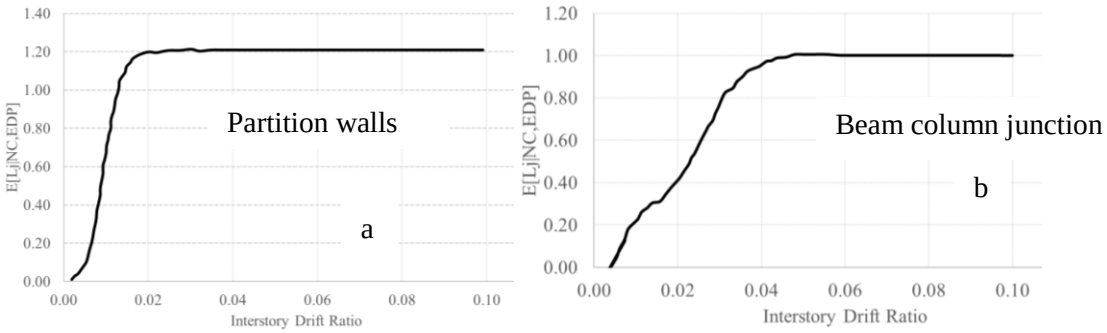


Fig. 8.2 a Expected loss conditioned on EDP for partition walls (Aslani and Miranda 2005); 8.2 b Expected loss conditioned on EDP for beam column junction (Aslani and Miranda 2005)

First order gradient based optimization schemes are used for the optimization framework described in the next chapter. Because of this, to integrate seismic loss into this framework, the expected loss functions need to be described as smooth functions. One way to describe the functions shown in figs. 8.2a and 8.2b is by using interpolation techniques. The simplest interpolations that can represent these functions are polynomial functions. Using polynomial functions, we get,

$$E\left[L_j \mid NC, EDP_j\right] = \sum_{i=1}^{k} A_i \left(\overline{EDP}_j\right)^{\eta_i} \tag{8.11}$$

Here, $A_i, \eta_i$ are the constants in the polynomial. These constants differ for different components and need to be explicitly evaluated. The values of $A_i, \eta_i$ for partition walls and beam column junctions are given in Appendix 8.

A more robust methodology of interpolation would be to use cubic spline functions; but to the knowledge of the author, as this the first time an attempt is initiated to integrate the seismic loss aspect into the first order gradient multi-objective optimization framework, the simplest polynomial based interpolation technique is adopted; considering the other uncertainties associated with the loss estimation process, this methodology is deemed to be acceptable.

## 8.4 Conclusion

A simplified framework of loss estimation is outlined in the chapter. The concept of lumped loss estimation is introduced, and a polynomial based interpolation technique is adopted to evaluate the loss. The simplified loss estimation method adopts the techniques described in Aslani and Miranda (2005) and uses Heaviside step function to indirectly reflect the effect of collapse by assuming total loss when the drift exceeds a certain value.

# 9. Design of viscous dampers for linear frames: a multi-objective framework

Puthanpurayil, A.M., Lavan.O and Dhakal, R.P. (2017). Multi-objective loss optimization of seismic retrofitting of moment resisting frames using viscous dampers, Paper No: 1321, 16th World conference in Earthquake Engineering, Santiago, Chile (Oral Presentation)

Lavan.O, Puthanpurayil A.M., and Dhakal, R.P. (2017). Optimal Viscous damper design for 3D Asymmetric structures., published in 8th European Workshop on the seismic behaviour of Irregular and Complex Structures held in Romania (Oral Presentation)

**Abstract:** In this chapter a first order gradient based optimization scheme is presented to optimally quantify and distribute linear viscous dampers along the height of a linear elastic building. The first order gradients are analytically derived using the very efficient Adjoint Variable method. A full detail description and the implementation of the gradients are presented. A multi- objective framework is presented, and the formulated optimization problem minimizes the initial cost and the total expected loss simultaneously. In the present chapter the total expected loss considered is mainly due to drift, but the framework is very generic, and acceleration related loss also can be incorporated with no additional effort. The framework is applicable to any type of building structures made of any type of material. The efficacy of the framework is illustrated with a 2D linear four storey frame and an eight storey linear 3D asymmetric building.

## 9.1 Introduction

Viscous dampers are very effective in reducing seismic responses. This is mainly attributed to the fact that the damper force is linearly or nonlinearly proportional to velocity and is out of

phase with the column displacements. As a result, the columns or foundations are not subjected to additional demand, and may not need to be strengthened (Constantinou *et al.*1993, Miyamoto & Scholl 1996, Lavan 2012). This chapter is mainly concerned with the application of linear viscous dampers for seismic performance enhancement of existing frames.

In a retrofitting design using viscous dampers the main task that needs to be addressed by the engineer is the "sizing" and the allocation of the dampers. Both these tasks are coupled, and a realistic optimum would be difficult to be achieved if both of them are treated as un-coupled. Nevertheless, the majority of the optimal design methodologies for retrofitting using viscous dampers address the problem of distributing a given total added damping to achieve the best performance (minimize damage measures) which results in decoupling the two tasks. Some of the works in this direction presented very efficient methods (Zhang & Soong 1992, Tsuji & Nakamura 1996, Takewaki, 1997a, 1997b, 1998, 1999, Singh& Moreschi, 2001, 2002, Garcia 2001). Note that in these works the total added damping is predetermined and the optimisation is mainly initiated for efficiently allocating the dampers only. The algorithms are thus used to determine the optimal positioning of this quantity along the height of the building. In some of these works, approaches to estimate a reasonable total added damping were also proposed.

From a different perspective, Lavan and Levy (2005, 2010) and Lavan (2015) minimized the total added damping subject to a constraint on the performance of the structure (allowable inter-story drifts). They also presented a practical analysis/redesign procedure for arriving at the optimal designs exploiting the advantage of the fully stressed characteristics of the optimal solution (Levy & Lavan, 2006, Lavan, 2015). While this formulation lends itself to the performance-based-design framework, the allowable inter-story drifts, or performance measures, are mainly determined based on code requirements. The performance measure is usually not determined explicitly based on the economic consequences.

All the above cited works involved optimization of a single objective with the other objectives adopted as constraints with predetermined values. For an ideal retrofitting scheme to be economically viable, the initial cost should be minimized without compromising the anticipated performance in terms of response reduction. A reduction in response directly translates to a reduction in loss. But it could clearly be seen that both criteria are mutually competing against each other; i.e. minimization of initial cost would result in lesser damping and hence an increase in the seismic loss due to increase in the system response and a minimization of seismic loss would result in an increase in initial cost due to the requirement of more damping. So how would one decide which of these two objectives is more important for a specific decision-making scenario?

### 9.1.1 Multi-objective optimization

In order to decide on which of the objectives is more important for a chosen decision-making scenario, one needs to know the effect of minimization on both objectives. A very well-established way of accomplishing this is by the notion of Pareto optimality (Pareto V 1927). The key concept of Pareto optimality is that rather than attempting to identify a single optimal design, one seeks to determine the entire family of designs that lie on a Pareto front. So basically, a Pareto front design represents a feasible solution for which an improvement in any of the objectives can only be realized by a degraded performance in the other. So, in the context of this chapter, the Pareto front presents a solution of decreased expected total loss only by accepting an increase in the initial cost; but the Pareto front as a whole is very attractive to the decision makers because it provides a complete picture of the potential design solutions and the implication of a specific decision in terms of its effect on both the expected loss and initial cost.

A focus to minimize both initial cost and expected total seismic loss together presents itself with the need for a multi-objective framework. One of the earlier works in this related to seismic control was by Lavan and Dargush (2009). Though a Pareto optimality criterion was adopted, there was no explicit consideration of seismic loss in the study. Also, Genetic Algorithm (GA), a zero order optimization scheme was used for generating the Pareto front. The main issue with a GA scheme is that a very large number of function evaluations are needed for the solution which poses a very high computational demand. The Other relevant reference which combined both the initial cost and seismic loss and assessed the performance in a framework of life cycle cost reduction was by Gidaris & Taflanidis (2015). But as the adopted optimization scheme was formulated as a single objective and again zero order, it required a very large number of function evaluations.

In this present chapter, a novel multi-objective gradient based first order optimization framework is proposed which attempts to generate the Pareto front by minimizing the initial cost and seismic loss simultaneously. Computationally the optimization framework is very efficient mainly because it adopts a gradient based approach and the amount of function evaluations required is very less. Also, the Pareto front generated gives a full sphere of the possible solutions helping a decision maker place his decision on informed quantified facts. Only linear frames are used in this chapter and nonlinear frame are discussed in chapter 10.

## 9.2 Why linear frame?: A socio-economic review

The conventional philosophy of seismic design accepts the fact that in a major earthquake the parent frames suffer inelastic excursions, but prevents collapse and hence ensures life safety. This is even true for a low damage control frame. One of the key motivations for the adoption

of this philosophy relies on the fact that earthquake is a rare event in the lifetime of a building; so, it would be economically non-viable to make it to perform in the elastic range in a major event.

Recent earthquakes especially in New Zealand have highlighted that there is a high socio-economic flaw with such a philosophy. To evidence this, as already mentioned in chapter 1.0, during the recent Kaikoura earthquakes in November-December 2016, though the deaths were minimum, the earthquake damage cost is estimated at ~NZ $ 15 billion; again, it is not very clear whether this includes the indirect costs associated with the business disruption and other hidden costs. Similarly, the Christchurch sequence of earthquakes (2010-2012); the estimated loss is around NZ $40 billion which corresponds to 20% of the Gross Domestic Product (Pampanin 2015); These figures are significant and have huge impact on the overall socio-economic fabric and calls for a design philosophy which not only ensures life safety but also safeguards economic resilience. As already mentioned in the introduction, this is furthered by the societal expectation that after a credible event life can move on without any major disruption which makes instilling economic resilience in the design philosophy an unavoidable task.

One of the ways to achieve this is to adopt low damage techniques like base isolation or adding viscous dampers and forcing the frames to remain linear or predominantly linear so that no major disruption occurs in the structure during a major event or associated events. To force the parent structure to be linear or close to linear (mildly inelastic within an economically repairable limits), there might be an increase in the initial cost; but holistically if we review the cost due to damage, disruption and rebuild that would be necessary to be made after a credible event, the increase in the initial cost would be justifiable in a qualitative manner even after inclusion of the possible inflation that may happen in the future. Again, lifeline buildings like hospitals, fire stations, and police stations etc. which need to be functional after an event

definitely should be designed in such a manner that they remain elastic and fully functional. So, in effect holistically it can be categorically stated that a design to achieve a linear response of a structure is justifiable in a geographic place where earthquake is not a rare event but more or less a common event which every building might feel at least once during its life span.

## 9.3 Optimization framework

This section presents the generic framework for multi-objective optimization. First order gradient based schemes are employed to solve the optimization problem. The optimization problem involves minimizing simultaneously the initial cost and the expected total loss. Expected total loss is computed as per the intensity based methodology described in chapter 8.0. A component strategy is adopted for the loss computation. In this study, seismic losses due to downtime and injury are not accounted for; thereby resulting in underestimation of the benefits of optimal intervention.

The framework presented here is applicable equally to strengthening existing buildings and to new buildings. In a new building, both stiffness and damping may be considered as variables and maybe optimized to achieve a target performance; but in this present work only the added damping is considered as the variable. If only damping is considered as the variable, then the initial cost in the case of enhancing seismic performance with viscous dampers can be assumed as the cost of added dampers and their installation.

### 9.3.1 Problem formulation

The optimization problem is formulated as given below,

$$
\left.
\begin{aligned}
&\min\left(\Gamma(\mathbf{c}_d),\Psi(\mathbf{c}_d)\right)\\
&\textit{here,}\\
&\Psi=\left\{H\left(\mathrm{X}-d_{al}\right)\right\}\times C_{total}\\
&+\left\{H\left(d_{al}-\mathrm{X}\right)\right\}\times\sum_{j=1}^{N_d}c_j\sum_{i=1}^{k}A_i\left(\frac{1}{N_{gm}}\sum_{r=1}^{N_{gm}}\left\{\max_t\left(abs\left(\mathbf{H}_T\mathbf{u}_r(t)\right)\right)\right\}\right)^{\eta_i}\\
&\textit{where}\quad\mathbf{u}_r(t)\quad\textit{follows}\\
&\mathbf{M}\ddot{\mathbf{u}}_r(t)+\left[\mathbf{C}+\mathbf{C}_{damper}(\mathbf{c}_d)\right]\dot{\mathbf{u}}_r(t)+\mathbf{K}\mathbf{u}_r(t)=-\mathbf{M}\mathbf{r}\ddot{u}_{g,r}(t)\\
&\mathbf{u}_r(0)=0;\dot{\mathbf{u}}_r(0)=0\\
&0\le\mathbf{c}_d\\
&r=1\rightarrow N_{gm}\\
&\mathrm{X}=Env\left(\max_i\left(\left\{\max_t\left(abs\left(\mathbf{H}_T\mathbf{u}_1(t)\right)\right),\max_t\left(abs\left(\mathbf{H}_T\mathbf{u}_2(t)\right)\right),..,\max_t\left(abs\left(\mathbf{H}_T\mathbf{u}_{N_{gm}}(t)\right)\right)\right\}\right)
\end{aligned}
\right\}\forall\ddot{u}_{g,r}(t)
\tag{9.1}
$$

In eq. (9.1) $H$ refers to the Heaviside step function; $\mathbf{H}_T$ refers to the drift transformation matrix; $\mathbf{c}_d$ refers to the damper vector; $\mathbf{u}_r, \dot{\mathbf{u}}_r$ and $\ddot{\mathbf{u}}_r$ are displacement vector, velocity vector and acceleration vector for the $r^{th}$ ground motion; $N_{gm}$ represents the number of ground motions; $\mathbf{M}, \mathbf{C}$ and $\mathbf{K}$ are the mass, inherent damping and stiffness matrices; $\mathbf{C}_{damper}(\mathbf{c}_d)$ is the added viscous damper matrix; **r** is the directionality vector; $\ddot{u}_{g,r}$ is the $r^{th}$ ground motion acceleration vector; $C_{total}$ is the total cost of the structure; $c_j$ is the cost of the $j^{th}$ component.

Eq. (9.1) represents the simultaneous minimization of damper quantities and expected total loss. As already mentioned in chapter 8, the effect of collapse is considered by incorporating the Heaviside step function with a kernel function comprising the capping drift $d_{al}$ and envelope drift. More on this is given in section 9.3.1.1.

#### *9.3.1.1 Allowable acceptable total loss*

Heaviside step function is used in eq. (9.1) to introduce a control on the limiting acceptable loss. The expected total loss is computed using a suite of ground motions as described in chapter 8.0. The kernel of the Heaviside step function involves the envelope computed drift which is basically the maximum of the drifts at all levels considering all ground motions and the allowable acceptable capping drift $d_{al}$. $d_{al}$ is chosen to make the frame remain predominantly linear. As explained in section 9.2, this is mainly justified from a socio-economic aspect after reviewing the recent Kaikoura and Christchurch earthquakes.

One aspect of eq. (9.1) is that when the envelope computed drift exceeds the $d_{al}$, it is assumed that the structure would be completely written off. To emphasize this point, in the recent 2016 Kaikoura earthquake in New Zealand, one multi-story building was demolished mainly classing it as non-repairable. The main damage in the building was in one of the columns where there was a reasonable hinge formation. Albeit the experienced engineer's belief that it could be repaired, and building be re-used, the building was marked for demolition mainly because the health and safety laws prevented the workers from going inside the building to do the repair. This is a very significant societal aspect which drives what is deemed as acceptable in the modern society. The selection of $d_{al}$ in eq. (9.1) may be used to indirectly reflect these societal aspects. This epitomizes the significance of eq. (9.1) from a pragmatic view point as it gives direct control of allowable acceptable damage to the designer.

Similar justifications for this may again be obtained from the Christchurch sequence of earthquakes. It had been observed during the Christchurch sequence of earthquakes that so many buildings though did not collapse had to be demolished as the damage was classed as

non-repairable; it was also observed that owners or stake holders had a strong tendency to write off their assets (buildings) when they suffered moderate repairable inelasticity mainly because they could claim insurance (Personal communications with experienced engineers). There are also many other non-technical reasons that can justify the demolition of many buildings. This is a huge economic burden on the society and gives a strong motivation for forcing the capping drift to a value such that the system is predominantly elastic in a design event.

#### *9.3.1.2 Optimization scheme*

Eq. (9.1) presents a nonlinear optimization problem. In the present study this problem is solved by discretizing the nonlinear objective functions and issolved by using an aggregate gradient based methodology (Izui et al. 2014). In this method the objective functions are evaluated at multiple points in the objective function space and the design variables at each point is aggregately updated using the information from all other points. The multi-objective problem is converted into a single objective problem using an adaptive weighting technique. The obtained single objective problem is then solved using a sequential linear programming (SLP) method and the design variables are updated. Optimization framework comprises of the following steps:

**Step 1: Selection of a suite of ground motions matching the specified intensity**

An ensemble of ground motions is selected to match the target mean spectrum corresponding to the specific intensity level of interest. It must be noted that the procedure outlined in this section is equally applicable to time based assessments in which case the expected annual loss will be minimized instead of the total expected loss used in the present study.

*9.3.1.2.1 Start of Multi-Objective Framework (Izui et al. 2014)*

The aggregate gradient based methodology adopted for the multi-objective optimization framework is presented in detail in this section.

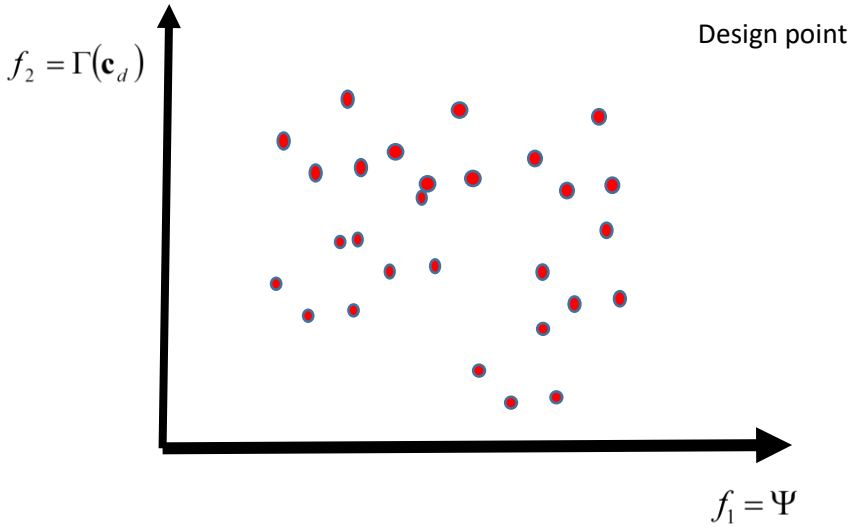


Fig. 9.1 Objective function space

**Step 2 Initialization of design variables and generation of initial design points**

Design point is basically obtained by computing the two objective functions given in eq. (9.1) assuming a specific random distribution for the design variables which are the damper coefficients. Mathematically this means, for *q* design variables (damper coefficients), generate *K* design points using random values for the design variables. For e.g. if we assume *q*=2 and *K*=7, then there are seven random distributions of the two dampers and each design point in the objective function space as shown in fig. 9.1 corresponds to evaluation of the objective functions in eq. (9.1) subject to the constraint on the damper coefficients. The objective function $\Gamma(\mathbf{c}_d)$ is simply the addition of the capacities of the two dampers which reflect the initial cost that is needed and the evaluation of the expected total loss $\Psi$ corresponds to the evaluation of the second function in eq. (9.1).

**Step 3 Compute weighting coefficients as per Data Envelopment Analysis (DEA)**

To generate the Pareto front, the design points shown in fig. 9.1 needs to move towards the Pareto frontier point that is closest to its current position in the objective function space. But as the Pareto frontier is not known prior to optimization calculation, the points in the objective function space need to be updated using an adaptive weighting method. Only a very brief detail is given in this step and for details interested readers should refer to Izui et al. (2014).

DEA computes the efficiency of the $M^{th}$ point by solving a linear programming problem as,

$$\left.\begin{array}{l} \min\left(\Lambda^M\right) = \sum_{i=1}^{m} w_i^M \, f_i^M \\ \text{Subject to,} \\ \sum_{i=1}^{m} w_i^M \, f_i^k \geq 1 \\ w_i^M \geq 0 \end{array}\right\} \text{(for k = 1,2,…..…..…..}K) \qquad (9.2)$$

Here $f_i^k$ is the $k^{th}$ point's $i^{th}$ objective function value and $w_i^M$ represents the weighting coefficients.

**Step 4 Compute the sensitivities of the objective functions for the $M^{th}$ point**

Gradient for the objective function $\Gamma^M$ is trivial as it is a direct function of the damping vector $\mathbf{c}_d$ and the sensitivity will return a vector **1.** But the gradient of the objective function $\Psi^M$ is not trivial. One way to determine the gradient is by finite difference approach; but this has serious limitations in terms of computational demand as it requires *n+1* analysis for *n* design

variables. So, in the present study, gradients are computed analytically using the Adjoint Variable method as outlined in section 9.3.2.

**Step 5 Update the design variables of the $M^{th}$ point**

A minimization of the weighted sum of the objective functions is done using sequential linear programming (SLP) and the design variables are updated. SLP uses a suitable move limit to arrive at the updated value of the design variable. For the $M^{th}$ point we get,

$$\min\ f^M = \sum_{i=1}^{m} w_i^M \sum_{j=1}^{n} \frac{\partial f_i\left(\mathbf{c}_d^M\right)}{\partial c_{dj}} c_{dj} \Bigg\} \tag{9.3}$$

Subject to

$$\mathbf{c}_d^L \le \mathbf{c}_d \le \mathbf{c}_d^U \tag{9.4}$$

Here $f^M$ is the weighted sum of the objective functions, $\mathbf{c}_d^M$ is the design variable vector of the $M^{th}$ point before updating, $\mathbf{c}_d^L$ and $\mathbf{c}_d^U$ are the lower and upper move limits of the design variable. If $M=n$ then proceed to step 6, else adopt $M=M+1$ and proceed to step 5. For more details on this step interested readers should refer Izui et al. (2014).

**Step 6 Check for termination condition**

If termination condition is satisfied (maximum number of iterations), the procedure ends else returns to step 2.

*9.3.1.2.2 Schematic illustration of the optimization framework*

Fig. 9.2 presents the schematic representation of the whole procedure involved in the multi-objective framework. The framework mainly consists of the analysis block where the points for the objective function space are generated. Each of the point on the objective function space comprises of a specific distribution of the dampers along the height of the frame. For e.g. the red point in the objective function space corresponds to the specific distribution in the analysis block with dampers represented as red boxes. Once the points are generated in the objective function space, adaptive weights of these points are computed. Using these weights, the multi-objective problem is converted to a single objective problem. The obtained nonlinear single objective problem is then discretized as piecewise linear programming problem and solved using SLP. The design vectors are then updated and the cycle repeats till termination condition is satisfied. This whole process takes place in the multi-objective engine.

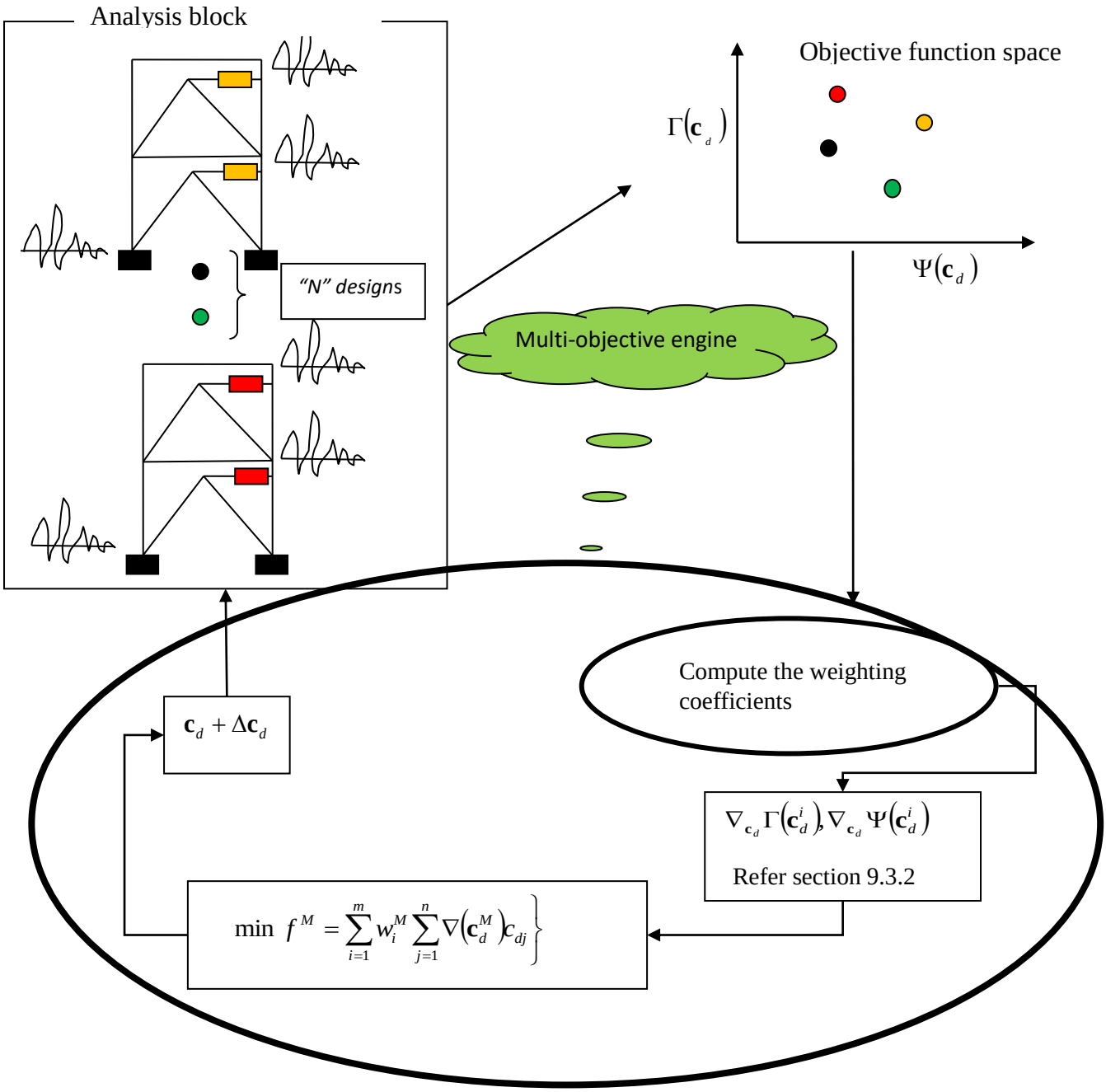


Fig.9.2 Schematic representation of the optimization procedure for $\Delta\mathbf{c}_d^i \geq \varepsilon_{tolerance}$

### 9.3.2 Gradient derivation

In this section an efficient way to compute $\nabla_{\mathbf{c}_d}\Psi$ is described in detail. The classical way to compute gradients is to use the classical Finite Difference Method; but this method is highly inefficient for large systems. So, an alternative indirect methodology of computing gradient is

described in this section. A very brief description on the state of the art of gradient computation is described here and then in the next subsection the mathematical derivation is described.

Hsieh and Arora (1985) derived the first variations on the point-wise as well as integral type constraints for linear elasticity and used a direct differentiation method to compute the variations on the displacements. Michaeleris *et al.* (1994) systematically presents the sensitivities for a generalized response functional using both the direct differentiation method and Adjoint Variable Method (AVM). The derived formulation is directly applicable in Finite Element implementations. A very detailed review of the state of the art of the field of sensitivity computation is given in Kang et al. (2004). They classify the methods into two categories: one is the direct differentiation method and the other one is the AVM. In AVM itself there are two ways of computing sensitivities: one is the differentiate-then discretize and discretize-then differentiate approach (Conte *et al.* 2003). Majority of the work done in optimization for transient problems incorporates differentiate then discretize approach (Jense *et al.*2014). Jense *et al.* (2014) presents a comparative review of both approaches for sensitivity computation and outlines the associated errors.

The gradient derivation in this thesis incorporates the differentiate-then discretize approach as outlined in Lavan (2006) and Jense *et al.* (2014).

#### *9.3.2.1 Mathematical derivation: Differentiate and Discretize procedure (Lavan 2006)*

To derive the analytical gradients by AVM approach, non-differentiable functions like *max* and *abs* in eq. (9.1) need to be replaced by a differentiable function. In this study a *p type* norm is used.

Using the differentiable *p type* norm version, $\mathbf{d}_{est,r} = \max_t\left(abs\left(\mathbf{H}_T\mathbf{u}_r(t)\right)\right)$ is replaced as,

$$\left.\begin{aligned}\mathbf{d}_{est,r}(t_f) &= \left(\frac{1}{t_f}\int_0^{t_f}\left(D\left(\mathbf{H}_T\mathbf{u}_r(t)\right)\right)^p dt.\right)^{\frac{1}{p}}\mathbf{1} = D\left(\mathbf{d}_{mp,r}(t_f)\right)^{\frac{1}{p}}\mathbf{1}\\ r &\to 1\,to\,N_{gm}\end{aligned}\right\} \tag{9.7}$$

where

$$\mathbf{d}_{mp,r}(t_f) = \frac{1}{t_f}\int_0^{t_f}\left(D\left(\mathbf{H}_T\mathbf{u}_r(t)\right)\right)^p dt.\mathbf{1} \tag{9.8}$$

$p$ is a large positive even number; $t_f$ is the final time.

Now in differential format eq. (9.8) can be written as,

$$\left.\begin{aligned}\dot{\mathbf{d}}_{mp,r}(t_f) &= \frac{1}{t_f}D\left(\mathbf{H}_T\mathbf{u}_r(t)\right)^p.\mathbf{1}\\ \mathbf{d}_{mp,r}(0) &= \mathbf{0};\end{aligned}\right\} \tag{9.9}$$

Now to compute the $Env\left(\max_i(..)\right)$, a weighted approach is adopted (Lavan 2006).

$$\begin{aligned}&Env\left\{\max\left\{\max_t\left(abs\left(H_T\mathbf{u}_1(t)\right)\right)\right\},.....\max\left\{\max_t\left\{abs\left\{H_T\mathbf{u}_{N_{gm}}(t)\right\}\right\}\right\}\right\}\\ &= \frac{\sum_{r=1}^{N_{gm}}\mathbf{1}^T\bullet\left\{D\left(\mathbf{d}_{mp,r}(t_f)\right)^{\frac{1}{p}}\right\}^{q+1}\bullet\mathbf{1}}{\sum_{r=1}^{N_{gm}}\mathbf{1}^T\bullet\left\{D\left(\mathbf{d}_{mp,r}(t_f)\right)^{\frac{1}{p}}\right\}^{q}\bullet\mathbf{1}}\end{aligned} \tag{9.10}$$

where $q$ is a large positive value.

Now applying eq. (9.10) into eq. (9.1) we get,

$$\Psi = \left\{ H\left( \frac{\sum_{r=1}^{N_{gm}} \mathbf{1}^T \bullet \left\{ D\left(\mathbf{d}_{mp,r}\left(t_f\right)\right)^{\frac{1}{p}} \right\}^{q+1} \bullet \mathbf{1}}{\sum_{r=1}^{N_{gm}} \mathbf{1}^T \bullet \left\{ D\left(\mathbf{d}_{mp,r}\left(t_f\right)\right)^{\frac{1}{p}} \right\}^{q} \bullet \mathbf{1}} - d_{al} \right) \right\} \times C_{total}$$

$$+ \left\{ H\left( d_{al} - \frac{\sum_{r=1}^{N_{gm}} \mathbf{1}^T \bullet \left\{ D\left(\mathbf{d}_{mp,r}\left(t_f\right)\right)^{\frac{1}{p}} \right\}^{q+1} \bullet \mathbf{1}}{\sum_{r=1}^{N_{gm}} \mathbf{1}^T \bullet \left\{ D\left(\mathbf{d}_{mp,r}\left(t_f\right)\right)^{\frac{1}{p}} \right\}^{q} \bullet \mathbf{1}} \right) \right\} \times \sum_{j=1}^{N_d} c_j \sum_{i=1}^{k} A_i \left( \frac{1}{N_{gm}} \sum_{r=1}^{N_{gm}} \left( d_{mp,r,j}\left(t_f\right)\right)^{\frac{1}{p}} \right)^{\eta_i}$$

(9.11)

On normalization by total cost, eq. (9.11) gets modified as,

$$\hat{\Psi} = \left\{ H\left( \frac{\sum_{r=1}^{N_{gm}} \mathbf{1}^T \bullet \left\{ D\left(\mathbf{d}_{mp,r}\left(t_f\right)\right)^{\frac{1}{p}} \right\}^{q+1} \bullet \mathbf{1}}{\sum_{r=1}^{N_{gm}} \mathbf{1}^T \bullet \left\{ D\left(\mathbf{d}_{mp,r}\left(t_f\right)\right)^{\frac{1}{p}} \right\}^{q} \bullet \mathbf{1}} - d_{al} \right) \right\} \times 1$$

$$+ \left\{ H\left( d_{al} - \frac{\sum_{r=1}^{N_{gm}} \mathbf{1}^T \bullet \left\{ D\left(\mathbf{d}_{mp,r}\left(t_f\right)\right)^{\frac{1}{p}} \right\}^{q+1} \bullet \mathbf{1}}{\sum_{r=1}^{N_{gm}} \mathbf{1}^T \bullet \left\{ D\left(\mathbf{d}_{mp,r}\left(t_f\right)\right)^{\frac{1}{p}} \right\}^{q} \bullet \mathbf{1}} \right) \right\} \times \frac{1}{C_{total}} \sum_{j=1}^{N_d} c_j \sum_{i=1}^{k} A_i \left( \frac{1}{N_{gm}} \sum_{r=1}^{N_{gm}} \left( d_{mp,r,j}\left(t_f\right)\right)^{\frac{1}{p}} \right)^{\eta_i}$$

(9.12)

Over here, $d_{al}$ represents the allowable drift, $H(\bullet)$ represents the Heaviside step function, $C_{total}$ represents the total cost of the building, $c_j$ represents the cost of the $j^{th}$ component, $A_i$ is the constant multiplier associated with the loss function, $\eta_i$ represents the power, $N$ represents the degrees of freedom and $N_{gm}$ is the number of ground motions. First term in eq. (9.12) represents the total loss (in the present study writing off of the building) and the second term represents the aggregate component loss.

Eq. (9.12) can be re-written with analytical expressions for Heaviside step function as follows,

$$\hat{\Psi} \cong \frac{1}{2}+\frac{1}{2}\tanh\left( k\left( \frac{\sum_{r=1}^{N_{gm}} \mathbf{1}^T \bullet \left\{ D\left(\mathbf{d}_{mp,r}\left(t_f\right)\right)^{\frac{1}{p}} \right\}^{q+1} \bullet \mathbf{1}}{\sum_{r=1}^{N_{gm}} \mathbf{1}^T \bullet \left\{ D\left(\mathbf{d}_{mp,r}\left(t_f\right)\right)^{\frac{1}{p}} \right\}^{q} \bullet \mathbf{1}} - d_{al} \right) \right) +$$

$$\left( \frac{1}{2}+\frac{1}{2}\tanh\left( k\left( d_{al} - \frac{\sum_{r=1}^{N_{gm}} \mathbf{1}^T \bullet \left\{ D\left(\mathbf{d}_{mp,r}\left(t_f\right)\right)^{\frac{1}{p}} \right\}^{q+1} \bullet \mathbf{1}}{\sum_{r=1}^{N_{gm}} \mathbf{1}^T \bullet \left\{ D\left(\mathbf{d}_{mp,r}\left(t_f\right)\right)^{\frac{1}{p}} \right\}^{q} \bullet \mathbf{1}} \right) \right) \right) \times \frac{1}{C_{total}} \sum_{j=1}^{N_d} c_j \sum_{i=1}^{k} A_i \left( \frac{1}{N_{gm}} \sum_{r=1}^{N_{gm}} \left( d_{mp,r,j}\left(t_f\right)\right)^{\frac{1}{p}} \right)^{\eta_i}$$

(9.13)

In eq. (9.13) when $k \to \infty$ the function will converge to the Heaviside step function. Now the augmented function is obtained by adding in effective zeros.

$$\hat{\Psi} = \frac{1}{2}+\frac{1}{2}\tanh\left( k\left( \frac{\sum_{r=1}^{N_{gm}} \mathbf{1}^T \bullet \left\{ D\left(\mathbf{d}_{mp,r}\left(t_f\right)\right)^{\frac{1}{p}} \right\}^{q+1} \bullet \mathbf{1}}{\sum_{r=1}^{N_{gm}} \mathbf{1}^T \bullet \left\{ D\left(\mathbf{d}_{mp,r}\left(t_f\right)\right)^{\frac{1}{p}} \right\}^{q} \bullet \mathbf{1}} - d_{al} \right) \right) +$$

$$\left( \frac{1}{2}+\frac{1}{2}\tanh\left( k\left( d_{al} - \frac{\sum_{r=1}^{N_{gm}} \mathbf{1}^T \bullet \left\{ D\left(\mathbf{d}_{mp,r}\left(t_f\right)\right)^{\frac{1}{p}} \right\}^{q+1} \bullet \mathbf{1}}{\sum_{r=1}^{N_{gm}} \mathbf{1}^T \bullet \left\{ D\left(\mathbf{d}_{mp,r}\left(t_f\right)\right)^{\frac{1}{p}} \right\}^{q} \bullet \mathbf{1}} \right) \right) \right) \times \frac{1}{C_{total}} \sum_{j=1}^{N_d} c_j \sum_{i=1}^{k} A_i \left( \frac{1}{N_{gm}} \sum_{r=1}^{N_{gm}} \left( d_{mp,r,j}\left(t_f\right)\right)^{\frac{1}{p}} \right)^{\eta_i}$$

$$+ \sum_{j=1}^{N_{gm}} \int_0^{t_f} \lambda_j^T(t) \left\{ \mathbf{M}\ddot{\mathbf{u}}_j(t) + \mathbf{C}\dot{\mathbf{u}}_j(t) + \mathbf{K}\mathbf{u}_j(t) + \mathbf{M}\mathbf{I}\ddot{u}_{g_j}(t) \right\} dt$$

$$+ \sum_{j=1}^{N_{gm}} \int_0^{t_f} \chi_j^T(t) \phi_j\left(\dot{\mathbf{d}}_{mp,j}\left(t_f\right), \mathbf{d}_{mp,j}\left(t_f\right), \mathbf{u}_j(t)\right) dt$$

(9.14)

Where,

$$\sum_{j=1}^{N_{gm}} \phi_j\left(\dot{\mathbf{d}}_{mp,j}\left(t_f\right), \mathbf{d}_{mp,j}\left(t_f\right), \mathbf{u}_j(t)\right) = \sum_{j=1}^{N_{gm}} \dot{\mathbf{d}}_{mp,j}\left(t_f\right) - \frac{1}{t_f} D\left(\mathbf{H}_T \mathbf{u}_j(t)\right)^p . \mathbf{1} \Bigg\} \tag{9.15}$$

and **C** represents the manufactured damping matrix. Just for convenience sake, we ignore the inherent damping matrix.

Now let's denote,

$$\left.\begin{aligned}
T_1 &= \frac{1}{2}+\frac{1}{2}\tanh\left(k\left(\frac{\sum_{r=1}^{N_{gm}}\mathbf{1}^T\bullet\left\{D\left(\mathbf{d}_{mp,r}\left(t_f\right)\right)^{\frac{1}{p}}\right\}^{q+1}\bullet\mathbf{1}}{\sum_{r=1}^{N_{gm}}\mathbf{1}^T\bullet\left\{D\left(\mathbf{d}_{mp,r}\left(t_f\right)\right)^{\frac{1}{p}}\right\}^{q}\bullet\mathbf{1}}-d_{al}\right)\right)\\
T_2 &= \left(\frac{1}{2}+\frac{1}{2}\tanh\left(k\left(d_{al}-\frac{\sum_{r=1}^{N_{gm}}\mathbf{1}^T\bullet\left\{D\left(\mathbf{d}_{mp,r}\left(t_f\right)\right)^{\frac{1}{p}}\right\}^{q+1}\bullet\mathbf{1}}{\sum_{r=1}^{N_{gm}}\mathbf{1}^T\bullet\left\{D\left(\mathbf{d}_{mp,r}\left(t_f\right)\right)^{\frac{1}{p}}\right\}^{q}\bullet\mathbf{1}}\right)\right)\right)\bullet\frac{1}{C_{total}}\sum_{j=1}^{N_d}c_j\sum_{i=1}^{k}A_i\left(\frac{1}{N_{gm}}\sum_{r=1}^{N_{gm}}\left(d_{mp,r,j}\left(t_f\right)\right)^{\frac{1}{p}}\right)\\
T_3 &= \sum_{j=1}^{N_{gm}}\int_0^{t_f}\lambda_j^T(t)\left\{\mathbf{M}\ddot{\mathbf{u}}_j(t)+\mathbf{C}\dot{\mathbf{u}}_j(t)+\mathbf{K}\mathbf{u}_j(t)+\mathbf{M}\mathbf{I}\ddot{u}_{g,j}(t)\right\}dt\\
T_4 &= \sum_{j=1}^{N_{gm}}\int_0^{t_f}\chi_j^T(t)\phi_j\left(\dot{\mathbf{d}}_{mp,j}\left(t_f\right),\mathbf{d}_{mp,j}\left(t_f\right),\mathbf{u}_j(t)\right)dt
\end{aligned}\right\} \tag{9.16}$$

So eq. (9.14) can be rewritten as,

$$\hat{\Psi} = T_1 + T_2 + T_3 + T_4 \tag{9.17}$$

Now taking the variation of eq. (9.14) we get,

$$\delta\hat{\Psi} = \delta T_1 + \delta T_2 + \delta T_3 + \delta T_4 \tag{9.20}$$

*9.3.2.1.1 Variation of first term* $(\delta T_1)$

Now let's denote,

$$y\left(\mathbf{d}_{mp,1},\mathbf{d}_{mp,2},\mathbf{d}_{mp,3}..\mathbf{d}_{mp,N_{gm}}\right)=\frac{num}{den}=\frac{\sum_{r=1}^{N_{gm}}\mathbf{1}^T\bullet\left\{D^{\frac{1}{p}}\left(\mathbf{d}_{mp,r}\left(t_f\right)\right)\right\}^{q+1}\bullet\mathbf{1}}{\sum_{r=1}^{N_{gm}}\mathbf{1}^T\bullet\left\{D^{\frac{1}{p}}\left(\mathbf{d}_{mp,r}\left(t_f\right)\right)\right\}^{q}\bullet\mathbf{1}} \tag{9.21}$$

Now inserting eq. (9.21) in eq. (9.20) we get,

$$T_1=\frac{1}{2}+\frac{1}{2}\tanh\left(k\left(y\left(\mathbf{d}_{mp,1},\mathbf{d}_{mp,2},\mathbf{d}_{mp,3}..\mathbf{d}_{mp,N_{gm}}\right)-d_{al}\right)\right) \tag{9.22}$$

$$\delta T_1=-\frac{1}{2}k\left(\tanh\left(k\left(y\left(\mathbf{d}_{mp,1},\mathbf{d}_{mp,2},\mathbf{d}_{mp,3}..\mathbf{d}_{mp,N_{gm}}\right)-d_{al}\right)\right)^2-1\right)\bullet k\left\{\sum_{r=1}^{N_{gm}}\frac{\partial^T y}{\partial\mathbf{d}_{mp,r}}\delta\mathbf{d}_{mp,r}\right\} \tag{9.23}$$

On applying variational calculus,

$$\delta T_1=-\frac{1}{2}k\left(\tanh\left(k\left(y\left(\mathbf{d}_{mp,1},\mathbf{d}_{mp,2},\mathbf{d}_{mp,3}.....\mathbf{d}_{mp,N_{gm}}\right)-d_{al}\right)\right)^2-1\right)\bullet$$
$$k\left\{\sum_{r=1}^{N_{gm}}\left(\begin{array}{l}\left(\frac{1}{den^2}\bullet\frac{1}{p}\left(D^{\frac{1}{p}-1}\left(\mathbf{d}_{mp,r}\left(t_f\right)\right)\bullet\mathbf{1}\right)\bullet\right.\\ \left\{\left\{den\bullet(q+1)\bullet\left(\mathbf{1}^T\bullet D^{\frac{1}{p}}\left(\mathbf{d}_{mp,r}\left(t_f\right)\right)\bullet\mathbf{1}\right)^q\right\}-\right.\\ \left.\left.\left\{num\bullet q\bullet\left(\mathbf{1}^T\bullet D^{\frac{1}{p}}\left(\mathbf{d}_{mp,r}\left(t_f\right)\right)\bullet\mathbf{1}\right)^{q-1}\right\}\right\}\end{array}\right)^T\delta\mathbf{d}_{mp,r}\right\} \tag{9.24}$$

*9.3.2.1.2 Variation of first term* $\left(\delta T_2\right)$

$$T_2 = \left( \frac{1}{2} + \frac{1}{2}\tanh\left( k\left( d_{al} - \frac{\sum_{r=1}^{N_{gm}} \mathbf{1}^T \bullet \left\{ D\left(\mathbf{d}_{mp,r}\left(t_f\right)\right)^{\frac{1}{p}} \right\}^{q+1} \bullet \mathbf{1}}{\sum_{r=1}^{N_{gm}} \mathbf{1}^T \bullet \left\{ D\left(\mathbf{d}_{mp,r}\left(t_f\right)\right)^{\frac{1}{p}} \right\}^{q} \bullet \mathbf{1}} \right) \right) \right) \bullet \frac{1}{C_{total}} \sum_{j=1}^{N_d} c_j \sum_{i=1}^{k} A_i \left( \frac{1}{N_{gm}} \sum_{r=1}^{N_{gm}} \left( d_{mp,r,j}\left(t_f\right)\right)^{\frac{1}{p}} \right)^{\eta_i}$$

(9.25)

$$\delta T_2 = \frac{1}{2} k \left( \tanh\left( k\left( d_{al} - y\left(\mathbf{d}_{mp,1},\ldots\mathbf{d}_{mp,N_{gm}}\right)\right)\right)^2 - 1\right) \bullet$$

$$k \left\{ \left\{ \sum_{r=1}^{N_{gm}} \left\{ \begin{array}{l} \frac{1}{den^2} \bullet \frac{1}{p} \left( D^{\frac{1}{p}-1}\left(\mathbf{d}_{mp,r}\left(t_f\right)\right) \bullet \mathbf{1} \right) \bullet \\ \left\{ \left\{ den \bullet (q+1) \bullet \left( \mathbf{1}^T \bullet D^{\frac{1}{p}}\left(\mathbf{d}_{mp,r}\left(t_f\right)\right) \bullet \mathbf{1} \right)^{q} \right\} - \\ \left\{ num \bullet q \bullet \left( \mathbf{1}^T \bullet D^{\frac{1}{p}}\left(\mathbf{d}_{mp,r}\left(t_f\right)\right) \bullet \mathbf{1} \right)^{q-1} \right\} \end{array} \right\}^T \delta\mathbf{d}_{mp,r} \right\} \right\} \bullet \frac{1}{C_{total}} \sum_{j=1}^{N_d} c_j \sum_{i=1}^{k} A_i \left( \frac{1}{N_{gm}} \sum_{r=1}^{N_{gm}} \left( d_{mp,r,j}\left(t_f\right)\right)^{\frac{1}{p}} \right) +$$

$$\frac{1}{2} + \frac{1}{2}\tanh\left( k\left( d_{al} - y\left(\mathbf{d}_{mp,1},\ldots\mathbf{d}_{mp,N_{gm}}\right)\right)\right) \bullet$$

$$\sum_{r=1}^{N_{gm}} \left\{ \begin{array}{l} \left( \frac{1}{C_{total}} \mathbf{c}_{\cos t\_ns} \sum_{i=1}^{k} A_i \eta_i \left( \frac{1}{N_{gm}} \sum_{r=1}^{N_{gm}} \left( D^{\frac{1}{p}}\left(\mathbf{d}_{mp,r}\left(t_f\right)\right) \bullet \mathbf{1} \right) \right)^{\eta_i - 1} \right) \bullet \\ \frac{1}{N_{gm}} \left( \frac{1}{p} \bullet D^{\frac{1}{p}-1}\left(\mathbf{d}_{mp,r}\left(t_f\right)\right) \bullet \mathbf{1} \right) \\ \bullet \delta\mathbf{d}_{mp,r} \end{array} \right\}$$

(9.26)

*9.3.2.1.3 Variation of third term* $\left(\delta T_3\right)$

$$T_3 = \sum_{r=1}^{N_{gm}} \int_0^{t_f} \lambda_j^T(t) \left\{ \mathbf{M}\ddot{\mathbf{u}}_r(t) + \mathbf{C}\dot{\mathbf{u}}_r(t) + \mathbf{K}\mathbf{u}_r(t) + \mathbf{M}\mathbf{I}\ddot{u}_{g_{,r}}(t) \right\} dt \qquad (9.27)$$

$$\delta T_3 = \sum_{r=1}^{N_{gm}} \left\{ \begin{array}{l} \int_0^{t_f} \lambda_r^T(t)\delta\mathbf{C}\dot{\mathbf{u}}_r(t)dt + \int_0^{t_f} \delta\mathbf{u}_r^T(t)\left\{\mathbf{M}\ddot{\lambda}_r(t) - \mathbf{C}\dot{\lambda}_r(t) + \mathbf{K}\lambda_r(t)\right\}dt + \delta\mathbf{u}_r^T(t)\left\{\mathbf{C}\lambda_r(t) - \mathbf{M}\dot{\lambda}_r(t)\right\}\Big|_0^{t_f} \\ + \delta\dot{\mathbf{u}}_r^T(t)\left\{\mathbf{M}\lambda_r(t)\right\}\Big|_0^{t_f} \end{array} \right\}$$

(9.28)

*9.3.2.1.4 Variation of fourth term* $(\delta T_4)$

$$T_4 = \sum_{r=1}^{N_{gm}} \int_0^{t_f} \chi_r^T(t)\phi_r\left(\dot{\mathbf{d}}_{mp,r}(t_f), \mathbf{d}_{mp,r}(t_f), \mathbf{u}_r(t)\right)dt \tag{9.29}$$

$$\delta T_4 = \sum_{r=1}^{N_{gm}} \left\{ \chi_r^T(t_f)\frac{\partial\phi_r}{\partial\dot{\mathbf{d}}_{m,p,r}}\delta\mathbf{d}_{m,p,r}(t_f)\Big|_0^{t_f} + \int_0^{t_f} \delta\mathbf{d}_{m,p,r}^T\left\{\frac{\partial\phi_r}{\partial\mathbf{d}_{m,p,r}}\chi_r(t) - \frac{\partial\phi_r}{\partial\dot{\mathbf{d}}_{m,p,r}}\dot{\chi}_r(t)\right\}dt + \int_0^{t_f} \delta\mathbf{u}_r^T(t)\left\{\frac{\partial\phi_r}{\partial\mathbf{u}_r}\chi_r(t)\right\}dt \right\}$$

(9.30)

Summing up the first two terms and re-ordering we get,

$$\delta T_2 + \delta T_1 = \sum_{r=1}^{N_{gm}} \left( k \left\{ \left\{ \left\{ \frac{U_{cap,\max}}{den^2} \bullet \frac{1}{p} \left( D^{\frac{1}{p}-1}\left(\mathbf{d}_{mp,r}\left(t_f\right)\right) \bullet \mathbf{1} \right) \bullet \left\{ den \bullet (q+1) \bullet \left( \mathbf{1}^T \bullet D^{\frac{1}{p}}\left(\mathbf{d}_{mp,r}\left(t_f\right)\right) \bullet \mathbf{1} \right)^q \right\} - \left\{ num \bullet q \bullet \left( \mathbf{1}^T \bullet D^{\frac{1}{p}}\left(\mathbf{d}_{mp,r}\left(t_f\right)\right) \bullet \mathbf{1} \right)^{q-1} \right\} \right\} \right\}^T \bullet \delta \mathbf{d}_{mp,r} \right.$$

$$\left. \frac{1}{C_{total}} \sum_{j=1}^{N_d} c_j \sum_{i=1}^{k} A_i \left( \frac{1}{N_{gm}} \sum_{r=1}^{N_{gm}} \left( d_{mp,r,j}\left(t_f\right) \right)^{\frac{1}{p}} \right) \right)$$

$$+ \left( \frac{1}{2} + \frac{1}{2} \tanh\left( k \left( d_{al} - y\left( \mathbf{d}_{mp,1}, \ldots \mathbf{d}_{mp,N_{gm}} \right) \right) \right) \bullet \right.$$

$$\left. \sum_{r=1}^{N_{gm}} \left\{ \begin{array}{l} \left( \frac{1}{C_{total}} \mathbf{c}_{\cos t\_ns} \sum_{i=1}^{k} A_i \eta_i \left( \frac{1}{N_{gm}} \sum_{r=1}^{N_{gm}} \left( D^{\frac{1}{p}}\left(\mathbf{d}_{mp,r}\left(t_f\right)\right) \bullet \mathbf{1} \right) \right)^{\eta_i - 1} \right) \bullet \\ \frac{1}{N_{gm}} \left( \frac{1}{p} \bullet D^{\frac{1}{p}-1}\left(\mathbf{d}_{mp,r}\left(t_f\right)\right) \bullet \mathbf{1} \right) \end{array} \right\} \bullet \delta \mathbf{d}_{mp,r} \right)$$

$$- \sum_{r=1}^{N_{gm}} \left[ k \left\{ \left\{ \left\{ \frac{U_{cap,\max}}{den^2} \bullet \frac{1}{p} \left( D^{\frac{1}{p}-1}\left(\mathbf{d}_{mp,r}\left(t_f\right)\right) \bullet \mathbf{1} \right) \bullet \left\{ den \bullet (q+1) \bullet \left( \mathbf{1}^T \bullet D^{\frac{1}{p}}\left(\mathbf{d}_{mp,r}\left(t_f\right)\right) \bullet \mathbf{1} \right)^q \right\} - \left\{ num \bullet q \bullet \left( \mathbf{1}^T \bullet D^{\frac{1}{p}}\left(\mathbf{d}_{mp,r}\left(t_f\right)\right) \bullet \mathbf{1} \right)^{q-1} \right\} \right\} \right\} \bullet \delta \mathbf{d}_{mp,r} \right.$$

$$\left. \left( \frac{1}{2} k \left( \tanh\left( k \left( y\left( \mathbf{d}_{mp,1}, \ldots\ldots \mathbf{d}_{mp,N_{gm}} \right) - d_{al} \right) \right)^2 - 1 \right) \bullet \right) \right]$$

(9.31)

Now introducing new notations for each of these terms we get,

$$
\left.
\begin{aligned}
&\mathbf{Q}_{1,r} = -\frac{1}{2}k\left(\tanh\left(k\left(y\left(\mathbf{d}_{mp,1},.....\mathbf{d}_{mp,N_{gm}}\right)-d_{al}\right)\right)^2-1\right)\bullet \\
&k\left\{\begin{Bmatrix}\frac{U_{cap,\max}}{den^2}\bullet\frac{1}{p}\left(D^{\frac{1}{p}-1}\left(\mathbf{d}_{mp,r}\left(t_f\right)\right)\bullet\mathbf{1}\right)\bullet \\ \left\{\left\{den\bullet(q+1)\bullet\left(\mathbf{1}^T\bullet D^{\frac{1}{p}}\left(\mathbf{d}_{mp,r}\left(t_f\right)\right)\bullet\mathbf{1}\right)^q\right\}-\right\}\end{Bmatrix}\right\} \\
&\mathbf{Q}_{2,r} = \\
&\frac{1}{2}k\left(\tanh\left(k\left(d_{al}-y\left(\mathbf{d}_{mp,1},...\mathbf{d}_{mp,N_{gm}}\right)\right)\right)^2-1\right)\bullet \\
&k\left\{\begin{Bmatrix}\frac{U_{cap,\max}}{den^2}\bullet\frac{1}{p}\left(D^{\frac{1}{p}-1}\left(\mathbf{d}_{mp,r}\left(t_f\right)\right)\bullet\mathbf{1}\right)\bullet \\ \left\{\left\{den\bullet(q+1)\bullet\left(\mathbf{1}^T\bullet D^{\frac{1}{p}}\left(\mathbf{d}_{mp,r}\left(t_f\right)\right)\bullet\mathbf{1}\right)^q\right\}-\right\}\end{Bmatrix}\right\}\bullet \\
&\left\{\begin{Bmatrix}\left\{num\bullet q\bullet\left(\mathbf{1}^T\bullet D^{\frac{1}{p}}\left(\mathbf{d}_{mp,r}\left(t_f\right)\right)\bullet\mathbf{1}\right)^{q-1}\right\}\end{Bmatrix}\right\} \\
&\frac{1}{C_{total}}\sum_{j=1}^{N_d}c_j\sum_{i=1}^{k}A_i\left(\frac{1}{N_{gm}}\sum_{r=1}^{N_{gm}}\left(d_{mp,r,j}\left(t_f\right)\right)^{\frac{1}{p}}\right) \\
&\mathbf{Q}_{3,r} = \frac{1}{2}+\frac{1}{2}\tanh\left(k\left(d_{al}-y\left(\mathbf{d}_{mp,1},...\mathbf{d}_{mp,N_{gm}}\right)\right)\right)\bullet \\
&\left\{\begin{Bmatrix}\left(\frac{1}{C_{total}}\mathbf{c}_{\cos t\_ns}\sum_{i=1}^{k}A_i\eta_i\left(\frac{1}{N_{gm}}\sum_{r=1}^{N_{gm}}\left(D^{\frac{1}{p}}\left(\mathbf{d}_{mp,r}\left(t_f\right)\right)\bullet\mathbf{1}\right)\right)^{\eta_i-1}\right)\bullet \\ \frac{1}{N_{gm}}\left(\frac{1}{p}\bullet D^{\frac{1}{p}-1}\left(\mathbf{d}_{mp,r}\left(t_f\right)\right)\bullet\mathbf{1}\right)\end{Bmatrix}\right\}
\end{aligned}
\right\} \qquad (9.32)
$$

Collecting all the $\delta\mathbf{d}_{m,p,r}$ terms, we get

$$
\sum_{r=1}^{N_{gm}}\left\{\delta\mathbf{d}_{m,p,r}^T\left(t_f\right)\left\{\frac{\partial\phi_r}{\partial\dot{\mathbf{d}}_{m,p,r}}\chi_r\left(t_f\right)+\mathbf{Q}_{1,r}+\mathbf{Q}_{2,r}+\mathbf{Q}_{3,r}\right\}+\int_0^{t_f}\delta\mathbf{d}_{m,p,r}^T(t)\left\{\frac{\partial\phi_r}{\partial\mathbf{d}_{m,p,r}}\chi_r(t)-\frac{\partial\phi_r}{\partial\dot{\mathbf{d}}_{m,p,r}}\dot{\chi}_r(t)\right\}dt\right\} \qquad (9.33)
$$

Collecting the $\delta\mathbf{u}_r(t)$ and $\delta\dot{\mathbf{u}}_r(t)$ terms we get,

$$\sum_{r=1}^{N_{gm}}\left\{\begin{array}{l}\int_0^{t_f}\delta\mathbf{u}_r^T(t)\left\{\mathbf{M}\ddot{\lambda}_r(t)-\mathbf{C}\dot{\lambda}_r(t)+\mathbf{K}\lambda_r(t)+\left\{\frac{\partial\phi_r}{\partial\mathbf{u}_r}\chi_r(t)\right\}\right\}dt+\delta\mathbf{u}_r^T(t)\left\{\mathbf{C}\lambda_r(t)-\mathbf{M}\dot{\lambda}_r(t)\right\}\Big|_0^{t_f}\\ +\delta\dot{\mathbf{u}}_r^T(t)\left\{\mathbf{M}\lambda_r(t)\right\}\Big|_0^{t_f}\end{array}\right\} \quad (9.34)$$

Eliminating $\delta\mathbf{d}_{m,p,r}(t_f)$, $\delta\mathbf{d}_{m,p,r}(t)$, $\delta\mathbf{u}_r(t)$ and $\delta\dot{\mathbf{u}}$ terms,

$$\left.\begin{array}{l}\mathbf{M}\ddot{\lambda}_r(t)-\mathbf{C}\dot{\lambda}_r(t)+\mathbf{K}\lambda_r(t)=-\frac{\partial\phi_r}{\partial\mathbf{u}_r}\chi_r(t)=-\frac{\partial\phi_r}{\partial\mathbf{u}_r}\chi_r(t_f)=\frac{\partial\phi_r}{\partial\mathbf{u}_r}\left\{\mathbf{Q}_{1,r}+\mathbf{Q}_{2,r}+\mathbf{Q}_{3,r}\right\}\\ \mathbf{C}\lambda_r(t_f)-\mathbf{M}\dot{\lambda}_r(t_f)=0\\ \mathbf{M}\lambda_r(t_f)=0\\ \lambda_r(t_f)=\dot{\lambda}_r(t_f)=\mathbf{0}\\ \frac{\partial\phi_r}{\partial\mathbf{u}_r}=-\frac{p}{t_f}\bullet\mathbf{H}_T^T\bullet D\left(\mathbf{H}_T\mathbf{u}_j(t)\right)^{p-1}\end{array}\right\} \quad (9.35)$$

On solving eq. (9.35), the gradients are given as,

$$\delta\hat{\Psi}=\sum_{i=1}^{N_{gm}}\int_0^{t_f}\lambda_i^T(t)\,\delta\mathbf{C}\dot{\mathbf{u}}_i(t)\,dt \quad (9.36)$$

Eq. (9.36) represents the analytical gradients. The computed analytical gradient has been compared against the gradients computed from the classical Finite difference scheme; the difference between both the gradients is almost close to zero (of the order of $10^{-20}$).

# 9.4 Numerical Study

### 9.4.1 Four storey frame

A four-story reinforced concrete frame described in Arede (2000), designed in accordance with Eurocode 8 (EC8) and Eurocode 2(EC2) is used to illustrate the proposed optimization procedure. The frame is designed for high seismicity assuming a PGA of 0.3g. The geometric dimensions of the frame with the location of the partition walls and the arrangement of the

dampers are given in Fig.9.3. It should be noted that in the analysis, partition wall was not modelled and only the bare frame with the dampers are analyzed.

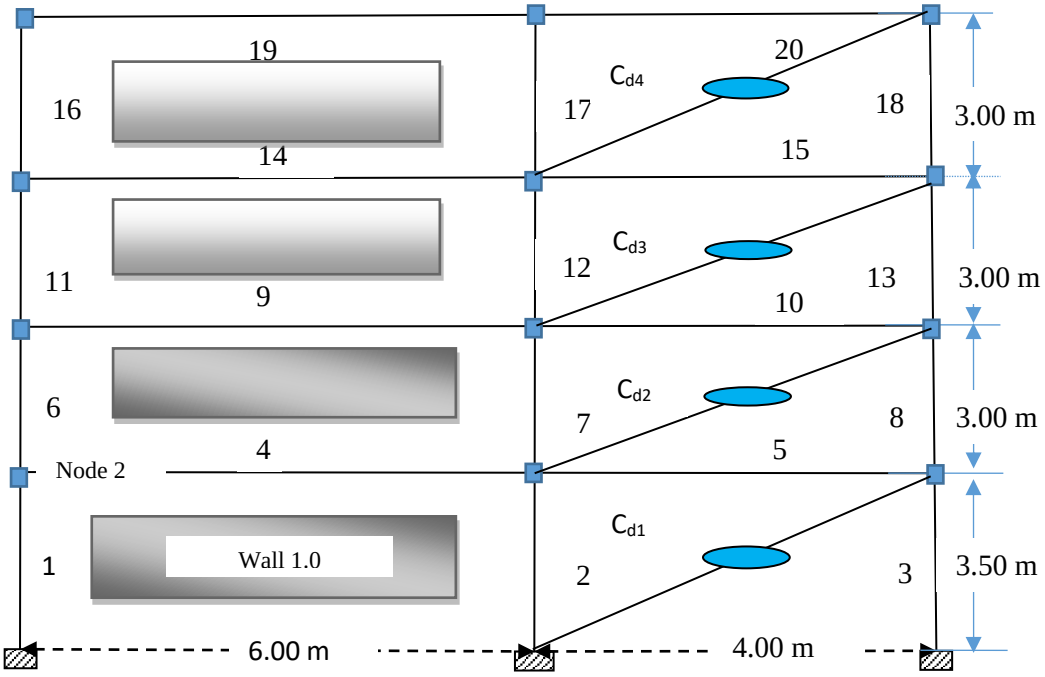


Fig. 9.3 $C_{di}$ refers to added dampers and $i=1....4$

Dynamic Young's modulus of concrete is assumed as $3.5\times10^{10}\,Nm^{-2}$. Geometric properties and nodal masses are given in Appendix 3.

The proposed framework is very generic and can include any number of components; but as the whole purpose of this example is to demonstrate the multi-objective optimization framework, only loss to partition walls and beam column joints are included in the study. Expected total loss is computed as described in chapter 8.0 adopting the coefficients from Appendix 8.0.

Realistic normalized cost for the two components considered in the loss is adopted from the Rawlinson's cost estimation schedule (Rawlison's 2012). The frame is assumed to be part of a three-dimensional building system with floor area of $100m^2$ per floor. As per the Rowlinson's

pricing manual 2012 (Rowlinson database, New Zealand), assuming the architectural functionality as hospitality, the floor cost is assumed to be \$4750/ $m^2$ which would then total to \$475,000 per floor and the total estimated cost would be \$1,900,000. For this present example, it is assumed that 70% of this total estimated cost is assigned to the frame under consideration which would amount to \$1,330,000. It should be remembered that this total cost estimate given by Rawlinson's schedule consists of approximate cost of all the components and as only two components (beam column joints and partitions) are considered in the present study, this total cost (~\$1,330,000) must be scaled down. Adopting the fact that partitions cost ~7.5% and the beam column junction costs ~5.2% of the total cost (Rawlinson's manual), the total cost gets scaled down to ~\$1,68,910.

Losses in the partition walls are assumed to be lumped to the nodes of the bay to which the wall is attached by assuming a suitable tributary area. For e.g., for wall 1, 50% of the loss is lumped to node 2 as shown in fig. 9.3. The interstorey drift associated with node 2 which is the same for the other nodes at the same level (in the case of node 2, the first floor level) causes the loss in this partition wall. Euler beam elements are used for the modelling of the frame. Elemental Wilson Penzien model is adopted to represent the inherent damping matrix. For more details on implementation of Elemental Wilson Penzien damping model, please refer to section 3.3.2 of chapter 3.0.

A suite of 7 artificial ground motions scaled to match an EC8 design spectra with PGA 0.4g is used for the present study. It must be mentioned that the framework is very generic and cater to any number of ground motions; as the purpose of this example is just to demonstrate the framework, only 7 ground motions are used. Un-controlled frame analysis has revealed that some the of the ground motions scaled to this level of intensity may incur inelastic excursions in the parent frame due to drifts greater than the order of about 1.3% (Arede 2000). As already

mentioned in section 9.2, it has been observed in the public response to the Christchurch/Kaikoura sequence of earthquakes that when the building tends to yield or enter inelastic state, the buildings had to be demolished either due to the tendency of owners to claim insurance to build new ones or due to inaccessibility to repair them. So, an effective damper based scheme should incur minimum yielding state in the parent structure. To achieve this objective in the present study, the capping drift $d_{al}$ is limited to 0.8% so that the parent frame is predominantly linear. Only drift sensitive loss is accounted in the present study. Multi-objective optimization is performed as per the methodology described in section 9.3.1.2. For the present study only 40 design points are generated in the objective space, i.e. $K$=40 in step 2 and $q=4$ as there are only 4 dampers. Constraint *move limit* as required by eq. (9.4) is adopted as 5% of the design damping vector.

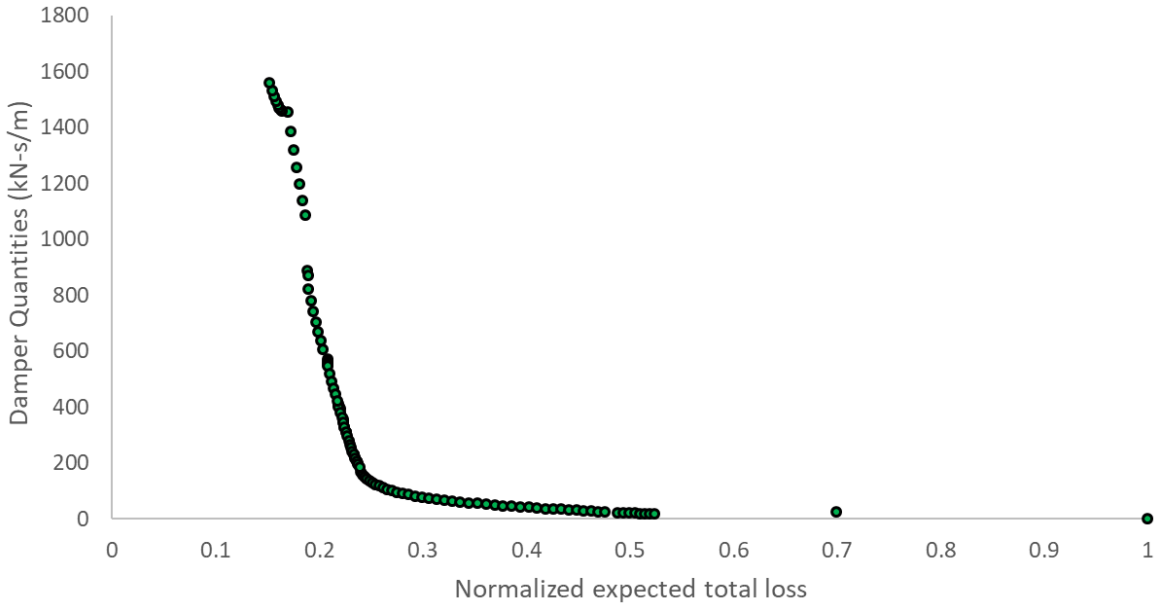


Fig. 9.4 pareto-front obtained for the four story frame

Fig. 9.4 shows the final Pareto front plotted between initial cost (damper quantities) and the normalized loss. Each of this point on the Pareto front corresponds to a specific quantity of dampers and its distribution. The uncontrolled frame results in a 100% loss as illustrated in fig

9.4 mainly because the drift generated exceeds $d_{al}$ (which is 0.8% for the present example) in at least one of the ground motion.

The Pareto front shown in fig. 9.4 illustrates a clear trade-off for the choice of the expected loss and the initial cost. Each point on the pareto front corresponds to a solution which is obtained by the degraded performance of one of the objectives. For e.g., a point on to the extreme right on the x-axis presents a solution where there is a very high loss with minimum initial cost ; similarly a point to left on the x axis shows a minimum loss scenario but with a very high initial cost. So, a whole sphere of possible solutions is represented by the Pareto front and enables the designer to quantitatively weigh the trade-offs; i.e. whether to favor one objective in the expense of a degraded performance of the other. Also in the Pareto front obtained it could also be seen that there is a substantial decrease in loss with minimum added damping. To illustrate this further, three points on the Pareto front with corresponding loss as 27%, 24% and 22% are selected. The respective quantity of dampers are $94kN-s/m, 135kN-s/m$ and $325kN-s/m$. Though the decrease in loss is marginal altogether, it may be clearly seen that the quantity of dampers required increases drastically, almost ~3 times for the 22% loss case. This is really a very useful insight for the stakeholder/owner as he or she can directly see the implications of their choice mainly because the entire front of solutions are available.

The point corresponding to loss of 24% is selected to generate fig 9.5. It may be clearly seen that for a further reduction in loss, a much larger quantity of added damping is required. This quantity corresponds to a first mode damping ratio of approximately 22%. It should be noted that this normalized loss quoted is the percentage loss that corresponds to the scaled down total cost (~$1,68,910) as described above. So, the approximate loss in dollars comes to ~$40,539 which is 24% of the scaled down total cost and 3% of the total cost of the frame which is ~$1,330,000.

To illustrate the benefits further in dollar terms, suppose we select point corresponding to 22% loss, then it would amount to a loss of ~$37,160. So basically, we obtain a reduction of ~$3,379; but to achieve this, the initial cost must be increased (approximately 3 times the cost for 24% loss). Similar comparative observations may be derived for all the points in the Pareto front; this illustrates the benefit of Pareto front.

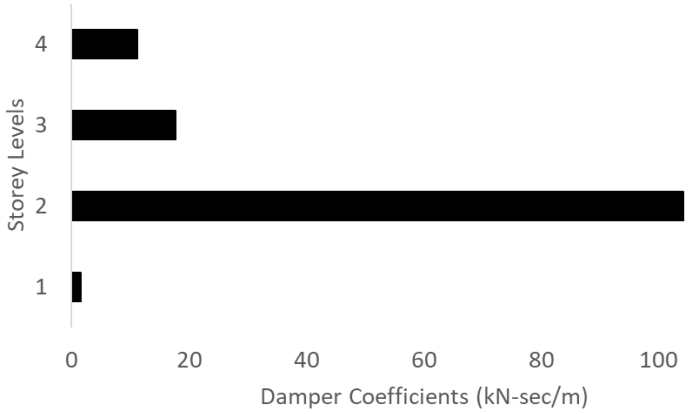


Fig. 9.5 Optimal distribution of dampers of the selected point in the pareto front

### 9.4.2 Eight storey 3D Asymmetric frame RC structure

An eight storey 3 bay by 3 bay asymmetric framed structure introduced by Tso and Yao (1994) and further studied by Lavan (2006) is used for the further study here. Plan and elevations of the structure is shown in fig 9.6.

The geometric properties of the structure are shown in table 1.0.

Table 1.0 Geometric properties of the structure

| Element location | Beams (width x depth) | Columns (width x depth) |
|---|---|---|
| Frames 1 & 4 | 400mm x 600 mm | 500 mm x 500 mm |
| Frames 2 & 3 | 400 mm x 600 mm | 700 mm x 700 mm |

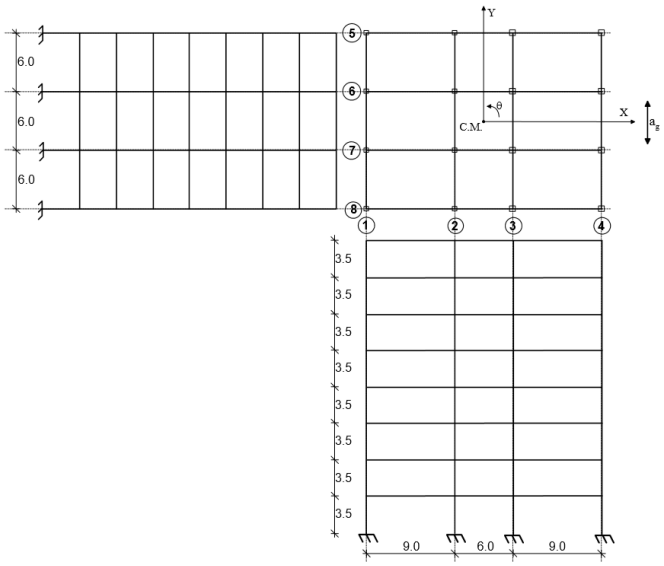


Fig. 9.6 Eight storey 3 bay by 3 bay RC structure

A uniform floor mass of $0.75\,^{ton}/_{m^2}$ is uniformly distributed in all floors. The fundamental period of the system in the y-direction is 1.15 seconds and in the x-direction it is 1.225 seconds.

The modelling of the 3D frame follows the philosophy of assembling the matrix adopted in Wilson and Dovey (1972). Only 3 degrees of freedom is assumed in each floor; The axial deformations are neglected and slab acts as a rigid diaphragm. In majority of the practical structures with in-situ slab construction the assumption of rigid diaphragm may be reasonably justified. Stiffness matrix of each independent frame is assembled first as a plane frame and then the contribution of each of this plane frames to the global 3D frame is computed. More details on this is given in Lavan (2006).

Since the present example is only used for demonstrating the applicability of the proposed framework, losses due to structural frame and partitions are only considered in the present study like the previous example. The partition walls are assumed to be distributed uniformly along the height in the outer bays of frame 1 and frame 4. The building is assumed to be in Christchurch, New Zealand and the functionality is categorized as hospitality. As per

Rowlinson's pricing manual 2012 (Rowlinson database, New Zealand), a typical cost per floor area is approx-imately NZ$ 4,750/$m^2$. The total floor area is given as 3456 $m^2$ which will give an approximate total cost of the building as NZ$16,416,000. This cost includes all components like structure, non-structural, services etc. Since only the structural frame and partitions are considered in the present study, the total cost had to be scaled down to reflect that and it amounts to NZ$ 2,101,248. This value is called the net considered cost in the present study. This cost is obtained by using the split up that 5.2% of the total cost is attribute to structural frames and 7.5% is attributed to the partitions. Therefore, the obtained Pareto front should be interpreted from this aspect. The losses are lumped at the relevant degrees of freedom and a component based assessment of loss is adopted as described in chapter 8.0. To simplify the loss computation, it has been assumed that the distribution of the total cost is the same in all storeys; i.e. if the total cost is "X" and there are "n" storeys, cost per storey is taken as "X/n". In a more realistic case, explicit storey level cost would need to be computed by summing up

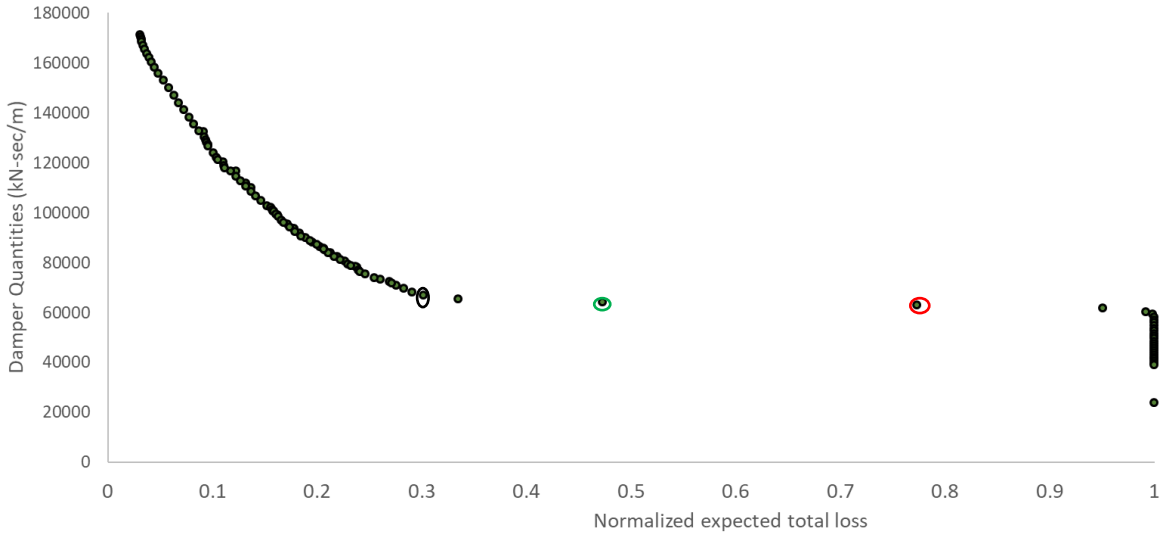


Fig. 9.7 Pareto front for the 3D structure

the re-placement value of each of the component comprising the storey. The framework proposed in this study is very generic and can easily incorporate this aspect. Fig 9.7 shows the Pareto front. The loss computed is normalized by the net considered cost as described above.

Fig 9.7 shows the obtained Pareto front. The loss computed is normalized by the net considered cost as described above. For further illustration let's consider three points as shown in fig. 9.7; red circled point corresponds to ~77% loss (NZ$ 1,617,961) given with a damper quantity of 62.8 MN-sec/m, green circled point refers to ~48% (NZ$ 1,008,599) with a total damper quantity of 64.1 MN-sec/m and black circled point refers to a loss of ~30% (NZ$ 630,375) with a total damper quantity of 67 MN-sec/m. Comparing the red circle and the green circle it is clearly seen that a reduction in loss of ~38% is obtained by an increase in total damper quantity by ~2%; so, basically when we shift from red circled point to green circled point a saving of ~NZ $ 609,362 is made; similarly comparing red circle and black circle it may be clearly seen that a reduction by 61% is achieved (saving of NZ $ 987,586) by an increase of just ~7% increase in the damper quantity. This is a very useful information and highlights the benefit of Pareto front emphatically.

Fig. 9.8 shows a typical viscous damper distribution with a damping ratio of ~40%, obtained for the peripheral frames for a typical point identified on the Pareto front of Fig. 9.7. This point corresponds to a total expected loss of 30% of the net considered cost i.e. a loss of NZ$ 630,374; now with respect to total structural cost this amounts to 3.8% of total building cost. As described above, only two components (Structural frames and partitions) are considered in this study and this value will increase when more and more components are added. For illustration purpose, this is deemed to be sufficient.

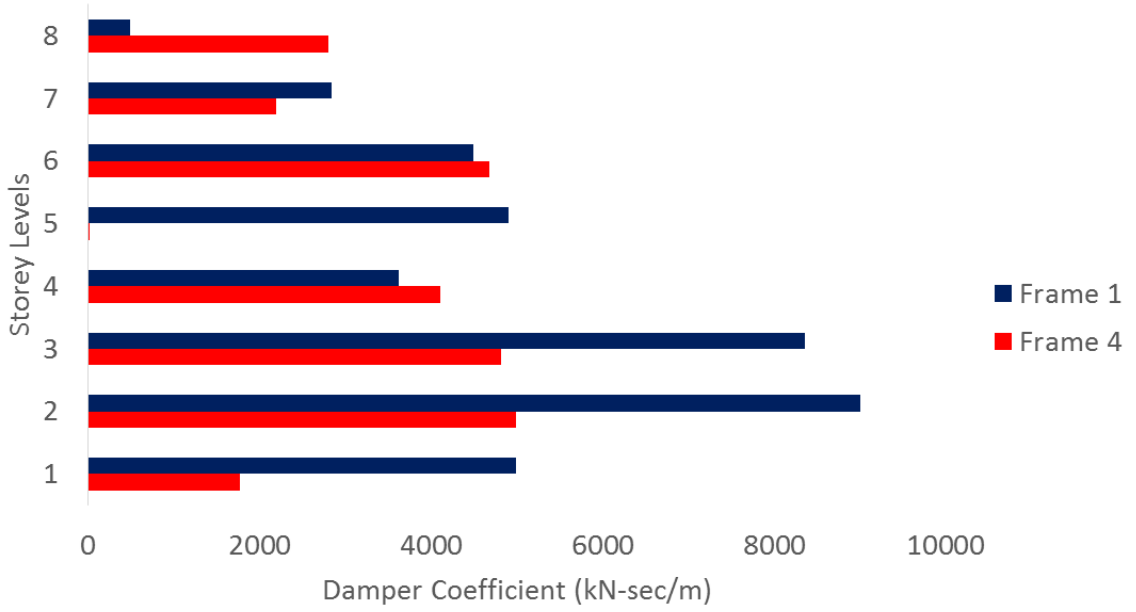


Fig. 9.8 Viscous damper distribution on the peripheral frames; frame 1 and frame 4

The *controlling* drift which is the $d_{al}$ in eq. (9.1) is limited to 0.8% of the story height; this will ensure a predominant elastic response. The presented framework is very generic and can cater to any number of ground motions. The total optimized quantity of dampers if the expected total loss needs to be restricted to 30% of the net considered cost (3.8% of total building cost) is 67 MN-sec/m. Similarly, all the points in the Pareto front represents a specific quantity and distribution.

## 9.5 Conclusion

A first order gradient based optimization scheme is presented to optimally quantify and distribute linear viscous dampers along the height of a building. Analytical derivation of the first order gradients using the very efficient Adjoint Variable method is presented in detail. A full detail description and the implementation of the analytical gradients are illustrated. An aggregate gradient based multi- objective framework is presented and the formulated optimization problem minimizes the initial cost by constraining the total expected loss. A 2D

four storey and a 3D eight storey asymmetrical frame system is used to depict the efficiency of the presented schemes.

# 10. Design of viscous dampers for nonlinear frames: a multi-objective framework

Puthanpurayil, A.M., Lavan.O and Dhakal, R.P. (2015). Seismic loss optimization of nonlinear moment frames fitted with viscous dampers, Proceedings of the tenth pacific conference in earthquake engineering, (Oral presentation)

**Abstract:** In this chapter the first order gradient based multi-objective optimization scheme presented in chapter 9 is extended to nonlinear frames.

## 10.1 Introduction

Earthquakes are random events and almost entirely non-predictable. Though from a societal aspect, it would be ideal for a viscous damper enhanced structure to remain linear for the re-usability and post-earthquake functioning of the building as described in previous chapters, it might not always be economically feasible to achieve this target in an extreme rare event. So, the optimal design of viscous dampers for a nonlinear system is important mainly because when inelastic excursions happen in the parent frame there will be real time modal migration and what is optimal in the linear case might not be optimal when the parent frame becomes inelastic. Though there has been a lot of research effort expended on formulating optimization framework for linear frames, till date very few schemes exist for nonlinear frames. Lavan and Levy (2005) pioneered this effort by minimizing the total added damping subject to a constraint on the performance of the structure (allowable inter-story drifts). Levy & Lavan (2006) and Lavan (2015) also presented highly efficient practical analysis/redesign procedure for arriving at the optimal designs exploiting the advantage of the fully stressed characteristics of the optimal solution. While these formulations lend itself to the performance-based-design

framework, the allowable inter-story drifts, or performance measures, are determined based on code requirements. These drifts are usually not determined based on the economic consequences and thus the formulated framework never reflected the economic aspect explicitly.

In the recent past with the advent of Performance Based Earthquake Engineering framework as described in chapter 8.0, direct estimation of seismic loss has become the deciding factor; one of the main reasons for this is because majority of the owners/stake holders involved in decision making are non-engineers and seismic loss is a more tangible and appealing decision variable. One relevant reference in optimal design of viscous dampers which combined both the initial cost and seismic loss and assessed the performance in a framework of life cycle cost reduction was by Gidaris & Taflanidis (2015); but the framework presented by them was based on a zero-order optimization scheme (Micro-Genetic Algorithm) and it required a very large number of function evaluations (as per the paper it required 6 million analyses to optimize a 2D three storey shear frame). The other most important aspect that may be noted is that all the above-mentioned works are single objective in nature.

In this present chapter, the novel multi-objective gradient based first order optimization framework (Izui et al. 2014) proposed for linear frames in chapter 9 is applied to nonlinear frames. Computationally, in comparison to the zero order schemes, the proposed first order optimization framework is very efficient mainly because it adopts a gradient based approach and the amount of function evaluations required are very less. Also, the Pareto front generated gives a full sphere of the possible solutions helping a decision maker place his decision on informed quantified facts.

## 10.2 Optimization framework

This section presents the extension of the generic framework for multi-objective optimization presented in chapter 9 for nonlinear frames. The optimization problem involves minimizing simultaneously the initial cost and the expected total cost. Expected total cost is computed in a similar manner as per the intensity based methodology as described in chapter 8.0 and the effect of collapse is indirectly considered by using the Heaviside step function. A capping on the peak drift is considered in the optimization framework to prevent real collapse of the structure. This is further illustrated in section 10.2.1. A component strategy is adopted for the loss computation. Again, in this study, no seismic losses due to downtime and injury are accounted.

The framework presented here is applicable equally to strengthening of existing buildings and to new buildings. In this present work only, the added damping is considered as the variable. If only damping is considered as the variable, then the initial cost in the case of enhancing seismic performance with viscous dampers can be assumed as the cost of added dampers and their installation.

### 10.2.1 Problem formulation

The optimization problem is formulated as,

$$
\left.
\begin{aligned}
&\min\left(\Gamma\left(\mathbf{c}_d\right),\Psi\left(\mathbf{c}_d\right)\right)\\
&\textit{here,}\\
&\Psi=\left\{H\left(\mathrm{X}-d_{al}\right)\right\}\times C_{total}+\left\{H\left(d_{al}-\mathrm{X}\right)\right\}\times\sum_{j=1}^{N_d}c_j\sum_{i=1}^{k}A_i\left(\frac{1}{N_{gm}}\sum_{r=1}^{N_{gm}}\left\{\max_t\left(abs\left(\mathbf{H}_T\mathbf{u}_r\left(t\right)\right)\right)\right\}\right)^{\eta_i}\\
&\textit{where}\quad\mathbf{u}_r\left(t\right)\quad\textit{follows}\\
&\mathbf{M}\ddot{\mathbf{u}}_r\left(t\right)+\left[\mathbf{C}+\mathbf{C}_{damper}\left(\mathbf{c}_d\right)\right]\dot{\mathbf{u}}_r\left(t\right)+\mathbf{f}_s\left(\mathbf{u}_r\left(t\right),\dot{\mathbf{u}}_r\left(t\right)\right)=-\mathbf{M}\mathbf{r}\ddot{u}_{g,r}\left(t\right)\\
&\mathbf{u}_r\left(0\right)=0;\dot{\mathbf{u}}_r\left(0\right)=0\\
&0\le\mathbf{c}_d\\
&r=1\rightarrow N_{gm}\\
&\mathrm{X}=Env\left(\max_i\left(\left\{\max_t\left(abs\left(\mathbf{H}_T\mathbf{u}_1\left(t\right)\right)\right),\max_t\left(abs\left(\mathbf{H}_T\mathbf{u}_2\left(t\right)\right)\right),..,\max_t\left(abs\left(\mathbf{H}_T\mathbf{u}_{N_{gm}}\left(t\right)\right)\right)\right\}\right)
\end{aligned}
\right\}\forall\ddot{u}_{g,r}\left(t\right)
$$

(10.1)

In eq. (10.1) $H$ refers to the Heaviside step function; $\mathbf{H}_T$ refers to the drift transformation matrix; $\mathbf{c}_d$ refers to the damper vector; $\mathbf{u}_r,\dot{\mathbf{u}}_r$ and $\ddot{\mathbf{u}}_r$ are displacement vector, velocity vector and acceleration vector for the $r^{th}$ ground motion; $N_{gm}$ represents the number of ground motions; $\mathbf{M},\mathbf{C}$ are the mass & inherent damping matrices; $\mathbf{f}_s\left(\mathbf{u}_r\left(t\right),\dot{\mathbf{u}}_r\left(t\right)\right)$ represents the nonlinear restoring forces vector at time *t*. $\mathbf{C}_{damper}\left(\mathbf{c}_d\right)$ is the added viscous damper matrix; **r** is the directionality vector; $\ddot{u}_{g,r}$ is the $r^{th}$ ground motion acceleration vector; $d_{al}$ is the allowable capping drift; $C_{total}$ is the total cost of the structure; $c_j$ is the cost of the $j^{th}$ component.

The allowable capping drift $d_{al}$ for linear frames described in the previous chapter was selected so that the parent frame did not incur any inelasticity; but the allowable capping drift $d_{al}$ for nonlinear frames are selected in such a way that the frame incurs controlled inelasticity with no real global collapse. As illustrated in eq. (10.1), when the peak drift in any ground motion

exceeds the allowable drift $d_{al}$, it is deemed to be a total loss. So, if $d_{al}$ is selected in such a way that only reasonable inelasticity is developed, then the framework presented by eq. (10.1) ensures sufficient resilience in case of an accidental very rare extreme event which exceeds the intensity of the ground motions considered for the present study. This is mainly achieved because though the frame work suggests total loss after exceeding $d_{al}$, in reality it would not be so. Thus, the definition of $d_{al}$ in inelastic framework should be selected judiciously so that real global collapse is prevented in a rare extreme event.

### 10.2.2 Optimization scheme

Eq. (10.1) presents a nonlinear optimization scheme. Optimization scheme is explained with reference to section 9.3.1.2. Optimization framework remains the same as outlined in section 9.3.1.2 except in step 4 of the scheme. The gradients for the present study employs a finite difference scheme to compute the gradients. It is true that finite difference method of gradient computation is not the most efficient way; but as the sole purpose of this chapter is to illustrate the application of the first order gradient based multi-objective framework in optimizing viscous dampers (both quantification and distribution) for nonlinear frames, this method of gradient computation is deemed to be acceptable. For more efficient computation of Gradients, interested readers should refer (Pollini et al. 2017). Though, even if the gradient computation is not efficient, still it could be clearly seen that the number of function evaluations required in arriving at the Pareto front is quite less in comparison to the zero order schemes used by other researchers.

## 10.3 Numerical Study

The same four story reinforced concrete frame described in chapter 9 is used to illustrate the proposed optimization procedure in the case when parent frame becomes nonlinear. The elemental Wilson Penzien damping model with consistent mass formulation is used for representing the inherent damping in the study. The elemental Wilson Penzien damping model as opposed to classical Rayleigh damping model is mainly employed to reduce the appearance of the spurious instantaneous damping force as illustrated in chapters 2.0 & 3.0.

The seismic loss computation used for this example computes the loss from both partition walls and the structural elements. The cost distribution remains the same as described in section 9.4.1. and the total scaled down cost remains the same which is ~$1,68,910. Losses in the partition walls are computed by the lumped tributary area approach described in chapter 8.0. All the losses computed are normalized against the scaled down building cost. As the losses are computed assuming probability of collapse to be zero, the $d_{al}$ is limited to 1.5% of the storey height. The selection of $d_{al}$ =1.5% provides with sufficient resilience in the case of an extreme rare event with an increased intensity than of the ground motions considered for the present study.

A suite of 7 artificial ground motions scaled to match a EC8 design spectra with PGA 0.63g (more than 2 times the design PGA) is used for the present study. Un-controlled frame analysis has revealed that this level of ground motion intensity can incur inelastic excursions in the parent frame due to drifts greater than the order of about >2.0% (Arede 2000).

As mentioned in section 9.2, though it has been observed in the public response to the Christchurch/Kaikoura sequence of earthquakes that they would expect the building to remain

elastic and re-occupiable after an event, it might not always be possible to satisfy that criterion, especially in the case of an extreme rare event. So, an effective damper based scheme should incur controlled yielding state in the parent structure in such a way that the damage incurred is repairable. To achieve this objective, as already mentioned in the present study, the limiting peak drift in any ground motion $d_{al}$ is limited to 1.5%. Only drift sensitive loss is accounted in the present study. Multi-objective optimization is performed as per the methodology described in section 9.3.1.2 with gradients being computed using the finite difference method. For the present study only 40 design points are generated in the objective space, i.e. $K$=40 in step 2 of section 9.3.1.2 and $q$=*4* as there are only 4 dampers. Constraint *move limit* is adopted as 2% of the design damping vector. Simplest bilinear hysteresis is used for the analysis. It may be critiqued that since the structure is RC, bilinear hysteresis might not be appropriate; but as the present study is intended only for illustrating the applicability of the optimization framework to the nonlinear scenario, it is deemed to be acceptable. Also, plasticity is limited (max drift = 1.5%) so the effect of the hysteretic model on the results is not expected to be large.

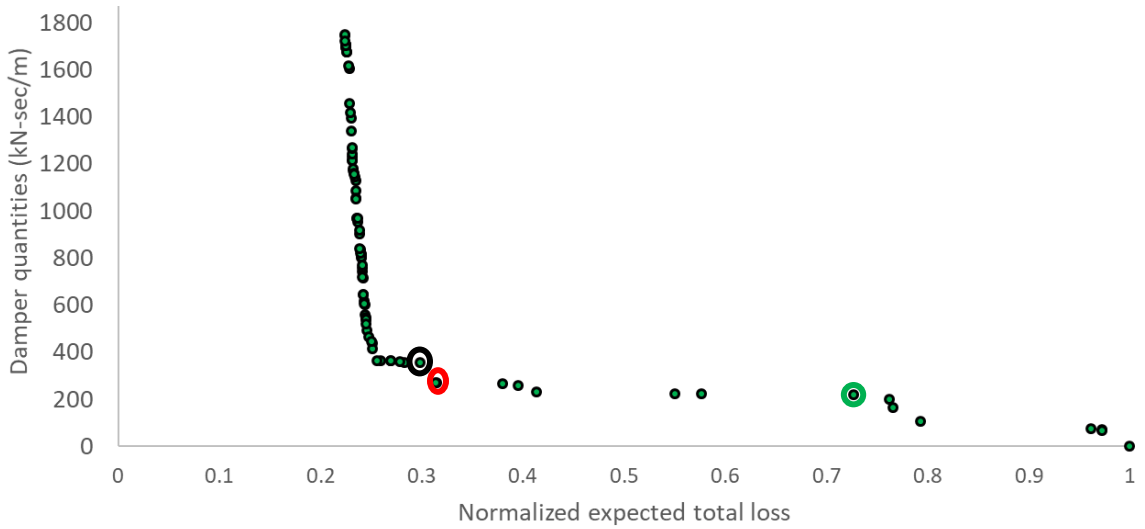


Fig. 10.1 pareto-front for the four story frame

Fig. 10.1 shows the final Pareto front. Each of this point on the Pareto front corresponds to a specific quantity of dampers and its distribution. To illustrate the benefit of Pareto front, let us focus on three points as shown on the front; points corresponding to ~72% (green circle), ~31% ( red circle) and ~29% (black circle). The associated quantities of dampers are as follows: $217kN-s/m$ (green circle), $270kN-s/m$ (red circle) and $353kN-s/m$ ( black circle). From this, it could be clearly seen that, a reduction of loss from 72% to 31% (~57% reduction) is obtained by an increase of 25% of the damper quantity (initial cost), but a further increase of 30% in damper quantity only results in a reduction of 7% in the loss (point with black circle). To put it in a different perspective, from the Pareto front, it is clearly seen that a slight increase in one of the objectives (in this case, the loss) results in a high reduction in the other objective function (the initial cost/damper quantities). This is a very powerful information as far as a stakeholder is concerned mainly because this gives him a clear understanding of the financial implications of his decisions.

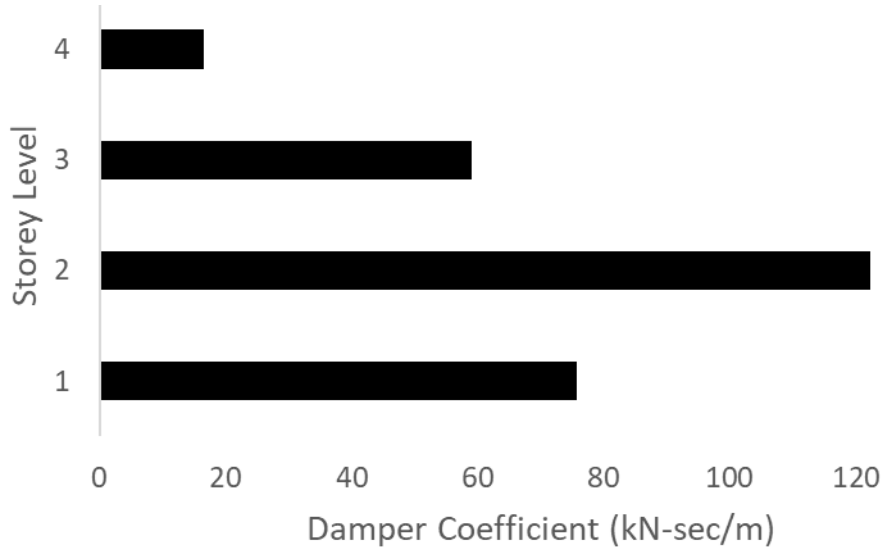


Fig. 10.2 Optimal distribution of dampers of the selected point in the pareto front

Fug. 10.2 presents the damper distribution for the total expected normalized loss of ~31% (red circle). It has to be noted that this level of damping corresponds to approximately 40% damping

ratio in the first mode. One of the advantages of this method is that both quantification and distribution of the dampers are achieved simultaneously. It could be clearly seen that as the initial cost increases the loss is minimized considerably.

## 10.4 Effect of choice of inherent damping models on optimal design of viscous dampers

To investigate the effect of choice of inherent damping models on the optimal "sizing" and "distribution" of the viscous dampers, a re-analysis of the system presented in section 10.3 is done by changing the inherent damping model to global initial stiffness Rayleigh damping model. Fig. 10.3 presents the comparison of the Pareto front plots generated using two different choices of damping model. Pareto front generated by elemental Wilson Penzien (EWP) in fig. 10.3 is directly adopted from fig.10.1.

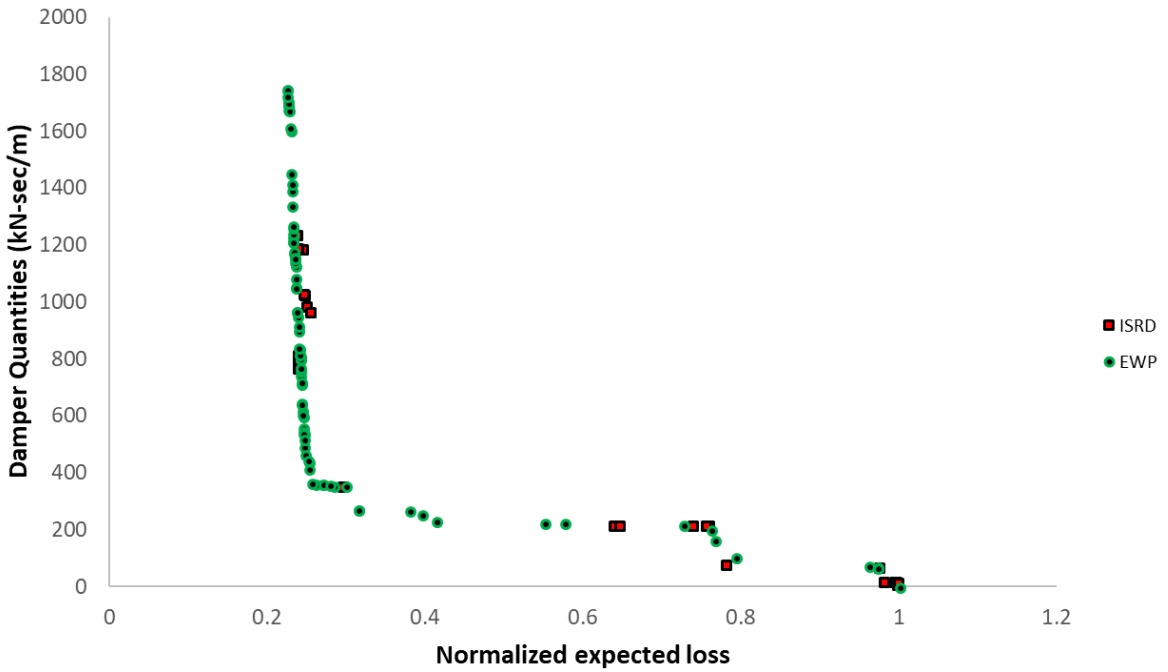


Fig. 10.3 Comparison of Pareto fronts generated with two different choices of inherent damping models.

From fig. 10.3, it may be clearly deduced that for high damping ratios the effect of the inherent damping modelling is minimum. It may also be deduced that when the damping ratio is comparatively low, the differences seems to be more. From this aspect it may be concluded that the effect of inherent damping model will be high when the added damping ratio is less and more inelasticity happens in the structure.

## 10.5 Conclusion

A first order gradient based multi-objective optimization scheme is presented to optimally quantify and distribute linear viscous dampers along the height of a nonlinear building frame. An aggregate gradient based multi- objective framework is presented and the formulated optimization problem minimizes the initial cost by constraining the total expected loss. The constraint on the total expected loss is incorporated via the use of a Heaviside step function incorporating a capping drift. As opposed to the linearity assumption, in the case of nonlinear frames, the main function of the capping drift is to ensure controlled inelasticity. A four storey frame is used to demonstrate the scheme. A comparative study on the effect of choice of inherent damping models on the obtained Pareto front is also presented. It is concluded that, when the added damping ratio is small and the inelasticity in the parent frame is high, the choice of inherent damping model is more pronounced.

# 11. Conclusions & Future research

This thesis presents (a) fundamental modelling approaches to capturing the phenomenon of inherent damping and (b) incorporating these approaches in a generic multi-objective framework for optimization of viscous dampers. Both linear and nonlinear parent frames are considered. Each individual chapter captures the relevant conclusions and the main purpose of this chapter is to consolidate the main developments and to propose some future research directions

### 11.1 Main Conclusions

The first part of the thesis (chapters 3-7) introduces a paradigm shift to inherent damping modelling by developing the novel concept of "elemental damping models" and chapters (9-10) develops an efficient multi-objective gradient based optimization framework for viscous damper design incorporating these elemental damping models.

As optimization is sensitive to the mathematical models used to represent the physical system, it becomes imperative that a realistic optimum will only be achieved if the inherent epistemic uncertainties are minimized. One of the epistemic uncertainty in structural dynamics is the representation of the phenomenon of inherent damping. Classical approach to modelling of inherent damping is by adopting the mathematically convenient Rayleigh damping model. The use of Rayleigh damping model in linear or nonlinear dynamics has no real justification as evidenced in this thesis. So, in this direction, the following has been achieved in the thesis:

1. The first part of the thesis develops a whole new paradigm of damping modelling in which the damping matrix is developed at the element level and assembled to system level in a similar manner to mass or stiffness matrices. Element level formulation of damping incurs no additional computational penalty and reflects the contribution of the elements in a more realistic manner. Six new damping models with increasing rigor are

introduced into the nonlinear seismic dynamic analysis scenario. The developments are described in detail in chapters 3, 5 and 6. This satisfies the first objective described in chapter 1.0.

2. A modified Newmark method is developed in chapter 4.0 which can solve integro-differential equations involving convolution damping models. The method is called AAR approach and is applicable to both linear and nonlinear equations of motion.
3. Chapter 7.0 presents a comparative performance of all the proposed models in nonlinear scenario and proposes the updated elemental Wilson Penzien model as the preferred model for representing inherent damping phenomenon in IDA study. When the system is linear this model converges to the constant elemental Wilson Penzien model. This satisfies the second objective proposed in chapter 2.0.
4. Adopting the most realistic in-structure damping model recommendation from chapter 7.0, a generic framework is developed which can simultaneously optimize the initial cost of the dampers as well as the seismic loss likely to be incurred in an earthquake. To this end, an aggregate gradient based multi-objective strategy adopted from the literature is applied to optimally quantify and distribute the dampers in frame buildings. The expected loss is computed as per classical Pacific Earthquake Engineering Research (PEER) center seismic risk assessment framework. A polynomial based interpolation is used to compute the expected loss conditioned on engineering demand parameters (EDPs). Gradients for the optimization framework is computed analytically using the highly efficient Adjoint Variable Method. Efficiency of the framework is demonstrated using a four-storey 2D linear frame and an eight-storey 3D asymmetric linear system. The results are presented in the form of Pareto front which is plotted between the initial cost and the expected seismic loss. Pareto front presents a set of feasible solutions and presents the owner and other stakeholders with a powerful

decision-making tool, as it clearly shows the implication of the decisions made. The methodology is described in detail in chapter 9.0. This satisfies the third objective proposed in chapter 1.0.

5. The optimization framework developed based on aggregate gradient based multi-objective strategy is extended to inelastic frames. The gradients are derived using the finite difference schemes. Chapter 10.0 describes in detail the procedure and presents with a comparison of linear and nonlinear frames. This satisfies the fourth objective proposed in chapter 1.0.
6. It has been shown in chapter 10 that in a highly inelastic system, when the added damping ratio due to the addition of viscous dampers is small, then the effect of choice of inherent damping models on the optimal quantity and distribution of the added viscous dampers is considerable.

In summary, this thesis puts forward with an advanced first order gradient based generic multi-objective framework for viscous damper quantification and distribution for linear / nonlinear structures which incorporates realistic advanced inherent elemental damping models.

### 11.2 Recommendations for future research

Based on the work presented in the thesis following recommendations are made for future research. They are as follows:

- The proposed elemental inherent damping models in this thesis is mainly developed for plane frame elements. The promising results presented in this thesis suggest that an extension of this new paradigm of elemental formulation for damping models into the 3D beam and shell elements would improve its applicability and prospects.

- The more reliable modified Newmark total equilibrium (Puthanpurayil et al. 2014) is adopted in this thesis. In the computation of damping forces which is required in the Newmark total equilibrium framework, the tangent damping matrix is treated as the secant matrix; refer chapter 3.0. It is envisaged that a more realistic implementation is achievable if a secant estimate of the damping force is used. Further research is recommended in this direction.
- In the optimization framework presented in this thesis, seismic loss computation is based on mean responses. It is recommended that future research be directed towards incorporating the median responses along with standard deviation into the optimization framework.
- The seismic loss is computed using polynomial interpolation in the thesis. It recommended that future research be undertaken to investigate the possibility of incorporating more robust interpolation techniques like cubic spline interpolation.
- The proposed optimization framework in chapter 10.0 presents the scenario where parent frame incurs controlled inelasticity. The gradient computation is done by Finite Difference method. Higher efficiency would be obtained if the nonlinear gradients are computed using Adjoint Variable Method. Further research is recommended in this direction.

# Appendix 1: Computation of elemental frequencies using consistent mass matrix

Elemental frequencies of beam elements are obtained by assuming free-free boundary condition. Using the consistent mass formulation, the mass matrix is given as,

$$\mathbf{M} = \frac{\rho A_e l_e}{420}\begin{bmatrix} 4l_e^2 & -3l_e^2 \\ -3l_e^2 & 4l_e^2 \end{bmatrix} \qquad \text{A.1.1}$$

and the flexibility matrix with plastic hinge spring flexibility $f_s$ in series is given as,

$$\mathbf{F} = \begin{bmatrix} \frac{2l_e}{6EI_e} + f_s & \frac{l_e}{6EI_e} \\ \frac{l_e}{6EI_e} & \frac{2l_e}{6EI_e} + f_s \end{bmatrix} \qquad \text{A.1.2}$$

Now elemental frequencies can be computed by solving eq. A1.3 given below as,

$$\begin{bmatrix} \frac{2l_e}{6EI_e} + f_s & \frac{l_e}{6EI_e} \\ \frac{l_e}{6EI_e} & \frac{2l_e}{6EI_e} + f_s \end{bmatrix} \frac{\rho A_e l_e^3}{420}\begin{bmatrix} 4 & -3 \\ -3 & 4 \end{bmatrix}\begin{Bmatrix} \phi_{e,1} \\ \phi_{e,2} \end{Bmatrix} = \frac{1}{\omega_e^2}\begin{bmatrix} 1 & 0 \\ 0 & 1 \end{bmatrix} \qquad \text{A1.3}$$

Solving eq. A1.3 gives the elemental frequencies and elemental mode shapes for the element under consideration. If the state of the element is elastic the plastic hinge spring flexibility $f_s$ would be zero otherwise the spring flexibility exists. It can be clearly seen that eq. A.1.3 can also be solved analytically if required.

# Appendix 2: Revised Newmark constant average acceleration method

First the classical Newmark constant average acceleration method is illustrated briefly in this section and then the revised Newmark formulation is presented which is the basic framework used in this thesis. The fundamental assumption in the classical Newmark formulation is that the acceleration is assumed to be constant during the time step with a value equal to the average of the accelerations at the beginning and end of the time step. The classical Newmark method starts with the difference in the response between two successive time steps $\Delta T$ apart. So, the equation of motion at time $t$ with $\{u(t)\}, \{\dot{u}(t)\}$ and $\{\ddot{u}(t)\}$ representing, displacement, velocity and acceleration becomes,

$$[M]\{\ddot{u}(t)\}+[C]\{\dot{u}(t)\}+[K]\{u(t)\}=\{P(t)\} \qquad \text{A2.1}$$

At time $(t+\Delta T)$,

$$[M]\{\ddot{u}(t+\Delta T)\}+[C]\{\dot{u}(t+\Delta T)\}+[K]\{u(t+\Delta T)\}=\{P(t+\Delta T)\} \qquad \text{A2.2}$$

Taking the difference between these two equations would result in,

$$[M_t]\{\Delta\ddot{u}\}+[C_t]\{\Delta\dot{u}\}+[K_t]\{\Delta u\}=\{\Delta P\} \qquad \text{A2.3}$$

In the above equation, $M_t$, $C_t$ and $K_t$ respectively are the tangent mass, tangent damping and the tangent stiffness matrices. The eq. A.3 is in incremental equilibrium with $\{\Delta\ddot{u}\}, \{\Delta\dot{u}\}$ and $\{\Delta u\}$ being the corresponding acceleration, velocity and displacement increments. Eq. A.2.1 has *n* equilibrium equations and *3n* unknowns including *n* displacements, *n* velocities and *n* accelerations. So, this incremental form of the equation can only be solved by expressing a relationship between the displacement, velocity and acceleration.

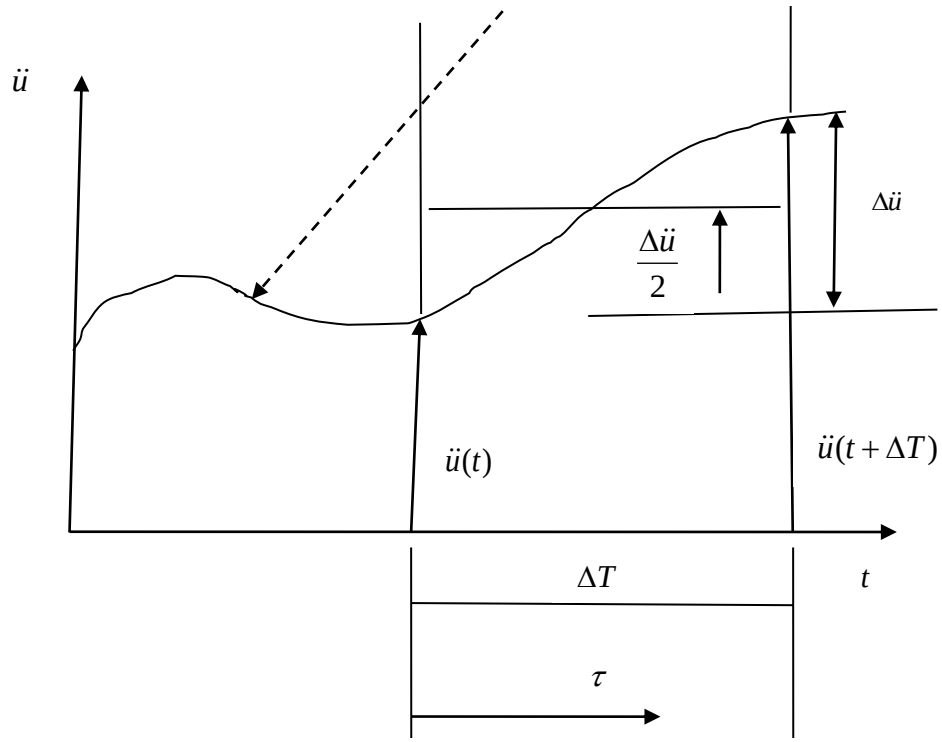


Fig A1.0 Illustration of the variation of the acceleration within a time step in constant average acceleration method

With reference to Fig. A1.0, the above assumption can be illustrated in mathematical terms as,

$$\{\ddot{u}(t+\tau\} = \{\ddot{u}(t)\} + \frac{1}{2}\{\Delta\ddot{u}\} \qquad \text{A2.4}$$

Let

$$\{\ddot{u}(t)\} = \{\ddot{u}_0\} \qquad \{\dot{u}(t)\} = \{\dot{u}_0\} \qquad \{u(t)\} = \{u_0\} \qquad \text{A2.5}$$

Then eq. A.4 can be rewritten as,

$$\{\ddot{u}(t+\tau\} = \{\ddot{u}_0\} + \frac{1}{2}\{\Delta\ddot{u}\} \qquad \text{A2.6}$$

Integrating with respect to $\tau$ , we get,

$$\{\dot{u}(t+\tau)\} = \{\dot{u}_0\} + \tau\{\ddot{u}_0\} + \frac{\tau}{2}\{\Delta\ddot{u}\} \qquad \text{A2.7}$$

and integrating again,

$$\{u(t+\tau)\} = \{u_0\} + \tau\{\dot{u}_0\} + \frac{\tau^2}{2}\{\ddot{u}_0\} + \frac{\tau^2}{4}\{\Delta\ddot{u}\} \quad \text{A2.8}$$

Now at the end of the time step, the velocity and displacement in terms of increments of acceleration is given as,

$$\{\dot{u}(t+\Delta T\} = \{\dot{u}_0\} + \Delta T\{\ddot{u}_0\} + \frac{\Delta T}{2}\{\Delta\ddot{u}\} \quad \text{A2.9}$$

$$\{u(t+\Delta T\} = \{u_0\} + \Delta T\{\dot{u}_0\} + \frac{(\Delta T)^2}{2}\{\ddot{u}_0\} + \frac{(\Delta T)^2}{4}\{\Delta\ddot{u}\} \quad \text{A2.10}$$

The increments of velocity and displacement expressed in terms of increments of acceleration in eqs. A2.9 and A2.10 are as follows,

$$\{\Delta\dot{u}\} = \Delta T\{\ddot{u}_0\} + \frac{\Delta T}{2}\{\Delta\ddot{u}\} \quad \text{A2.11}$$

$$\{\Delta u\} = \Delta T\{\dot{u}_0\} + \frac{(\Delta T)^2}{2}\{\ddot{u}_0\} + \frac{(\Delta T)^2}{4}\{\Delta\ddot{u}\} \quad \text{A2.12}$$

Now rearranging the above equations in terms of increments of displacement results in,

$$\{\Delta\ddot{u}\} = \frac{4}{\Delta T^2}\{\Delta u\} - \frac{4}{\Delta T}\{\dot{u}(t)\} - 2\{\ddot{u}(t)\} \quad \text{A2.13}$$

$$\{\Delta\dot{u}\} = \frac{2}{\Delta T}\{\Delta u\} - 2\{\dot{u}(t)\} \quad \text{A2.14}$$

The revised Newmark scheme starts with equation of equilibrium at time $t + \Delta T$ ,

$$[M]\{\ddot{u}(t+\Delta T)\} + [C]\{\dot{u}(t+\Delta T)\} + [K]\{u(t+\Delta T)\} = \{P(t+\Delta T)\} \quad \text{A2.15}$$

The following relations are used for the development of the scheme,

$$[K(t+\Delta T)]\{u(t+\Delta T)\} = [K(t)]\{u(t)\} + [K_t]\{\Delta u\} \quad \text{A2.16}$$

$$[C(t+\Delta T)]\{\dot{u}(t+\Delta T)\} = [C(t)]\{\dot{u}(t)\} + [C_t]\{\Delta\dot{u}\} \quad \text{A2.17}$$

$$[M(t+\Delta T)]\{\ddot{u}(t+\Delta T)\} = [M(t)]\{\ddot{u}(t)\} + [M_t]\{\Delta\ddot{u}\} \quad \text{A2.18}$$

where $K_t, C_t$ and $M_t$ are the corresponding tangent stiffness, tangent damping and tangent mass matrices and $K(t), C(t)$ and $M(t)$ are the corresponding secant stiffness, secant damping and secant mass matrices. In the further development of the method these secant matrices are denoted as $M, C$ & $K$. Now substituting the above equations, A2.16-A2.18 in A2.15 gives,

$$[M]\{\ddot{u}(t)\} + [M_t]\{\Delta\ddot{u}\} + [C]\{\dot{u}(t)\} + [C_t]\{\Delta\dot{u}\} + [K]\{u(t)\} + [K_t]\{\Delta u\} = \{P(t+\Delta T)\} \quad \text{A2.19}$$

Now collecting the increment terms on one side,

$$[M_t]\{\Delta\ddot{u}\} + [C_t]\{\Delta\dot{u}\} + [K_t]\{\Delta u\} = \{P(t+\Delta T)\} - [M]\{\ddot{u}(t)\} - [C]\{\dot{u}(t)\} - [K]\{u(t)\} \quad \text{A2.20}$$

Now by using eqs. A2.13 and A2.14, the increments of acceleration and velocity can be expressed in terms of increments of displacement and finally the equilibrium can be written as,

$$[\hat{K}_t]\{\Delta u\} = \{P(t+\Delta T)\} + [M]\left\{\{\ddot{u}(t)\} + \frac{4}{\Delta T}\{\dot{u}(t)\}\right\} + 2[C_t]\{\dot{u}(t)\} - [C]\{\dot{u}(t)\} - [K]\{u(t)\} \quad \text{A2.21}$$

where dynamic or augmented stiffness $[\hat{K}_t]$ is given as,

$$[\hat{K}_t] = \frac{4}{\Delta T^2}[M_t] + \frac{2}{\Delta T}[C_t] + [K_t] \quad \text{A2.22}$$

# Appendix 3: Description of the four-story frame

The four story structure used in the present study is a test frame tested in European laboratory for structural assessment (ELSA) designed according to previous versions of Eurocodes 2 and 8 (Arede 1997). As already stated the structure falls in the high ductility class and is designed for a PGA of 0.3g with soil type B and behavioural factor of 5. For full reinforcement details refer (Arede 1997). Fig. A 2.1 represents the geometric dimensions of the frame elevation. Floor slab masses are assumed to be lumped at the beam column joints. C25/30 grade concrete with B500 Tempcore reinforcing steel with yield strength of 500 MPa was used for the actual construction. As the frame is already experimentally tested more information regarding the material characteristics of the frame is available in (Arede 1997). As our focus is to qualitatively illustrate the performance of the proposed damping models, following simplified structural data is used for the present study.

**A3.1 Material Property** (Dolsek 2010)

Considerable discrepancies in the material characteristics were observed in the testing in comparison to the nominal value as given by Eurocode 2. Adopted value for the present study is given as below:

Mean concrete strength= 33 MPa

Modulus of elasticity = $3.1\times10^{10}\ N/m^2$

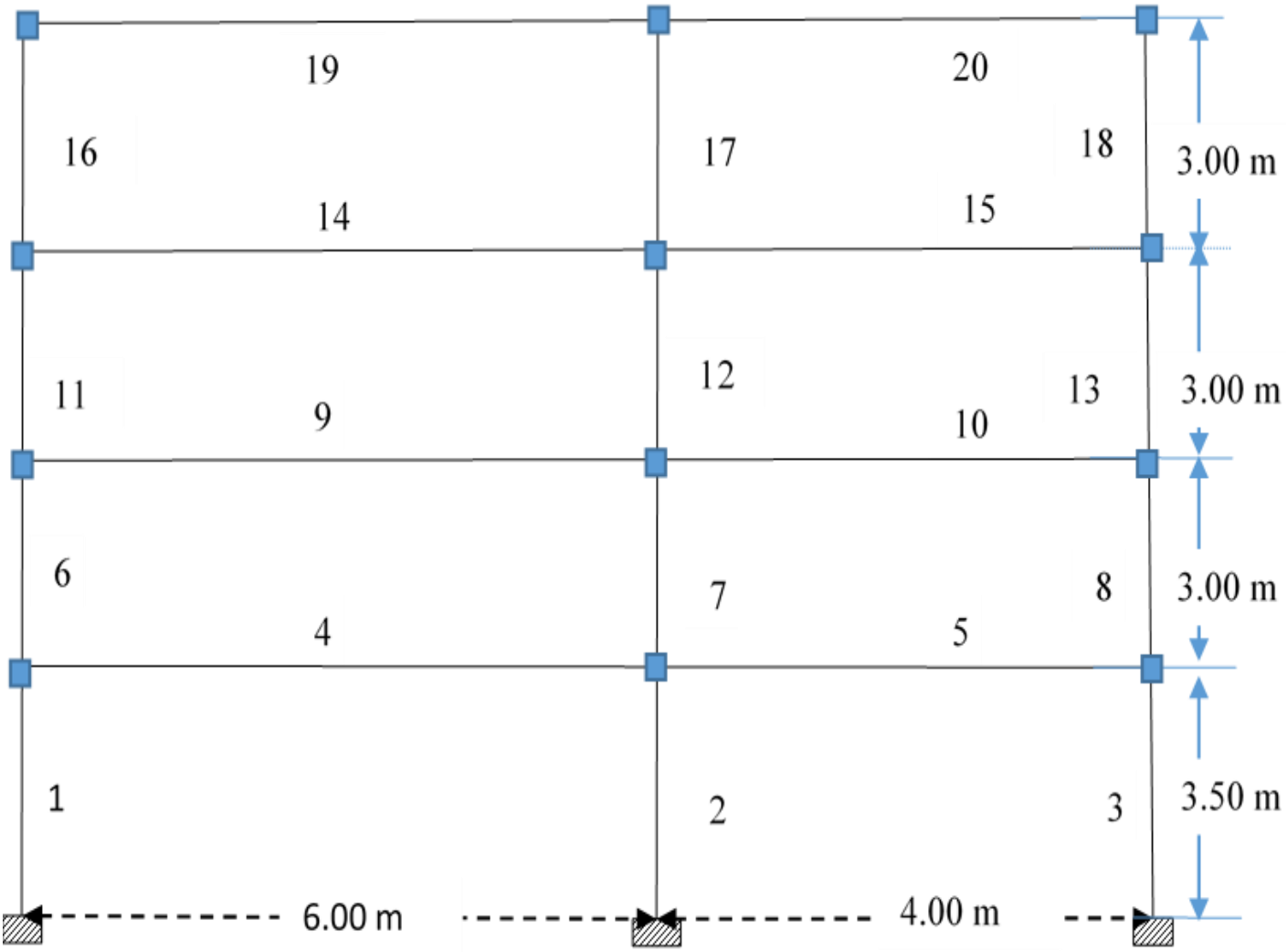


Fig. A2.1 Four story frame

**A3.2 Geometric Properties** (Arede 1997)

| Member number | Width of the member (mm) | Depth of the member(mm) |
|---|---|---|
| 1,6,11,16,17,12,7,2,3,8,13,18 | 450 | 450 |
| 4,5,9,10,14,15,19,20 | 300 | 450 |

**A3.3 Nodal Mass** (Arede 1997)

| Floor level | Mass per node (kg) |
|---|---|
| 1st floor | 29800 |
| 2nd -4th floor | 29500 |

**A3.4 Yield Rotations**

Yield rotations are computed as per Fardis (2007). if section yielding is identified as yielding of steel reinforcement, yield curvature is given as,

$$\varphi_y = \frac{f_y}{E_s\left(1-\xi_y\right)d} \tag{A3.1}$$

In eq.(A2.1),

$$\xi_y = \left(\alpha^2 A^2 + 2\alpha B\right)^{\frac{1}{2}} - \alpha A \tag{A3.2}$$

where

$$\alpha = \frac{E_s}{E_c}, A = \rho_1 + \rho_2 + \rho_v + \frac{N}{bdf_y}, B = \rho_1 + \rho_2\delta_1 + 0.5\rho_v\left(1+\delta_1\right) + \frac{N}{bdf_y} \tag{A3.3}$$

$b$ is the width of the compression zone, $d$ is the effective depth of the section, $\rho_1$ and $\rho_2$ are the ratio of the tension and compression reinforcements normalized on $bd$, $\rho_v$ is the ratio of the web reinforcement, $\delta_1$ is the ratio of the distance of center of compression reinforcement from the extreme compression

fibers to the effective depth of the section, $E_s$ and $E_c$ are elastic modulus for steel and concrete. Only yield rotation corresponding to flexural yielding is considered in the present study and is given as,

$$\theta_y = \frac{\phi_y L_s}{3} \tag{A3.4}$$

where $L_s$ is the shear span.

| **Member number** | **Yield Rotation (i$^{th}$ node) (Positive/negative) (rad)** | **Yield Rotation (j$^{th}$ node) (Positive/negative)(rad)** |
|---|---|---|
| 1,2,3 | 0.04 | 0.0074 |
| 6,8,11,13,16,18 | 0.0064 | 0.0064 |
| 7 | 0.0054 | 0.0061 |
| 12,17 | 0.0061 | 0.0061 |
| 4,9 | 0.0093 | 0.0093 |
| 5,10 | 0.0062 | 0.0062 |
| 14,19 | 0.009 | 0.009 |
| 15,20 | 0.006 | 0.006 |

# Appendix 4 : Algorithm for implementation of the the AAR method

The implementation is carried out using eq. (4.15) in most cases where a closed form solution as described in Section 3.0 exists for the integrals containing the kernel function. Here, the implementation strategy is illustrated for the generic case in which the damping kernel function $g(t)$ adopts any causal dissipative model. For the generic case, the equation of motion is given as,

$$M\{\ddot{u}(t)\}+\int_0^t C_k g(t-\tau)\{\dot{u}(\tau)\}d\tau + K\{u(t)\}=\{P(t)\} \qquad \text{A4.1}$$

The initial conditions are as specified in eq. (4.4). Now, the implementation using eq. (4.15) involves the evaluation of two integrals in close form.

**Steps involved in the algorithm**

1. Initialise the displacement vector $d_{old}=\{d_0\}=\{u(0)\}$ and velocity vector $v_{old}=\{v_0\}=\{\dot{u}(0)\}$
2. To evaluate initial acceleration consider eq. A4.1 and we get,

$$\{\ddot{u}(t)\}=M^{-1}\left\{\{P(t)\}-\int_0^t C_k g(t-\tau)\{\dot{u}(\tau)\}d\tau - K\{u(t)\}\right\} \qquad \text{A4.2}$$

$t=0,$

$$\{\ddot{u}(0)\}=M^{-1}\left\{\{P(0)\}-\int_0^0 C_k g(0-0)\{\dot{u}(0)\}d\tau - K\{u(0)\}\right\} \qquad \text{A4.3}$$

$$a_{old}=\{\ddot{u}(0)\}=M^{-1}\{P(0)-C_k g(0)v_{old}-Kd_{old}\} \qquad \text{A4.4}$$

3. Evaluate in closed form the following integrals

$$I_{damp1} = \int_{t}^{t+\Delta T} C_k g(t+\Delta T-\tau)d\tau \qquad \text{A4.5}$$

$$I_{damp2} = \int_{t}^{t+\Delta T} C_k g(t+\Delta T-\tau)\pi d\tau \qquad \text{A4.6}$$

4. Initialise $\{F_{damp1}\} = I_{damp1} v_{old}$ and $\{F_{damp2}\} = I_{damp2} v_{old} \frac{2}{\Delta T}$ at *t=0* A4.7

5. Initialise $\{F_{damp}\}$ term at *t=0* (Refer eq.4.8a and eq.4.15) A4.8

6. Choose a sufficiently small time step. For the first time step,

   *i. Calculate effective load vector* $F_{new}$ *at time* $t+\Delta T$

- $$\{F_{new}\} = \{P(t+\Delta T)\} + M\left\{a_{old} + v_{old}\left[\frac{4}{\Delta T}\right]\right\} - K_s\{d_{old}\} - \{F_{damp1}\} - \{F_{damp}\} + \{F_{damp2}\}$$

A4.9

where $\{P(t+\Delta T)\}$ is the applied load vector in eq. A4.1.

   *ii. Solve for the displacement increment,*

- $$\{\Delta u\} = \left[\frac{4}{\Delta T^2} M + \frac{2}{\Delta T^2} I_{damp2} + K_T\right]^{-1} \{F_{new}\} \qquad \text{A4.10}$$

   *iii. Calculate the displacement for time* $t+\Delta T$

- $$d_{new} = d_{old} + \{\Delta u\} \qquad \text{A4.11}$$

   *iv. Solve for acceleration increment and velocity increment*

- $$\{\Delta \ddot{u}\} = \left[\frac{4}{\Delta T^2}\{\Delta u\} - \frac{4}{\Delta T} v_{old} - 2a_{old}\right] \qquad \text{A4.12}$$

- $$\{\Delta \dot{u}\} = \left[\frac{2}{\Delta T}\{\Delta u\} - 2v_{old}\right] \qquad \text{A4.13}$$

   *v. Calculate the velocity and acceleration for* $t+\Delta T$

- $v_{new} = v_{old} + \{\Delta \dot{u}\}$ A4.14
- $a_{new} = a_{old} + \{\Delta \ddot{u}\}$ A4.15
- Update the $d_{old}, v_{old}$ and $a_{old}$
- Update $\{F_{damp}\}, \{F_{damp1}\}$ and $\{F_{damp2}\}$

7. Repeat the steps (i-v) in 6 for other time steps.

# Appendix 5: Timoshenko beam element formulation

The mass matrix $M$ and stiffness matrix $K$ of the Timoshenko beam model used for the study in Section 4.6 is given as below.

$$[M]=\frac{I_0 h}{420\mu^2}\begin{bmatrix}156 & -22h & 54 & 13h\\ -22h & 4h^2 & -13h & -3h^2\\ 54 & -13h & 156 & 22h\\ 13h & -3h^2 & 22h & 4h^2\end{bmatrix}+\frac{I_2}{30h\mu^2}\begin{bmatrix}36 & -3h & -36 & -3h\\ -3h & 4h^2 & -3h & -h^2\\ -36 & -3h & 36 & 3h\\ -3h & -h^2 & 3h & 4h^2\end{bmatrix}+$$
$$\Omega\left(\frac{I_0 h}{10\mu^2}\begin{bmatrix}84 & -11h & 36 & 9h\\ -11h & 2h^2 & -9h & -2h^2\\ 36 & -9h & 84 & 11h\\ 9h & -2h^2 & 11h & 2h^2\end{bmatrix}+\frac{I_2}{\mu^2}\begin{bmatrix}0 & 6 & 0 & 6\\ 6 & 2h & -6 & -2h\\ 0 & -6 & 0 & -6\\ 6 & -2h & -6 & 2h\end{bmatrix}\right)$$
$$+\Omega^2\left(\frac{I_0 h}{5\mu^2}\begin{bmatrix}240 & -30h & 120 & 30h\\ -30h & 6h^2 & -30h & -6h^2\\ 120 & -30h & 240 & 30h\\ 30h & -6h^2 & 30h & 6h^2\end{bmatrix}+\frac{24I_2 h}{\mu^2}\begin{bmatrix}0 & 0 & 0 & 0\\ 0 & 2 & 0 & 1\\ 0 & 0 & 0 & 0\\ 0 & 1 & 0 & 2\end{bmatrix}\right) \quad \text{A5.1}$$

$$[K]=\frac{2EI}{\mu h^3}\begin{bmatrix}6 & -3h & -6 & -3h\\ -3h & 2h^2\lambda & 3h & h^2\xi\\ -6 & 3h & 6 & 3h\\ -3h & h^2\xi & 3h & 2h^2\lambda\end{bmatrix} \quad \text{A5.2}$$

$$\Omega=\frac{EI}{GAK_s h^2} \quad \text{A5.3}$$

$$\xi=1-6\Omega \quad \text{A5.4}$$

$$\lambda=1+3\Omega \quad \text{A5.5}$$

$$\mu=1+12\Omega \quad \text{A5.6}$$

$$I_0 = \rho A$$
$$I_2 = \frac{\rho A h^2}{12} \qquad \text{A5.7}$$

where

$E$ is the Young's Modulus,

$I$ is the second moment of area,

$\rho$ is the mass density and $h$ is the elemental length.

# Appendix 6: Derivation of damping coefficients for the Russell damping model

Only the coefficient matrix for the symmetric upper triangular coefficient matrix is given here, where $c_{ij}$ refers to the $i^{th}$ row and $j^{th}$ column element.

These coefficients are computed using eq. (6.11) for Gaussian kernel function by applying the classical Hermitian cubic shape functions. For details on the variables in the coefficient matrix refer section 6.3.1.

$$\Re_\theta = \sqrt{2}be^{-\left(\frac{1}{2}\frac{L^2}{b^2}\right)}L^2 + erf\left(\frac{L}{\sqrt{2}b}\right)\sqrt{\pi}L^3 - 6\sqrt{2}bL^2 - 8\sqrt{2}b^3 + 9L\sqrt{\pi}\left(erf\left(\frac{L}{\sqrt{2}b}\right)\right)b^2 + 8\sqrt{2}e^{\left(-\frac{1}{2}\frac{L^2}{b^2}\right)}b^3$$

$$\Re_\eta = 5\sqrt{2}be^{-\left(\frac{1}{2}\frac{L^2}{b^2}\right)}L^2 - 20\sqrt{2}bL^2 - 24\sqrt{2}b^3\left(1 - e^{-\left(\frac{1}{2}\frac{L^2}{b^2}\right)}\right) + 27L\sqrt{\pi}erf\left(\frac{1}{2}\frac{L\sqrt{2}}{b}\right)b^2 + 4erf\left(\frac{L}{\sqrt{2}b}\right)\sqrt{\pi}L^3$$

$$\Re_\lambda = \sqrt{2}be^{-\left(\frac{1}{2}\frac{L^2}{b^2}\right)}L^2 - 16\sqrt{2}bL^2 - 24\sqrt{2}b^3\left(1 - e^{-\left(\frac{1}{2}\frac{L^2}{b^2}\right)}\right) + 27L\sqrt{\pi}erf\left(\frac{1}{2}\frac{L\sqrt{2}}{b}\right)b^2 + 2erf\left(\frac{L}{\sqrt{2}b}\right)\sqrt{\pi}L^3$$

$$c_{11} = \frac{6b^2a}{L^6\sqrt{\pi}}\Re_\theta$$

$$c_{12} = \frac{3b^2a}{L^5\sqrt{\pi}}\Re_\theta$$

$$c_{13} = -c_{11}$$

$$c_{14} = c_{12}$$

$$c_{22} = \frac{b^2 a}{2L^4\sqrt{\pi}}\Re_{\eta}$$

$$c_{23} = -c_{12}$$

$$c_{24} = \frac{b^2 a}{2L^4\sqrt{\pi}}\Re_{\lambda}$$

$$c_{33} = c_{11}$$

$$c_{34} = -c_{14}$$

$$c_{44} = c_{22}$$

# Appendix 7: Derivation of damping coefficients for the ESM damping model

The internal direct damping coefficient matrix obtained by computing eq. (6.34) using classical Hermitian cubic shape functions are given as follows.

$$c_{11} = -\frac{\left(288\left(\frac{1}{e^{\alpha L_e}}\right) - 24\alpha^3 L_e^3 + \frac{288\alpha L_e}{e^{\alpha L_e}} + 72\alpha^2 L_e^2\left(\frac{1}{e^{\alpha L_e}} + 1\right) - 288\right)}{\alpha^4 L_e^6} \tag{A7.1}$$

$$c_{12} = \frac{-\left(144\left(\frac{1}{e^{\alpha L_e}}\right) - 12\alpha^3 L_e^3 + 144\alpha L_e\left(\frac{1}{e^{\alpha L_e}}\right) + 36\alpha^2 L_e^2\left(\frac{1}{e^{\alpha L_e}} + 1\right) - 144\right)}{\alpha^4 L_e^5} \tag{A7.2}$$

$$c_{13} = \frac{\left(288\left(\frac{1}{e^{\alpha L_e}}\right) - 24\alpha^3 L_e^3 + 288\alpha L_e\left(\frac{1}{e^{\alpha L_e}}\right) + 72\alpha^2 L_e^2\left(\frac{1}{e^{\alpha L_e}} + 1\right) - 288\right)}{\alpha^4 L_e^6} \tag{A7.3}$$

$$c_{14} = -\frac{\left(144\left(\frac{1}{e^{\alpha L_e}}\right) - 12\alpha^3 L_e^3 + 144\alpha L_e\left(\frac{1}{e^{\alpha L_e}}\right) + 36\alpha^2 L_e^2\left(\frac{1}{e^{\alpha L_e}} + 1\right) - 144\right)}{\alpha^4 L_e^5} \tag{A7.4}$$

$$c_{22} = -\frac{\left(4\left(2\alpha L_e + 3\right)\left(\frac{6}{e^{\alpha L_e}}\right) - \alpha^2 L_e^2 + 4\alpha L_e + 2\alpha L_e\left(\frac{1}{e^{\alpha L_e}}\right) - 6\right)}{\alpha^4 L_e^4} \tag{A7.5}$$

$$c_{23} = \frac{\left(144\left(\frac{1}{e^{\alpha L_e}}\right) - 12\alpha^3 L_e^3 + 144\alpha L_e\left(\frac{1}{e^{\alpha L_e}}\right) + 36\alpha^2 L_e^2\left(\frac{1}{e^{\alpha L_e}} + 1\right) - 144\right)}{\alpha^4 L_e^5} \quad \text{(A7.6)}$$

$$c_{24} = -\frac{\left(72\left(\frac{1}{e^{\alpha L_e}}\right) - 4\alpha^3 L_e^3 + 72\alpha L_e\left(\frac{1}{e^{\alpha L_e}}\right) + \alpha^2 L_e^2\left(\frac{20}{e^{\alpha L_e}} + 16\right) - 72\right)}{\alpha^4 L_e^4} \quad \text{(A7.7)}$$

$$c_{33} = -\frac{\left(288\left(\frac{1}{e^{\alpha L_e}}\right) - 24\alpha^3 L_e^3 + \frac{288\alpha L_e}{e^{\alpha L_e}} + 72\alpha^2 L_e^2\left(\frac{1}{e^{\alpha L_e}} + 1\right) - 288\right)}{\alpha^4 L_e^6} \quad \text{(A7.8)}$$

$$c_{34} = \frac{\left(144\left(\frac{1}{e^{\alpha L_e}}\right) - 12\alpha^3 L_e^3 + 144\alpha L_e\left(\frac{1}{e^{\alpha L_e}}\right) + 36\alpha^2 L_e^2\left(\frac{1}{e^{\alpha L_e}} + 1\right) - 144\right)}{\alpha^4 L_e^5} \quad \text{(A7.9)}$$

$$c_{44} = -\frac{\left(4\left(2\alpha L_e + 3\right)\left(\frac{6}{e^{\alpha L_e}}\right) - \alpha^2 L_e^2 + 4\alpha L_e + 2\alpha L_e\left(\frac{1}{e^{\alpha L_e}}\right) - 6\right)}{\alpha^4 L_e^4} \quad \text{(A7.10)}$$

# Appendix 8

The polynomial interpolation constants for the expected loss function conditioned on the mean EDP is given in the below table

| Constants | Partition walls | Beam column junction |
|---|---|---|
| $A_1$ | 288489 | 1845 |
| $A_2$ | 67788 | -526 |
| $A_3$ | -5467 | 45.8 |
| $\eta_1$ | 3 | 3 |
| $\eta_2$ | 2 | 2 |
| $\eta_3$ | 1 | 1 |

## REFERENCES


Adachi F,Fujita K, Tsuji M, Takewaki I(2013): Importance of interstory velocity on optimal along-height allocation of viscous oil dampers in super high-rise buildings *Engineering Structures,* **56,** 489-500.

Adachi F,Yoshitomi S, Tsuji M, Takewaki I (2013): Nonlinear optimal oil damper design in seismically controlled multi-story building frame *Soil Dynamics& Earthquake Engineering,* **44,** 1-3.

Adhikari S. (2000). *Damping models for structural vibration.* PhD Dissertation, University of Cambridge.

Adhikari S (2007) On the quantification of damping model uncertainity J. Sound and Vibration. 306: 153-171.

Adhikari S, Wagner N (2004) Direct time–domain integration method for exponentially damped linear systems. Comp.& Struct.82: 2453–2461.

Adhikari S., & Woodhouse J. (2003). Quantification of non-viscous damping in discrete linear systems *Journal of Sound and Vibration*. *260* . 499-518.

Ahmadi, G. (1979). "On the application of the critical excitation method to aseismic design." *Journal of Structural Mechanics, 7,* 55–63.

Aifantis EC., (1984) On the microstructural origins of certain inelastic models. Journal of Engineering Materials. Transaction of ASME 106: 326-330.

Aifantis EC., (1999) Gradient deformation models at nano, micro, and macroscales. Journal of Engineering Material Technology-Transactions of ASME 121:189-202.

Ajeet, S.K., & Shirkhande, M. (2007). Optimal placement of supplemental dampers in seismic design of structures. *Japanese Society of Engineering Education, 9(3),* 125-135.

Arede A.J.C.D. (1997). Seismic assessment of reinforced concrete frame structures with a new flexibility based element. Research Thesis, Universidade Do Porto

ASCE 41(2017) Seismic Evaluation and Retrofit of existing buildings, American Society of Civil Engineers

Aslani, H. & Miranda E. (2005). Probabilistic earthquake loss estimation and loss disaggregation in buildings. Research report No:15, University of Stanford.

Askes H., Metrikine AV., (2002) One-dimensional dynamically consistent gradient elasticity models derived from a microstructure. Part 2: Static and dynamic response. European journal of Mechanics A/Solids 21:573-588

Aydin, E., Boduroglub, M.H., & Guney D. (2007). Optimal Dampers Placements for Seismic rehabilitation of planar building structures, *Engineering Structures, 29,*176-185.

Baburaj, V., & Matsukai, Y. (1994). A study on the material damping of thin angle-ply laminated plates, *Journal of Sound and Vibration, 172 (3),* 415–419.

Bandstra, J. P. (1983). Comparison of equivalent viscous damping in discrete and continuous vibrating system, *Transaction of ASME, Journal of Vibration, Acoustics, Stress and Reliabilityin Design, 105,* 382–392.

Banks, H.T., & Inman, D.J. (1991). On damping mechanisms in beams, *Transactions of ASME, Journal of Applied Mechanics. 58,* 716-723.

Berg GV The analysis of structural response to earthquake forces. Report, University of Michigan industry program of the college of engineering.

Bradley B.A., Dhakal R.P., Cubrinovski M., MacRae G.A., Lee S.D. (2009). Seismic loss estimation for efficient decision making. *Bulletin of the New Zealand Society for Earthquake Engineering*. 42 (2). 96-110.

Bernal D (1994) Viscous damping in inelastic structural response. *ASCE Journal of Structural Engineering*, **120**( 4): 1240-1254..

Carr AJ (1982) Ruaumoko manual. *Report,* University of Canterbury, Christchurch.

Carr, A. J. (1997). Damping Models for Inelastic Structures, *Proceedings of Asia Pacific Vibration Conference '97,* (pp 287–293), Kyongju, Korea, Nov. 9–13, Vol. 1.

Carr AJ (1998) Ruaumoko manual. *Report,* University of Canterbury, Christchurch.

Carr, A. J. (2005). Damping Models for Time-history Structural Analyses, *Proceedings of Asia Pacific Vibration Conference '05*, (pp 42–48), Langkawi, Malaysia, Nov 27.

Carr A.J (2007). Ruaumoko Manual-Theory *University of Canterbury*. 3-14.

Carr AJ (2016) Ruaumoko Users Guide, (5 Volumes). Carr Research Ltd. Christchurch.

Carr AJ, Puthanpurayil AM, Lavan O, Dhakal RP (2017) Damping models for inelastic time history analysis: A proposed modelling approach. 16th World Conference in Earthquake Engineering, Santiago, Chile, January 2017.

Caughey TK (1960) Classical normal modes in damped linear dynamic systems. Transaction of ASME, Journal of Applied Mechanics 27: 269-271.

Chai YH, Kowalsky MJ (2015) Influence of nonviscous damping on seismic inelastic displacements. Int J Struct Stab Dyn. https ://doi.org/10.1142/S0219 45541 45007 46

Charney F.A. (2008). Unintended consequences of modelling damping in structures. *Journal of Structural Engineering*. *134 (4).* 581-592.

Cheng, F. Y., & Pantelides, C. P. (1988). *Optimal placement of actuators for structural control*, Technical Report NCEER-88-0037, State University of New York, Buffalo, New York.

Chopra AK (1995) Dynamics of structures-theory and applications to earthquake engineering. Prentice Hall inc.

Chopra AK (2012) Dynamics of Structures: Theory and application to Earthquake Engineering, Prentice Hall.

Chopra A.K and McKenna F., (2016) Modeling Viscous Damping in Nonlinear Response History Analysis of Buildings for Earthquake Excitation," *Earthquake Engineering and Structural Dynamics*

Cimellaro, G.P. (2007). Simultaneous stiffness-damping optimization of structures with respect to acceleration, displacement and base shear, *Engineering structures, 29*, 2853-2870.

Cimellaro, G.P., & Retamales, R. (2007). Optimal softening and damping design for buildings. *Structural Control and Health Monitoring, 14 (6),* 831-857.

Cimellaro, G.P., Lavan, O.,& Reinhorn, A.M., (2009). Design of passive systems for control of inelastic structures. *Earthquake Engineering and Structural Dynamics, 38,* 783–804.

Clough RW, Penzien J (2003) Dynamics of Structures, Computers and Structures

Constantinou MC. Syman MD. Tsopelas P. Taylor DP. 1993. Fluid viscous dampers in applications of seismic energy dissipation and seismic isolation. *ATC-17-1*.581-591

Constantinou, M.C., & Tadjabakhsh I.G. (1983). Optimum design of a first story damping system. *Computers and Structures, 17 (2),* 305-310.

Conte JP, Vijalapura PK, Meghella M (2003) Consistent finite-element response sensitivity analysis. Journal of Engineering Mechanics, ASCE: 1380-1393.

Connor, J.J. & Klink, B.S.A. (1996) *Introduction to Motion-Based Design,* WIT Press.

Connor, J.J., Wada, A., Iwata, M., & Huang, Y.H. (1997). Damage-controlled structures, I: preliminary design methodology for seismically active regions. *Journal of Structural Engineering,123(4),*423-431.

Cortes F, Mateos M, Elejabarriata MJ, (2009) A direct formulation for exponentially damped systems, Comp. and Struct.87:391-394.

Crisp DJ (1980) Damping models for inelastic structures. *Dissertation,* University of Canterbury, Christchurch.

CSI, User Guide PERFORM-3D, Computers and Structures Inc. Berkeley California, USA. June 2011.

De Silva, C.W. (1981). An algorithm for the optimal design of vibration controllers for flexible systems. *Journal of Sound and Vibration, 75 (4),* 495-502.

Dolsek M (2010) Development of computing environment for the seismic performance assessment of reinforced concrete frames by using simplified nonlinear models. Bulletin of Earthquake Engineering 8:1309–1329.

Drenick, R.F. (1970). Model-free design of aseismic structures. *Journal of Engineering Mechanics Division, ASCE, 96(EM4),* 483–493.

Drenick, R.F. (1973). Aseismic design by way of critical excitation. *Journal of Engineering Mechanics Division, ASCE, 99(EM4),* 649–667.

Drenick, R.F. (1977a). On a class of non-robust problems in stochastic dynamics. B.L. Clarkson (Ed.). *Stochastic Problems in Dynamics* (pp. 237–255), Pitman, London.

Drenick, R.F. (1977b). The critical excitation of nonlinear systems. *Journal of Engineering Mechanics Division, 44(E2),*333–336.

Drenick, R.F., & Park, C.B. (1975). Comments on worst inputs and a bound on the highest peak statistics of a class of non-linear systems. *Journal of Sound and Vibration, 41,* 129–131.

Eringen AC., (1972) Nonlocal polar elastic continnua, International Journal of engineering Science 10:1-16

Eringen AC., (1983) On differential equations of nonlocal elasticity and solutions of screw dislocation and surface waves. Journal of Applied Physics 54: 4703-4710

Eringen AC., (1987) Theory of nonlocal elasticity and some applications Res Mechanics 21:313-342

Filippou FC, D'Ambrisi A, Issa A (1992) Nonlinear static and dynamic analysis of Reinforced Concrete subassemblages. Report, University of California, Berkeley.

Flugge W, (1978) Viscoelasticity, Second revised, ed. Springer Verlag Berlin

Friswell MI, Sondipon A, Lei Y (2007) Non-local finite element analysis of damped beams, International journal of Solids and Structures 44:7564-7576

Fujita K., Kasagi M., Lang Z. Q, Takewaki, I. (2014): Optimal placement and design of nonlinear dampers for building structures in the frequency domain. *Earthquake and Structures,* **7(6)**

Garcia, D.L. (2001). A simple method for the design of optimal damper configuration in MDOF structures. *Earthquake Spectra, 17(3),* 38-398.

Garcia, D.L., & Soong, T.T. (2002). Efficiency of a simple approach to damper allocation in MDOF structures. *Journal of Structural Control, 9 (1),* 19-30.

Gidaris I, Taflanidis AA (2015): Performance assessment and optimization of fluid viscous dampers through life-cycle cost criteria and comparison to alternative design approaches, *Bulletin of Earthquake Engineering,***13(4),** 1003-1028

Gluck, N., Reinhorn, A.M., Gluck, J., & Levy, R. (1996). Design of supplemental dampers for control of structures. *Journal of Structural Engineering, ASCE, 122(12),* 1394-1399.

Golla, D. F., and Hughes, P. C , 1985, "Dynamics of Viscoelastic Structures—A Time-Domain, Finite Element Formulation," ASME *Journal of AppliedMechanics,* Vol. 52.

Gonzalez_lopez.S, Fernandez-Saez J. (2012), " Vibrations in euler-Bernoulli beams treated with non-local damping patches, *Computers and Structures,* 108-109; 125-134

Gurgoze, M., & Muller, P.C. (1992). Optimal positioning of dampers in multi-body systems. *Journal of Sound and Vibration, 158(3),* 517-530.

Hahn, G.D., & Sathiavageeswaran, K.R. (1992). Effects of added-damper distribution on the seismic response of buildings. *Computers & Structures, 43 (5),* 941-950.

Hall J.F. (2006). Problems encountered from the use (or misuse) of Rayleigh damping. *Earthquake and Structural Dynamics, 35,* 522-545.

Hall JF (2016) Discussion of 'Modelling viscous damping in nonlinear response history analysis of buildings for earthquake excitation' by Anil K. Chopra and Frank McKenna. *Earthquake and Structural Dynamics*. Vol.45, 2229-2233. DOI:10.1002/eqe.2761

Hsieh CC, Arora JS (1985) Structural design sensitivity analysis with general boundary conditions: dynamic problem. International Journal for Numerical Methods in Engineering 21: 267-283.

Humar JL (2012) Dynamics of Structures, CRC Press

Iyengar, R.N. (1970). *Matched inputs.* Report No. 47, Series J, Center for Applied Stochastics, Purdue University,W. Lafayette, IN.

Iyengar, R.N. (1972). Worst inputs and a bound on the highest peak statistics of a class of non-linear systems. *Journal of Sound and Vibration, 25*, 29–37.

Iyengar, R.N., & Manohar, C.S. (1985). System dependent critical stochastic seismic excitations. *M15/6, Proceedings of the 8th International Conference on SMiRT*, Brussels, Belgium.

Iyengar, R.N., & Manohar, C.S. (1987). Nonstationary random critical seismic excitations. *Journal of Engineering Mechanics, ASCE, 113(4),* 529–541.

Iyengar, R.N. (1989). Critical seismic excitation for structures. *Proceedings of the 5th ICOSSAR,* San Francisco, ASCE Publications, NewYork.

Izui K.,Yamada T.,Nishiwaki S., Tanaka K (2014): *Multi-objective optimization using an aggregative gradient-based methos*, Structural Multidisciplinary Optimization

Jehel P, Leger P, Ibrahimbegovic A (2014) "Initial versus tangent stiffness-based Rayleigh damping in inelastic time history analysis," Earthquake and Structural Dynamics, vol. 43, pp. 467-484.

Jensen SJ, Nakshtrathala PB ,Tortorelli DA (2014):On the consistency of adjoint sensitivity analysis for structural optimization of linear dynamic problems, *Structural and Multidisciplinary Optimization,***49(5),** 831-837.

Kang B-S, Park G-J, Arora JS (2006) A review of optimization of structures subjected to transient loads. Struct Multidiscip Optim31:81–95

Lavan O. (2012). On the efficiency of viscous dampers in reducing various seismic responses of wall structures. *Earthquake and Structural Dynamics.* 41. 1673-1692.

Lavan, O. (2015). Optimal Design of Viscous Dampers and Their Supporting Members for the Seismic Retrofitting of 3D Irregular Frame Structures. *Journal of Structural Engineering.*

Lavan, O. (2015). A methodology for the integrated seismic design of nonlinear buildings with supplemental damping. *Structural Control and Health Monitoring*. 22 (3). pp 484–499.

Lavan, O., Amir.O (2014): Simultaneous topology and sizing optimization of viscous dampers in seismic

retrofitting of 3D irregular frame structures *Earthquake Engineering and Structural Dynamics,* **43(9),** 1325-1342,

Lavan, O., Cimellaro,G.P.,& Reinhorn, A.M., (2008). Noniterative optimization procedure for seismic weakening and damping of inelastic structures. *Journal of Structural Engineering, Vol.134,10,* 1638-1648.

Lavan, O., & Dargush, G.F., (2009). Multi-objective Evolutionary seismic design with passive energy dissipation systems. *Journal of Earthquake Engineering, 13,* 758-790.

Lavan, O., & Levy, R. (2004). Optimal design of supplemental viscous dampers for linear framed structures. *Proceedings of 13th World Conference on Earthquake Engineering,* Paper no: 42.

Lavan, O., & Levy, R. (2005). Optimal design of supplemental viscous dampers for irregular shear frames in the presence of yielding. *Earthquake Engineering & Structural Dynamics, 34(8),* 889-907.

Lavan, O., & Levy, R. (2006a). Optimal design of supplemental viscous dampers for linear framed structures. *Earthquake Engineering & Structural Dynamics, 35(3),* 337-356.

Lavan, O., & Levy, R. (2006b). Optimal peripheral drift control of 3D irregular framed structures using supplemental viscous dampers. *Journal of Earthquake Engineering, 10(6),* 903-923.

Lavan, O., & Levy, R. 2010. Performance based optimal seismic retrofitting of yielding plane frames using added viscous damping. *Earthquakes & structures.* 3. 307-326.

Leger, P., & Duassault, S. (1992). Seismic energy dissipation in MDOF structures. *ASCE Journal of Structural Engineering, 118 (5),* 1251-1269.

Lei Y, Friswell MI, Adhikari S., (2006) A Galerkin method of distributed systems with non-local damping. International of Journal of Solids and Structures. 43:3381-3400

Levy, R. & Lavan, O. (2006). Fully stressed design of passive controllers in framed structures for seismic loadings. *Structural Multidisciplinary Optimization.* 32. 485-498.

Liang Z.,Lee G.C.,Dargush G.F., Song J. 2012. Structural Damping: Applications in seismic response modification. *CRC press*.

Lopez-Garcia, D. (2001): A simple method for the design of optimal damper configuration in MDOF structures. *Earthquake Spectra,* **17(3),** 38-398.

Lopez G, Fernandez-Saez J., (2012) Vibrations in Euler Bernoulli beams treated with non-local damping patches. Computers and Structures

Lord Rayleigh (1877 (Re-issued 1945)) Theory of sound, Second ed., New York: Dover Publication.

Love AEH (1906) A Treatise on the Mathematical Theory of Elasticity, Cambridge: Cambridge University press.

Mander JB, Dhakal RP, Mashiko N & Solberg K M (2007) Incremental dynamic analysis applied to seismic financial risk assessment of bridges. *Engineering Structures* 29 (10) : 2662-2672

Martinez-Rodrigo, M., & Romero, M.L. (2003).An optimum retrofit strategy for moment resisting frames with nonlinear viscous dampers for seismic applications. *Engineering Structures, 25 (2),* 913–925.

Metrikine AV, Askes H., (2002) One-dimensional dynamically consistent gradient elasticity models derived from a microstructure. Part 2: Static and dynamic response. European journal of Mechanics A/Solids 21:555-572

Michaleris P, Tortorelli DA, & Vidal CA (1994). Tangent Operators and Design Sensitivity Formulations for Transient Nonlinear Coupled Problems with Applications to Elasto-Plasticity, *International journal for numerical methods in Engineering,* 37 (14), 2471-2499

Miyamoto HK, Scholl R.E.(1996). Case study: seismic rehabilitation of non-ductile soft story concrete structure using viscous dampers. *11th World Conference on Earthquake Engineering* , Acapulco, Mexico.

Moreschi L.M. (2000). *Seismic design of energy dissipation systems for optimal performance.* PhD. Dissertation, Virginia Polytechnic Institute and State University.

Muravskii G.B. (2004). On frequency independent damping. *Journal of Sound and Vibration, 274.* 653-668.

Palazzo,B., Petti, L., & De Iuliis. (2004). A modal approach to optimally place dampers in framed structures. *Proceedings of 13th World Conference on Earthquake Engineering,* Paper no: 769.

Palazzo,B., Petti, L., & De Iuliis. (2004). A modal approach to optimally place dampers in framed structures. *Proceedings of 13th World Conference on Earthquake Engineering,* Paper no: 769.

Pampanin (2015), Towards the "ultimate earthquake-proof" building: development of an integrated low-damage system. : 321-358. http://dx.doi.org/10.1007/978-3-319-16964-4_13.

Paolo DM, Failla G, Zingales M (2013) Non-local stiffness and damping models for shear deformable beams. European journal of Mechanics A/Solids 40:69-83

Paola, M.D., & Navarra, G. (2009). Stochastic seismic analysis of MDOF structures with nonlinear viscous dampers. *Structural Control and Health Monitoring, 16, (3),* 303-318.

Pareto,V. (1927). Manuel d'e´conomie Politique, Giard, Paris.

PEER/ATC 72-1 (2010) Modeling and acceptance criteria for seismic design and analysis of tall buildings.

PERFORM 3D (2006) Nonlinear Analysis and performance assessment for 3D structures. *user manual.* Computers and Structures inc.

Pollini. N, Lavan.O & Amir. O,(2015): Towards minimum-cost optimization of viscous fluid dampers for seismic retrofitting. *Bulletin of Earthquake Engineering,* **14(3)**. 971-998

Puthanpurayil AM, Carr AJ, Dhakal RP (2014) A generic time domain implementation scheme for non-classical convolution damping models. Engineering Structures 71 : 88-98.

Puthanpurayil,A.M., Dhakal,R.J.,&Carr,A.J.,(2011), Modelling of in-structure damping damping: a review of the state of the art. *Proceedings of 9th Pacific Conference on Earthquake Engineering,* Paper no: 091.

Puthanpurayil AM, Lavan O, Carr AJ, Dhakal RP (2016) Elemental damping formulation: an alternative modelling of inherent damping in nonlinear dynamic analysis. Bulletin of Earthquake Engineering 14:2405-2434

Ramirez.MC, Miranda E (2009): Building-Specific loss estimation methods & tools for simplified performance-based earthquake engineering, *Report No:171,* Stanford University

Reddy JN., (2007) Nonlocal theories for bending, buckling and vibration of beams. Internation Journal of Engineering Science 45:288-307.

Reid T.J. (1956). Free vibration and hysteretic damping. *Journal of Royal Aeronautical Society*. *60*, 283.

Rowlinsons Handbook (2012)

RP Dhakal and JB Mander. (2006): Financial risk assessment methodology for natural hazards, *Bulletin of the New Zealand Society for Earthquake Engineering*, **39**(2), 91-105.

Russell, D. L., (1991), "On Mathematical Models for the Elastic Beam with Frequency Proportional Damping," *Control and Estimation in Distributed Parameter Systems*, SIAM. 125-169

Scanlan RH (1970) Linear damping models and causality in vibrations. Journal of Sound and Vibration 13(4): 499-503.

Sarlis, A.A. and Constantinou, M.C., "Modeling triple friction pendulum isolators in program SAP2000", document distributed to the engineering community together with example files, University at Buffalo, 2010

Sharpe RD (1974) The Seismic Response of Inelastic Structures. Dissertation, University of Canterbury, Christchurch.

Shing PB, Mahin SA (1987) Elimination of spurious higher-mode response in pseudodynamic tests. Earthquake and Structural Dynamics 15: 425-445.

Shukla, A.K., & Datta, T.K. (1999). Optimal use of viscoelastic dampers in building frames for seismic force. *Journal of Structural Engineering, ASCE, 125(4),* 401-409.

Silling SA.,(2000) Reformulation of elasticity theory for discontinuities and long range forces. Journal of Mechanics and Physics of solids 48:(1) 175-209

Silling SA, Zimmermann M., Abeyaratne R., (2003) Deformation of a peridynamic bar. Journal of Elasticity. 73:173-190

Singh M.P., & Moreschi, L.M. (2001). Optimal seismic response control with dampers. *Earthquake and Structural Dynamics, 30 (4),* 553-572.

Singh M.P., & Moreschi, L.M. (2002). Optimal placement of dampers for passive response control. *Earthquake and Structural Dynamics, 31 (4),* 955-976.

Smyrou,E., Priestley,M.J.,&Carr,A.J., (2011). Modelling of elastic damping in nonlinear time-history analyses of cantilever RC walls. *Bulletin of Earthquake Engineering*

Sorrentino S, Marchesiello S, Piombo BAD., (2003) A new analytical technique for vibration analysis of non-proportionally damped beams. Journal of Sound and Vibration. (4) 265:765-782

Takewaki, I. (1997a). Optimal damper placements for minimum transfer functions. *Earthquake Engineering & Structural Dynamics, 26 (11),* 1113-1124.

Takewaki, I. (1997b). Efficient redesign of damped structural systems for target transfer functions. *Computer Methods in Applied Mechanics & Engineering, 147(3-4),* 275-286.

Takewaki, I. (1998). Optimal damper positioning in beams for minimum dynamic compliance. *Computer Methods in Applied Mechanics & Engineering, 156(1-4),* 363-373.

Takewaki, I. (1999). Displacement-acceleration control via stiffness-damping collaboration. *Earthquake Engineering & Structural Dynamics, 28,* 1567-1585.

Takewaki, I. (2000). Optimal damper placement for planar building frames using transfer functions. *Structural and Multidisciplinary Optimization, 20 (4),* 280-287.

Takewaki, I. (2000a). Optimal damper placement for critical excitation. *Probabilistic Engineering Mechanics,15(4),* 317–325.

Takewaki, I. (2000b). Effective damper placement for critical excitation. *Confronting Urban Earthquakes, Report of Fundamental Research on the Mitigation of Urban Disasters Caused by Near-Field Earthquakes*, 558–561.

Takewaki, I. (2000c). A new probabilistic critical excitation method. *Journal of Structural and Construction Engineering, AIJ, 533,* 69–74.

Takewaki, I. (2000d). A nonstationary random critical excitation method for MDOF linear structural models. *Journal of Structural and Construction Engineering, AIJ, 536,* 71–77.

Takewaki, I. (2001a). Anewmethod for nonstationary random critical excitation. *Earthquake Engineering and Structural Dynamics*, *30(4)*, 519–535.

Takewaki, I. (2001b). Nonstationary random critical excitation for nonproportionally damped structural systems. *Computer Methods and Applied Mechanics Engineering*, *190(31),* 3927–3943.

Takewaki, I. (2001c). Nonstationary random critical excitation for acceleration response. *Journal of Engineering Mechanics. ASCE*, *127(6),* 544–556.

Takewaki, I. (2001d). Critical excitation for elastic–plastic structures via statistical equivalent linearization. *Probabilistic Engineering Mechanics*, *17(1),* 73–84.

Takewaki, I. (2001e). Critical excitation for MDOF elastic–plastic structures via statistical equivalent linearization. *Journal of Structural Engineering AIJ*, *47B*, 187–194.

Takewaki, I. (2001f). Probabilistic critical excitation for MDOF elastic–plastic structures on compliant ground. *Earthquake Engineering and Structural Dynamics*, *30(9)*, 1345–1360.

Takewaki, I. (2001g). Maximum global performance design for variable critical excitations. *Journal of Structural and Construction Engineering, AIJ, 539,* 63–69.

Takewaki, I. (2004a). Critical envelope functions for non-stationary random earthquake input. *Computers & Structures 82(20–21),* 1671–1683.

Takewaki, I. (2004b). Bound of earthquake input energy. *Journal of Structural Engineering ASCE, 130 (9),* 1289–1297.

Takewaki, I. (2005). Bound of earthquake input energy to soil–structure interaction systems. *Soil Dynamics & Earthquake Engineering*, *25(7–10),* 741–752.

Takewaki, I. (2007). *Critical Excitation Methods in Earthquake Engineering*, Netherlands: Elsevier.

Takewaki, I. (2009). *Building Control With Passive Dampers: Optimal Performance Based Design of Earthquakes*, John Wiley and Sons.

Takewaki I., Fujita K., Yamamoto K., & Takabatake H. (2010). Smart passive damper control for greater building earthquake resilience in sustainable cities, *Sustainable Cities and Society, doi:10.1016/j.scs.2010.08.002*

Takewaki, I., & Nakamura, T. (1995). Hybrid inverse mode problems for FEM-shear models. *Journal of Engineering Mechanics, 121 (8),* 873-880.

Takewaki, I., & Nakamura, T. (1997). Hybrid inverse mode problems for a structure-foundation system. *Journal of Engineering Mechanics, 123 (4),* 312-321.

Takewaki, I., & Uetani, K. (1999). Optimal damper placement in shear-flexural building models. *Proceedings of second world conference on structural control*, vol 2. (pp 1273-1282), John Wiley & Sons Ltd, Chichester.

Takewaki, I., & Yoshitomi, S. (1998). Effects of support stiffnesses on optimal damper placement for a planar building frame. *Journal of the Structural Design of Tall Buildings, 7 (4),* 323-336.

Tan, P., Dyke, S.J., Richardson, A., & Abdullah, M. (2005). Integrated device placement and control design in civil structures using genetic algorithms. *Journal of Structural Engineering, 131 (10),* 1489-1496.

Taylor, D.P., (1999). Buildings: Design for Damping. Taylor Devices Inc, NY.

Trombetti, T., Silvestri, S., & Ceccoli,C. (2003). *On the first modal damping ratio of MPD and SPD systems*. Technical Report, Department DISTART, University of Bologna, Italy.

Trombetti, T., & Silvestri, S. (2004). Added viscous dampers in shear type structures: the effectiveness of mass proportional damping. *Journal of Earthquake Engineering, 8 (2),* 275-313.

Trombetti, T. & Silvestri, S. (2006). On the modal damping ratios of shear-type structures equipped with Rayleigh damping systems. *Journal of Sound and Vibration, 292 (1-2),* 21-58.

Trombetti, T. & Silvestri, S. (2007). Novel schemes for inserting seismic dampers in shear type systems based upon the mass proportional component of Rayleigh damping matrix. *Journal of Sound and Vibration, 302 (3),* 486-526.

Tsopelas, P., Constantinou, M.C., Kircher, C.A. and Whittaker, A.S., "Evaluation of simplified methods of analysis for yielding structures," Report No. NCEER-97-0012, National Center for Earthquake Engineering Research, 1997

Tsuji, M. & Nakamura, T. (1996). Optimum viscous dampers for stiffness design of shear buildings. *Journal of the Structural Design of Tall Buildings 5,* 217-234.

Val, V.D & Segal, F. (2005). Effect of damping model on pre-yielding earthquake response of structures. *Engineering Structures 27,* 1968-1980.

Vamavatsikos, D & Cornell C A (2002). Incremental Dynamic Analysis. *Earthquake & Structural Dynamics,13(3)* 491-514

Viola, E., & Guidi, F. (2009). Influence of the supporting braces on the dynamic control of buildings with added viscous dampers. *Structural Control and Health Monitoring, 16 (3),* 267-286.

Vision 2000 SEAOC (1995) -A framework for performance based design, Vol I, Vol II, Vol III: Structural Engineers Association of California, Vision 2000 committee, Sacramento, California

Wada, A., Huang,Y., & Bertero,V.V., (2004). Innovative Strategies in Earthquake Engineering. Bozorgnia, Y., Bertero, V.V.,(Ed), *Earthquake Engineering, From Engineering Seismology to Perfomance-Based Engineering*, (pp. 10-1-10-33). CRC Press, London.

Whittaker, A.S., Constantinou, M.C. and Tsopelas, P., "Displacement estimates for performance-based seismic design", Journal of Structural Engineering, ASCE, Vol. 124, No. 8,1998.

Wilson, EL and Clough R (1962) Dynamic response by step by step matrix analysis. in *Symposium on the use of computers in civil engineering, Lisbon.*

Wilson EL and Penzien J (1972) Evaluation of orthogonal damping matrices. *International Journal for numerical methods in engineering* **4** : 5-10.

Wongprasert, N., & Symans, M.D. (2004). Application of a genetic algorithm for optimal damper distribution within the nonlinear seismic benchmark building. *Journal of Engineering Mechanics, 130 (4),* 401-406.

Woodhouse J. (1998). Linear damping models for structural vibration *Journal of Sound and Vibration*. *215 (3).* 547-569.

Wu, B., Ou, J.P., Soong, T.T. (1997). Optimal placement of energy dissipation devices for three-dimensional structures. *Engineering Structures, 19,*113 -125.

Xi Lin (1999). *Analysis and design of building structures with supplemental lead dampers under earthquake and wind loads.* PhD. Dissertation, University of Canterbury, Christchurch

Xu Z.D., Shen Y.P., & Zhao H.T.(2003) .A synthetic optimization analysis method on structures with viscoelastic dampers, *Soil Dynamics and Earthquake engineering,23,*683-689.

Xu Z.D., Zhao, H.T., & Li.A.Q. (2004). Optimal analysis and experimental study on structures with viscoelastic dampers, *Journal of Sound and Vibration,273 (3),*607-618.

Zareian F., & Medina R.A. (2010). A practical method for proper modelling of structural damping in inelastic plane structural systems *Computers and Structures. 88.* 45-53.

Zhang, R.H., & Soong T.T. (1992). Seismic design of visco-elastic dampers for structural applications. *Journal of Structural Engineering, 118 (5),* 1375-1392.